SEISMIC PERFORMANCE EVALUATION AND DESIGN OF A NOVEL PISTON BASED SELF-CENTERING BRACING SYSTEM

by

A. B. M. Rafiqul Haque

B.Sc. (Civil Engineering), Bangladesh University of Engineering and Technology, 2007

M.A.Sc. (Civil Engineering), The University of British Columbia, 2012

A THESIS SUBMITTED IN PARTIAL FULFILLMENT OF
THE REQUIREMENTS FOR THE DEGREE OF

DOCTOR OF PHILOSOPHY

in

THE COLLEGE OF GRADUATE STUDIES
(Civil Engineering)

THE UNIVERSITY OF BRITISH COLUMBIA
(Okanagan Campus)

June 2017

The undersigned certify that they have read, and recommend to the College of Graduate Studies for acceptance, a thesis entitled:

SEISMIC PERFORMANCE EVALUATION AND DESIGN OF A NOVEL PISTON BASED SELF-CENTERING BRACING SYSTEM

Submitted by A. B. M. Rafiqul Haque in partial fulfillment of the requirements of

The degree of DOCTOR OF PHILOSOPHY.

Dr. M. Shahria Alam, Associate Professor, School of Engineering, UBC

Supervisor, Professor

Dr. Ahmad Rteil, Assistant Professor, School of Engineering, UBC

Supervisory Committee Member, Professor

Dr. Abbas Milani, Professor, School of Engineering, UBC

Supervisory Committee Member, Professor

Dr. Keith Culver, Professor, Faculty of Management, UBC

University Examiner, Professor

Dr. Michael J. Tait, Professor, Faculty of Engineering, McMaster University

External Examiner, Professor

22 June 2017

(Date submitted to Grad Studies)

Additional Committee Members include:

Dr. Stephen Karrer O'Leary, Associate Professor, School of Engineering, UBC

Neutral Chair

ABSTRACT

Buildings designed and constructed using current seismic design codes experience nonlinear deformation during strong earthquakes; resulting in hysteretic damping. This behavior is necessary for dissipating energy from an earthquake. Thus, buildings with traditional structural systems experience permanent deformation after seismic events, resulting in enormous economic losses. To resolve this issue, researchers have developed various smart structural systems in the past decades. One such system is the novel piston based self-centering bracing (PBSC) system. This study investigates the cyclic performance of this bracing system in finite element environment to predict its load-deformation response during seismic events. This newly developed bracing system utilizes Nickel Titanium (Nitinol) based shape memory alloy (SMA) bars inside a sleeve-piston assembly for the self-centering mechanism. During cyclic loading, the bars are pulled from opposite directions to avoid compressive loading on the bars. The energy dissipation is achieved through nonlinear load deformation hysteresis. Furthermore, this bracing system can be designed to be buckling restraint. The system exhibits flag shaped force-deformation hysteresis. A unique hysteresis model is proposed from the simulated hysteresis response of this bracing system. This hysteresis model is implemented in a commercial structural analysis and design software known as "S-FRAME." In the next phase, seismic performance of steel frames equipped with the PBSC bracing system has been evaluated. Overstrength and force reduction factors were determined using FEMA P695 methodology. Using these factors, PBSC braced frames were designed and their seismic performance was assessed in terms of inter-story drift ratios. Furthermore, the seismic performance of PBSC braced frame was also compared against buckling restrained braced frames in terms of fragility function. Finally, this research presents a design methodology for this bracing system.

PREFACE

A significant part of this study has been submitted to peer-reviewed journals and conference proceedings for publication. All literature review, mathematical calculations and analytical models presented in the following journal and conference papers have been exclusively carried out by the author. The academic supervisor was only responsible for guidance and review of the work produced.

List of publications related to this thesis

Haque, A.B.M.R. & Alam, M.S. (2014). Piston-based self-centering brace apparatus, Patent US 20160326742 A1, CA2935575A1, WO2015100497A1.

Haque, A.B.M.R. & Alam, M.S. (2015). Cyclic Performance of a Piston Based Self-Centering Bracing System. ASCE Structural Congress. April 23–25, 2015, Portland, Oregon.

Haque, A.B.M.R. Sasibut, S. Rong, F. & Alam, M.S. (2016). A Hysteresis Model for the Piston-Based Self-Centering Bracing System Considering Residual Deformation. 5th International Structures Specialty Conference, CSCE, London, ON, June 2016, Paper ID: 978.

Haque, A.B.M.R. & Alam, M.S. (2017). Hysteretic behaviour of a piston-based self-centering (PBSC) bracing system made of superelastic SMA bars - a feasibility study. Tentatively accepted, Structures, Elsevier.

Haque, A.B.M.R. & Alam, M.S. (2017). SMA flag hysteresis model with sliding response for the piston based self-centering bracing system. To be Submitted, Engineering Structures, Elsevier.

Haque, A.B.M.R. & Alam, M.S. (2017). Seismic response modification factor of braced frame buildings equipped with piston based self-centering SMA bracing system. To be Submitted, Journal of Constructional Steel Research, Elsevier.

TABLE OF CONTENTS

LIST OF TABLES

LIST OF FIGURES

LIST OF NOTATIONS

A_b Area of the steel brace

A_s Austenite start temperature

A_{sma} Area of the SMA bars

A_f Austenite finish temperature

C_o Factor relating roof displacement to the fundamental mode displacement

CMR Collapse margin ratio

E_{steel} Modulus of elasticity of steel

E_{sma} Modulus of elasticity of SMA

E_i Initial modulus

E_p Post-yield modulus

E_t Tangent modulus

E_v Variable modulus

$F_{y,steel}$ Yield strength of steel

$F_{y,sma}$ Yield strength of SMA

g Acceleration due to gravity

h_n Height of building to roof level

H Height

IDA Incremental dynamic analysis

I_E Importance factor

K_i Initial stiffness

k Effective length factor for buckling load calculation

K_b Stiffness of the steel brace

K_{eq} Equivalent axial stiffness of the brace

K_i Initial stiffness

K_p Post-yield stiffness

K_{shaft} Stiffness of the brace shaft

K_{sma} Stiffness of the SMA bars

L Length

L_b Length of the brace

L_i Increased length

L_a Actual length

L_{shaft} Length of the brace shaft

L_{sma} Length of the SMA bars

m_x Mass at story x

M_f Martensite finish temperature

M_s Martensite start temperature

M_w Moment magnitude of earthquake

M_v Higher mode effect

nm Nanometer

P Axial load

P_y Yield force

P_{amf} Austenite to martensite finishing force

PGA Peak ground acceleration

PGV Peak ground velocity

r_y Residual strain coefficient

R Response modification factor

R_d Ductility related force reduction factor

R_o Overstrength factor

RTR Record to record variability

S_a Spectral acceleration

S_aT Spectral acceleration at fundamental period of the structure; also denoted as $S(T_a)$

S_{MT} Spectral acceleration for MCE ground motion at the fundamental period (T_1)

S_{CT} Median spectral acceleration at the collapse level ground motion at T_1

S_{DCT} Median spectral displacement at the collapse level ground motion at T_1

S_{DMT} Spectral displacement for MCE ground motion at T_1

SSF Spectral shape factor

T Natural period/Temperature

T_1 Fundamental period from eigenvalue analysis

V_d Design base shear force

V_E Elastic Structure base shear demand

V_{max} Maximum base shear of the base shear vs. displacement curve

V_y Yield base shear capacity

W Seismic weight of the structure

α Unloading force turn factor in PBSC hysteresis model

β Residual deformation factor

β_{RTR} Uncertainty parameter for record to record variability

β_{TD} Test data uncertainty

β_{MDL} Modeling uncertainty

β_{DR} Design requirement related uncertainty

β_{TOT} Total system collapse uncertainty

ε_1 Current strain

$\varepsilon_{\_limit}$ Limiting strain on the hysteresis backbone

ε_L Plateau strain

ε_r Residual strain

ε_{ri} Residual strain of the ith cycle

Δ_y Yield displacement

Δ_{max} Maximum/Ultimate displacement

δ Displacement

$\delta_{y,eff}$ Effective yield displacement

δ_u Ultimate displacement

μ Displacement Ductility

μ_T	Period based ductility
σ_1	Current stress point
σ_2	Next stress point
$\sigma_{\_limit}$	Stress limit on the hysteresis backbone
σ_{ams}	Austenite to martensite starting stress
σ_{amf}	Austenite to martensite finishing stress
σ_{mas}	Martensite to austenite starting stress
σ_{ams}	Martensite to austenite finishing stress
σ_{ams}	Martensite to austenite finishing stress
λ_r	Brace elongation ratio (elongated length/original length)
$Ø_{1,x}$	Ordinate of the modal displacement at level x
$Ø_{1,r}$	Ordinate of the modal displacement at roof

ACKNOWLEDGEMENTS

This research would not have been possible without the help, support and contribution of many individuals. Firstly, I would especially like to thank my Ph.D. supervisor Dr. M. Shahria Alam for his continuous support and mentoring during my research. His deep knowledge and passion for research have inspired me throughout my graduate studies at UBC. I would also like to thank my course teachers and committee members Dr. Kasun Hewage, Dr. Abbas Milani and Dr. Ahmad Rteil for providing valuable knowledge which helped me in every aspect of my research. I would also like to mention the aid and support of Dr. Marinos Stylianou, Dr. Siriwut Sasibut and Dr. Feng Rong of S-FRAME Software Inc. Their knowledge and support were pivotal in the implementation of this research output in a commercial finite element software. Their continuous feedback and review were immensely helpful in developing the algorithms and finite element models necessary for this study.

UBC's Okanagan campus has provided an outstanding scholastic and work atmosphere through their excellent management system which was crucial for my research work. The research presented in this Ph.D. thesis was jointly funded by Natural Sciences and Engineering Research Council of Canada and S-FRAME Software Inc. through the Collaborative Research and Development Grants.

I am also very thankful for being a member of an exceptional research group. It is very challenging to tackle a doctoral thesis. I would like to thank the research teammates and fellow graduate students who made this journey enjoyable. Specifically, I would like to thank Dr. Muntasir Billah, Shahin Zareie, Dr. Shahidul Islam, Dr. Farshad Hedayati Dezfuli and Zillur Rahman, Lukman Sarker for their continued good spirits and help in this research. The highly

knowledgeable research group mates provided remarkable support in my research through criticism, dialogue, and technical reviews.

Through the ups and downs of life and graduate research, my beautiful wife Fahmida Islam was always there for me. Her constant support, encouragement, and love were indispensable in my success. I am also grateful for my beautiful daughter Samia Haque, who is the inspiration of my life. Finally, I would like to thank my parents (Miah Mahmudul Haque and Mrs. Rokeya Haque) and siblings (Kaniz Mahmuda Sharmeen and M. Mohaimenul Haque) for all their support during this long and arduous study life. I would like to express my deepest gratitude to them.

Dedicated to my parents

Mr. Miah Mahmudul Haque

and

Mrs. Rokeya Haque

CHAPTER 1: INTRODUCTION AND THESIS ORGANIZATION

1.1 General

Earthquake is one of the most destructive catastrophes of nature. A high-intensity earthquake can cause serious havoc by destroying infrastructure and taking away countless lives. Every year, more than a thousand earthquakes are reported in Western Canada by the seismologists and the Geological Survey of Canada (NRC 2016). During the past 70 years, more than one hundred earthquakes with greater than moment magnitude (M_w) 5.0 occurred in the offshore region of the west of Vancouver Island (NRC 2016). For this reason, the Pacific coast is considered as the most earthquake prone region in Canada. This region is a part of the Pacific ring of fire, which is a concentration of earthquake activities related to the presence of active faults in the earth's crust. Per Natural Resources Canada, all three types of tectonic plate movements such as sliding past each other, colliding and diverging occur in this region; which causes substantial earthquake activity. The M_w 8.1 Queen Charlotte Island earthquake of 1949 happened along the faults in the BC's offshore region. A M_w 6.5 earthquake occurred in subduction ocean plate boundary under downtown Seattle in 1965. Finally, in 1946, a M_w 7.3 earthquake took place in central Vancouver Island within the continental crust. The frequency and the size of these earthquakes decrease with the distance from the coast and the active tectonic plate boundaries; this makes Saskatchewan and Manitoba the least earthquake-prone zones in Canada (NRC 2016).

If we look at some other significant earthquakes which happened between 1990's and 2010, we can see the earthquakes like the 1994 Northridge, which caused $40 billion in direct damage to Southern California (Eguchi et al. 1998). This event exposed vulnerabilities of welded moment connections in hundreds of buildings which was previously unknown. In 1995's Kobe earthquake,

central Japan was violently shaken, elevated highways collapsed and numerous buildings were destroyed. Around five thousand people lost their lives and the earthquake caused over $130 billion in direct damage (Scawthorn and Yanev 1995). Finally, the M_w 7.9 earthquake which struck the Sichuan Province in China on March 12, 2008, caused tens-of-thousands of casualties; which is a stark reminder on the consequence of constructing weak structures in active seismic hazard zones.

In a more recent event like 2010 Maule (Chile) earthquake, the infrastructure losses were approximately $20.9 billion (Elnashai et al. 2010). Furthermore, this number is around $20 billion in the 2011 Christchurch (New Zealand) earthquake; which is equivalent to 13% of New Zealand's GDP. The destruction in the wake of this earthquake was substantial, which included the demolition of about 70% of business district buildings and a loss of more than 50% of heritage buildings. The major business district was closed for over 18 months, and thousands of residents were forced to out-migrate (Elwood 2013).

These events demonstrate the severity of seismic events and their effect on the economy. These enormous losses from earthquakes triggered the awareness of building owners on how to reduce such damages. In the last century, our knowledge of seismicity and earthquake resistant structures has significantly improved. Scientists and engineers have come up with various methods for resisting seismic loads on structures. Some noteworthy methods include but are not limited to ductile moment resisting frames, base isolation systems, and seismic bracing systems. The ductile moment resisting system is currently the most widely used method for resisting seismic loading. This approach is prevalent in the construction industry due to its simplicity in design and construction. However, the fundamental concept of this method is to allow nonlinear deformation in specific locations on the primary force resisting elements of the structures during an earthquake

event; which is known as plastic hinge formation. A ductile moment resisting framing system dissipates earthquake-induced energy by hysteresis energy dissipation in these plastic hinges. This causes severe plastic deformations which are irreversible in most cases. If this deformation goes beyond a certain limit, the structure might have to be demolished and rebuilt afterward. Hence, regarding re-use or reparability, this method is not very efficient.

The base isolation system is considered an effective alternative for resisting seismic loads. This system isolates a structure from earthquake excitation by disrupting the force transfer between the ground and the structure. This method is effective in preventing structural damage and saving lives. However, this approach is not efficient for a broad range of structural height, mass, and stiffness; since the difference in these parameters results in different natural frequencies. Sometimes the use of base isolation system could shift this frequency to an unfavorable domain in the earthquake response spectrum. Furthermore, the base isolation system is often too expensive to see a widespread use around the world.

The bracing system is another option for resisting seismic loads. However, the use of traditional structural bracings against seismic loading has its challenges. The two key challenges are compression buckling and permanent deformation. Buckling has a dramatic effect on strength and stiffness of a brace. Once it occurs, strength is reduced, and the brace loses stiffness in every successive load cycle. To resolve this issue, different types of seismic bracing systems have been developed. Most notable ones are the buckling restrained braces (BRBs) (Takeuchi et al. 2004) and cast steel yielding fuses (Christopoulos et al. 2008). BRBs resist seismic forces by hysteretic energy dissipation. They exhibit fat bilinear hysteresis response, which is very efficient in dissipating seismic energy. However, this high-energy dissipation comes with a price since the

BRBs experience significant nonlinear deformation during the energy dissipation process. This nonlinear deformation is permanent and cannot be easily reverted. It also causes nonlinear deformation in the connecting elements such as the connections, beams, and columns.

In order to prevent such permanent damages, researchers have come up with smart self-centering bracing systems such as the Self-Centering Energy Dissipation Device (SCED) (Tremblay and Christopoulos 2012), Memory Alloys for New Seismic Isolation Devices (MANSIDE) (Dolce et al. 2000) and RHDB (Zhang and Zhu 2007) braces. These braces offer some special advantages over their counterparts. These braces are buckling restrained; they have moderate energy dissipation capacity, and they experience very low permanent or residual deformation after an earthquake. This low residual deformation is due to their self-centering capability. The self-centering mechanism of these braces is either achieved using Nickel-Titanium based shape memory alloys (Nitinol SMA) (MANSIDE and RHDB braces) or high-strength steel or composite materials such as Kevlar or Aramid cables (SCED brace). SMAs are a type of alloy, which can experience significant nonlinear/plastic deformation and can revert to their original shape upon heating or stress removal. The regaining of original shape upon heating is known as the shape memory effect and the returning to original shape under stress removal is known as superelasticity. The one used in braces are usually Nitinol based superelastic SMAs. However, these smart self-centering bracing systems are either difficult to construct, have low strength or energy dissipation capability (Haque and Alam 2015a).

This thesis focuses on a newly developed self-centering bracing system invented by the author. This device is known as the Piston Based Self-Centering brace or in short, PBSC brace (Haque and Alam 2014). The PBSC bracing system is made using a cylinder-piston mechanism. The

energy dissipation and self-centering capability are achieved with Nitinol tie bars. Furthermore, the PBSC brace is designed to be fully buckling restrained. The concept of the PBSC brace is novel in terms of design and constructability. The design of this brace allows the use of both SMA bars and wires; whereas previous designs could only accommodate SMA bars. Furthermore, this brace can be very easily constructed and disassembled for repair or recycling purpose as illustrated in the patent document (Haque and Alam 2014). This research focuses on the cyclic performance, design and seismic load resistance of this bracing system. This proposed structural system will have the potential to not only save peoples' lives but also retain the structure after a massive earthquake.

1.2 Objective of the study

The primary purpose of this research is to develop a novel self-centering bracing system which will be able to bring a structure back to its original position after significant nonlinear deformation induced by a seismic event. The secondary objective of this research is to propose seismic response modification factor values required for the seismic design of this new bracing system.

To fulfill the objective mentioned above, a step by step development process has been carried out. This study has focused on the following

1. Development of a novel piston based self-centering bracing system: A gradual development process is shown for the piston based self-centering bracing system. The mechanism of this bracing system has been explained in detail. The bracing system has been modeled using a finite-element analysis software ABAQUS (2014). The load-deformation hysteresis shape have been determined and discussed.

2. Development of a hysteresis model for the PBSC bracing system: This objective was achieved by creating a hysteresis material model for Nitinol shape memory alloy with residual deformation. This material model was used in a custom made MATLAB (2012) based finite element software developed specifically for the PBSC bracing system. This finite element program was used to generate PBSC brace's load deformation hysteresis. The hysteresis results were used to develop an algorithm which was implemented in a commercial finite element software.
3. Determination of seismic response modification factors such as overstrength (R_o) and force reduction (R_d) factor: FEMA P695's (FEMA 2009) quantification of building seismic performance factor methodology was used to determine the overstrength and force reduction factors for the PBSC bracing system.
4. Seismic performance comparison between PBSC and buckling-restrained braced frame: Two different sets of braced frames were designed, one with the PBSC bracing system and the other with the buckling restrained bracing system. These frames were subjected to forty-four different earthquake ground motion records. The seismic performance of these two systems was compared against each other using fragility functions developed using four different damage states.

1.3 Scope of this research

With the purpose of accomplishing the objectives mentioned above, first, a comprehensive literature review was carried out to understand various innovative bracing systems developed by the previous researchers. There are different types of buckling restrained and self-centering systems, some of which depend on the hysteretic energy dissipation or post-tensioning of

steel/composite materials; whereas, others use various types of self-centering materials. Understanding these different types of systems is essential for the development of the PBSC bracing system proposed by the author. To fulfill the objectives stated in the previous section, the following studies were carried out:

1. ABAQUS (2014) based finite element models of the PBSC bracing system were built. To accurately predict the cyclic performance of the system, these models were constructed using continuum/solid elements. As PBSC bracing system uses both steel and Nitinol SMA components, the hysteresis models of these materials were first calibrated and then incorporated in these models. Displacement based quasi-static analyses were carried out on these brace models to determine the load deformation hysteresis. The resultant hysteresis was found to be flag-shaped.
2. The flag shaped SMA hysteresis model found in the earlier step (ABAQUS analysis) was coded and implemented in S-FRAME (2016) software which follows the loading and unloading rules defined in Auricchio and Sacco (1997). However, as this hysteresis model can not simulate residual deformation, another hysteresis model was developed specifically to include this behavior. First, Auricchio and Sacco (1997)'s Nitinol hysteresis rule was modified to include residual deformation. This novel material hysteresis model was implemented in a specialized finite element program developed for the PBSC bracing system in the MATLAB (2012) environment. This finite element program was used to establish a force deformation hysteresis model for the PBSC bracing system. The hysteresis model was found to exhibit sliding response near the origin of the force-deformation plot. Finally, this new hysteresis model was implemented in the S-FRAME Software.

3. Designing buildings equipped with the PBSC bracing system as per NBCC (2010) requires two critical parameters for seismic design, these are known as overstrength (R_o) and ductility related force reduction (R_d) factors. To calculate these parameters, four, six and eight storied PBSC braced frames were designed using tentative/approximate values of R_d and R_o. In the next step, FEMA P695 (FEMA 2009) suggested seismic performance factor determination analysis was carried out. Collapse margin ratios (CMR) were calculated and adjusted for spectral shape factors. These adjusted CMR values were checked against the acceptable CMR values provided in the guideline (FEMA 2009), and they were found satisfactory; indicating the tentative values of R_d and R_o were adequate for the seismic design.
4. To determine the seismic performance of building frames equipped with PBSC bracing system, four, six and eight-storied PBSC braced frames were designed and built in the S-FRAME's finite element environment. The flag-shaped SMA hysteresis model with sliding response was used to represent the cyclic load deformation behavior of the PBSC braces. Another set of these frames were equipped with the BRB braces and designed as per NBCC (2010). Nonlinear dynamic time history analysis was carried out on these two groups of frames using 44 ground motion records. Fragility functions were calculated from four different damage states to determine seismic vulnerability under a wide range of seismic intensity. Finally, these fragility functions were used to determine the advantages/disadvantages of the PBSC bracing system against the buckling restrained bracing system.

1.4 Thesis organization

This thesis is composed of seven chapters. The current chapter provides an introduction, objective and scope of the research. Brief descriptions of the contents of these chapters are given below along a flow-chart (Figure 1-1).

In **Chapter 2**, a literature review on various innovative structural force resisting systems (both energy dissipative and self-centering) have been discussed. The topics cover traditional energy dissipative and self-centering bracing systems. First, the traditional energy dissipative braces are reviewed; their advantages and disadvantages are discussed. Then self-centering braces are covered. Finally, some relevant studies are presented in a tabular format.

In **Chapter 3**, the development process of the PBSC bracing system is discussed in detail. The force transfer mechanism is explained. Finite element models are built in ABAQUS (2014) to examine the cyclic behavior of this bracing system. Finally, the results are presented and discussed in detail.

In Chapter 4 Two force-deformation hysteresis models are developed. First one is the traditional SMA flag shaped hysteresis model and the second one is specifically developed for capturing the sliding response of the PBSC bracing system. The development and implementation process of these hysteresis models are discussed in details. The algorithm, flow charts, verification, and codes are also presented.

Chapter 5 demonstrates the determination of overstrength and ductility related force reduction factors for the PBSC bracing system. These factors were determined using the guideline stated in FEMA P695. Incremental dynamic time history analysis was carried out on three different building

frames. Collapse margin ratio values were calculated, and they were used to validate the preliminary values of these factors utilized in the design.

Chapter 6 shows the performance comparison between a BRB and a PBSC braced frame. The BRB frame is designed using established code and guidelines such as NBCC (2010) and CSA (2009). Whereas, the PBSC braced frame is designed using the preliminary values of R_d and R_o determined in chapter 5 and the design method proposed by the author. The performance of these designed frames was evaluated using nonlinear dynamic time history analysis. Fragility function was developed for performance comparison using interstory drift ratio responses of these frames.

Finally, **Chapter 7** presents the research conclusion. Furthermore, some recommendations for future research have been suggested in this chapter.

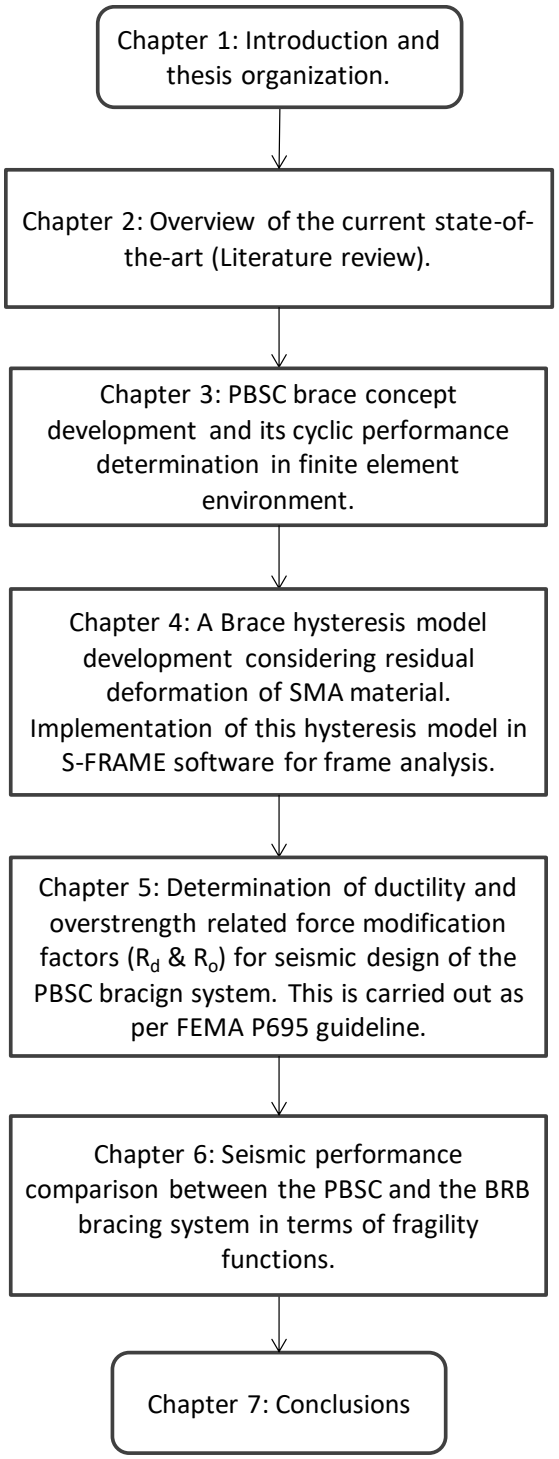

Figure 1-1: Thesis organization flow-chart

CHAPTER 2: OVERVIEW OF THE CURRENT STATE-OF-THE-ART

2.1 General

Various types of seismic bracing system have been developed, and some of them are available in the market. These systems can be grouped into two major categories: energy dissipative and self-centering systems. The following systems can be classified as energy dissipative systems: Traditional tension only braces, Buckling Restrained Brace (BRB), Cast Steel Yielding Fuse (CSYF). These braces resist seismic load by hysteretic energy dissipation characterized by large nonlinear deformation and fat hysteresis loops. On the other hand, the self-centering braces also go to the nonlinear range; however, these bracing systems can recover from large nonlinear deformation, which sets them apart from the others. This results in negligible (not more than 0.1%) residual interstory drift for the connected structure (Zhang and Zhu 2007). After an earthquake, these braces can pull back the structure to its original position resulting in very low post-earthquake repair costs. Some other self-centering systems are as follows: PBSC (Haque and Alam 2014), SCED (Tremblay and Christopoulos 2012), MANSIDE (Dolce et al. 2000), RHDB (Zhang and Zhu 2007) braces or the post-tensioned beam-column joints. Researchers have also developed base isolation systems with good self-centering capabilities (Dezfuli et al. 2013). Most of these systems rely on one of these following materials: high-strength steel strands, composite cables or superelastic shape memory alloy (SE SMA) wires/bars. Among these materials, SE SMA is a smart thermomechanical alloy composed of roughly equal atomic percentage of Nickel and Titanium. This material is also known as Nitinol, which is an abbreviated form of Nickel-Titanium Naval Ordnance Laboratory; named after the laboratory where it was invented. At room temperature, this material can come back to its original shape after large strains (6%-8%) with moderate hysteretic

energy dissipation. This lucrative property has made it one of the most interesting materials in the research of smart structures. More details on the above-mentioned bracing systems are given below.

2.1.1 Energy dissipative bracing systems

2.1.1.1 Buckling restrained bracing system

Among the numerous seismic load resisting bracing systems, the buckling restrained brace is the most notable one. Although numerous variations exist (Bystricky and Fanucci 2010; Chung-Che et al. 2014; Hinchman 2013; Iwata and Murai 2006) under the name, the one developed by Takeuchi et al. (2004) and produced and marketed by Nippon Steel Corporation has seen widespread use all around the world. This brace is essentially composed of concrete/grout filled steel tube and an inner steel core. The steel core can freely move inside the concrete sleeve thus reducing the possibility of axial load transfer from the core to the sleeve. When buckling load is reached, the core steel is prevented from buckling by the strong concrete sleeve. Figure 2-1 shows the comparison between traditional tension-compression steel brace and buckling restrained brace frame hysteresis; which shows that the traditional steel brace buckles under a compressive load, which is only a fraction of its tensile strength and loses most of its stiffness and load carrying capacity. The stiffness in the subsequent load cycles also diminishes and deformation increases significantly. On the contrary, the buckling restrained brace shows stable bilinear hysteresis loops under cyclic loading condition and exhibits excellent energy dissipation indicated by the large area inside the hysteresis loops. According to the experimental results of Fahnestock et al. (2007), a well detailed BRB frame can withstand significant drifts and ductility demand in the braces with almost no damage. They were subjected to a maximum ductility demand of 26 without any

damage. However, one potential limitation observed for the buckling restrained braces is its high residual deformation during design basis earthquake (DBE) and maximum considered earthquake (MCE) simulations. These large residual drifts may pose substantial challenges while restoring buildings with BRB frames to service condition after a major seismic incident.

The hysteretic mechanism (Figure 2-1(b)) shows that after a large nonlinear excursion if the load becomes zero the deformation does not reduce by a significant margin. This large residual deformation induces substantial beam-to-column connection deformation resulting in significant repair or rebuilding cost. Besides residual drift, BRBs are also susceptible core plate local buckling if the sleeve width to thickness ratio is not adequate to prevent it (Takeuchi et al. 2010).

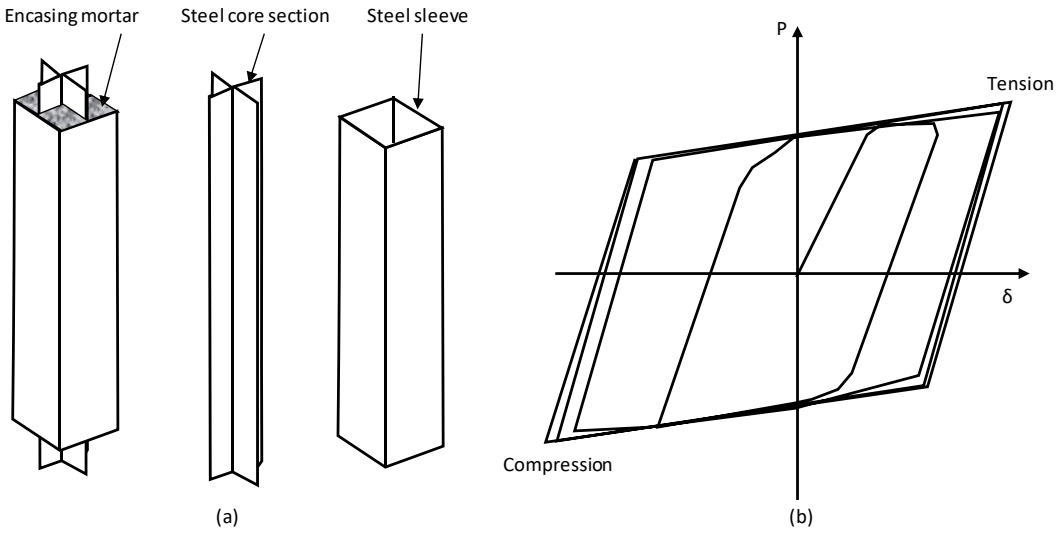

Figure 2-1: (a) A typical design of a buckling restrained brace (b)Hysteresis of a BRB brace (adapted from Asgarian and Shokrgozar (2009))

2.1.1.2 Cast-steel yielding fuse

The cast steel yielding fuse (Christopoulos et al. 2008) or commercially known as the Scorpion yielding brace is a device for improved seismic performance of concentrically braced frames (CBF) which is characterized by its Stable, full, symmetric and repeatable hysteretic behavior and

its large ductility capacity (Gray et al. 2012b) . The concept was presented as a novel seismic energy-dissipative device for CBFs. The use of a cast steel yielding device removes the inelastic compressive buckling and cyclic tensile yielding of traditional braces. It replaces traditional unstable brace hysteresis with a stable symmetric hysteretic response (Gray et al. 2010)

In this system, seismic energy is dissipated by yielding fingers of specially engineered connectors made of cast steel. Figure 2-2 shows a prototype yielding bracing system under experimental investigation. Under severe compression and tension loading, the fingers yield in flexure. This way they provide a full symmetric hysteresis.

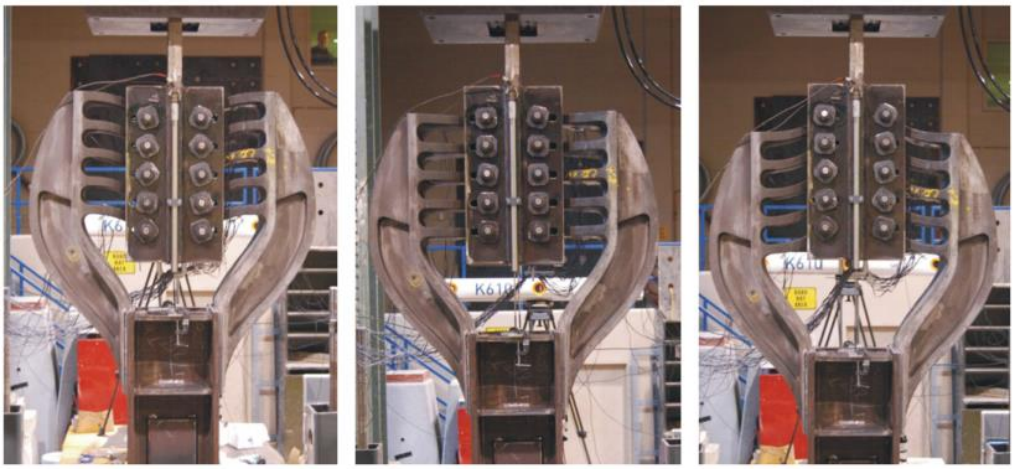

Figure 2-2: Yielding brace prototype test showing deformed shape of the fingers (Gray et al. 2014a)

A full-scale quasi-static testing of yielding brace is shown in Figure 2-3(a). The hysteresis response of the brace is shown in Figure 2-3(b). This system shows stable hysteresis response up to a certain deformation range; after this range is exceeded, the hysteresis drastically degrades. It can also be observed that this bracing system has almost no self-centering capability. It should also be noted that the maximum displacement achieved by this brace is around 75mm, which is approximately 1% of the 7m long brace.

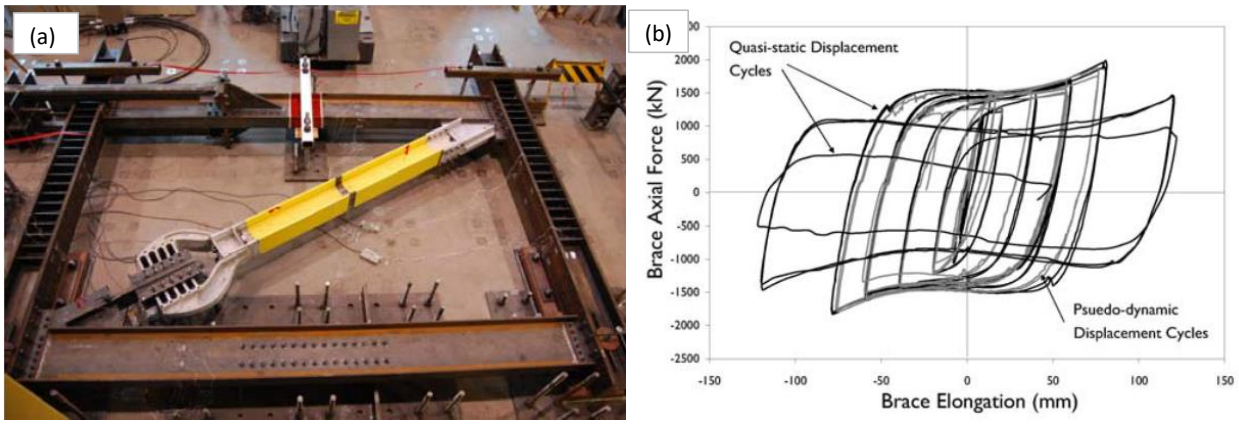

Figure 2-3: (a) A 7m long full-scale test specimen (b) Hysteresis of the full-scale yielding brace (Gray et al. 2012a)

Gray et al. (2014b) carried out time-history analysis on a twelve-story sample building designed with BRBs and Cast Steel Yielding braces. They demonstrated that the performance of both systems is very similar when designed with a similar design philosophy. Very Similar peak and residual inter-story drift ratios and accelerations were observed for both frames subjected to the same ground motions scaled to the DBE spectrum. A similar number of collapses were observed for both systems when subjected to the same ground motions scaled to the MCE spectrum.

2.1.2 Self-centering bracing systems

2.1.2.1 Advantages of self-centering systems

Although the above-mentioned self-centering braces are different in design, they produce an almost similar force-deformation response. Their force-deformation responses are flag-shaped with slight variations in their loading or unloading responses. If properly designed, they can bring back the structures to their original position after an earthquake.

2.1.2.2 Disadvantages of self-centering systems

Flag-shaped hysteresis generates less hysteretic energy dissipation or hysteretic damping compared to bilinear kinematic or isotropic hysteresis typically observed in buckling restraint braces. This low hysteretic damping results in a higher acceleration during earthquakes. Another important feature common to these systems is that they are never fully self-centering; although low, they experience a small amount of residual deformation.

2.2 Some notable self-centering systems

Different types of self-centering bracing systems have been developed by the researchers around the world. Some of these systems are discussed in this section. These smart self-centering bracing systems can recover from significant nonlinear deformation, which sets them apart from traditional bracing systems. Their use can result in insignificant residual interstory drift ratio in buildings. To understand their behavior, some noteworthy self-centering bracing systems are discussed below.

2.2.1 PBSC brace

The piston based self-centering bracing system is a novel invention by Haque and Alam (2014). This system is essentially composed of a piston, shaft and SMA bars/wires. Nickel-titanium-based shape memory alloy bars are used to transfer axial load from the shaft to the connected structure directly or through the sleeve for tension or compression forces respectively. From the detailed solid model based analysis done in ABAQUS (2014), it was found out that the brace has a hysteresis response almost similar to the flag shaped hysteresis (Haque and Alam 2015a), which signifies excellent self-centering capability. Figure 2-4 shows a translucent view of the PBSC bracing system taken from ABAQUS (2014).

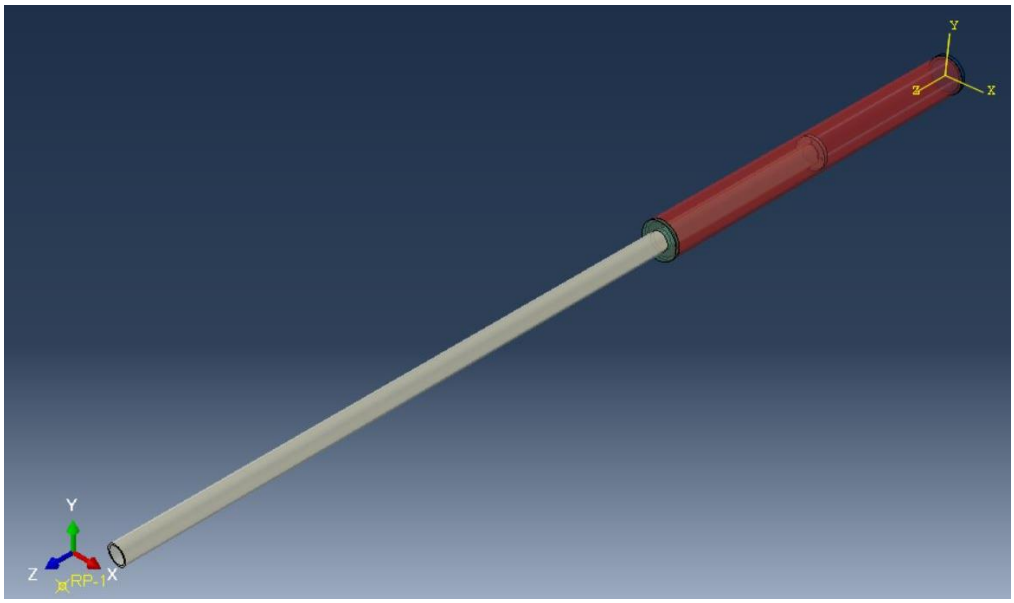

Figure 2-4: A 3D model of the PBSC bracing system

2.2.2 MANSIDE brace

A Nitinol wire based self-centering brace was developed under the Memory Alloys for New Seismic Isolation and Energy Dissipation Devices (MANSIDE) project (Dolce et al. (2001), Dolce and Cardone (2006)). This device employs two sets of wire loops; one set is kept at austenite state, and the other set is prestressed to the martensite state. The austenite wire loop provides re-centering capability while the martensite wire loop provides high-energy dissipation capacity. Figure 2-5(a) shows a cross-section of the device and Figure 2-5(b) shows a 3D view of the system.

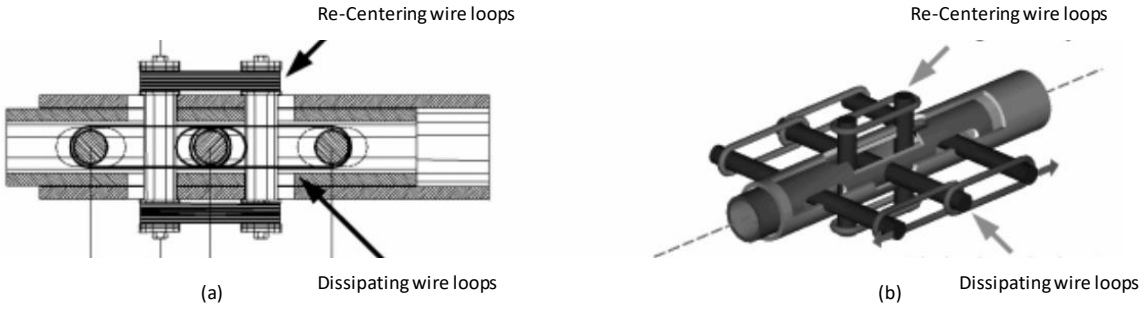

Figure 2-5: MANSIDE brace (a) cross section (b) 3D view (adapted from Dolce et al. (2000))

2.2.3 SCED brace

The self-centering energy dissipative device (SCED), developed by Christopoulos and Tremblay (2005), uses high strength Kevlar/Aramid cables and friction between two concentric steel members to achieve its self-centering and energy dissipation capability respectively. Like MANSIDE brace, the SCED brace also exhibits flag shaped hysteresis response, which translates to good self-centering capability. A cross-section (Figure 2-6(a)) and hysteresis model (Figure 2-6(b)) of the SCED brace is shown below.

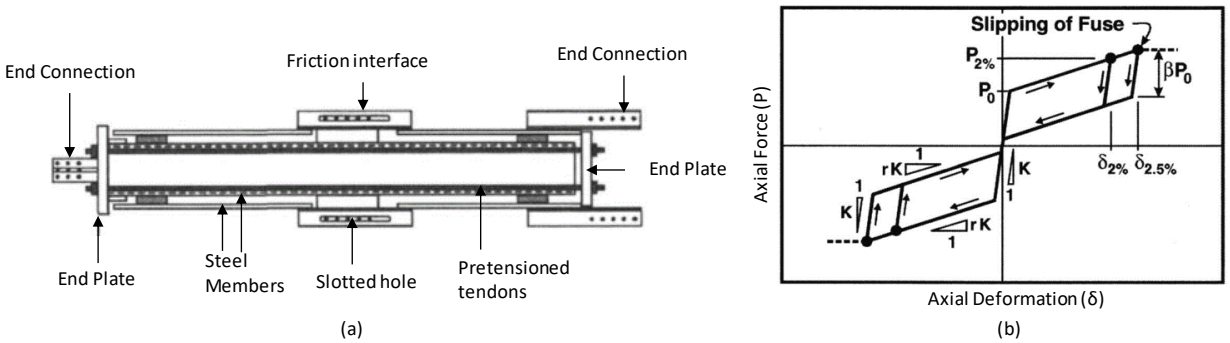

Figure 2-6: (a) SCED brace (b) Hysteresis model for SCED brace (adapted from Christopoulos et al. (2008))

2.2.4 RHDB device

Reusable Hysteretic Damping Brace (RHDB) developed by Zhang and Zhu (2007) is a passive energy dissipation device, in which the core energy-dissipating components are made of superelastic SMA (Nitinol) wires. RHDB has several performance advantages compared to the conventional bracing systems. As per the inventors, RHDB will experience minimal residual drifts due to its self-centring capability and can survive multiple strong earthquakes without repair or replacement. A seismic performance study on RHDB frames was carried out using a non-linear time history analysis of 3 and 6-storey RHDB building frames subjected to two suites of 20 earthquake ground motions. A similar analysis was carried out on BRB frames and the results were

compared. From this analysis, the authors found out that RHDBs not only can significantly reduce the residual drifts but also can control their peak inter-storey drifts during strong earthquakes. They observed that the residual story drifts of the RHDB frames are almost zero in all cases.

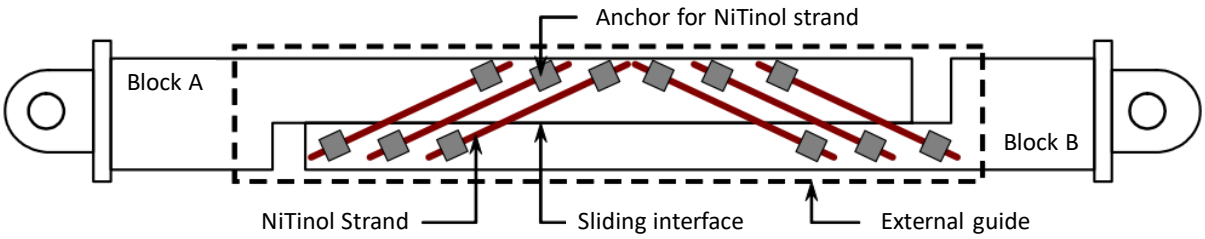

Figure 2-7: Longitudinal cross section of the RHDB brace (adapted from Zhang and Zhu (2007))

2.2.5 SC-BRB

Self-centering buckling restrained brace or SC-BRB developed by Miller et al. (2012) is composed of a typical BRB component and pre-tensioned superelastic nickel-titanium shape memory alloy rods. The system is held inside two concentric hollow steel tubes and a pair of slotted anchorage end plates; a concept introduced by Christopoulos et al. (2008). The BRB provides energy dissipation capacity whereas the shape memory alloy rod provides self-centering and additional energy dissipation capability. The SC-BRB prototype test showed robust performance, and it was found out that even after BRB core fracture, the SC-BRB had significant load carrying capacity due to the redundancy of the SMA rods. The residual deformation of SC-BRB was only half of the maximum brace deformation. The authors also concluded that the SC-BRB provides excellent energy dissipation and equivalent viscous damping capacity.

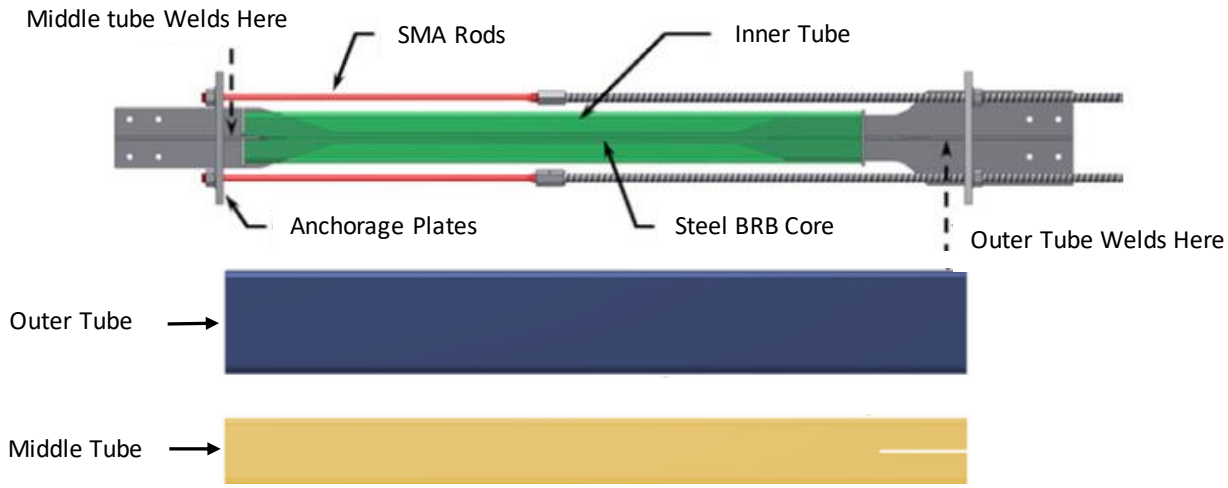

Figure 2-8: Self-centering buckling restraint brace components (adapted from Miller et al. (2012))

2.2.6 Hybrid steel-SMA device

An innovative hybrid steel-SMA device was developed by Yang et al. (2010) to mitigate structural damage induced by seismic events. The device is made of three major components: SMA re-centering wires, two energy absorption struts and two high strength steel tubes for guiding the movement of this device. A three-storied building model was built in OpenSees finite element environment with two different hybrid device installation as follows: Configuration 1: horizontal installation and Configuration 2: inverted "V" brace. Both pushover and nonlinear dynamic time history analyses were carried out to understand its behavior. Based on the analysis results the authors concluded that when designed by their proposed formula the device could re-center while maximizing its energy dissipation. The three-storied building with hybrid brace in configuration 2 showed comparable performance to the BRB frame in terms of peak interstory drift ratio; while configuration 1 showed good performance in terms of both interstory and residual interstory drift ratio.

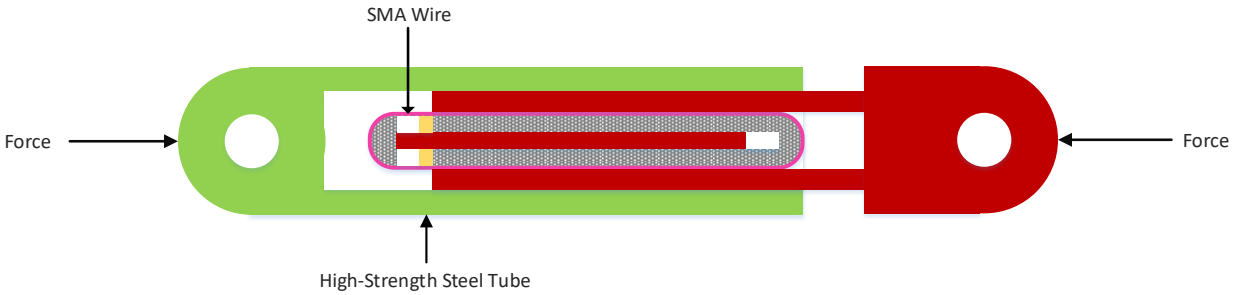

Figure 2-9: Cross-section of the hybrid device (adapted from Yang et al. (2010))

2.3 Other notable studies

Auricchio et al. (2006) carried out a numerical investigation on building frames equipped with Nitinol chevron braces. They compared the performance of these SMA braced structure with that of buckling restrained brace frame structure. To match the yield strength and time periods of the structure, the Nitinol braces were sized to have same yield force and axial stiffness as those of BRBs. Nitinol braces were modeled with a length ranging from 330mm to 453mm whereas the BRBs were in the range of 6000mm. To compensate for these reduced lengths, rigid elements were added to the Nitinol braces to achieve similar lengths. From this analysis, the authors concluded that, although the maximum interstory drift ratio of the SMA braced frames came higher compared to the counterpart, the residual interstory drift ratio was significantly lower. The low residual interstory drift indicates very low repair and rehabilitation cost after an earthquake. However, there is a limitation to this study, as much shorter length SMA braces were used compared to the steel braces. It was found that the SMA braces were elongated close to 30mm, which is around 8% of their lengths. This high elongation pushed SMA braces to martensite range, which resulted in very high axial force. This type of high axial force can severely damage the connected steel components (e.g. connections, beams or columns). Therefore, using shorter length Nitinol bars paired with rigid members may damage the connection. To eliminate this problem, the Nitinol bar length could be calculated based on the expected deformation demand in the braces, and thus their lengths could

be optimized. Furthermore, using longer Nitinol bars could have reduced the stiffness of the braces and decreased the natural frequency of the structure resulting in lower seismic base shear demand.

In another study, the researchers (Moradi et al. 2014) carried out incremental dynamic analysis on SMA (Nitinol) braced frames and compared their results against BRB frames. Similar to the previous investigation (Auricchio et al. 2006), they also used shorter Nitinol braces and added rigid links to compensate for the length reduction. They compared the maximum interstory drift and permanent roof drift ratios between these two types of frames. They found that at design ground motion intensity level both Nitinol and BRB braced frames exhibited maximum interstory drift lower than the design drift limits. They also found that the Nitinol braced frames exhibited more evenly distributed nonlinearity along the height of the buildings compared to BRBs. Furthermore, the authors observed that under severe ground motion excitations, the Nitinol braces are more beneficial. Also, Nitinol braced frames were found to experience significantly lower permanent roof drift compared to BRB braced frames.

Another group of researchers (Hu et al. 2013) carried out a similar comparative investigation between BRB frames and buckling restrained Nitinol braced frames. They observed that if Nitinol is used at the end of BRBs, the hysteresis of the BRBs become more flag shaped and enables them to re-center after load removal. However, this combination does not ensure full self-centering. Similar to the previous studies, they also found excellent residual interstory drift reduction while using Nitinol in buckling restrained braces.

In order to fully understand the mechanism of self-centering bracing systems made with Nitinol alloy, it is of utmost importance to thoroughly understand this material behavior under cyclic

loading. Therefore, the next section peeks into the properties and load-deformation behavior of this material in detail.

2.4 Shape memory alloy

Materials that can undergo phase transitions have received tremendous attention in the scientific community. This type of behavior has innovative applications in both medical science and engineering. The most notable example of such materials is shape memory alloy; specifically, the Nickel Titanium based one. This unique material although discovered in 1960's has seen very little or no use in the construction industry because of the high production cost, lack of understanding of their thermo-mechanical processing and very little knowledge for predicting their behavior. Nitinol has only seen some functional use in the last 30 years in biomedical, commercial and aerospace industries. The reason for this increased use can be attributed to a significant reduction in price and improvement in the quality and reliability of the product (DesRoches et al. 2004).

Also, in recent times many structural systems have been developed using SMA wires and bars (Alam et al. 2007). SMA wires have been used mostly for steel braces, for example in MANSIDE braces (Dolce et al. 2000), in RHDB braces (Zhang and Zhu 2007), in structural vibration control (Ma et al. 2004), in pre-strained wire braces (Lafortune et al. 2007) and in seismic isolation devices (Dezfuli et al. 2013). Nitinol bars have been used for reinforced concrete bridge piers (Billah and Alam 2015), bridge restrainers (Alam et al. 2012), and concrete beam-column joints (Youssef et al. 2008). There has been no use of SMA bars in structural braces so far. Only analytical investigation using SMA structural elements at brace-ends has been carried out by some researchers. A study on special concentrically braced frames made of Nitinol showed that SMA

braces are effective in reducing both maximum and residual interstory drifts under seismic loading (McCormick et al. 2007). A similar study was carried out on diagonal, split x and chevron brace and the performance of SMA braced structures were compared against BRB braced frames; and it was found out that SMA braces are effective in reducing peak interstory and residual roof drift ratio under seismic loading (Asgarian and Moradi 2011).

2.4.1 Microstructure of Nitinol

There are two basic atomic phases of Nickel-Titanium alloy; they are called the austenite and the martensite phase. Nitinol alloy can transform from one of these phases to the other under the application of pressure or heat, without any form of permanent damage. A three-dimensional diagram of these phases is shown in Figure 2-10. Austenite has a simple cubic structure (B_2 body-centered atomic structure). This phase is stable at high temperature and low stress. On the other hand, martensite phase has a body-centered tetragonal crystal structure (B_{19} rhombic geometry); which is stable at low temperature and high stresses.

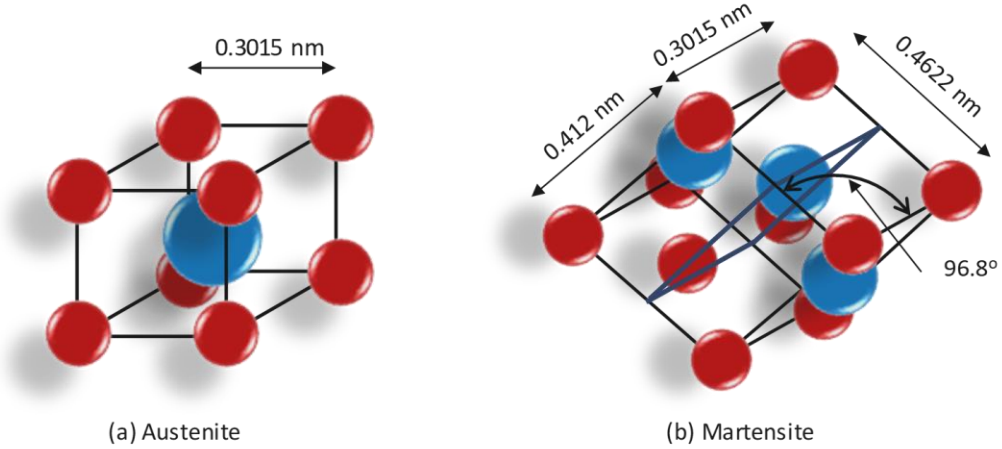

Figure 2-10: Three-dimensional microstructure of the Nickel-Titanium alloy (a) Austenite (b) Martensite

A two-dimensional representation of the austenite and martensite phase is shown in Figure 2-11. martensite can exist in two different forms; twin variant (Figure 2-11(b)) or a single favored variant (Figure 2-11(c)) (Wayman and Duerig 1990). These two variants are crucial in shape memory effect, which will be explained in the next section. More detail about the crystallography and microstructure of nickel-titanium alloy can be found in the literature (Duerig et al. 2013; Gall et al. 1999; Hane and Shield 1999; Otsuka and Shimizu 1986; Otsuka and Wayman 1998; Perkins 1981; Tadaki et al. 1988).

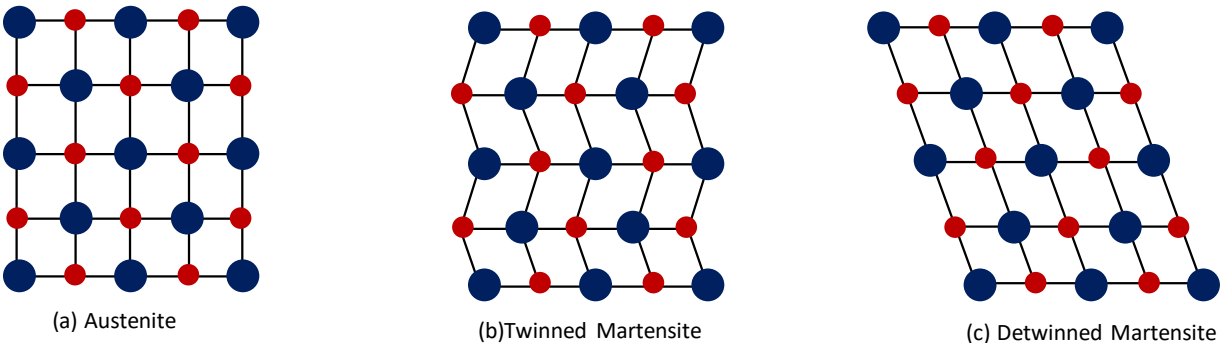

Figure 2-11: Two-dimensional microstructural of Nitinol in (a) Austenite (b) Twinned martensite and (c) Detwinned martensite phase (adapted from Speicher (2009))

The Nitinol based shape-memory alloy has two important properties. One of them is the shape memory effect, and the other one is known as the superelasticity. These two properties are briefly discussed below. More detailed explanation is given in the mechanism section.

2.4.2 Shape-memory effect

Typically, at a low temperature (below M_f as shown in Figure 2-12) if the shape memory alloy in twinned martensite phase is stressed/strained beyond yield, significant nonlinear deformation occurs (Up to 10%-15%), and the shape memory alloy goes to the detwinned martensite phase. However, upon heating beyond a certain temperature (Above A_f as shown in Figure 2-12), the alloy transforms to austenite state and recovers all plastic deformation (comes back to its original shape).

After cooling, the alloy transforms to twinned martensite phase without any residual deformation; which is known as the shape memory effect and is illustrated using green arrowed cycle in Figure 2-12.

2.4.3 Superelasticity

Above a certain high temperature (Above A_f in Figure 2-12), after a mechanical loading resulting in substantial plastic deformation (Up to 10%-15% strain), the alloy recovers all plastic deformations and comes back to the original shape with almost no residual deformation instantly after the removal of the load. This loading-unloading path results in hysteretic energy dissipation. This effect is known as superelasticity. The effect is shown using blue cyclic arrows in Figure 2-12. The phase transformation temperatures (A_s, A_f, M_s, and M_f) are explained in Figure 2-13.

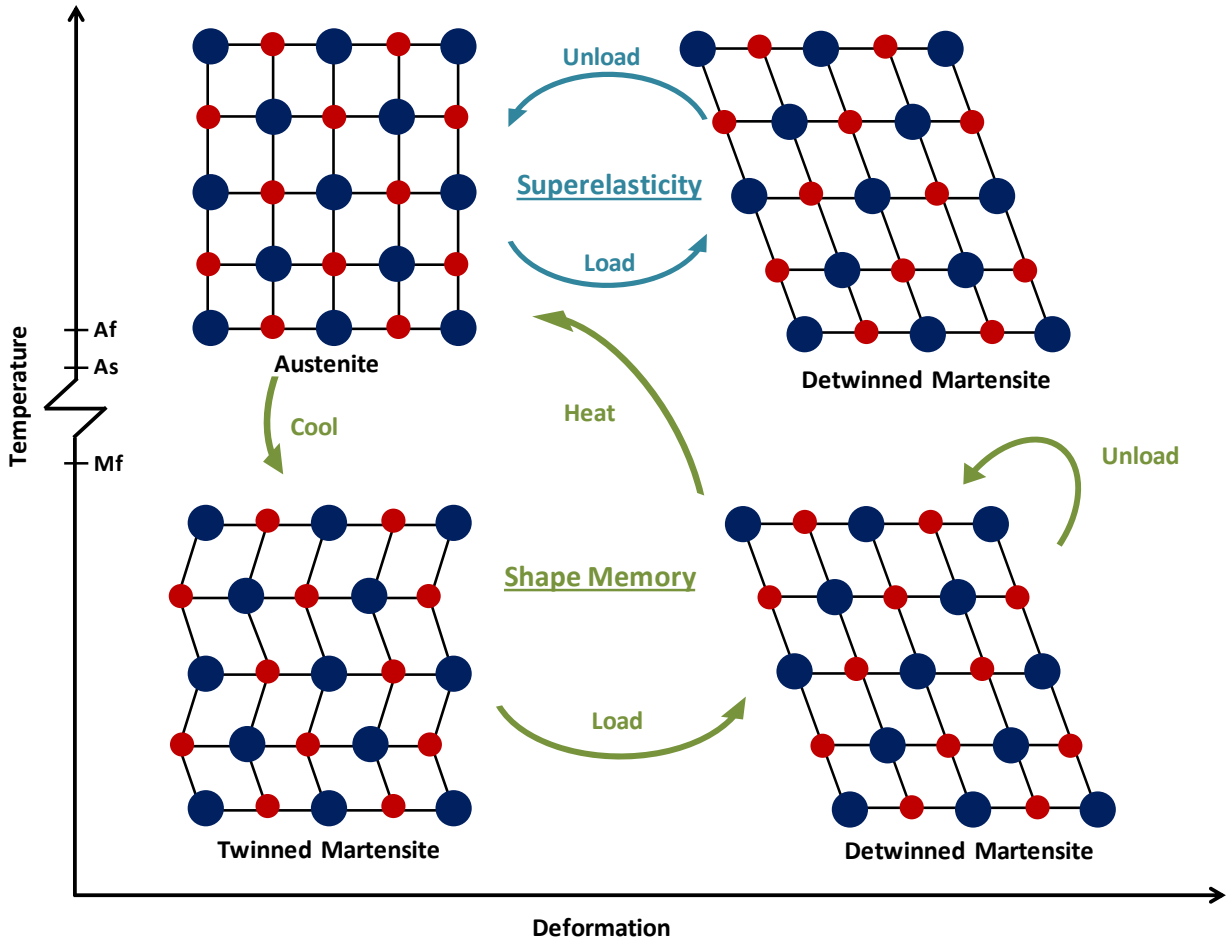

Figure 2-12: Two-dimensional microstructure of Nitinol during superelastic and shape memory effect (adapted from Speicher (2009))

2.4.4 Mechanism

According to Khachaturyan (1983) and Wayman (1964), both of these behaviors mentioned above are the result of martensitic transformations; which is a diffusionless, solid-solid transition between an austenite parent phase and martensite product phase. The austenite parent phase is crystallographically more ordered than the martensite phase. For SMA, this transformation is reversible and in some cases rate-dependent as well.

The thermo-mechanical behavior of SMA as a function of strain, temperature, and stress is summarized in Figure 2-13. SMA exhibits the shape memory effect below the martensite finish

temperature, M_f. If the SMA is heated beyond austenite finish temperature (A_f), any deformation experienced during the martensite phase is instantly recovered. The SMA is in its austenite phase at a temperature above A_f. At this phase stress-induced martensite is formed upon loading. However, upon unloading, the material returns to austenite phase at a lower stress level, thus causing the superelastic behavior. This ensuing nonlinear stress–strain relationship results in a hysteresis. Furthermore, the SMA undergoes ordinary plastic deformation with much higher strength at a higher temperature above M_d (DesRoches et al. 2004).

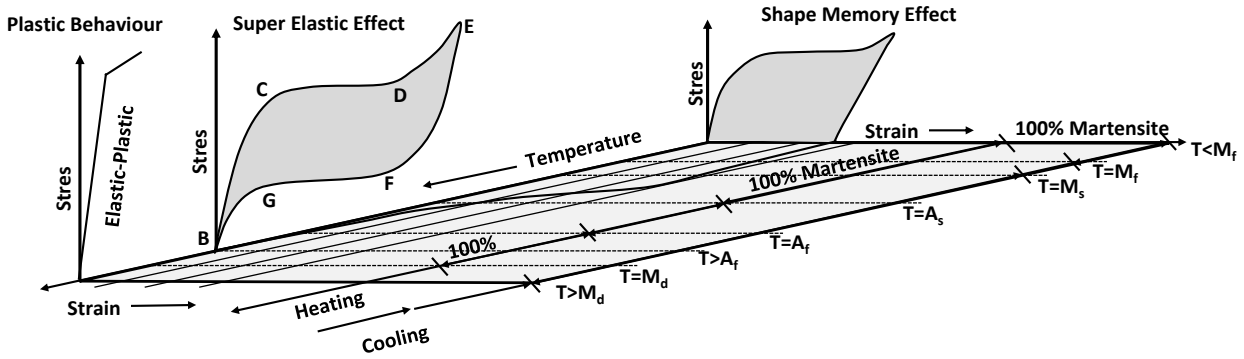

Figure 2-13: 3D stress–strain temperature diagram depicting deformation and shape memory behavior of Nitinol-based shape memory alloy (adapted from Alam et al. (2007))

The change in microstructure under loading and unloading at a constant temperature is shown in a two-dimensional plot in Figure 2-14. Figure 2-14(a) shows the stress-strain diagram for superelastic effect. This figure depicts how austenite phase transforms to detwinned martensite phase under the application of stress and thus accommodate the strain; creating a loading plateau. At the end of the loading plateau, the alloy fully transforms to the stress induced detwinned martensite phase. This figure is true for temperature above austenite finish temperature (A_f). Upon unloading the stress-strain curve comes back to the origin, thus recovering all plastic deformations. The resulting hysteresis gives Nitinol its energy dissipation capacity. However, if the Nitinol alloy is continued to be stressed beyond the martensite phase, slip planes will form (like common

metals), and the alloy will experience permanent plastic deformation from which it will not be able to recover to its original shape.

Figure 2-14(b) shows the stress-strain diagram of Nitinol SMA below martensite finish temperature (M_f). At this temperature, application of stress changes the twinned martensite to detwinned martensite. Upon unloading the alloy experiences significant plastic strain as shown in the figure. However, this plastic strain can be recovered by heating the alloy above austenite finish temperature (A_f) thus exhibiting the shape memory effect.

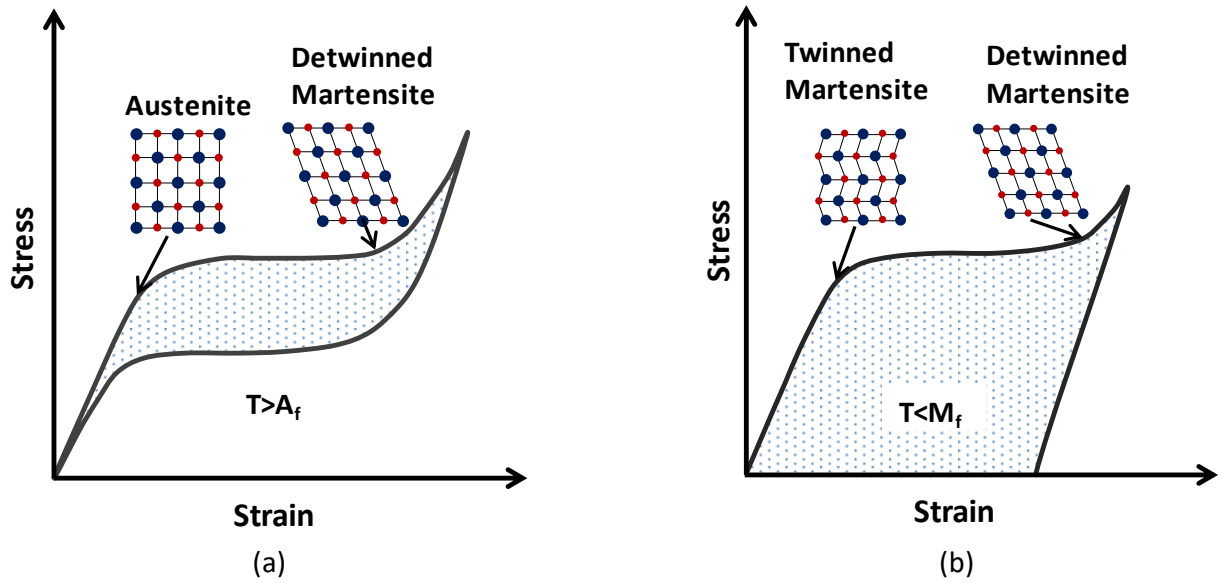

Figure 2-14: 2D stress–strain behavior of (a)Superelastic SMA (b)Shape memory SMA (adapted from Speicher (2009))

2.4.5 SMA bar behavior

Quasi-static and dynamic cyclic loading tests which are typically observed during earthquakes were carried out on SMA wires and large diameter bars (DesRoches et al. 2004). The diameters of the specimens tested include 1.8mm wire and 7.1mm, 12.7mm and 25.4mm bars. The authors observed that contrary to popular belief, SMA bars also show outstanding re-centering capacity (Figure 2-15). The residual strain observed for the test specimens were on an average 0.65% for

all the specimens where the maximum strain was 6%. The only disadvantage of using SMA bars over wires is its lower hysteretic energy dissipation capacity. The equivalent viscous damping represented by the fatness of the hysteresis loops (Figure 2-15) was found to vary from 2% for the 12.7mm bar to a maximum of 7.6% for the 1.8mm wire.

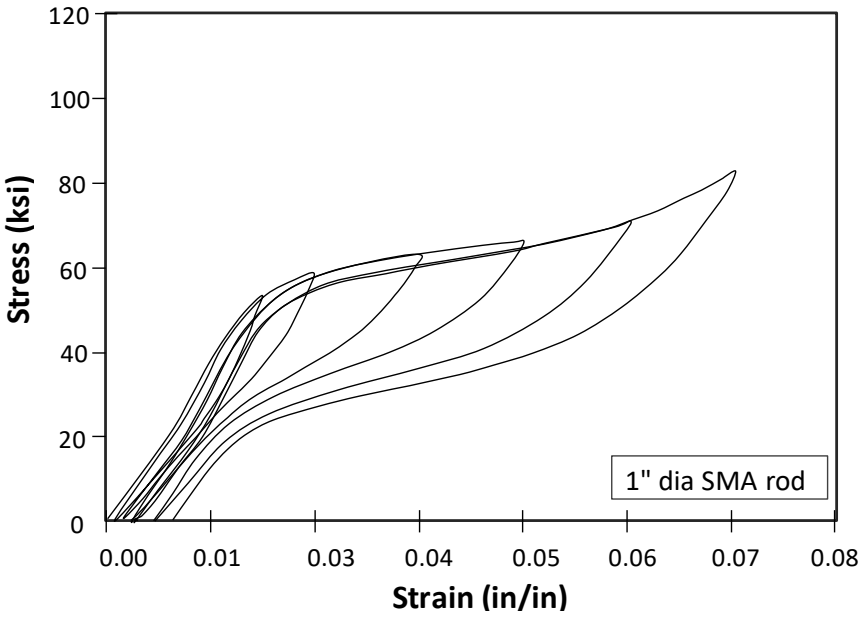

Figure 2-15: Stress–strain plot for 25.4 mm diameter nitinol SMA bar subjected to quasi-static cyclic loading (adapted from DesRoches et al. (2004)).

CHAPTER 3: HYSTERETIC BEHAVIOR OF A PISTON BASED SELF-CENTERING BRACING SYSTEM

3.1 General

This chapter presents the conceptual design and development process of the piston based self-centering bracing system. In the first step, the concept of the system with different SMA configuration is proposed and depicted using two-dimensional sketches. The possible usage of the brace in various types of structural systems is proposed. The predicted mechanism of the brace is described under cyclic loading conditions. A brief description of the brace construction method is also presented. Finally, a three-dimensional continuum finite element model is developed. The model is used for carrying out quasi-static time history analysis to understand the cyclic performance of the brace. The hysteretic response of this bracing system is compared against a similar system made with steel energy dissipative elements. The advantages and disadvantages of the SMA based system compared the steel tie based system is discussed. The scope of this chapter is limited to finite element investigation only. No experimental investigation has been carried on the brace prototype.

3.2 PBSC brace design

To resolve the shortcomings of the current self-centering bracing systems discussed in the previous chapter, the authors have developed a novel system known as the Piston Based Self-Centering Bracing System (PBSC brace) (Haque and Alam 2014). The PBSC bracing system is designed to have an excellent self-centering capability, moderate damping, and easy constructability. Furthermore, the brace will be buckling resistant under earthquake loading.

The PBSC brace is made of two concentric steel members connected in a cylinder-piston arrangement as shown in Figure 3-1. The concentric steel members could be made of circular, rectangular or any other standard structural sections. The piston in this assembly is designed to act as the shaft and the sleeve/cylinder is intended to house the Nitinol SMA bars, steel plates, and the locks/nuts. Two configurations are shown in Figure 3-1; in configuration 1 Nitinol bars are continuous through the piston plate and in configuration two the bars are discontinuous. The configuration one can incorporate twice the number of Nitinol bars compared to configuration 2; making it capable of carrying twice the load relative to the study published earlier (Haque and Alam 2015a).

Figure 3-1 shows the internal details of the PBSC brace. In this arrangement, the shaft has a smaller cross section compared to the sleeve for ease of installation inside the sleeve. Two sets of equal length Nitinol SMA bars are connected from the piston plate to the front and back caps using couplers or threaded nuts. The diameter of the orifices (openings) on the front cap, back cap, and the piston plate are made slightly larger than the SMA bar diameter. This is done to allow unrestrained rotational movement of the Nitinol tie bars during loading. This also eliminates the possibility of bending moment generation in ties. Moreover, in the case of plate rotation/bending, the ties mostly remain unaffected and straight. Furthermore, the piston plate is also made slightly smaller than the sleeve to reduce excessive friction during sliding movement. This size difference also reduces the possibility of sleeve inner surface damage from piston plate bending. The brace shaft and the sleeve are made of the same material, and the cross-sectional area of the sleeve is designed to be higher than that of the brace shaft; this is done to reduce the possibility of global or local buckling of the sleeve before the brace shaft. Similarly, the Nitinol SMA bars are designed

to have lower force carrying capacity than the brace shaft. This ensures that the SMA bars are the weakest link in the system and they go to nonlinear range before the other components

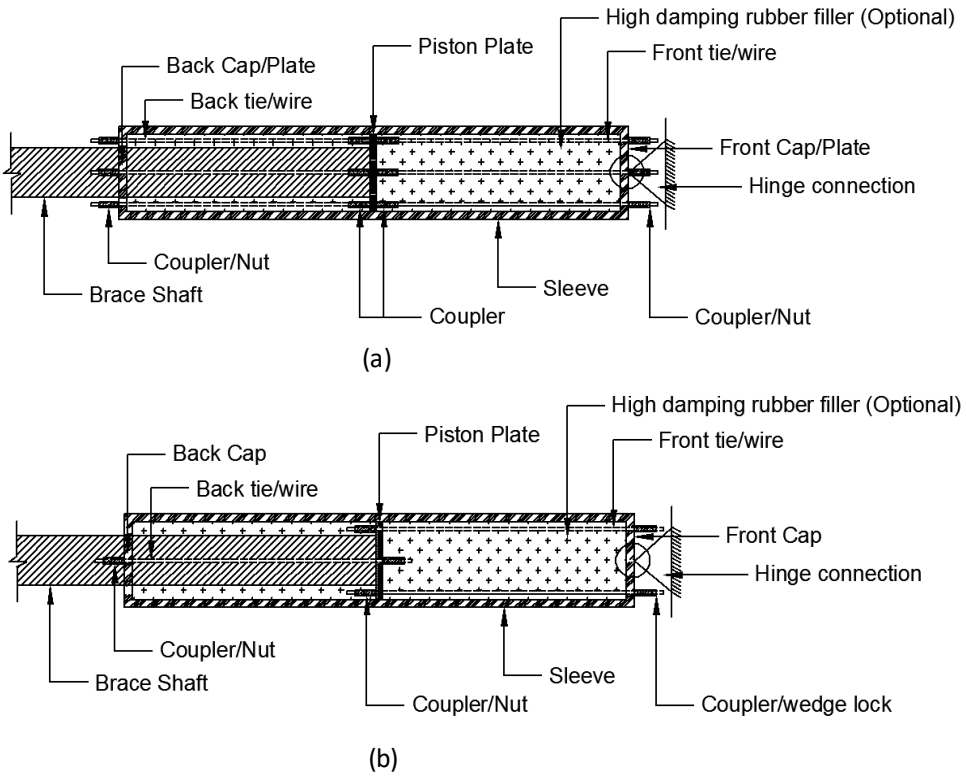

Figure 3-1: Internal details of the PBSC brace with optional high damping rubber filler (a) Configuration 1 and (b) Configuration 2

The PBSC bracing system is designed to work in any standard configuration such as Single/Chevron/V/X etc. A possible arrangement in a building frame is shown in Figure 3-2. In general, the design tensile and compressive load carrying capacity of the brace should be equal. This can be achieved by using the same cross-sectional area for both front and back ties. Furthermore, in order to have equal deformation capacity under compressive and tensile load, both front and back ties should be of equal lengths. The space inside the sleeve could be filled with high damping rubber. This rubber should be cut in a way to accommodate the ties and the brace shaft. This rubber filler could reduce impact energy during the change of loading direction (e.g. seismic

load). The diameter of the rubber filler should be smaller than the sleeve diameter to accommodate for the transverse bulging of the rubber filler during compressive deformation. The required gap can be calculated using the Poisson's ratio and the maximum design axial deformation of the rubber filler. The end plates should be designed with enough thickness to eliminate plate deformation due to forces coming from the Nitinol bars.

The Nitinol bars should be connected to the front and black cap/plates in a way that the bars can move out without any resistance; however, they should be prevented from moving inside the sleeve by couplers/nuts. This ensures that during tensile loading, only front ties get locked with the front cap and the back ties get structurally disconnected from the back cap and vice versa. By this mechanism, the front and back ties are alternately loaded during brace tensile and compressive load cycles and the ties only carry a tensile load.

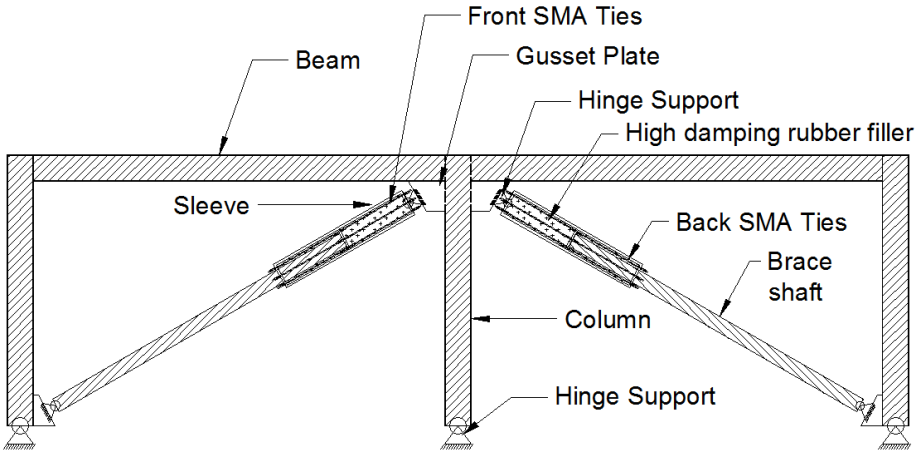

Figure 3-2: The use of the piston-based self-centering bracing system in a steel frame.

3.3 Materials

For this study, it is assumed that the brace shaft, sleeve, piston plate and front/back caps are made of structural steel. The following material properties were used for modeling steel in the finite element environment: modulus of elasticity of steel (200 GPa), Poisson's ration (0.3), yield

stress (345 MPa), ultimate stress (508 MPa) and ultimate strain (15.4%). As the finite element analysis package ABAQUS (2014) requires material properties data to be entered as true stress vs. true strain, all of the material properties data were input as such. The density of steel was set to 7850kg/m^3.

Various types of shape memory alloys have been developed over the past decades; such as Cu–Zn–Al–Mn–Zr, Ag–Cd, Au–Cd, Cu–Al–Ni, Cu–Zn, Cu–Zn–Al, Fe–Pd, , Cu–Al–Be, Ti–Ni–Cu, Ti–Ni–Hf, Fe–Mn, Mn–Cu, Ni–Ti–Fe, and Ni–Ti (Otsuka and Wayman 1999). However, for this study, only Ni-Ti based shape memory was chosen as the tie bar material for the following reasons: a rich collection of experimental results, availability of material hysteresis models, and ease of availability of the material. However, other SMA alloys could be used instead of Nitinol-based one if test results show similar or superior performance.

The material properties used for NiTinol are as follows: density (6500kg/m^3), modulus of elasticity (62.5 GPa), Poisson's ratio (0.33), austenite to martensite starting stress (400 MPa), austenite to martensite finishing stress (510 MPa), martensite to austenite starting stress (370 MPa) and martensite to austenite finishing stress (130 MPa) (Youssef et al. 2008). The superelastic plateau strain ($\mathcal{E}_L$) was set to 6% as shown using a dashed arrow in Figure 3-3. This material property data is also presented in Table A-1.

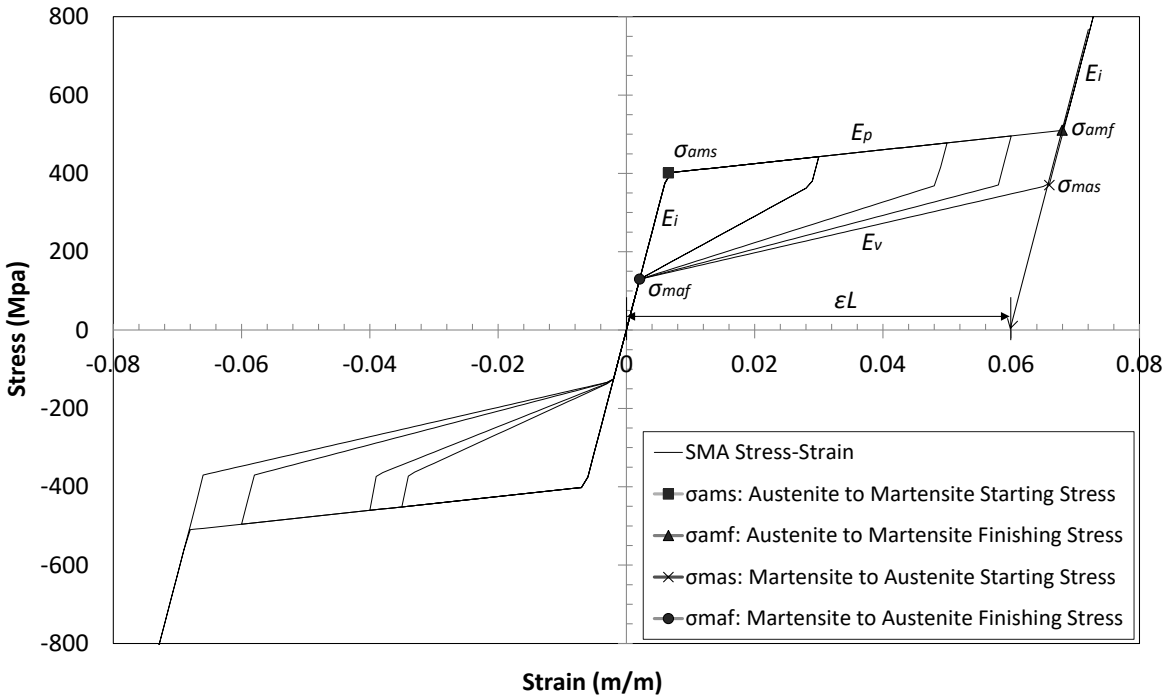

Figure 3-3: Stress–strain diagram of SE SMA used in the finite element analysis.

3.4 Brace mechanism

During compressive loading, when the stress in the back SMA ties/bars exceeds the austenite to martensite starting stress (Figure 3-3), their stiffness decreases and the bars deform significantly. This low tie bar stiffness reduces the global stiffness of the brace. Since the shaft, the SMA bars, and the sleeve are connected in series, the equivalent stiffness of the bracing system will not exceed the lowest stiffness of these three elements. This low stiffness results in less force sharing from the connected structure and thus limits the maximum load on the brace. This mechanism ensures that the buckling load is never reached for the shaft. This assumption remains valid if the shaft is designed for an axial load larger than the austenite to martensite finishing force of the SMA bars. To understand this mechanism clearly, Figure 3-4(a) and Figure 3-4(b) depict a translucent and a longitudinal view of the PBSC bracing system without the sleeve, respectively.

Similarly, during tensile loading, the shaft pulls the front ties while the front ties get locked with the front plate/cap by the couplers/nuts (as shown in Figure 3-4(c)). During this part of the loading cycle, the load flows through the following path: brace shaft → piston plate → front ties → front cap → external support. During this loading phase, the back ties get disconnected from the sleeve back cap, and they can freely move out of the sleeve by approximately the amount of tensile deformation experienced by the front ties. In this way, the back ties do not participate in the load transfer mechanism during tensile loading. During compressive loading, the piston plate pulls the back ties, and they lock with the back cap and thus transfer the load to the sleeve as compression (as shown in Figure 3-4(d)). So, the load path in compression is brace shaft → piston plate → back ties → back cap → sleeve →external support. During compressive loading, the front ties get disconnected from the sleeve front cap, and they can freely move out of the sleeve by approximately the amount of tensile deformation experienced by the back ties. This way the front ties never participate during the compressive loading phase. The connection between the ties and the front/end caps/plates are made in a way that they only lock during inward movement of the ties. However, the tie bars can move freely through the openings when ties move outward. The main objective of this mechanism is that the ties are never under compressive loading at any point in time during static or cyclic loading. This way buckling of ties is always prevented. To make sure that the above mechanism works, only axial load needs to be resisted by the PBSC bracing system. Therefore, the connection between the brace and the structure should be designed as pinned or hinged.

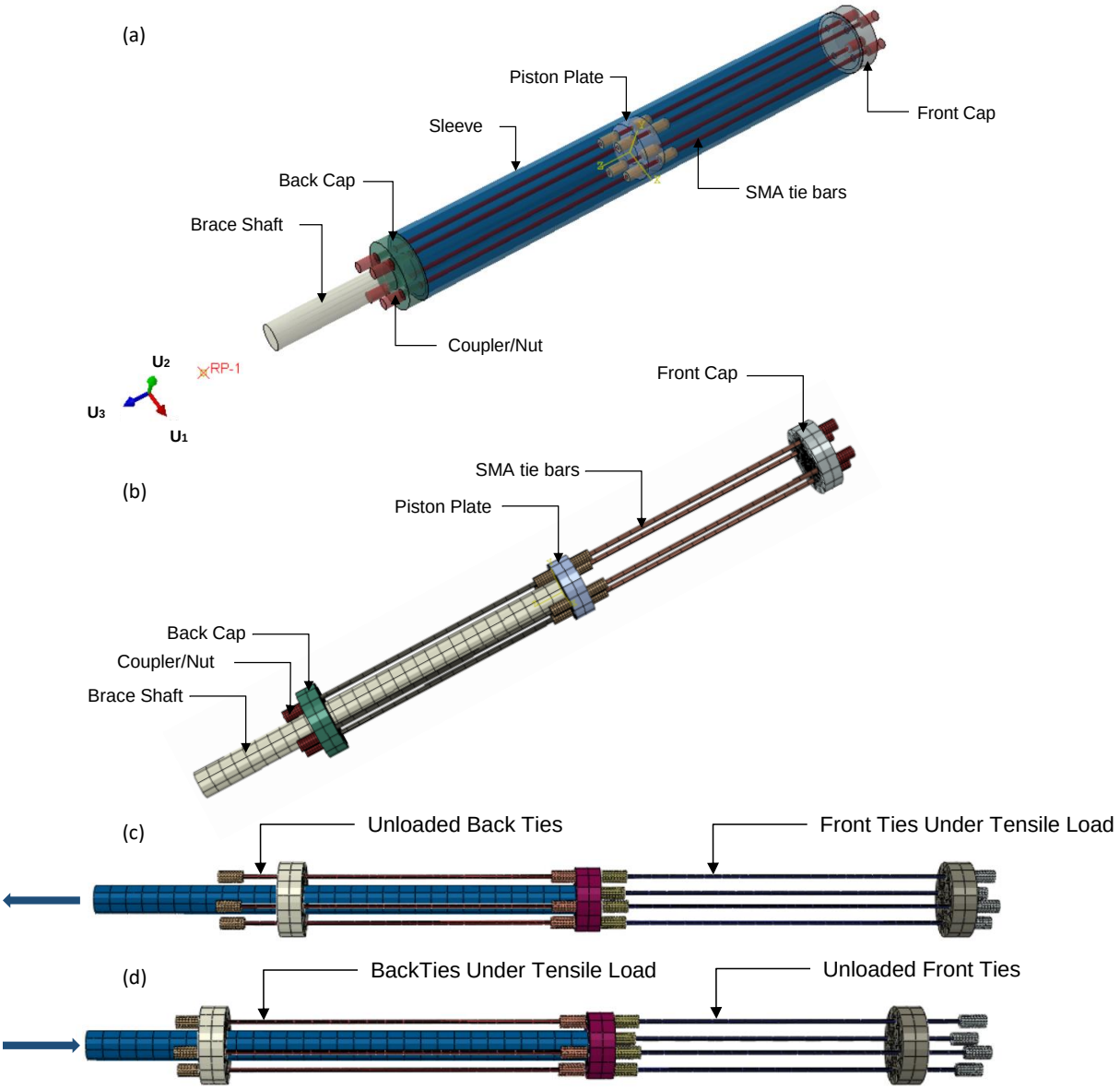

Figure 3-4: (a) Semi-transparent view of the PBSC brace from ABAQUS (2014) (b) Longitudinal profile of the PBSC brace with sleeve hidden from view (c) State of the internal elements during tensile loading (sleeve hidden from view) (d) State of the internal elements during compressive loading (sleeve hidden from view).

3.5 Construction of the brace

To prevent SMA bars from fully entering the sleeve, the ends of the SMA bars needs to be made larger using either threaded nuts, couplers or centerless grinding. The use of nuts will require pre-threading which is easy to do at the ends but not practical for the middle portions (as the nuts

could not be moved there). Therefore, use of nuts will be restricted to configuration 2 (Figure 3-1(b)) only or tie bar ends for configuration 1. A five-step construction method for the PBSC bracing system (configuration 1) is shown in Figure 3-5.

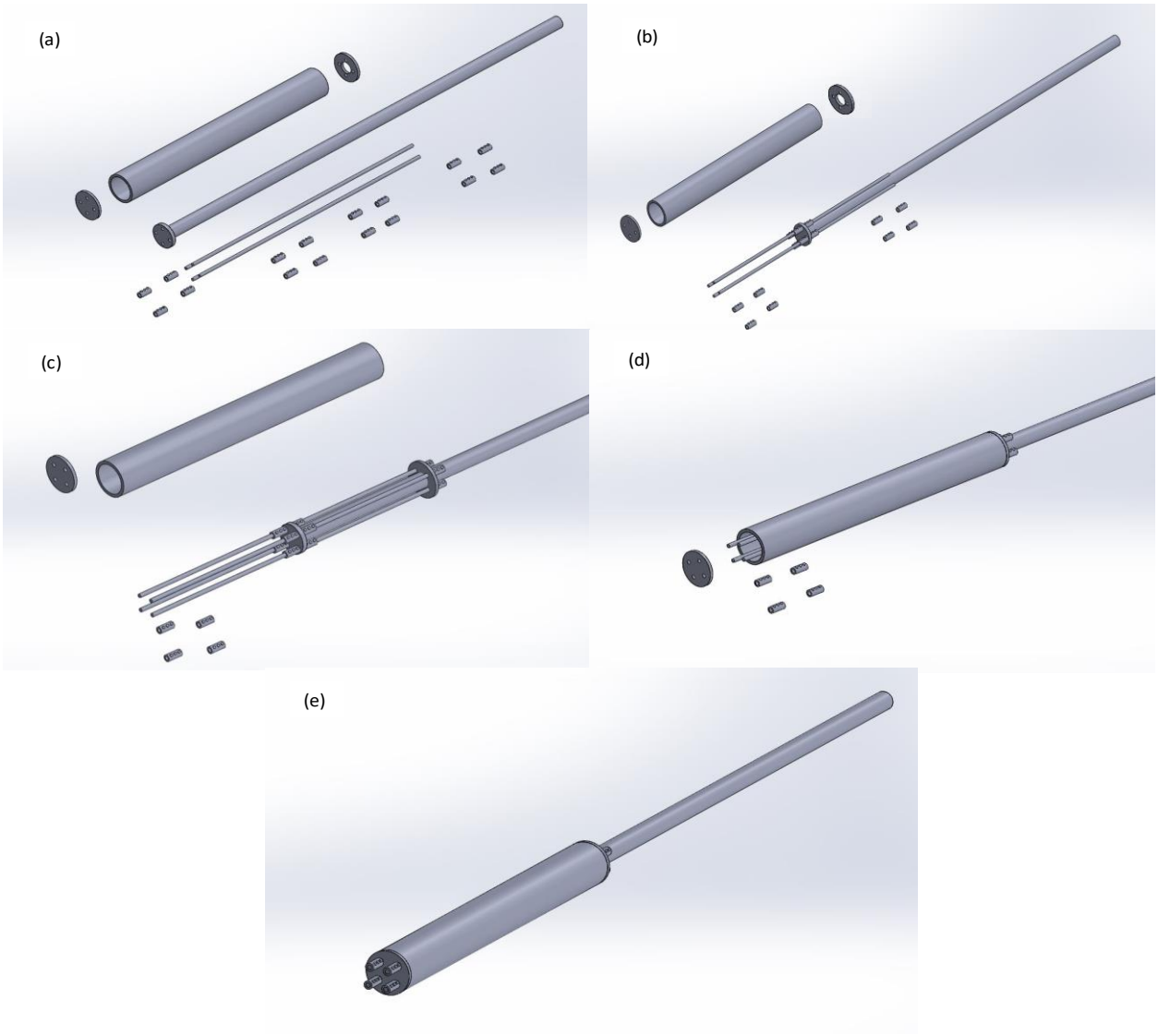

Figure 3-5: Construction of the PBSC Bracing System (a) Individual components (b) attachment of the SMA bars with the piston plate and the couplers (c) attachment of the back plate and the couplers/nuts (d) Attachment of the sleeve (e) attachment of the front plate and the couplers/nuts.

3.6 Finite element model

The finite element model is shown in Figure 3-6. Furthermore, for better understanding, every individual part of the PBSC brace has also been labeled in this figure and Figure 3-4(a). The section is taken at exactly mid-depth to illustrate how the SMA bars pass through front, piston, back plate and the couplers/nuts

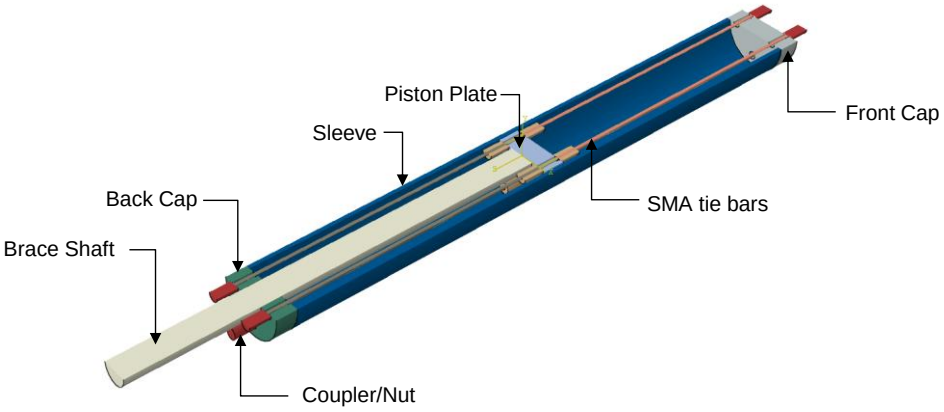

Figure 3-6: Longitudinal section of the PBSC brace.

A transverse cross section of the PBSC brace is shown in Figure 3-7. This figure illustrates the connection between the following elements: piston plate and brace shaft, SMA bars and the couplers/nuts. Adequate gap has been provided between the couplers/nuts and the sleeve. Also, a similar gap is provided between the couplers/nuts and the brace shaft. This gap prevents unwanted friction between the coupler and other brace components in the event of SMA bars and couplers going out of alignment.

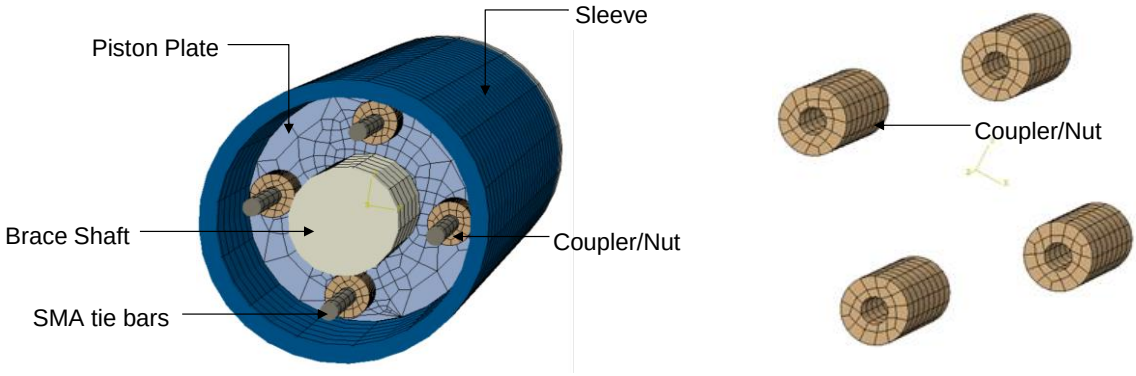

Figure 3-7: (a) Transverse section of the PBSC brace (b) Couplers for connecting SMA bars with piston plate or end caps.

Figure 3-7(b) shows the model of the coupler/nuts used in the finite element environment. A detail coupler/nut model was not constructed to keep the model simple. Therefore, no threads (for nuts) or screws (for couplers) were modeled. A detailed study using threads for nuts or screws for coupler will be carried out in future.

Figure 3-8 shows the back, piston and front plate used for the PBSC brace model utilized in this study. Unlike the other two plates, the back cap/plate has a larger opening at the center to allow shaft movement. The opening is made slightly greater than the brace shaft diameter to accommodate shaft diameter expansion during compressive loading. The required opening diameter is calculated based on maximum allowable compressive strain and Poisson's ratio of the brace shaft material. As the maximum stress in the brace shaft will be kept below the lower of the buckling and yield stress, the strains generated will be below yield and buckling strain. Even if we consider that the yield strain will be smaller than the buckling strain (which is quite uncommon for a slender member), the maximum diameter expansion will be Poisson's ratio times the yield strain, which is very low for structural steel members. For example, for a 345 MPa steel, the yield strain is only 0.15%, and the transverse strain will be 0.05%.

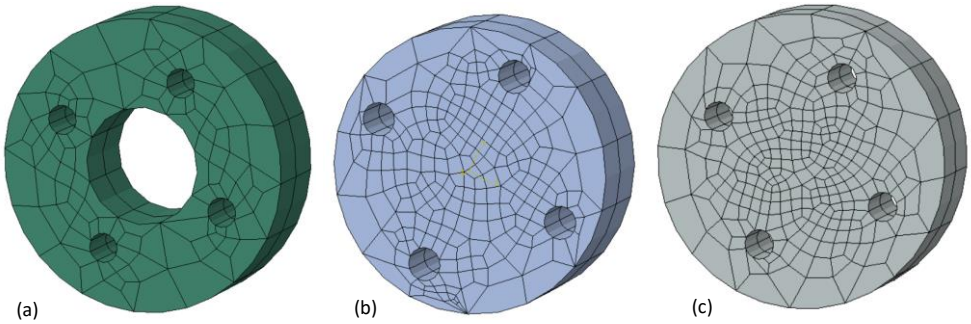

Figure 3-8: (a) Backplate(b) Piston plate and (c) Front plate with openings to accommodate SMA bars and/or brace shaft.

Figure 3-9(a) shows a typical example of the gaps kept between the SMA bars and the plates (Front, back and Piston plate) where the couplers/nuts are excluded to show the plate openings. This gap is kept to prevent SMA bars from bending in case of plate deformation. This also prevents unwanted load transfer (loads other than axial) from the plates to the bars.

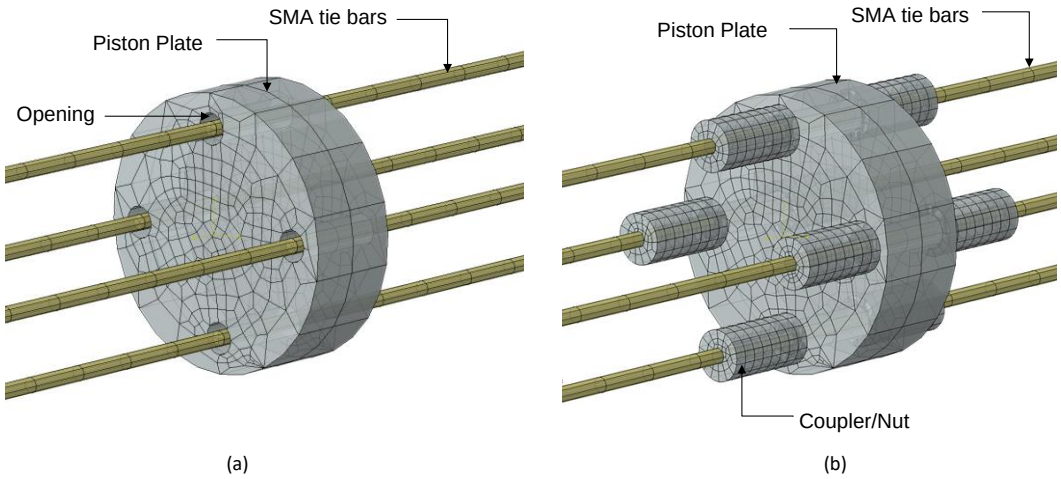

Figure 3-9: (a) Connection details between piston plate and SMA bars (a) nuts/couplers excluded from the face. (b) nuts/couplers included.

Figure 3-9(b) shows the connection between the couplers/nuts and the SMA bars. Here the couplers are connected to the SMA bars using hard contact formulation available in ABAQUS (2014). Hard contact is a pressure overclosure relationship that enforces zero penetration condition (not strict) between the surfaces and any contact pressure can be transmitted between the surfaces

when they are in contact. However, separable contact is created between the couplers/nuts and the piston plate.

3.6.1 Meshing

After the initial construction of the finite element model of PBSC brace, the edges of the part instances were seeded for mesh generation. Seeding was done before the mesh operation to set the approximate element sizes for the mesh. The seeding operation was done using the "seed part instance" tool available in the graphical user interface. Different seed sizes were selected for various parts of the model using the approximate global size option. The seed sizes for the couplers/nuts and SMA bars were made noticeably smaller than the shaft, piston, front, end plates and the sleeve. This size difference was done to ensure better convergence during slave and master contact surface interactions (ABAQUS 2014). The mesh size difference between the coupler/nut (slave) and the piston plate (master) is shown in Figure 3-9(b). It can be observed that the coupler/nut mesh is made denser compared to the piston plate.

An extremely dense mesh can produce highly accurate results. However, very dense mesh requires a significant amount of computer memory and exponentially high computational power. Otherwise, it could take very long time to solve these finite element problems. Therefore, it is necessary to optimize mesh size to achieve a balance between accuracy and analysis runtime. A trial and error based mesh sensitivity analysis was carried out to find out the optimum size of the mesh required for individual elements of the brace. The goal of this analysis was to maximize the mesh size without sacrificing accuracy. The full PBSC brace finite element model consists a total number of 40381 nodes, 6886 quadratic hexahedron elements (C3D20R). C3D20R is a general purpose 20-node quadratic brick element with reduced integration option. This element has 2x2x2

integration point and these are about one-quarter of the typical element size away from the element boundary. A trilinear extrapolation is done for converting values between integration points and nodes (Dhondt 2014). C3D20R elements require significantly more computational time compared to linear elements like C3D8R. For this reason, the meshing of the PBSC brace model was carefully optimized to provide a high degree of accuracy without causing too much increase in computation time.

3.6.2 Contact surfaces

Three different contact interaction properties were defined for the brace model. These were defined under the following categories: (1) friction sliding, (2) frictionless sliding, and (3) non-separable (welded) contact. These contact surface formulations are described below in details.

1. Friction sliding: The friction sliding contact surface has a penalty friction formulation with isotropic directionality in the tangential direction. The friction coefficient in this direction was taken 0.51. The friction coefficient value was chosen assuming grit blasted A36 steel (Kulak et al. 1987). The normal behavior was defined as hard contact where separation after the contact was allowed.
2. Frictionless sliding: For the frictionless sliding interaction, tangential behavior was set as frictionless and the normal behavior was kept the same as the "sliding with friction" contact.
3. Non-separable (welded) contact: The non-separable contact interaction was defined as follows, Tangential behavior was set to rough, and the normal behavior was set to hard contact without separation after contact.

The following interactions were defined between the PBSC brace components. Sliding with friction contact was defined between the following surface pairs: cylinder inner surface to SMA bar surfaces, shaft outer surface to back tie surfaces, back/front/ piston plate holes to SMA bars, shaft outer surface to coupler/nut surfaces, back cap to back couplers/nuts, front cap to front couplers/nuts, piston plate to middle couplers. Frictionless sliding contact was defined between the following surface pairs: middle couplers to cylinder inner, piston plate to cylinder inner, shaft to back cap inner and finally non-separable (welded) contact was defined between these pairs: back ties' ends to back couplers/nuts, front ties' ends to front couplers/nuts, cylinder to back cap, cylinder to front cap, shaft to piston plate, middle couplers to front and back ties. Frictionless contact was assumed between the cylinder inner surface and other components as Teflon coating will be used on the cylinder inner surface to allow free movement. No contact was defined between the shaft outer surface and the cylinder/sleeve inner surface as there is no chance of these two surfaces coming into contact. Although ignored in this analysis, friction can develop during the sliding mechanism if the axis of the shaft rotates with respect to the cylinder/sleeve. In this case, the piston plate might encounter the sleeve inner surface during cyclic movement. Depending upon the friction coefficient between these two metal surfaces there can be some friction force development. However, in the current ABAQUS finite element model this friction force is neglected based on the following two assumptions: (a) The shaft will not rotate enough to generate a significant normal force due to guidance through the thick back plate. Therefore, if the normal force is small, friction will be negligible. (b) Teflon coating on the sleeve/cylinder inner surface and the piston plate will reduce friction significantly. Furthermore, a low friction force will be beneficial in dissipating some earthquake energy; however, if the friction force is too large, it might damage the cylinder, piston plate or the shaft.

For the interacting contact surfaces, small and finite sliding formulation was defined based on the anticipated movement between the surfaces. Small sliding was defined for non-separable contacts, and finite sliding was defined for the rest (frictionless sliding and sliding with friction). Surface to surface discretization method was used for all interactions. Furthermore, no surface smoothing or slave adjustment was done for any of these interactions.

3.6.3 Boundary conditions and loading

Three boundary conditions were defined for the PBSC brace model in the finite element environment (ABAQUS 2014). The boundary conditions are as follows: Pinned for the front cap, displacement restrained for shaft free end (normal surface close to reference point 1 (*RP-1) point in Figure 3-4(a)) and displacement for the reference point (Figure 3-10). The front cap of the PBSC brace was restrained in three translational directions (U1=U2=U3=0). Here, U3 is the brace axial z direction and U1 and U2 are the two transverse x and y directions at 90 degrees apart (Figure 3-4(a)); this ensured that the front end of the brace remained in a fixed location. As the C3D20R solid elements do not have rotational degrees of freedom, no rotational restraint was applied. Secondly, the free end of the shaft was also restrained in two transverse directions (U1=U2=0), but the axial U3 direction was kept free to allow movement in the axial direction. A reference point (*RP-1) was created to represent the entire free end surface of the shaft which is shown in Figure 3-4(a). A constraint was defined between the reference point and the shaft end surface of the brace model so that any movement of the reference point is translated into an equal displacement for the brace shaft end. Later, a displacement boundary condition was defined for this reference point. The boundary condition for this reference point was set as follows: U1=U2=0 and U3=1.

Figure 3-10: Boundary conditions of the PBSC brace model in ABAQUS (2014).

3.7 Analysis and results

Four finite element models of the PBSC bracing systems were built in ABAQUS (2014). The length of the PBSC device (Sleeve length) was chosen to be 2m. The full shaft was not modeled for this analysis based on the assumption that the shaft will be in the linear range of response during the load cycles and the elastic deformation of the shaft will be insignificant compared to the nonlinear deformation of the PBSC device. The SMA bars are only allowed to go into the nonlinear range in this system to prevent nonlinear deformation in other components. Hence, studying the cyclic behavior of the PBSC brace device with a short part of the brace shaft is adequate in understanding the brace behavior. Besides, for retrofit works, the brace device with a short brace shaft will be manufactured, and then they will be connected to the existing braces. Furthermore, during frame analysis using the PBSC bracing system, the elastic shaft deformation will be calculated and will be added to the PBSC device deformation in finite element analysis software.

To eliminate the brace shaft deformation, a very rigid steel section has been used for the brace shaft. The section is made of solid circular steel with 96mm diameter and having a length of 1.5m. The ties were modeled as solid circular sections with a length of 2m. The Bar diameters chosen for this study are as follows: 10mm, 12mm, 16mm, and 20mm. These four different diameters were used for four cyclic analyses. The sleeve is modeled as a hollow circular section with a diameter of 250mm and a wall thickness of 15mm. 75mm thick steel plates have been used for the front, back cap, and the piston plate. The plate openings size was set to 25mm so that it becomes at least 5 mm larger than the largest diameter SMA bar in this analysis; this is done to allow unrestrained rotational movement of the tie bars. A total number of four SMA bars were used for each of these models. Each of these bars spanned between the three plates as shown in Figure 3-4.

The superelastic behavior of SMA bars was simulated using NiTinol superelastic-plastic ABAQUS/CAE plugin. The four transformation stresses used for SMA material model is given in the materials section. The remaining elements (shaft, sleeve and the plates) are made of steel. The material properties of steel are provided in the materials section.

Figure 3-11 represents the cyclic loading time history used for the PBSC brace model. This time history with a maximum value of 60mm was associated with the U3 direction of the *RP-1 reference point. The reference point *RP-1 was created for the centroid of the brace shaft and it was offset 250mm (an arbitrary value with no effect on the analysis). During result extraction, this reference point provided an easier way to retrieve both force and deformation results. Any deformation applied to the reference point was transformed to equal deformation for the shaft end surface.

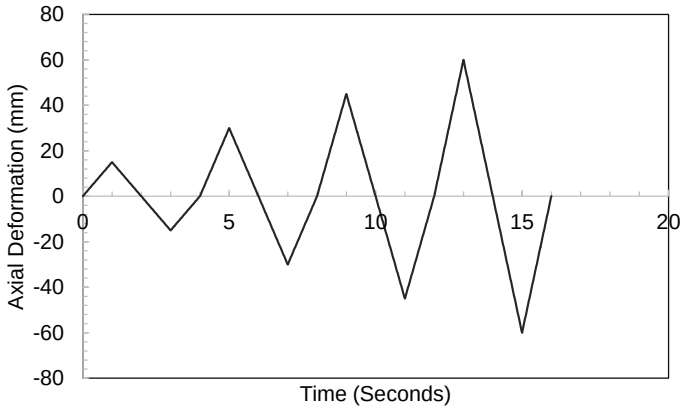

Figure 3-11: Quasi-static deformation loading history.

Figure 3-12 shows the velocity history of the deformation load shown in Figure 3-11. This figure was generated by differentiating the deformation time history with respect to time. It can be seen that the velocity time history has constant velocity plateaus where the deformation history has a constant slope. The velocity history shows sudden jumps where the deformation history has a change in slope positive to negative or vice versa. The change in slope in the max/min points of the deformation history plot indicates load reversal points.

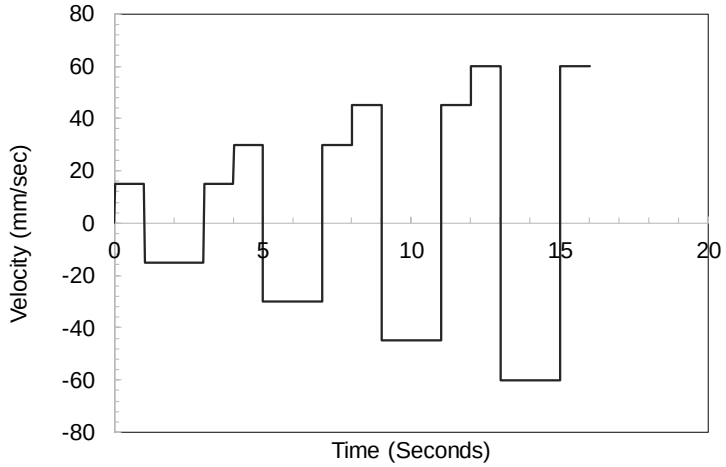

Figure 3-12: Velocity time history of the load.

Figure 3-13 shows the acceleration time history of the applied load. This history was calculated by differentiating the velocity time history with respect to time. In the velocity time history (Figure

3-12) where the velocity is constant, the corresponding acceleration values are zero. However, the acceleration has a large spike where the velocity plot has a sudden shift in value (e.g. load reversal points). This sudden acceleration occurs when the shaft reverses from loading to unloading state or vice versa.

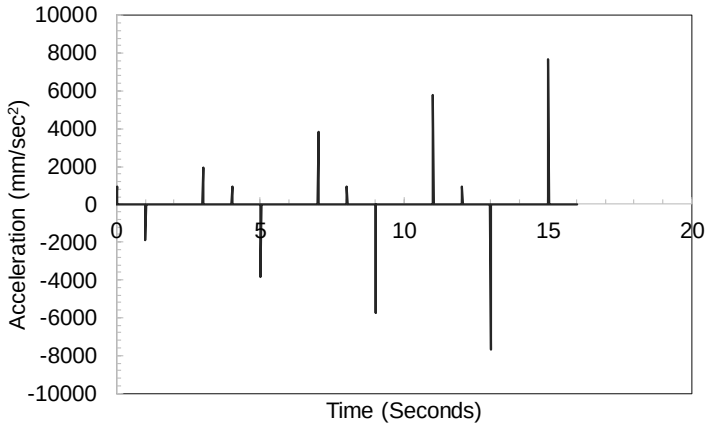

Figure 3-13: Acceleration time history of the load.

Figure 3-4 (c) and Figure 3-4 (d) depict the deformation states of the internal elements of the PBSC bracing system during tensile and compressive loading, respectively. The sleeve is intentionally kept hidden from this view in these figures. For a proper understanding of the deformed shape, the longitudinal deformation was three times exaggerated. From Figure 3-4 (c), it can be observed that the front end of the ties is under tension and this part is tightly locked between the front cap and piston plate. On the other hand, the back ends of the ties are structurally disconnected, and no load is shared by this part. The back end of these ties freely moved out of the back cap in this figure. Figure 3-4 (d) shows the compressive load cycle for the PBSC bracing system. In this loading phase, the back portions of the tie bars are locked between the piston plate and the back cap whereas the front ends of the tie bars are structurally disconnected from the front cap and freely moved out of the front cap.

Figure 3-14 shows the maximum von Mises stresses observed in the middle eight couplers/nuts during the reverse cyclic loading test. The stresses depicted here are in terms of quilt contours. For quilt contours, the variable values are extrapolated to element faces on the surface of the model. No averaging between elements is carried out. Quilt contours are useful when results are evaluated on an element-by-element basis. Only a single color per element is plotted for axisymmetric elements with asymmetric deformation. It can be observed that the maximum stresses are observed on the inside surfaces of the couplers. Figure 3-14 to Figure 3-17 present the brace analysis results with 16mm dia NiTi rods. All the stresses in these figures are quilt stresses to eliminate element local corner stresses from these figures.

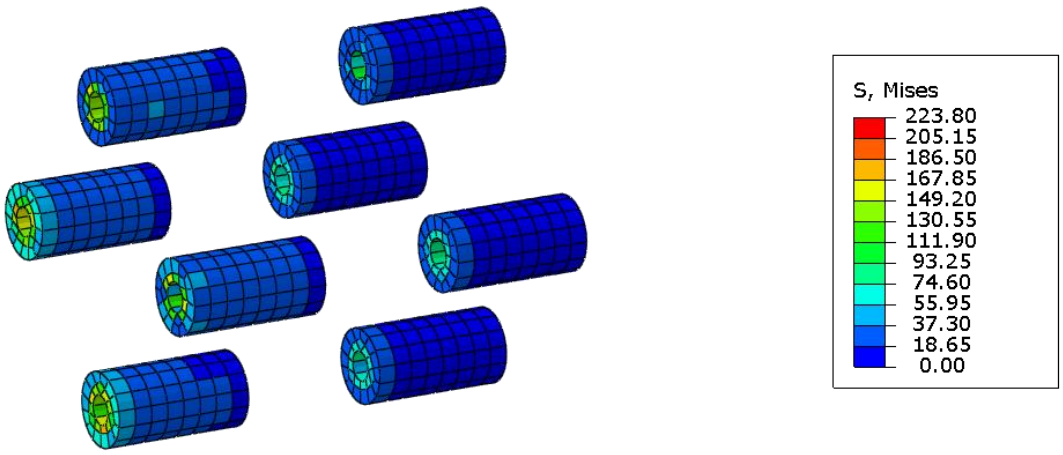

Figure 3-14: von Mises stress distribution on the couplers.

Figure 3-15 shows the maximum stresses experienced by the plates during the cyclic load test. In this figure, the piston plate is showing the maximum stresses around its openings. The maximum quilt stress was found to be 80.37 MPa.

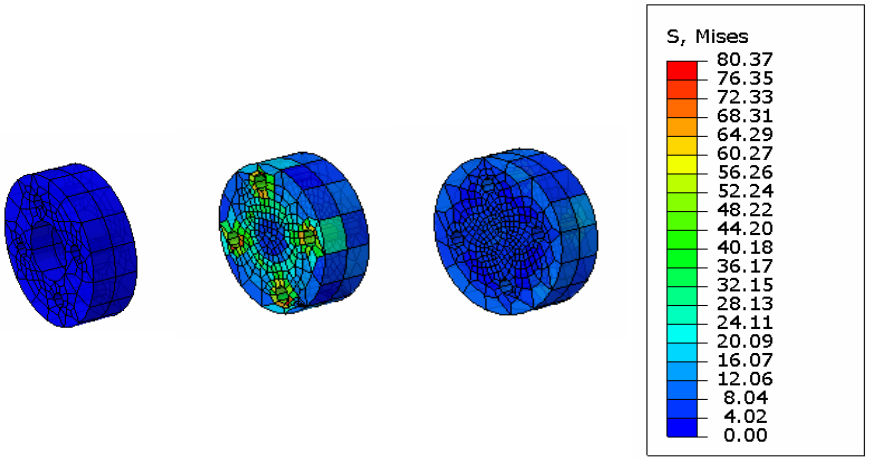

Figure 3-15: von Mises stress distribution on the plates.

Figure 3-16 (a) and (b) show the maximum stresses on the sleeve and shaft of the PBSC bracing system, respectively. It was observed that the sleeve experienced very low maximum stress (48.28 MPa) as intended by design. In contrast, the yield and the theoretical buckling strength for the sleeve are 345MPa and 855 MPa (assuming effective length factor $k = 2$), respectively. This low stress is critical in lowering any chance of global or local buckling in the sleeve. Figure 3-16(b) shows the von Mises stress distribution on the shaft. As per this figure, the maximum stress observed by the shaft is approximately 42 MPa. This stress is lower than the yield (345Mpa) and buckling strength (126.62Mpa assuming $k = 2$) for this section.

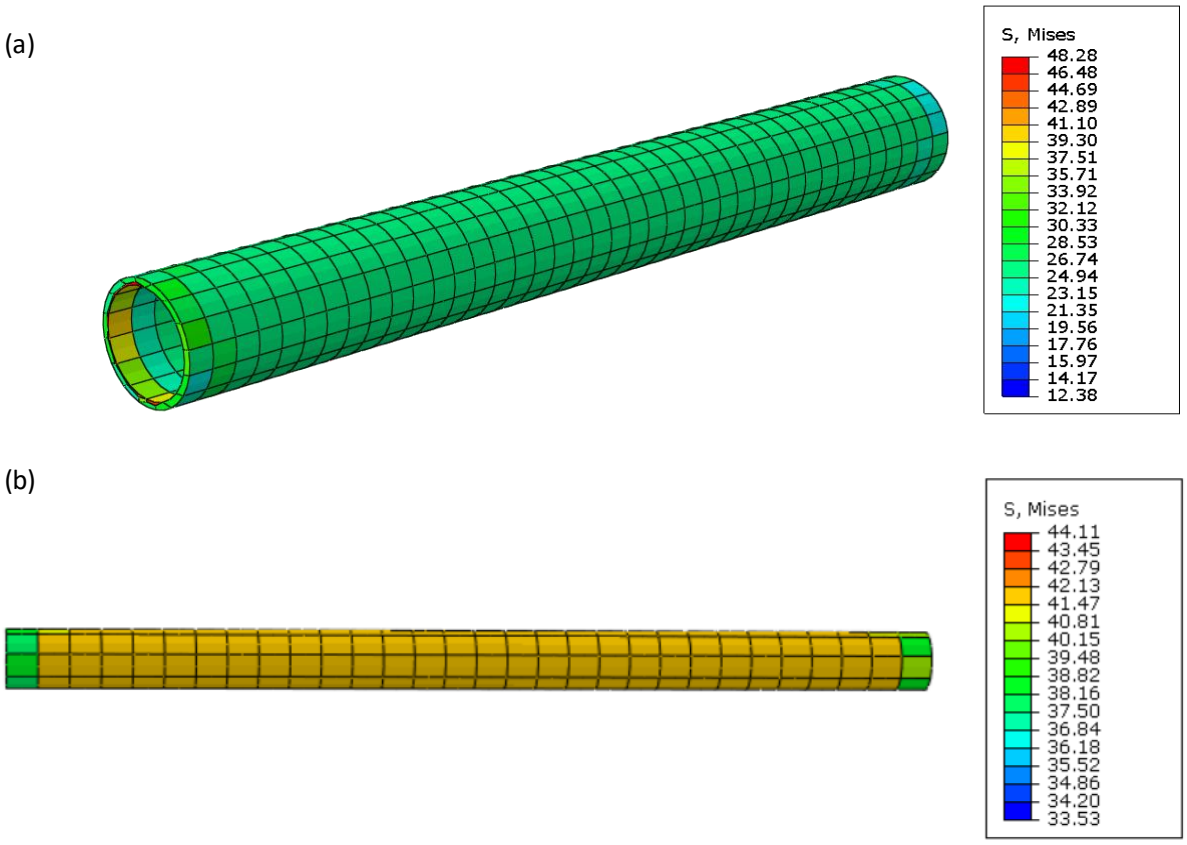

Figure 3-16: Von Mises stress distribution on (a) Sleeve and (b) Shaft.

Finally, Figure 3-17 shows the maximum stresses on the SMA bars. It was found that the quilt contour values were less than or equal to 391.01 MPa as shown in Figure 3-17. However, the banded contour values (not shown in this figure) were found to be higher. Those local stresses pushed the bars in the nonlinear range of response. The banded contours represent values as color-filled bands. These contours are computed by extrapolating results to the nodes and conditionally averaged. Averaging depends on the options selected and characteristics of the model (ABAQUS 2014).

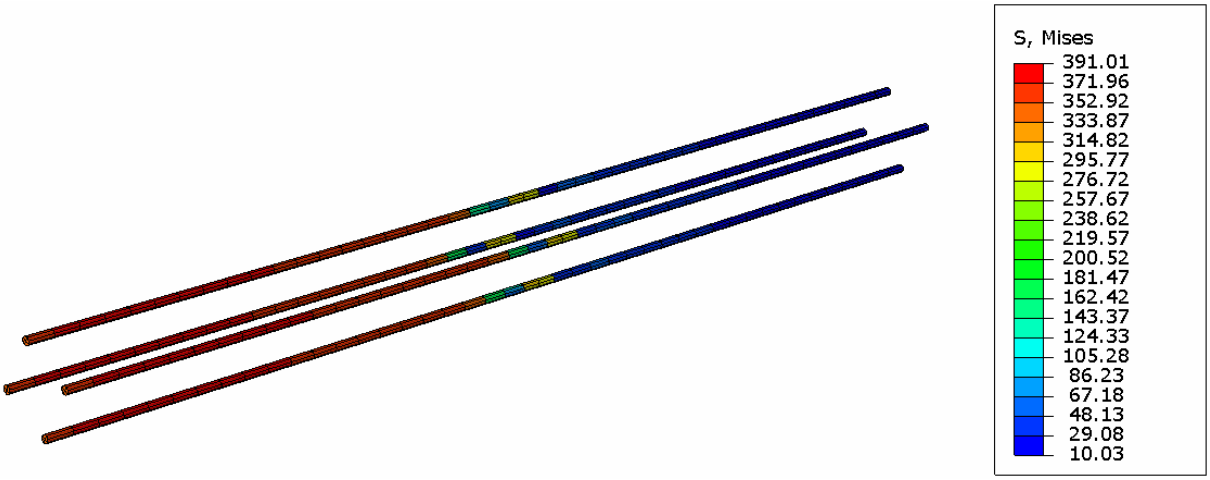

Figure 3-17: Von Mises stress distribution on the NiTinol ties

The whole reverse cyclic loading process was repeated for four different bar sizes mentioned earlier, and the load deformation hysteresis results are plotted in Figure 3-18(a)-(d). From this figure, it can be observed that the hysteresis of the PBSC system is very similar to the flag shape hysteresis.

It was observed in previous studies that flag shaped hysteresis signifies superior self-centering capability (Zhang and Zhu 2007). When installed in a structure, this type of smart systems could reduce permanent residual deformation by a very significant amount after an earthquake.

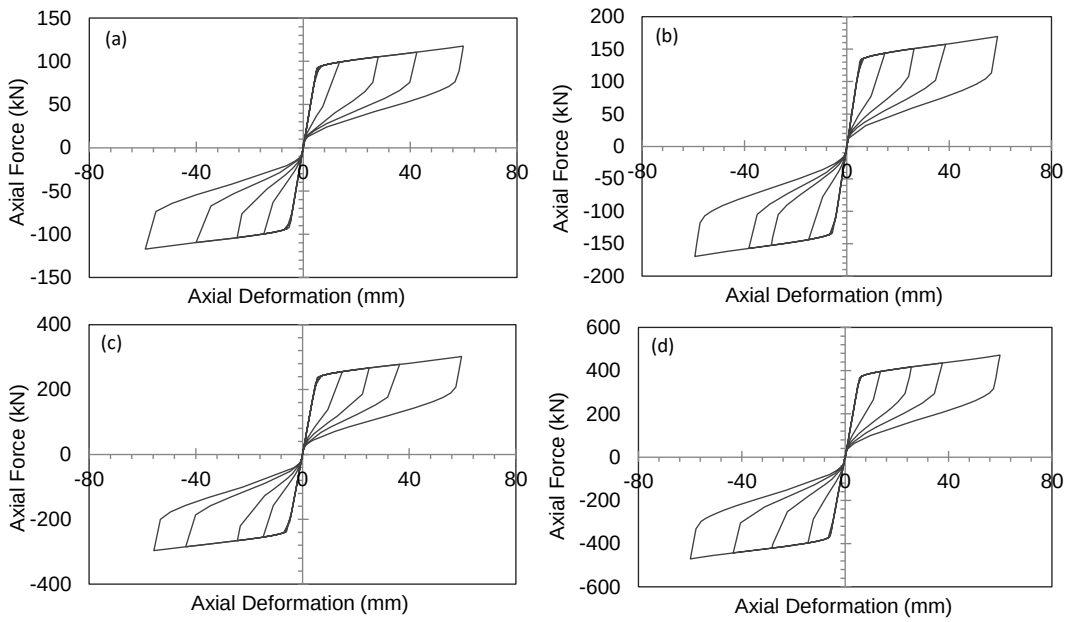

Figure 3-18: Hysteretic response of the PBSC bracing system with (a) 4-10mm (b) 4-12mm (c) 4-16mm and (d) 4-20mm dia NiTinol Bars.

Figure 3-18 (a) shows the load deformation hysteresis response of the PBSC bracing system with four numbers of 10mm diameter NiTinol based SMA bars. From this figure, it can be seen that the yield force of this brace is around 95kN. After the yielding, the stiffness is reduced. The post-elastic stiffness is also noteworthy which is helpful in resisting excessive plastic deformation. The maximum force and deformation observed for this brace are 110kN and 60mm, respectively. The observed hysteresis behavior is symmetric and stable as they do not show any strength degradation in subsequent load cycles. The flow direction of the hysteresis shape is provided in Figure 3-20(a). The symmetric behavior also indicates buckling has not occurred in the system. Similar behavior was observed for three other PBSC brace models utilizing 12mm, 16mm, and 20mm diameter SMA bars. The global yield forces of the brace with four numbers of 12mm, 16mm and 20mm bars were 140kN, 240kN and 375kNand the maximum forces were 160kN, 272kN, and 453kN, respectively. The highest deformation for these systems was limited to 60mm. This 60mm

maximum deformation was chosen based on approximately 6% elongation of the half-lengths (1075mm) of the SMA bars.

To understand the advantage of SMA bars used in this bracing system, a similar model was run using similar diameter steel rebar in place of SMA bars. The steel used in this analysis has the following material properties: Modulus of elasticity 200 GPa, Yield Strength 414 MPa and maximum elongation capability of 10.3%. The analyses results are presented in Figure 3-19, and the hysteresis flow paths are shown in Figure 3-20(b). It was observed that the hysteresis with steel rebar is similar to a sliding device. After a full reverse cyclic loading, the brace starts to slide between the unloaded state to the load reversal state. The stiffness of the brace becomes zero between these points. This large zero stiffness plateau makes the brace unsuitable for use against any lateral and vertical loading. This occurs due to permanent elongation of the steel rebars as steel cannot come back to its original size after load removal. Figure 3-19(a) to Figure 3-19(d) show the hysteretic responses for four braces with four numbers of 10mm, 12mm, 16mm and 20mm diameter 60-grade steel rebar.

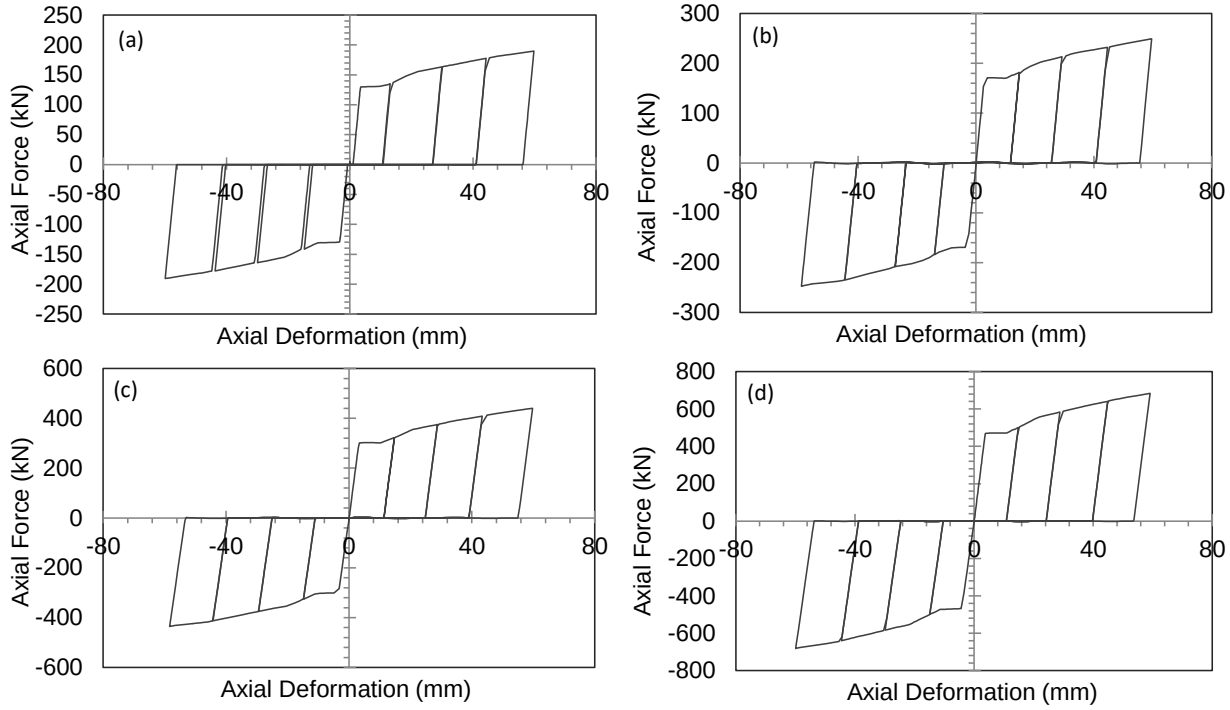

Figure 3-19: Hysteretic response of the bracing system with (a) 4-10mm diameter steel bar (b) 4-12mm diameter steel bar (c) 4-16mm diameter steel bar (d) 4-20mm diameter steel bar.

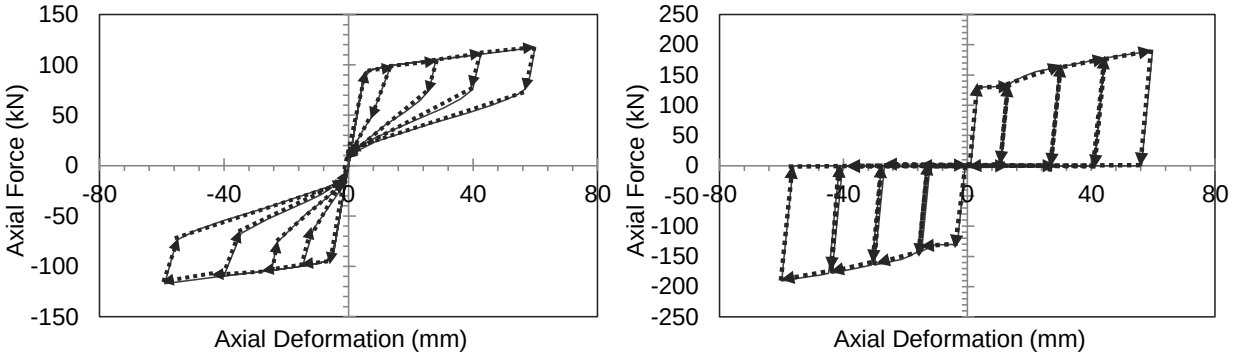

Figure 3-20: Hysteretic flow paths for the brace with (a) SMA tie bars (b) Steel ties bars.

Finally, the energy dissipation capability of the PBSC brace was compared to the same configuration fitted with steel rebar. As the yield strength of the braces made with SMA and steel rebar are not similar, for a more reasonable comparison, the calculated values were normalized with respect to the respective brace yield forces (Table 3-1). It was found out that, the brace with SMA rebar has a higher energy dissipation capacity compared to the same configuration of this brace made with steel rebar. It was found out that the SMA based system has around 10%-20%

higher energy dissipation capacity compared to the steel based one. This is due to the sliding hysteresis of steel based configuration relative to a flag hysteresis observed for the SMA based one.

Table 3-1: Normalized energy dissipation comparison.

	Dissipated Energy (kN-m/kN)			
Description	4-10mm	4-12mm	4-16mm	4-120mm
With SMA Bar	0.15	0.15	0.15	0.14
With Steel Rebar	0.13	0.13	0.13	0.13
% Higher	14.66	15.42	19.19	10.98

3.8 Summary

Four different PBSC brace models were built in the finite element environment and were tested under reverse cyclic quasi-static loading. From this analysis, the following observations were made.

- The PBSC brace exhibits flag shaped hysteresis response that is an excellent indicator of self-centering capability.
- The brace hysteresis was found to be symmetric with respect to both deformation and force response. This indicates that no buckling occurred during the analysis.
- Only SMA bars went to the nonlinear range during the cyclic load test while all other parts of the brace remained elastic. This ensures that the steel parts will require almost no repair or replacement after an earthquake event.

The PBSC bracing system has the following limitations compared to other bracing systems.

- Deformation capacity of the PBSC brace is limited to the deformation capacity of the SMA bars spanning between the piston plate and the end plates. Therefore, the theoretical maximum SMA bar length that could be utilized for the PBSC brace is equal to the half of the brace length. This implies that the maximum superelastic elongation capacity of the PBSC brace will be limited by this length constraint.

The current study has few limitations that need to be addressed in future research. No coupler/nut to SMA bar load slip model has been used in this study, which is necessary for determining proper load deformation behavior of these connections. In real world scenario, slippage could affect the self-centering capability. The SMA material model did not account for residual strain, and hence, the PBSC bracing system showed zero residual deformation. This is less conservative than what is expected from a PBSC brace prototype. An experimental investigation needs to be carried out for the validation of the finite element model test results.

The cyclic performance of the PBSC bracing system is highly dependent on the shape memory alloy ties. The hysteresis of SMA is dependent upon ambient temperature. If the ambient temperature drops below austenite finish temperature, SMA starts to lose its self-centering capability. If the temperature goes down to martensite finish temperature, SMA looses its superelastic ability. Therefore, the SMA alloy to be used in cold climate should be carefully calibrated/manufactured to have their austenite finish temperature lower than the expected lowest temperature in those regions.

Furthermore, hot weather or fire can be detrimental to the PBSC bracing system. After a major earthquake, fire can break out in a building and aftershocks can coincide. At a high temperature, such as M_d (a temperature much higher than A_f as shown in Figure 2-13), NiTinol becomes elastoplastic and loses both shape memory effect and superelasticity. Therefore, if NiTinol ties get warmed up beyond M_d due to fire, the PBSC bracing system will not be able to bring back the structure to its original position after the earthquake.

CHAPTER 4: A HYSTERESIS MODEL FOR THE PBSC BRACING SYSTEM

4.1 General

The piston based self-centering (PBSC) bracing system uses superelastic shape memory alloy (SE SMA) bars for its energy dissipation and self-centering capability. These SE SMA bars exhibit flag-shaped hysteresis; in theory, these bars are supposed to bring back the bracing system fully to its original position after significant nonlinear deformations. However, shape memory alloy undergoes some residual deformation after large plastic strains. This residual strain occurs when planes of tightly packed atoms slide past each other; individual bonds are broken and reformed with new atoms in a step-by-step process. Under repeated cyclic loading, these residual deformations add up and deviate from the anticipated zero residual strain flag shaped response. To accurately simulate this behavior during nonlinear dynamic time history analysis, an SMA flag shaped hysteresis model with sliding response has been developed by the author. This chapter shows the gradual development process of this new hysteresis model and provides analysis and verification results to support this claim. To validate the material hysteresis model, a MATLAB based superelastic uniaxial SMA material hysteresis model was developed and incorporated into a custom-made finite element program (MATLAB-based) specifically designed and developed for the PBSC bracing system. This custom made finite element program reduced hours of analysis run-time to seconds. For this reason, the SMA material hysteresis model was implemented in the MATLAB based finite element program instead of ABAQUS (2014). This finite element program was utilized to capture the nonlinear quasi-static response of the PBSC brace. Finally, the PBSC brace response from this analysis was used to develop a novel SMA flag shaped hysteresis model

with residual deformation and sliding response for implementation in a commercial structural analysis and design software known as S-FRAME. The hysteresis model was developed in a way to simulate not only PBSC bracing system but also other self-centering structural systems such as MANSIDE and RHDB brace. This hysteresis can also be calibrated to simulated SMA reinforced concrete elements; this will help researchers and engineers around the world simulate different types of self-centering structural systems in the finite element environment; which will enable them to design these systems more accurately and efficiently than before.

4.2 SMA bar behavior

For this study, we will critically analyze the NiTinol bar test results discussed in the previous chapter. The diameters of the specimens tested include 1.8mm wire and 7.1mm, 12.7mm and 25.4mm bars. DesRoches et al. (2004) confirmed that both SMA bars and wires show excellent re-centering capacity (Figure 4-1). The residual strain observed for the test specimens were on an average 0.65% for all the specimens where the maximum strain was 6%. The only disadvantage of using SMA bars over wires is its lower hysteretic energy dissipation capacity. The equivalent viscous damping represented by the fatness of the hysteresis loops was found to vary from 2% for the 12.7mm bar to a maximum of 7.6% for the 1.8mm wire.

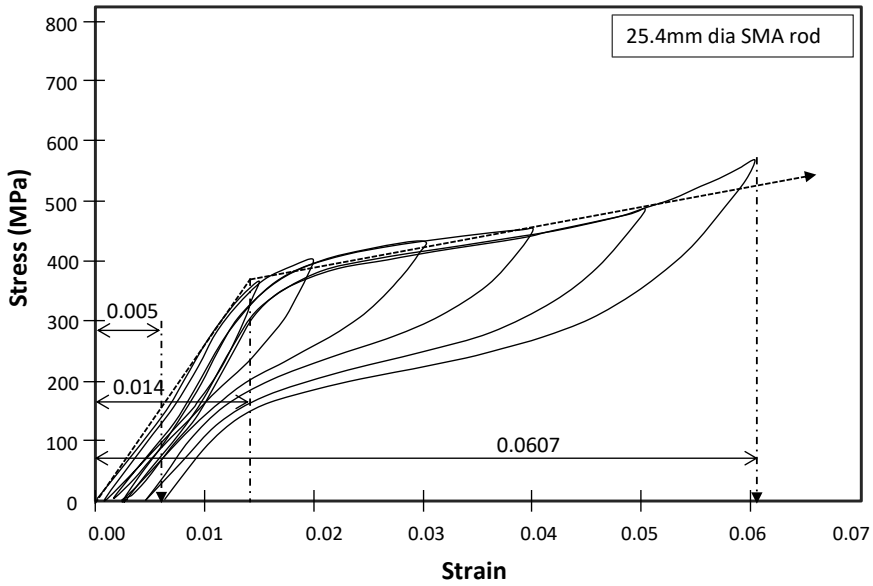

Figure 4-1: Stress–strain plot for 25.4 mm diameter nitinol SMA bar subjected to quasi-static cyclic loading (adapted from DesRoches et al. (2004)).

The maximum plastic, residual and yield strain of the 25.4mm dia SMA bar specimen were calculated from Figure 4-1, and the values are shown on the plot. From this figure, the accumulated residual strain is around 9.4% (0.0057/.0607) of the maximum strain; which is 12% of the maximum plastic strain. Here plastic strain is the strain value after deducting the yield strain of the specimen. However, other test results (DesRoches et al. 2004, Nemat-Nasser and Guo 2006) exhibited NiTinol having a residual strain in the range of 5%-12% of the maximum strain. Therefore a slightly lower (10%) residual to plastic strain ratio is used for the rest of this study.

4.3 SMA flag hysteresis rule

Based on the behavior observed in experimental investigations researchers have come up with both material and link hysteresis models for SE SMA material and SE SMA built elements respectively. A widely used material model for SMA is shown in Figure 4-2 (Auricchio and Sacco 1997). In this hysteresis model, unloading happens in two different stages. From a stress beyond martensite to austenite starting stress (σ_{mas}), the material unloads at initial elastic modulus (E_i) until

it reaches the martensite to austenite starting stress (σ_{mas}). After arriving at this stress level, the tangent modulus is drastically reduced to variable modulus, (E_v) and the line move towards martensite to austenite finishing stress point (σ_{mas}/E_i, σ_{mas}) on the backbone curve. This is very close to what the experimental results suggest (Figure 4-1). This material hysteresis model has been implemented in SeismoSoft (2016) finite element analysis software. The only shortcoming of this model is the absence of residual strain formulation, which is very important for accurate representation of this material behavior.

Some other notable features of this hysteresis models are the austenite to martensite starting stress (σ_{ams}), plastic modulus (E_p) and austenite to martensite finishing stress (σ_{amf}). For structural applications, σ_{ams} can be considered as yield stress. σ_{amf} is the stress level beyond which SMA becomes fully martensite and the tangent modulus changes back to E_i. The tangent modulus between σ_{ams} and σ_{amf} points on the backbone curve can be designated as the plastic modulus E_p. $\mathcal{E}_L$ is known as the plateau strain, and it represents the strain plateau in the austenite to martensite transition zone.

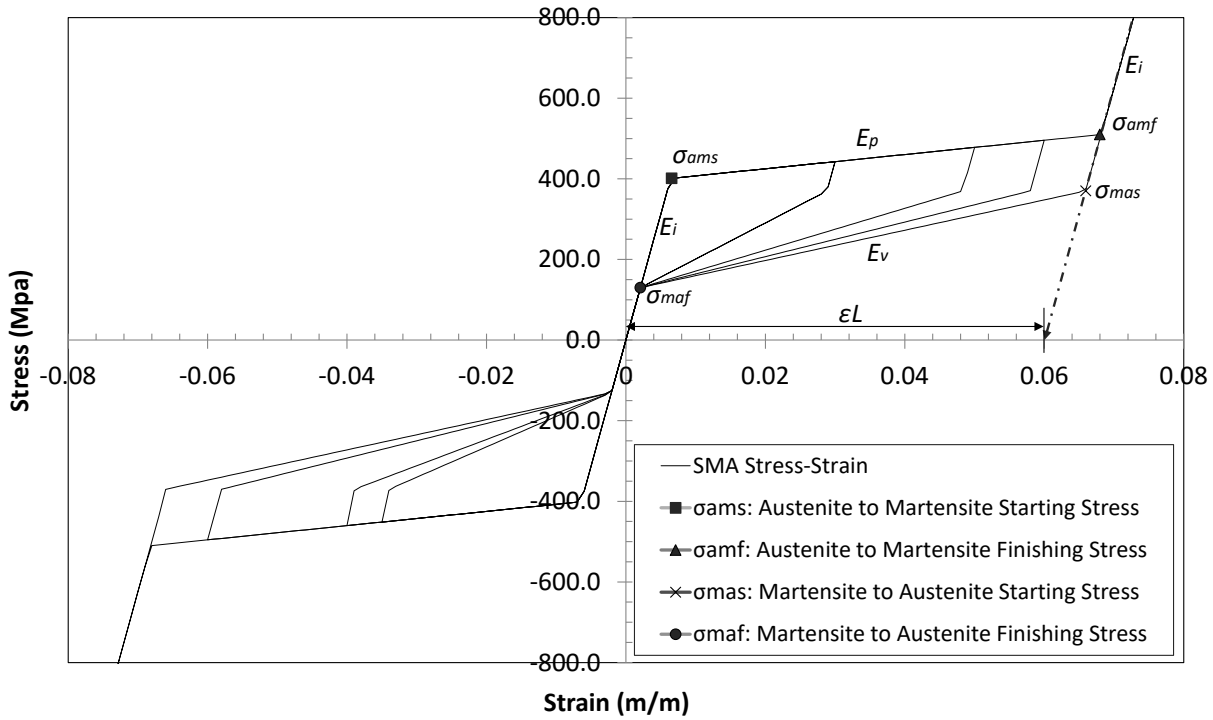

Figure 4-2: Uniaxial SMA flag-shaped hysteresis (adapted from Auricchio and Sacco (1997))

The next hysteresis model for representing SMA based structural elements in finite element software is the SMA flag-shaped hysteresis model available in Ruaumoko finite element software (Carr 2008). A diagram of this hysteresis model is shown in Figure 4-3. Comparison between Figure 4-3 and Figure 4-2 indicates that there is a clear distinction between the unloading rules. In the Ruaumoko model, there is no fixed force level representing the martensite to austenite starting force/stress. The unloading stiffness changes when the unloading line reaches a line parallel to the post-yield stiffness line going through *ALPHA*YP* point. Therefore, this model is less accurate in representing SMA based elements compared to the one implemented in SeismoStruct. Additionally, this model also lacks residual deformation. Nevertheless, this model has some additional parameters for controlling some important behavior; they are as follows: the parameter '*DELTA'* represents the point where material in the sections finishes transforming to martensite and starts stiffening up again. *PHI*YP* and *PSI*dy* point represent the fracture point. Additionally,

the unloading line has a stiffness of *BETA*K*$_o$. Therefore, the stiffness of this line can be different compared to the initial stiffness line. Furthermore, in this hysteresis model ALPHA, *YP,* k_o, *r, BETA, DELTA, PHI and PSI* values can be changed.

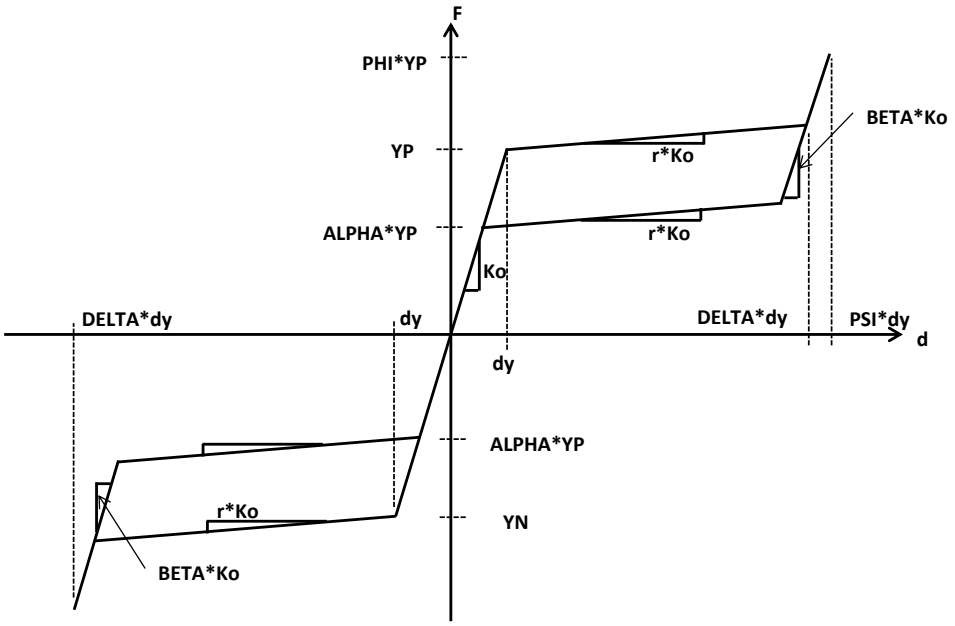

Figure 4-3: Graphical rule of flag-shaped hysteresis (adapted from Carr (2008))

4.4 PBSC brace hysteresis model development

From Figure 4-1, it can be observed that SMA bars are not entirely capable of re-centering. The residual plastic deformation is around 10% of the maximum plastic deformation. Both Ruaumoko and Auricchio & Sacco's hysteresis rules are missing this important feature. Due to these limitations mentioned above, the current hysteresis models are not very accurate in capturing residual deformations of elements made of SMA under cyclic loading conditions. To resolve this issue, a new SE SMA material model has been proposed. This model follows the basic hysteresis rule established earlier (Auricchio and Sacco 1997). In addition to the previous rules, it can simulate the residual strain accumulation. This modified model is only for simulating superelasticity but not the shape memory effect; therefore, it will not be able to simulate the

thermomechanical behavior of SMA. Furthermore, this model is specifically designed for frame element based finite element analysis; therefore, it cannot be used in solid or shell element modeling, which warrants more complex continuum mechanics and volume fraction based formulations. Furthermore, no strain rate dependent behavior has been incorporated. Therefore, this modified SE SMA hysteresis model will be only useful in specific applications such as accurately determining the PBSC brace hysteresis or modeling beam-column elements made of SE SMA.

The previous study on the PBSC brace (Haque and Alam 2015a) used NiTinol UMAT subroutine available in ABAQUS (2014) for the NiTinol material model. For calibrating the hysteresis parameters, superelastic-plastic ABAQUS/CAE plugin was used. This NiTinol material model was developed from the works of Auricchio and Sacco (1997); therefore, it is also missing the residual strain calculation algorithm. In the PBSC bracing system the SE SMA bars only get loaded in tension. Therefore an SE SMA material model with only tension loading unloading rule is sufficient in simulating the brace behavior. A brief description of the PBSC brace mechanism is given below which is later used to develop a simplified finite element model necessary for MATLAB implementation.

4.5 PBSC mechanism

PBSC bracing system is designed to be used in portal frames typically in a Diagonal/Chevron/V configuration. Figure 3-2 shows an example of such arrangement. The details of two different brace configurations have already been presented in Figure 3-1(a) and (b). Please refer to section 3.4 for reviewing the mechanism of this bracing system for understanding the simplified model discussed in section 4.6.

4.6 Simplified finite element model

In order to develop a simple MATLAB finite element program for the PBSC bracing system, the model was idealized using one-dimensional bar/strut elements. Below is a systematic description of the process by which the model was simplified.

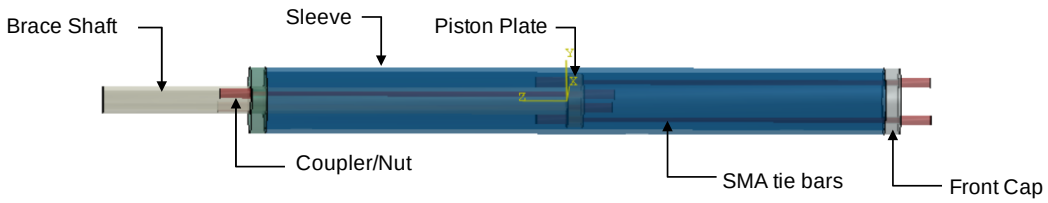

Figure 4-4: Longitudinal section of the PBSC bracing system

It can be seen from Figure 3-1 and Figure 4-4 that the PBSC bracing system has three major components; they are the shaft, the sleeve, and the internal SMA tie bars. The plates are provided to connect the ties to the other parts. From brace mechanism section and Figure 4-4, it can be understood that the sleeve is acting as a support for the back cap/plate, which transfers load from the SMA bars to the support when the brace is under compressive loading. Furthermore, the sleeve cross section is designed to take much larger loads than the ties and the shaft; This ensures minimal longitudinal deformation for the sleeve. Therefore, a finite element model made without the sleeve should behave almost similarly as the one with the sleeve if the plates are restrained from translation.

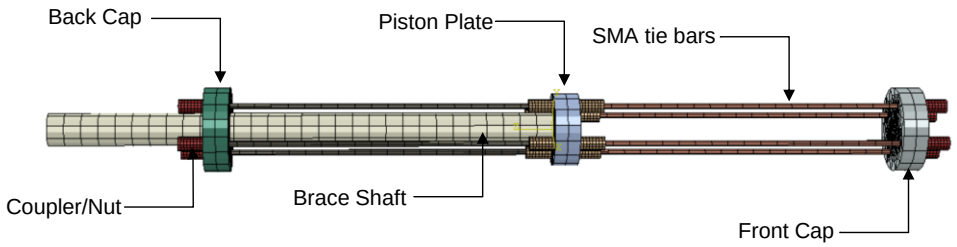

Figure 4-5: PBSC bracing system shown without the sleeve

Figure 4-5 shows the PBSC brace model without the explicit sleeve model. For MATLAB implementation, we can further assume that both the shaft and the SMA bars are bar elements and the plates are the nodal points. This simplified model is shown in Figure 4-6.

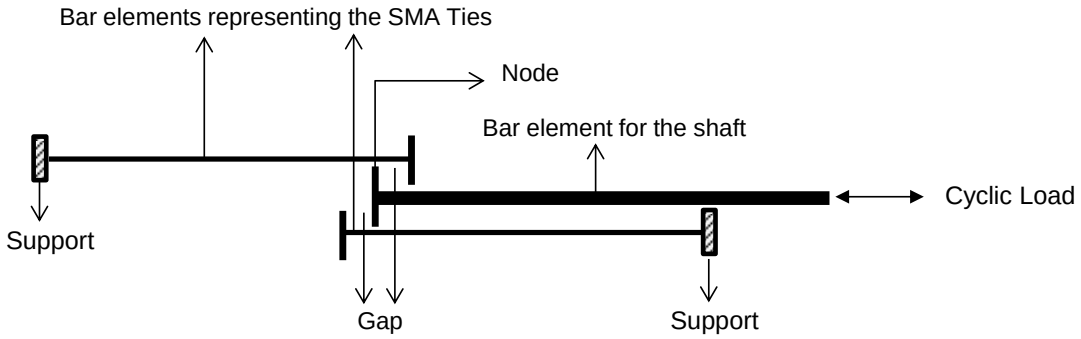

Figure 4-6: Simplified PBSC brace model

Finite element modeling the simplified representation of the brace shown in Figure 4-6 using one-dimensional bar/truss element is not possible as the right support node will reside in the same line of the shaft. Therefore, the shaft will be prevented from movement. To resolve this issue, this model was further simplified by moving the right support on the left side and reversing the front tie bars. This further simplified model is shown in Figure 4-7. However, moving the front ties to the back side converted the tensile load to compressive and subsequently, the deformations also became compressive (axial shortening for the front tie bars). However, it can be understood that in this configuration, if buckling is ignored, the compressive deformations experienced by the reversed tie bars are same the as that of the tensile deformations of the model shown in Figure 4-6. Hence, the overall load deformation hysteresis of the brace remains the same as the original model.

If we observe this model carefully, it can also be understood that the ties are occupying the same space if they are modeled in one dimension. To resolve this issue, only one set of tie bar could exist at any point in time depending upon the loading condition. Under tensile loading the

compression tie bars were deactivated and vice versa. During the deactivated state, all load deformation history of the tie bars was saved in the memory to be used in the subsequent cycle when that tie gets reactivated.

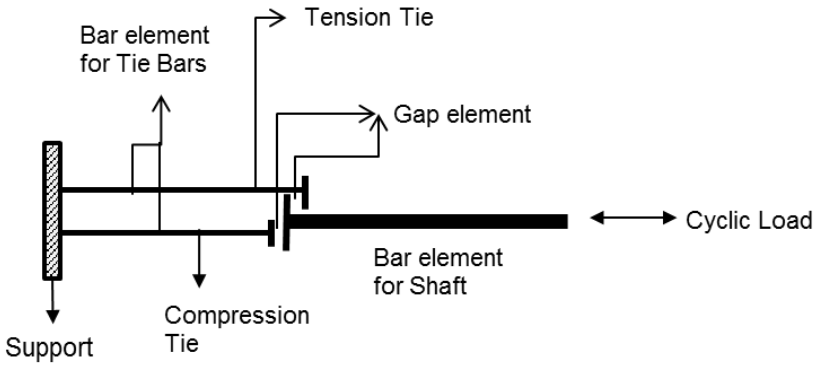

Figure 4-7: Further simplification of the PBSC brace model

4.7 SMA material model

In this section, a tension only SE SMA material hysteresis model with residual strain is developed. In the next step, it is incorporated into the MATLAB finite element program discussed above. This section briefly discusses the rules of SE SMA material model with residual deformation. As this material model is for tensile stresses only, no rules are available for the negative stresses. The following definitions and notations should be used for interpreting the hysteresis rules: loading refers to an increase in the absolute value of the stress without a change in sign. On the other hand, unloading refers to a decrease in the absolute value of the stress without a change in sign. Yielding refers to reaching a line with E_p tangent modulus passing through (σ_{ams}/E_i, σ_{ams}) point. E_v is the variable tangent modulus line connecting (σ_{maf}/E_i, σ_{maf}) point on the backbone curve to the unloading line coming from σ_{mas} stress level. Please check Figure 4-8 for interpreting the other notations.

The uniaxial SE SMA hysteresis rules with residual deformation is given below

1. Below yield stress
    1.1. Loading: Loading occurs on the right side or on the line with "E_i" tangent modulus and passing through (ε_{ri}, *0*) point. The loading line follows E_i tangent modulus until yielding. After yielding go to rule 2.
    1.2. Unloading:
        1.2.1. If unloading from a stress higher than *'σ_{mas}'* then the unloading line follows E_i tangent modulus. When the line reaches *'σ_{mas}'* go to 1.2.2.
        1.2.2. If unloading from a stress less than or equal to *'σ_{mas}'* then unloading line follows E_v tangent modulus. E_v is the variable tangent modulus of a line originating between σ_{amf} and σ_{ams} stress level and directed towards (σ_{amf}/E_i, σ_{amf}) point on the backbone curve. This line follows E_v tangent modulus until this line intersects a line with E_i tangent passing through (ε_{ri}, *0*) point. ε_{ri} is calculated using current hysteresis loops maximum strain and residual strain coefficient (Equation 1). After the intersection go to rule 1.2.3
        1.2.3. If unloading from a point on or below the intersection point defined in 1.2.2: The unloading line follows E_i tangent modulus.
2. After Yielding
    2.1. The line follows the post-yield tangent (E_p) until it reaches σ_{amf} or Austenite to martensite finishing stress. After reaching σ_{amf} go to rule 3
    2.2. Unloading: Go to rule 1.2.1
3. At or above σ_{amf} stress
    3.1. Loading: The loading line follows E_i tangent modulus.
    3.2. Unloading: Go to 1.2.1

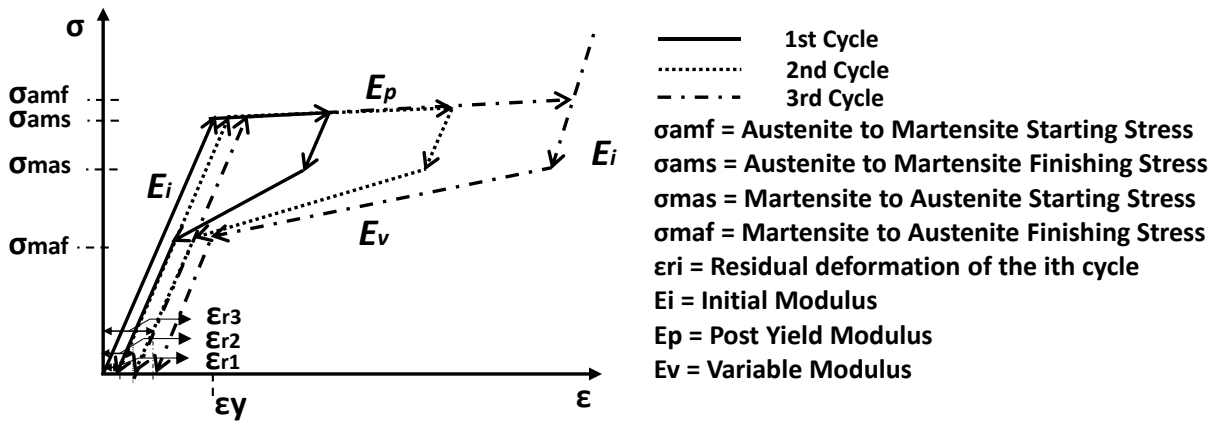

Figure 4-8: SMA uniaxial stress-strain hysteresis model with residual deformation (Tension Cycles Only)

A typical tension only cyclic response from the developed SE SMA material model is shown in Figure 4-9. The residual strain is calculated using equation (1). For simplification, a linear relationship has been used between the residual and plastic strain.

*Residual strain = (Maximum strain of the cycle-Yield Strain) *Residual Strain Coefficient (1)*

Here, the "Maximum strain of the cycle -Yield Strain" is the plastic strain for the current cycle under consideration. Furthermore, the Yield Strain is calculated from the original backbone curve. In this hysteresis model, residual strain is only allowed to increase. Therefore, if the current cycle has a maximum strain value less than the maximum strain of one of the previous cycles then the new residual strain will not be calculated, and the previous residual strain will be used for the current cycle. As per this rule, if the material experiences large strain cycles at the beginning, then the residual strain will be set to a higher value and will not be reduced if the subsequent cycle's maximum deformations are smaller.

This SMA hysteresis model with residual strain was validated against the experimental results presented in (DesRoches et al. 2004). The result of this validation is shown in Figure 4-9. In the material hysteresis model, the residual strain coefficient can be set to any value between 0 and 1.

However, a value of 0.128 was set for this validation (Figure 4-9). The material hysteresis model response (shown using blue lines) showed excellent agreement with the experimental result. The energy dissipation from of the experimental result and the MATLAB simulation are 11.03 kN-m/m and 10.73 kN-m/m respectively (calculated using the area inside the hysteresis loops and the cross-sectional area of the bar). The energy dissipation from the MATLAB simulation is only 2.8% lower than the experimental result. Therefore, it can be safely concluded that this material hysteresis model could be utilized to simulate SMA with residual strain/deformation.

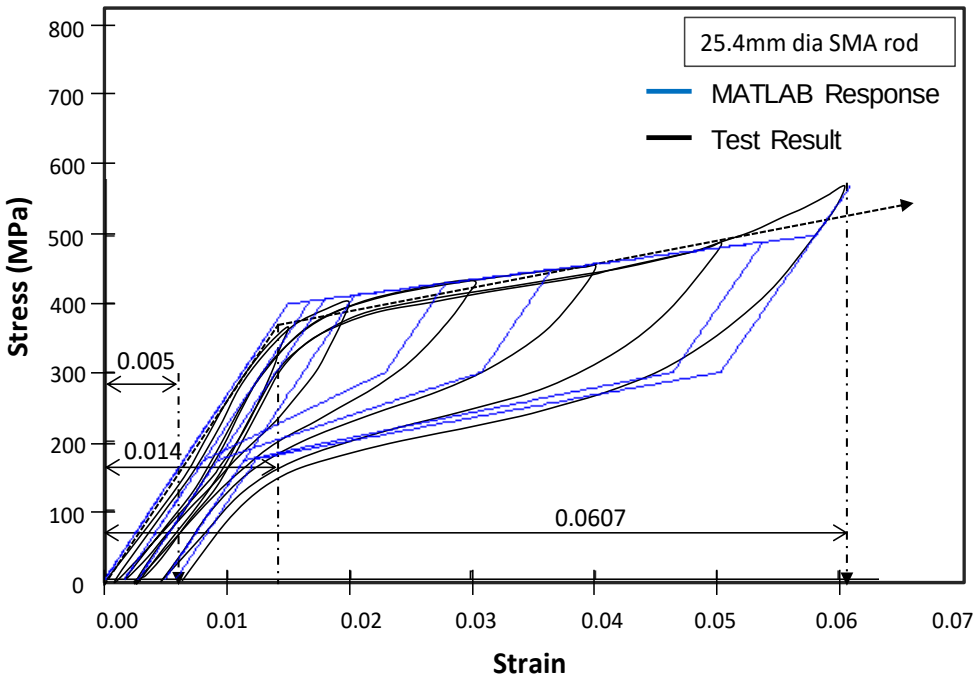

Figure 4-9: Validation of SMA material hysteresis model against experimental result by (DesRoches et al. 2004).

The SE SMA hysteresis model discussed above was coded as a function in MATLAB (2012), and a flow chart of this function is provided in Figure 4-10.

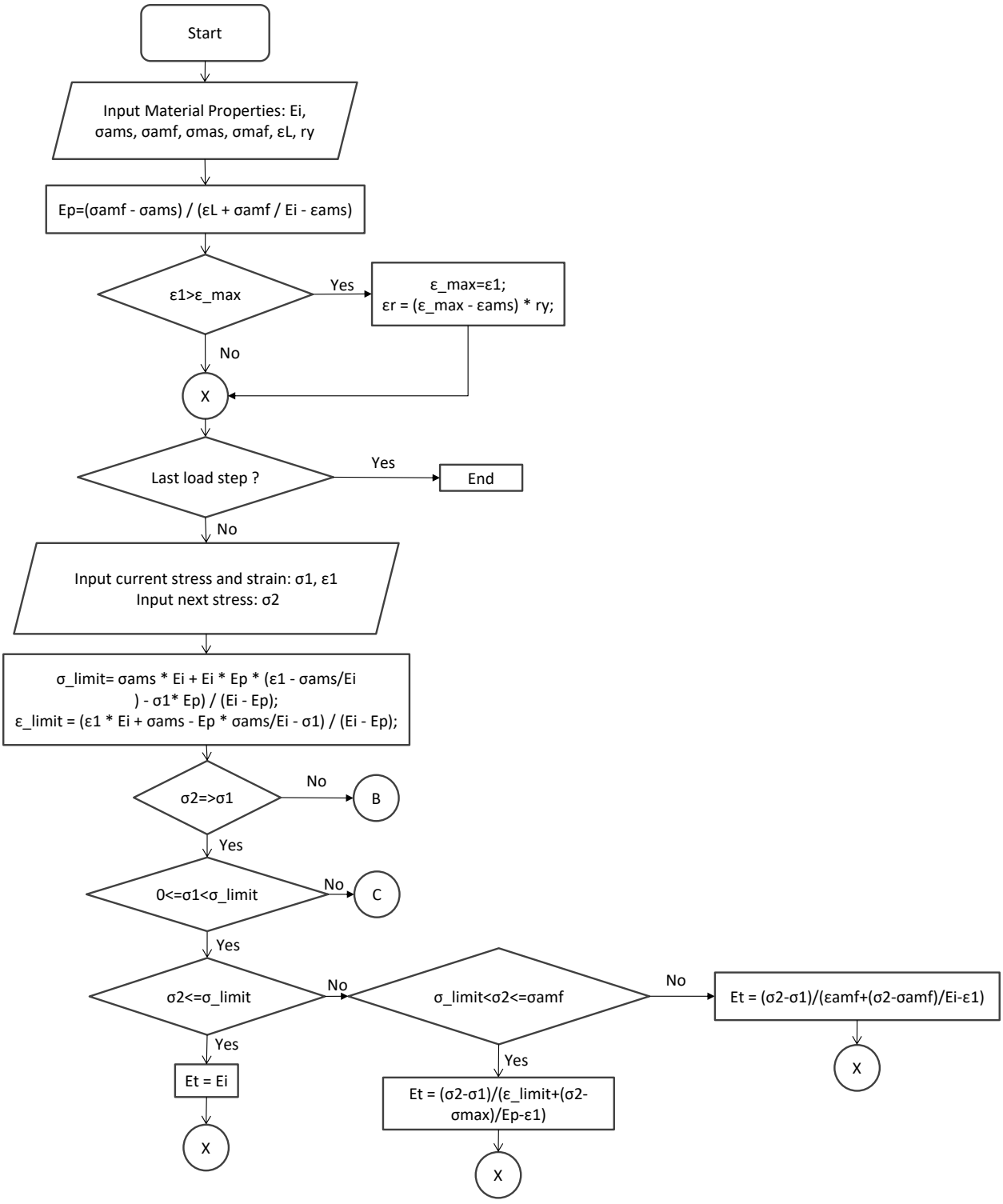

Figure 4-10: Flowchart of the SMA material hysteresis model

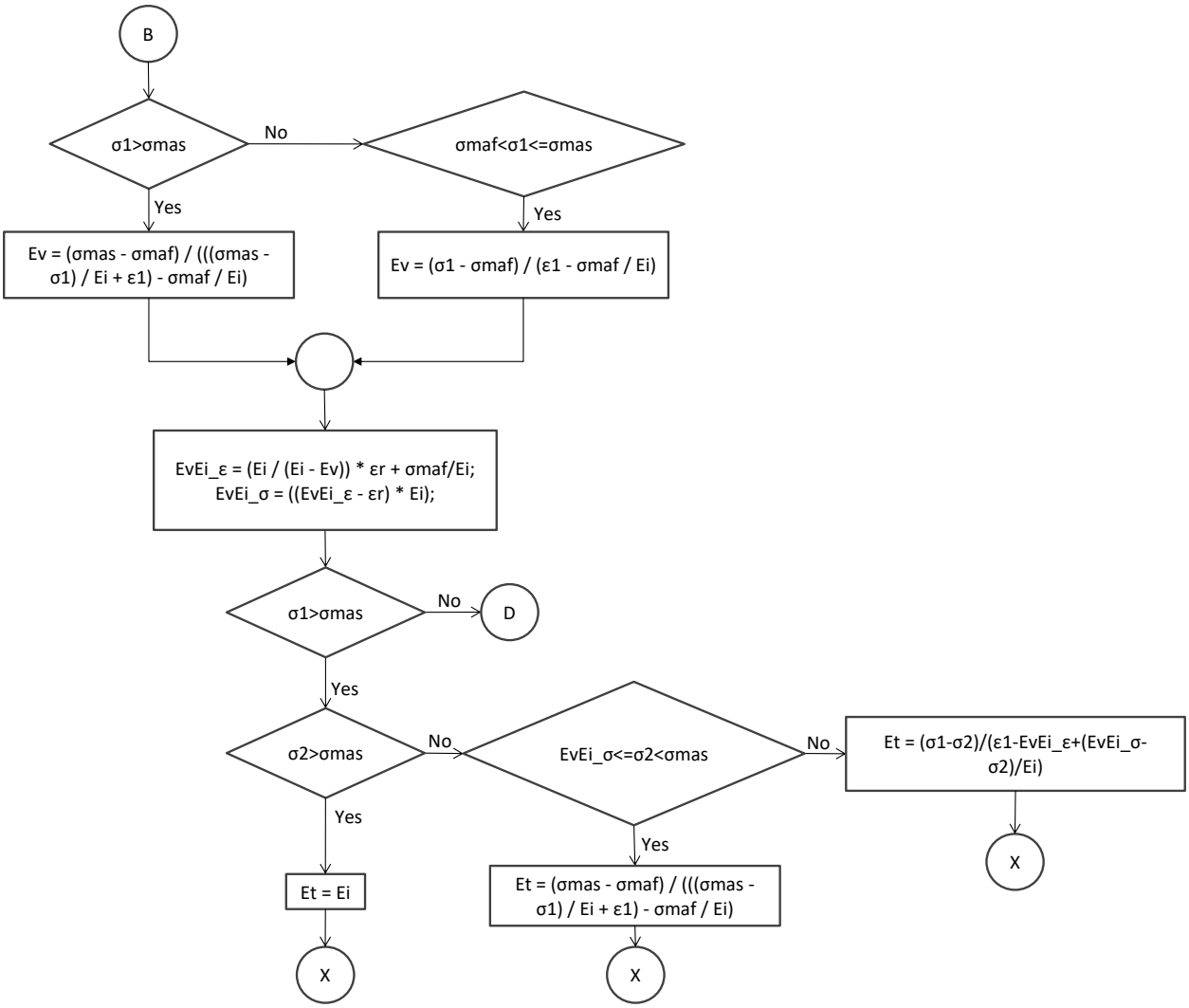

Figure 4-10: Flowchart of the SMA material hysteresis model (Continued)

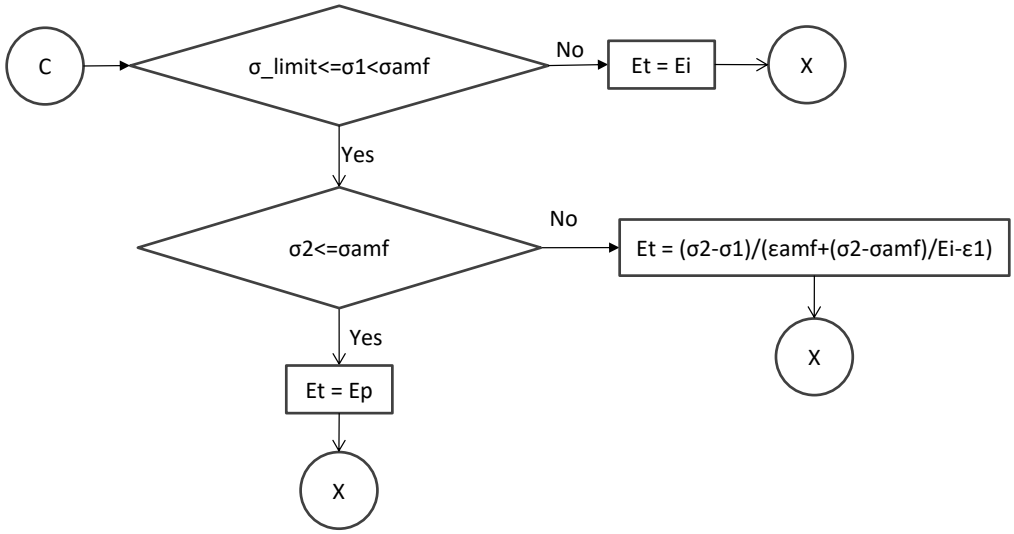

Figure 4-10: Flowchart of the SMA material hysteresis model (Continued)

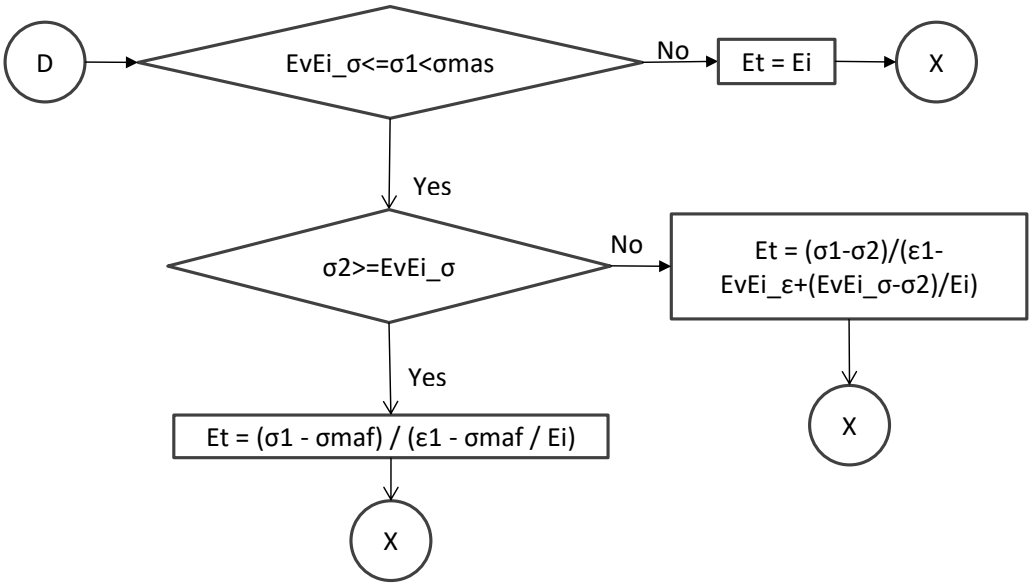

Figure 4-10: Flowchart of the SMA material hysteresis model (Continued)

The explanation of the parameters used in the flow chart (Figure 4-10) is given in Table 4-1.

Table 4-1: Description of the flow chart parameters

Parameter	Description	Typical value
E_i	Initial elastic modulus of SMA	62500 Mpa
σ_{ams}	Austenite to martensite starting stress	400 Mpa
σ_{amf}	Austenite to martensite finishing stress	510 Mpa
σ_{mas}	Martensite to austenite starting stress	370 Mpa
σ_{maf}	Martensite to austenite finishing stress	130 Mpa
ε_L	Plateau Strain	0.06
r_y	Residual to plastic strain ratio	0.1
E_p	Modulus during austenite to martensite transition state	3%-4% of Ei
ε_1	Current Strain	N/A
$\varepsilon_{\_max}$	Previous Maximum Strain	N/A
ε_r	Residual strain	N/A
σ_1	Current Stress	N/A
σ_2	Stress at next loading step	N/A
σ_{limit}	Stress limit of a line with E_i tangent passing through $(\varepsilon_{ams}, \sigma_{ams})$ point	N/A
ε_{limit}	Strain at σ_{limit} point	N/A
E_t	Tangent modulus	N/A
E_v	Variable tangent modulus of a line unloading from σmas stress level and directed towards $(\varepsilon_{maf}, \sigma_{maf})$ point of the backbone curve	N/A
$E_vE_i\_\varepsilon$	Strain at the intersection point between an unloading line with E_v tangent and a line with Ei tangent going through $(\varepsilon_r, 0)$ point	N/A
$E_vE_i\_\sigma$	Stress at the intersection point between an unloading line with E_v tangent and a line with Ei tangent passing through $(\varepsilon_r, 0)$ point	N/A

The function mentioned above was called from a MATLAB (2012) finite element program specifically developed for the PBSC bracing system. Another material model function was used for the steel shaft of the PBSC brace. That material model is based on bilinear kinematic hysteresis typically used for steel sections. The finite element program takes quasi-static loading as input and at every load step calls the corresponding material models for the relevant brace elements. For example, it calls the SE SMA material model for the SMA bars and bilinear kinematic hysteresis model for the steel shaft. Based on the current stresses in the elements, the material hysteresis models return the appropriate tangent modulus values to the solver. The solver calculates the element stiffnesses from the material tangent modulus. These stiffness values are used to create the global stiffness matrix. Finally, the global deformation matrix is calculated based on the global

force and stiffness matrix. The brace geometry is updated, and the program fetches the incremental loading data from the next load step. A flow chart of this overall process is shown in Figure 4-11. It can be seen from the flow chart that there is no particular element for representing the gap element. The gap is automatically taken care of by keeping the elongated tie bar lengths in memory. Due to the use of SMA material model with residual deformation, the tie bars are subjected to plastic deformation which changes their lengths permanently. When the load reverses from either tension to compression or vice versa, the previously loaded ties are deactivated, and their final elongated lengths are kept in the memory. The length data is reloaded to the memory when the load reverses its sign again. When this sudden length change occurs inside the brace, this generates a displacement data without any force; which results in a sliding response in the hysteresis shape.

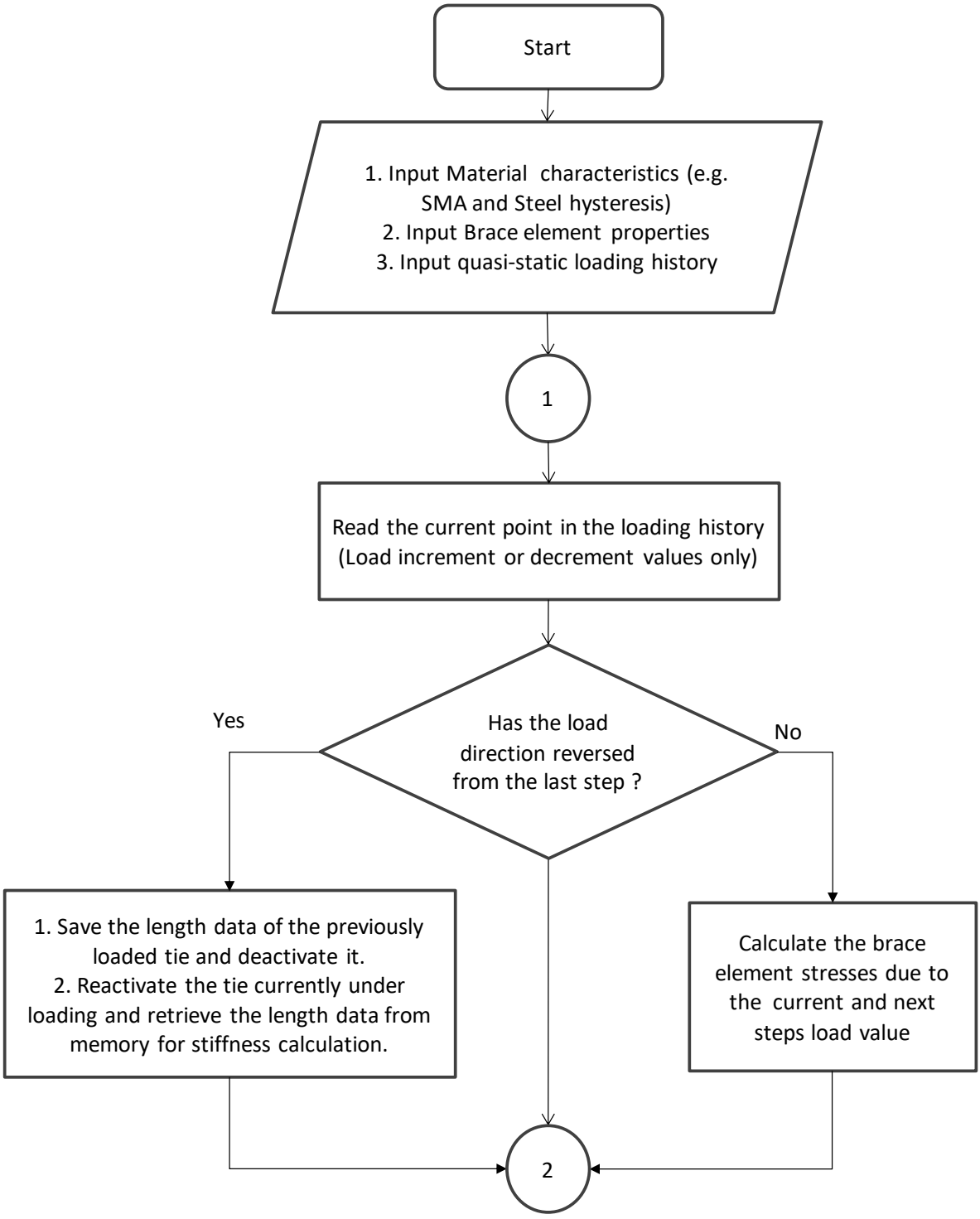

Figure 4-11: Flow-chart of the MATLAB PBSC analysis program

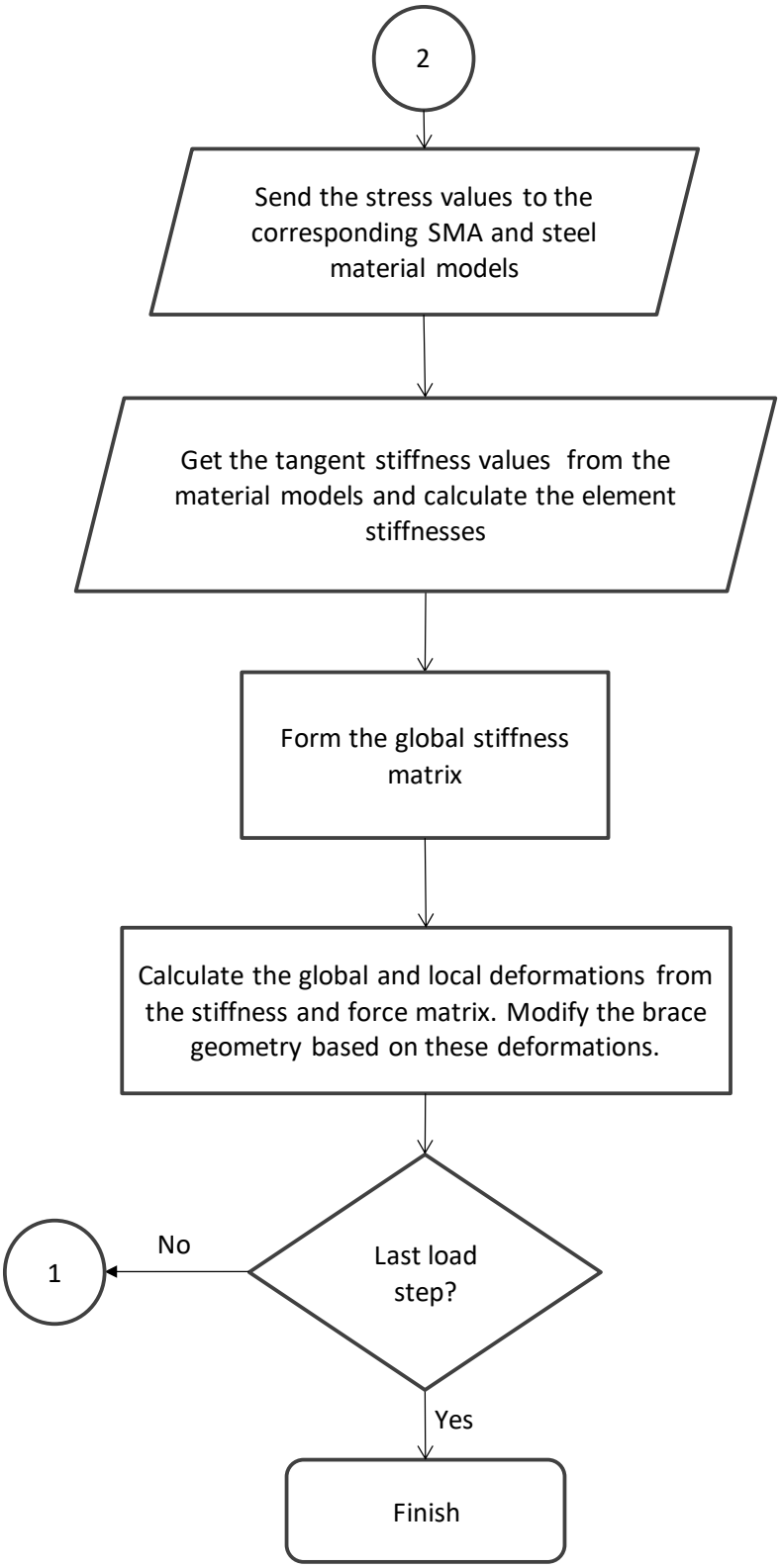

Figure 4-11: Flow-chart of the MATLAB PBSC analysis program (Continued)

4.8 Quasi-static response from MATLAB

Based on the procedure described above, a load controlled quasi-static analysis was carried out on the PBSC bracing system. Figure 4-12, Figure 4-13 and Figure 4-14 show the input loading history, deformation response and the global brace hysteresis response, respectively. With residual deformation taken into consideration, the brace shows different behavior compared to the one without residual deformation (Haque and Alam 2015a). The system shows a sliding response at the force-deformation origin. In this analysis, residual strain was 10% of the maximum plastic strain. The following section property data shown in Table 4-2 were used for this analysis.

Table 4-2: Section properties used for the PBSC MATLAB model

Description	Length (m)	Number	Cross section	Material
Shaft	4	1	HS219x9.5	Steel
Tie	1	2 in each direction	20mm diameter	SMA

For the SMA model, following transformation stresses were used. Austenite to martensite starting stress (400MPa), austenite to martensite finishing stress (510MPa), martensite to austenite starting stress (370MPa) and martensite to austenite finishing stress (130MPa). The modulus of elasticity of SMA was set to 62.5GPa. The plateau strain was assumed to be 0.06%, and the residual to plastic deformation ratio was set to 0.1 or 10%. Using these section properties and the loading history shown in Figure 4-12, a quasi-static analysis was carried out. Figure 4-12 shows the global brace deformation response due to this applied loading and Figure 4-13 shows the global load deformation hysteresis response of the brace. The previously mentioned sliding behavior can be observed near the origin. This is generated due to the 10% residual to plastic deformation ratio included in the SMA material model.

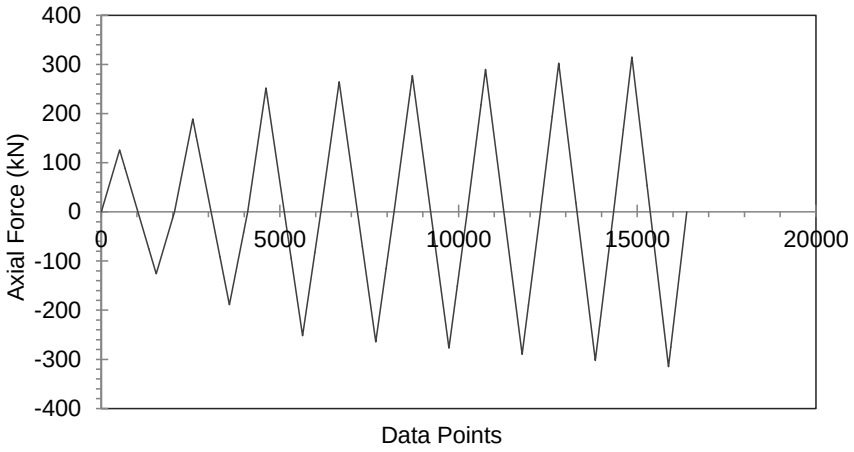

Figure 4-12: Input loading history for the MATLAB FE model

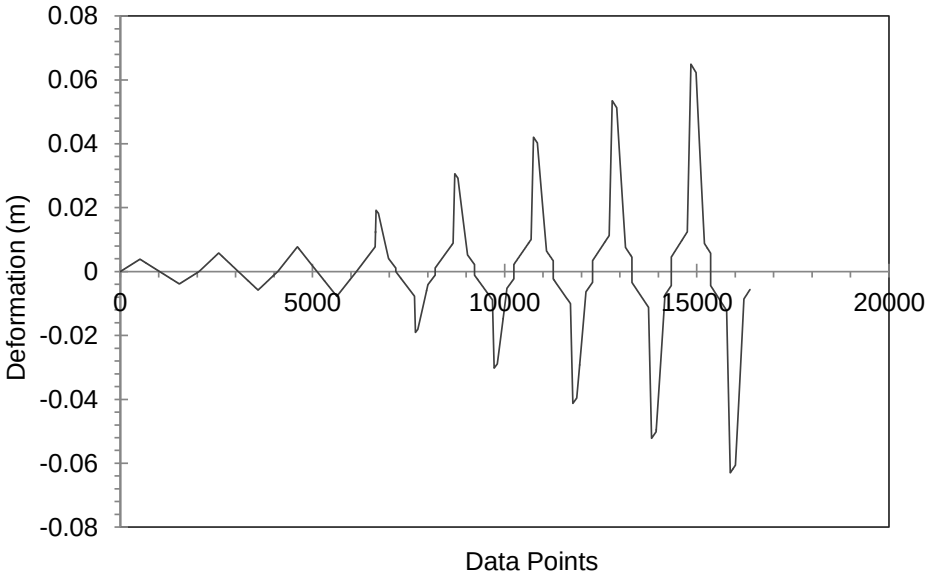

Figure 4-13: Output deformation history from the MATLAB FE model

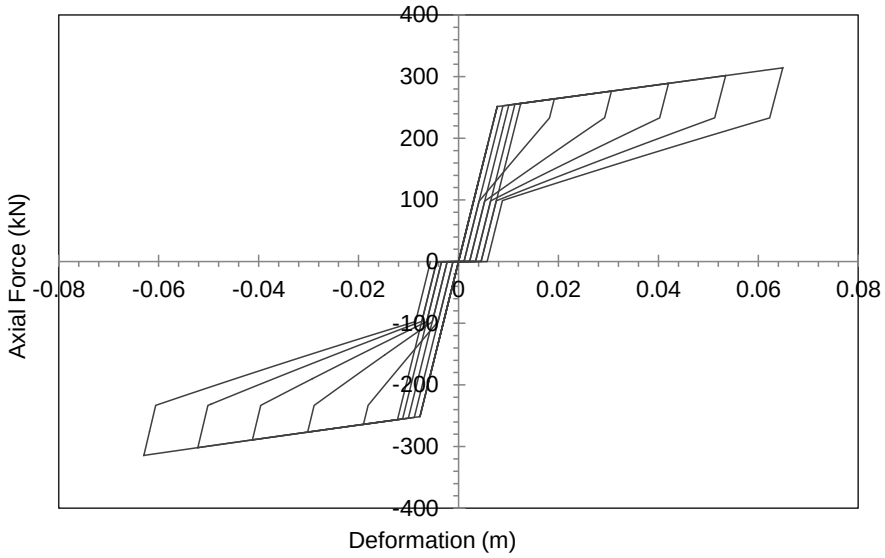

Figure 4-14: Hysteresis response of the PBSC bracing system from MATLAB FE model

The sliding or slippage at the force-deformation origin could result in an impact loading between the piston plate and the nuts/couplers during load reversal. However, this slippage and related impact could be significantly reduced by using Belleville springs/washers between the couplers/nuts and the piston plates.

4.9 Validation

The hysteresis model developed for the PBSC bracing system was validated using an ABAQUS FE model of the PBSC bracing system. As ABAQUS (2014) does not have an SMA material model capable of simulating residual strain, the model was used to test the MATLAB hysteresis model with residual deformation coefficient set to zero. The ABAQUS FE model utilized for this validation is shown in Figure 4-15; which is designed as per configuration 2 in Figure 3-1(b).

Figure 4-15: ABAQUS FE model of PBSC brace configuration 2.

In the model mentioned above, 2-16mm dia SMA tie bars were used for energy dissipation and self-centering of the brace. The shaft was modeled as custom hollow tubular steel section with an external diameter of 44.45mm and wall thickness of 12mm. The hollow circular sleeve section has an outer diameter of 110mm and wall thickness of 15mm. The length of the shaft, the sleeve and the SMA tie bars in the model, are 1500mm, 2000mm and 1075mm respectively. The modulus of elasticity of steel was set at 200GPa and was modeled as linear elastic. The SMA material properties used for the tie bars are provided in Table A-1 of Appendix A. A deformation loading history shown in Figure 3-11 was applied to the RP-1 reference point of the brace, and a quasi-static analysis was carried out. After the analysis, the hysteresis response shown in Figure 4-16 was observed; which is similar to the hysteresis response of configuration 1 of the PBSC bracing system (Figure 3-18). For validation of the MATLAB FE model, the loading history from the ABAQUS analysis output was extracted and provided as input to the MATLAB PBSC brace model. After some minor parameter adjustment using trial and error, the following hysteresis was observed in the MATLAB model (Figure 4-16). It has been found that the MATLAB-based model

of the PBSC bracing system can very accurately simulate the hysteresis of the ABAQUS PBSC brace model. Furthermore, the MATLAB-based model requires few seconds of run time compared to multiple hours in ABAQUS. Therefore, the MATLAB model can be used for very rapid analysis and design of the PBSC brace.

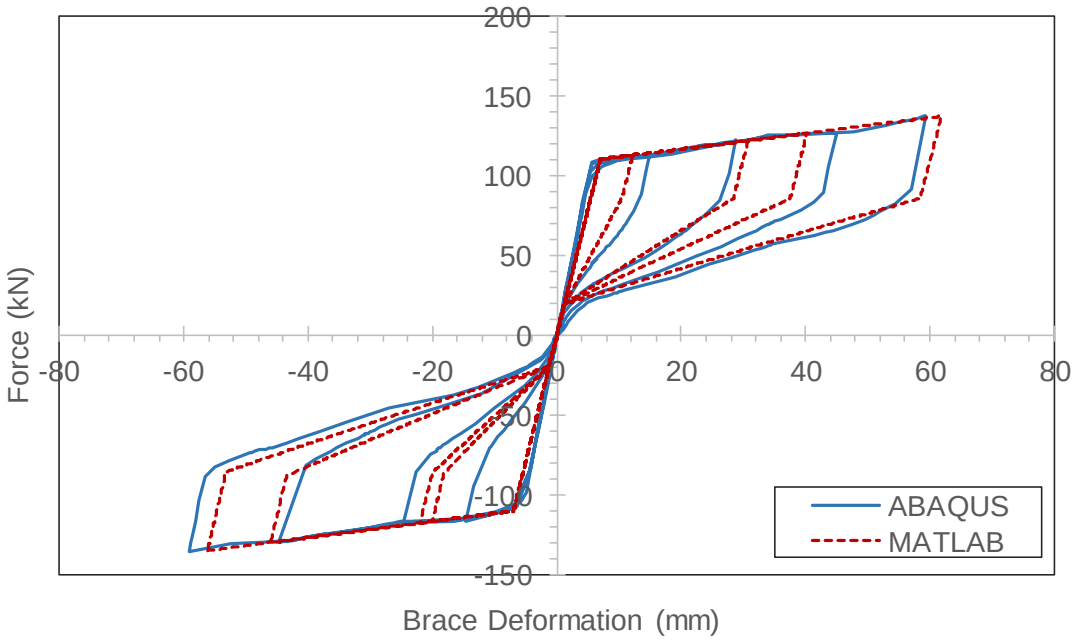

Figure 4-16: Hysteresis Model validation using ABAQUS FE model.

4.10 Hysteresis rules

Based on the observed response (Figure 4-14), a novel SMA flag hysteresis rule has been developed for simulating the behavior of PBSC bracing system. This novel flag hysteresis rule with sliding response is presented below. The following definitions should be taken into consideration for interpreting the hysteresis rules: loading refers to an increase in the absolute magnitude of the force (disregarding the sign of the force). This means that in positive force quadrants loading relates to an increase in value and vice versa. “Load reversal” refers to a situation where the loading or unloading line crosses the horizontal deformation axis, and the sign of the

load gets reversed. Yielding refers to reaching a line with k_2 stiffness passing through either the positive (d_y, F_y) or negative ($-d_y$, $-F_y$) yield deformation-action point. Furthermore, K_v is a variable stiffness of any line coming from the constant 'F_r' force level and going towards ($\alpha F_y/k_1, \alpha F_y$) point on the backbone curve. Refer to Figure 4-17 for understanding other parameters discussed in the following hysteresis rules.

4.10.1 In positive force direction

1. Below positive yield force level
   1.1. Loading: Loading occurs if the load deformation point is on the right side or on the line with k_1 stiffness and passing through (d_{ri}, 0) point. Any deformation left of this line follows zero stiffness, which results in zero force/Action. The loading line follows k_1 stiffness and loading continues at this stiffness until the loading line reaches a line with stiffness k_2 passing through backbone curve's yield deformation-action point ($F_y/k_1, F_y$). Arriving at this line yields the system. Go to rule 2.
   1.2. Unloading:
      1.2.1. If unloading from a force level higher than *'F_r'* then the unloading line follows k_1 stiffness. When the line reaches F_r force level go to rule 1.2.2.
      1.2.2. If unloading from a force level lower than or equal to *'F_r'* but higher than the intersection point between a line with stiffness k_1 passing through (d_{ri}, 0) and the unloading line with k_v stiffness coming from F_r force level; the unloading line is directed towards ($\alpha F_y/k_1, \alpha F_y$) point on the backbone curve. When the line with k_v stiffness intersects the line with k_1 stiffness passing through (d_{ri},0) point then go to rule 1.2.3
      1.2.3. If unloading from a point on or below the intersection point defined in 1.2.2: The unloading line follows k_1 stiffness.
   1.3. Load reversal: Go to the section named "In negative force direction".
2. After Yielding

2.1. The line follows the post-yield stiffness (k_2) until it reaches the forward (Austenite to martensite finishing force) transformation finishing force level (F_{ff}). After reaching F_{ff} go to rule 3

2.2. Unloading: Go to rule 1.2.1

3. At or above F_{ff} force level:

3.1. Loading: The loading line follows k_1 stiffness.

3.2. Unloading: Go to 1.2.1

4.10.2 In negative force direction

4. Above negative yield force level

4.1. Loading: Loading occurs if the load deformation point is on the left side or on the line with k_1 stiffness and passing through ($-d_{ri}$, 0) point. Any deformation on the right side of this line follows zero stiffness, which results in zero force/Action. The loading line follows k_1 stiffness and loading continues at this stiffness until the loading line reaches a line with stiffness k_2 passing through the negative yield deformation-action point ($-F_y/k_1$, $-F_y$). Reaching this line yields the system. Go to rule 5.

4.2. Unloading:

4.2.1. If unloading from a force level lower than *'$-F_r$'*, the unloading line follows k_1 stiffness. When the unloading line reaches F_r go to 4.2.2.

4.2.2. If unloading from a force level higher than or equal to *'$-F_r$'* but lower than the intersection point between a line with stiffness k_1 passing through *($-d_{ri}$, 0)* and the unloading line with k_v stiffness coming from $-F_r$ force level; the unloading line is directed towards *($-\alpha F_y/k_1$, $-\alpha F_y$)* point on the backbone curve. When the line with k_v stiffness intersects the line with k_1 stiffness passing through *($-d_{ri}$,0)* point then go to rule 4.2.3

4.2.3. If unloading from a point on or above the intersection point defined in 4.2.2: The unloading line follows k_1 stiffness.

4.3. Load reversal: Go to rule "In positive force direction".

5. After Yielding

5.1. The line follows the post-yield stiffness (k_2) until it reaches the forward (Austenite to martensite finishing force/action) transformation finishing force/action level (-F_{ff}). After reaching F_{ff} go to rule 6

5.2. Unloading: Go to rule 4.2.1

6. At or below -F_{ff} force level:

6.1. Loading: The loading line follows k_1 stiffness.

6.2. Unloading: Go to 4.2.1

Residual deformation values are calculated every time a deformation cycle exceeds the previous maximum deformation in the respective direction. This means that positive and negative deformations are independently calculated and they do not affect each other. The residual deformation "d_r" is calculated using the following expression.

*(Maximum deformation of the cycle - Yield deformation) *Residual deformation Coefficient*

Figure 4-17 depicts the proposed PBSC brace hysteresis model with sliding deformation. Three consecutive cycles have been shown here with loading/unloading directions marked with arrows. As this hysteresis has many rules and branch prediction equations, for the brevity of this thesis the flow chart is not given here. However, the visual basic macro code developed for generating this hysteresis model plots is provided in the appendix.

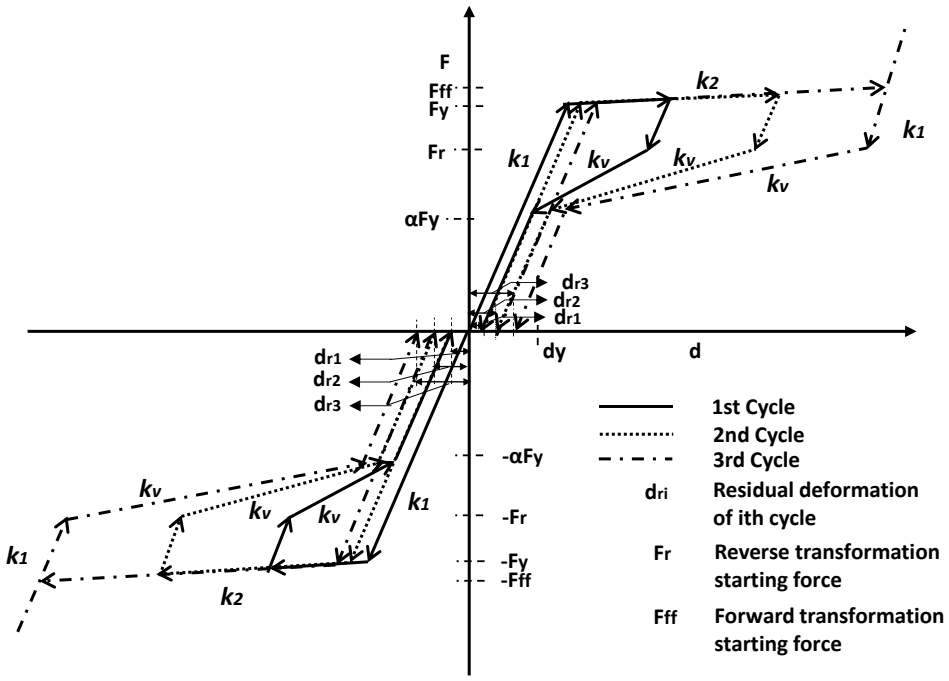

Figure 4-17: SMA flag-shaped hysteresis model with sliding response.

4.11 Response under quasi-static loading

The hysteresis rule presented above was coded in Visual Basic for Application (VBA) for testing/debugging with various loading histories. The program was coded in deformation controlled manner; therefore, the program takes deformation history as input and produces loading history as output; which is necessary for implementation in traditional finite element analysis and design software. Three types of deformation loading histories were used for this exercise; these are Triangular, harmonic and transient. These deformation histories were carefully scaled to produce a nonlinear response, which resulted in a full cyclic response. Full hysteresis responses are very helpful in finding out anomalies/bugs in the code. At the initial stage of this hysteresis model development, the resultant hysteresis response had many outlier points. For some of the test cases, the resultant hysteresis was asymmetric for a symmetric input deformation history; which is an indication of a bug in the code. The test cases shown in Figure 4-18, Figure 4-19 and Figure 4-20 were used for detecting such bugs. After detection of these bugs, they were carefully fixed

until the desired response was found as per the hysteresis rules laid out earlier in section 4.10. Figure 4-18 shows the link hysteresis code response under three types of triangular loading histories. Figure 4-18(a) is the most common loading protocol which starts from zero and gradually increases in magnitude in every subsequent load cycles. The hysteresis response due to this deformation loading history is shown in Figure 4-18(b). The result shows two flag-shaped hysteresis plots separated by both force and deformation axes. The hysteresis response is symmetric; which validates the input deformation history. Figure 4-18(c) shows a deformation history which starts with larger magnitude cycles and eventually decreases to zero and then again increases to the initial values. This loading history was specifically chosen to see the effect of large residual deformation in the initial cycles on the response of latter smaller magnitude cycles. The hysteresis response (Figure 4-18(d)) shows that the initial larger cycles have a profound effect on the subsequent cycles. As residual deformation in the PBSC bracing system cannot decrease, the subsequent cycles even with smaller magnitudes had same large residual deformations as the initial cycle. It can also be observed that the smaller magnitude cycles did not add any residual deformation to the initial cycles which is in agreement with experimental results by Paradis et al. (2009). They found that once SMA has strained to a large value any subsequent cycle to a strain near that value add up residual strain at a much lower rate. This additional residual strain accumulation can be safely ignored in engineering analysis. The last loading history (Figure 4-18 (e)) is saw tooth shaped with only single directional/signed deformation history. The resulting hysteresis (Figure 4-18(f)) shows no negative force even though the unloading lines touched the deformation axis at non-zero deformation points. After reaching the deformation axis, the stiffness changed to zero which resulted in zero forces.

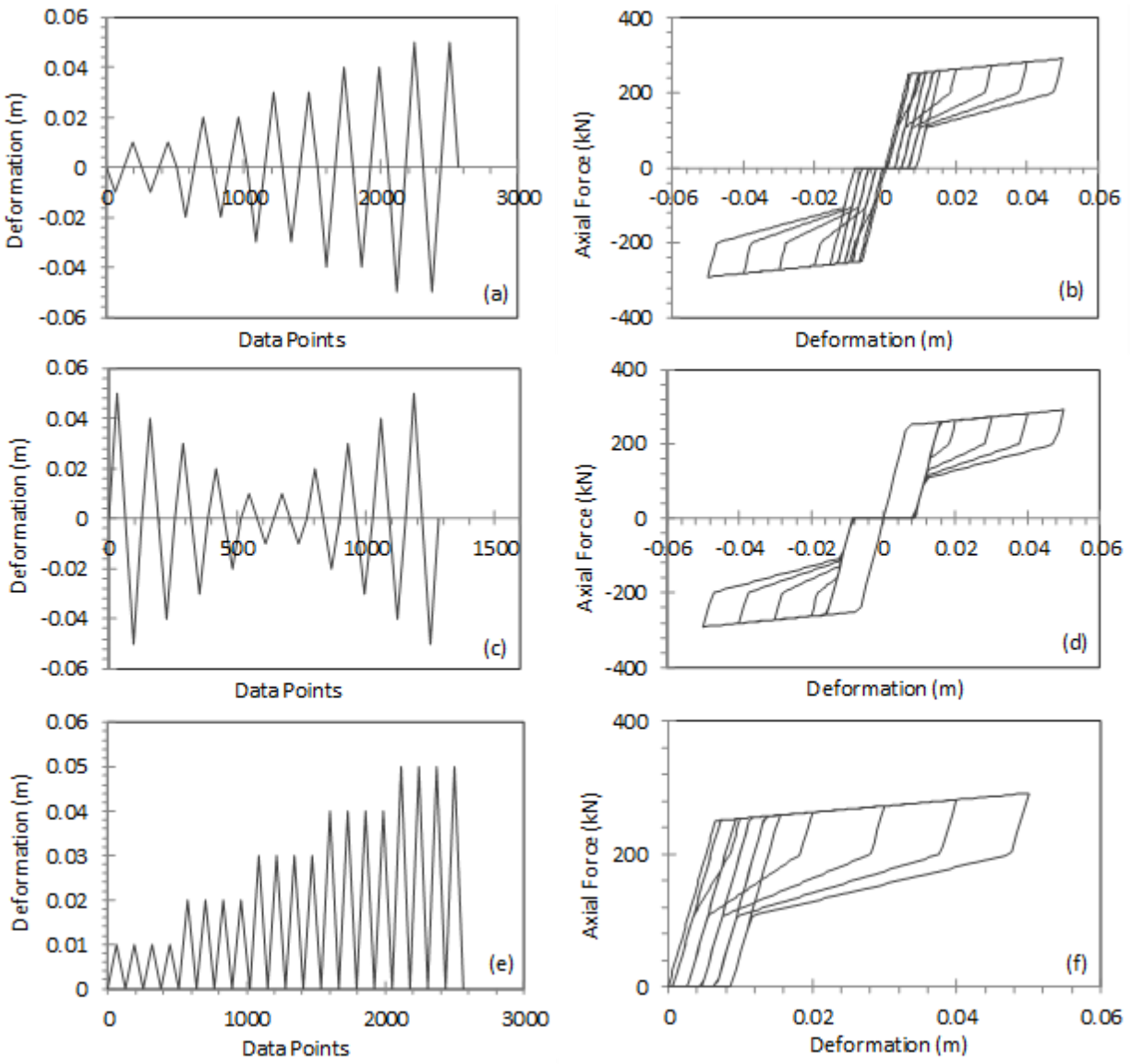

Figure 4-18: PBSC brace hysteresis under different types of triangular loading

Figure 4-19 (b) and Figure 4-19 (d) show the responses of the PBSC hysteresis model under harmonic excitation shown in Figure 4-19 (a) and Figure 4-19 (c), respectively. Both deformation histories are similar where the only difference is that their signs are reversed. This sign reversal was done to find bugs in the symmetric part of the code as any asymmetric response is a sign of asymmetry in the code. However, the resultant hysteresis was found satisfactory as per expectation.

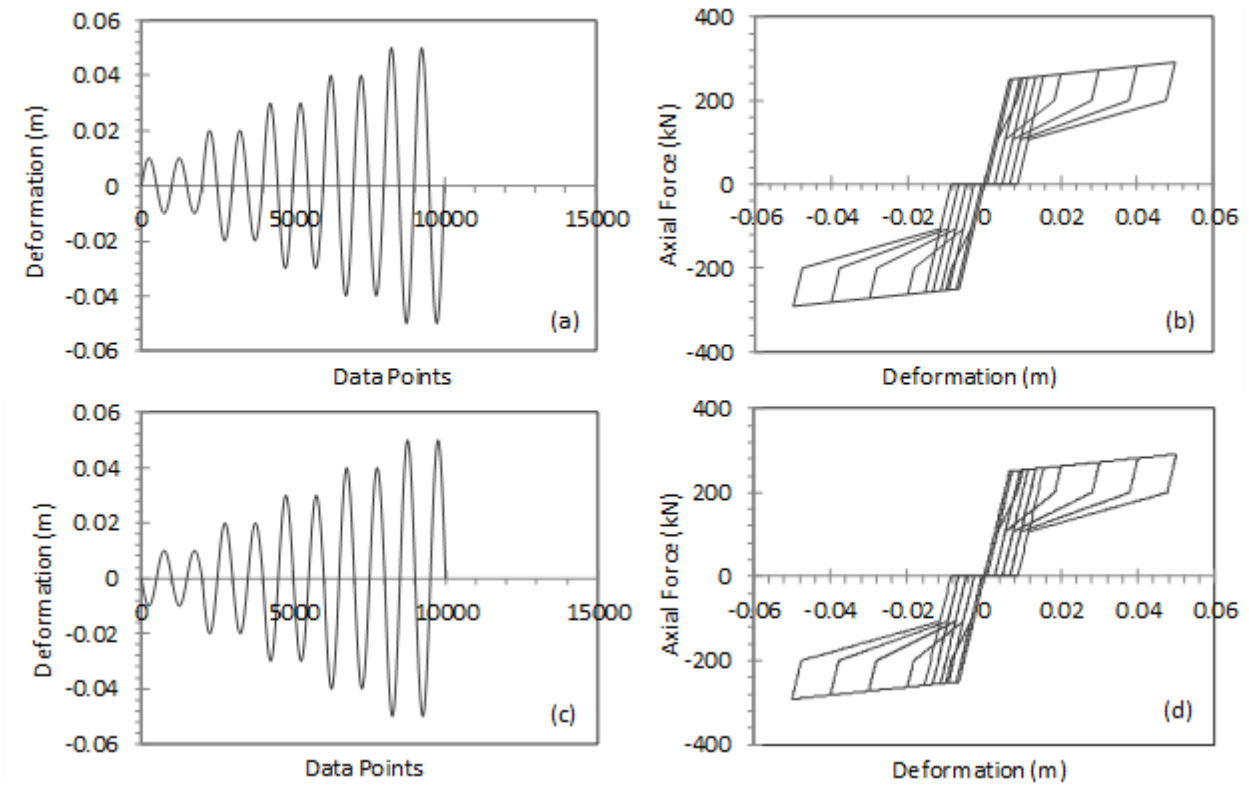

Figure 4-19: PBSC brace hysteresis under harmonic loading with increasing magnitude

Figure 4-20 (b), Figure 4-20 (d) and Figure 4-20 (f) show the PBSC hysteresis model response under irregular transient loading histories shown in Figure 4-20 (a), Figure 4-20 (c) and Figure 4-20 (e) respectively. Figure 4-20 (a) shows a highly asymmetric input deformation history and the resultant response is shown in Figure 4-20 (b). Figure 4-20 (b) shows a loading history comparable to an earthquake deformation history record. The resultant hysteresis response (Figure 4-20 (d)) is shown on the right-hand side. As the input deformation is asymmetric, the output hysteresis was also found similar. Figure 4-20 (e) shows a very unusual loading history; this sine plus step function is created using very few number of data points. The gaps between some of the points are intentionally made very large. These large gaps require multiple hysteresis branches to be predicted in advance. To create a hysteresis response for these loading histories, a branch prediction algorithm was developed inside the hysteresis code. This code can accurately predict

which hysteresis branch/rule to follow if there is a large gap in the input data. This prediction not only makes response calculations more accurate but also requires much less time history data points than usual. Therefore, during time history analysis, if larger time steps are used than usual, the accuracy does not get affected.

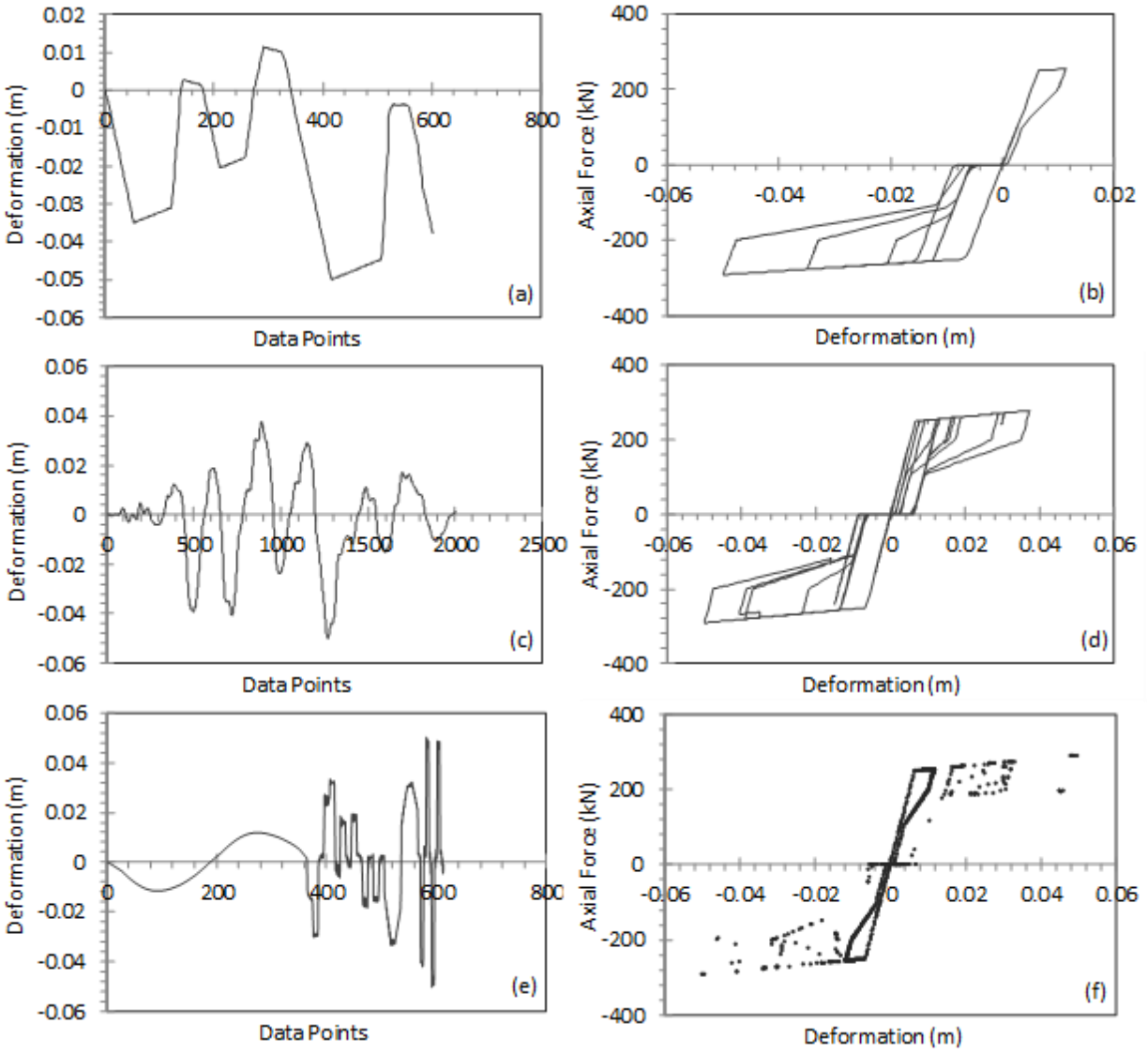

Figure 4-20: PBSC brace hysteresis under transient loading

To show the validity of the response obtained from the input deformation history of Figure 4-20 (e), only the points are plotted in Figure 4-20 (f). All the data points in this plot fall inside the flag shaped hysteresis.

4.12 Analysis model

A six-storied tall, 4x4 bay steel braced frame was considered in this study. The bay widths are 5m, and story heights are 3m each. Therefore, the total width of the building in two orthogonal directions is 20m, and the total height is 18m. The braces are only installed on the perimeter frames of the building. To design the braces for full lateral-load arising from the seismic events, all beams were connected to the columns using moment released connections; and the columns were restrained to the foundation using hinges. Nevertheless, the columns were modeled as continuous members along their heights. The modeling was done in a way that the structure becomes unstable under lateral loading if braces are not installed. The braces were modeled using pin ended connections and were installed as inverted "V" in the middle two bays. In this configuration, only the braces will resist the lateral load arising from the earthquake. The slabs were modeled using 150mm deep concrete shell sections. However, for clarity, it is hidden from the view in Figure 4-21. The following loading was applied to the floor slabs (except the roof) in the gravity direction. Superimposed Dead Load: 2kN/m^2, live load: 2.4kN/m^2. On the roof, the dead load was considered as 0.5 kN/$m^{2,}$ and snow load was taken as 2.2 kN/m^2. Furthermore, another 1.6kN/m^2 on the roof was considered for miscellaneous storage and mechanical services loads. After the structural modeling, the frame was analyzed under both gravity and seismic loading. The seismic zone considered for this analysis was "Vancouver, " and the soil class was taken as class "C."

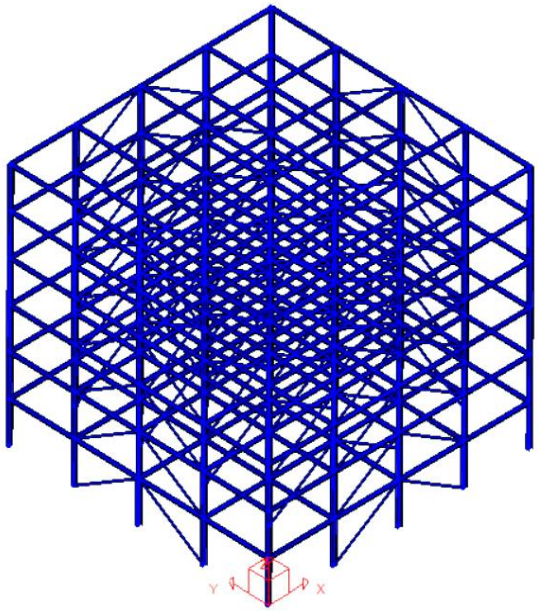

Figure 4-21: Three-dimensional model of the steel building

The peak ground acceleration value for Vancouver response spectrum is 0.47g. The peak spectral acceleration values for this seismic zone is given in Table 4-3. For this building, both the importance factor and higher mode effect were taken as 1.0. As R_d and R_o are unknown for the PBSC braced frames, they were estimated based on preliminary analysis using FEMA P695 (FEMA 2009) guideline. This preliminary analysis suggested an R_d value of 6.0 and R_o value of 1.1. These values were later confirmed using detailed analysis; the details of which can be found in CHAPTER 5: Furthermore, designing this braced frame with a low R_d value (4 or below), may not induce nonlinearity in the braces; which will prevent us from utilizing the self-centering capability of this bracing system. Furthermore, if this building can resist seismic load and can also self-center after designing with a large R_d value (6.0), then the performance advantage of this novel bracing system will be confirmed.

Table 4-3: Spectral acceleration values for Vancouver Soil Class "C"

Sa(T)	Sa (0.2)	Sa (0.5)	Sa (1.0)	Sa (2.0)	Sa (4.0)
Acceleration (g)	0.95	0.65	0.34	0.17	0.085

After carrying out the analysis and design using CSA S16-14, it was found that the minimum required sections for the beams and columns are W250x24 and W310x67, respectively. It was also figured out that the minimum required size for the brace for the upper three floors is HS127x4.8. For the 2nd and 3rd floor the required section is HS127x6.4, and finally, on the ground floor, the required size is HS127x8.0.

As nonlinear dynamic time history analysis of three-dimensional building frames is computationally intensive, a two-dimensional model was created using the outer perimeter frame. To run the analysis only in two-dimensions, the following restraint condition was applied to the nodes. All the nodes except the foundation were restrained in U_y, R_z and R_x degrees of freedom. The foundation nodes were restrained in U_x, U_y and U_z directions only. Furthermore, the brace ends were moment released in both local orthogonal planes (M_y and M_z); additionally, the torsion was also released at one end. This end release condition prevents bending moment generation or transfer to and from the building frame. The previously mentioned gravity loading (Dead, Snow, and Storage) and self-weight of the slab were calculated and applied to the beams as uniformly distributed load as a seismic mass. For dead, and self-weight a multiplier of 1.0 was used; whereas, for the snow and storage loads 0.25 and 0.6 were used. The nodal restraint conditions and the gravity loading on the beams are shown Figure 4-22(a) and the uniformly distributed loading condition is shown in Figure 4-22(b).

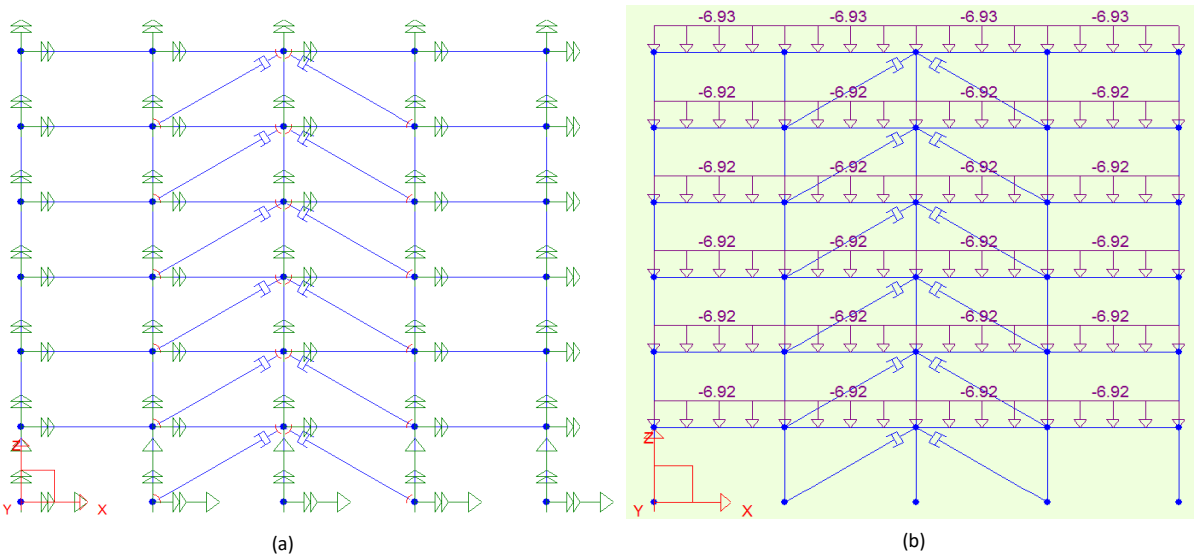

Figure 4-22: (a) Nodal Restraint Conditions (b) Uniformly distributed gravity loading on the beam for the 2D model.

The dashpot shapes shown at the end of the braces represents the zero length link elements. To calculate the hysteresis model's input parameters, three different PBSC braces were designed for the three different brace sections used in this frame. In order to design the PBSC braces, the ultimate design loads which were used to design the brace sections were retrieved from the software. The envelopes of all the design load cases were taken and the PBSC brace was designed for it. The amount of required SMA needed for each brace was calculated using a spreadsheet specifically developed for this task. The PBSC brace design process used in the spreadsheet is as follows: the ultimate design load was divided using the austenite to martensite starting stress (σ_{ams}) of SMA to find out the required cross-sectional area of SMA bars. For this study, the value of σ_{ams} was taken as 400 N/mm^2. The result gave the necessary cross-sectional area of the SMA bars. Bar diameters were selected in a way to provide an integer value or as close to that as possible. In the next step, a design length of the SMA bars was chosen. The estimated length of the SMA bars was taken as 1/6th of the brace length or approximately 1m. This ratio has been selected based on the following assumption: buildings are generally designed for a maximum interstory drift of 2%-

2.5%. As braces are diagonal members, they typically experience 40%-50% of this drift in their axial direction; which results in a drift of approximately 1%. As NiTinol based SMAs can recover from 6%-9% strain (Dolce and Cardone 2001), we can comfortably make the NiTinol bars of the PBSC brace 1/6th to 1/9th of the total brace length. This will also result in a lot of material and cost savings. The parameters mentioned above were provided as input to the MATLAB quasi-static analyzer developed for the PBSC brace, and a hysteresis was generated. The hysteresis results were used to find out the initial and post-yield stiffness as well as the SMA unloading stiffness. These values were provided as input in the S-FRAME Software link hysteresis input window. This process was repeated three times for the three brace sections, and three links were generated. Finally, these links were assigned to the appropriate brace ends. Figure 10 shows the link input parameters used for the HS127x8 brace section.

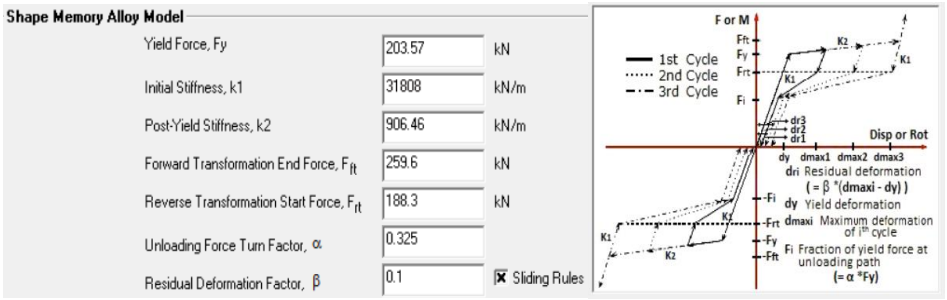

Figure 4-23: Sample input data for PBSC link hysteresis

4.13 Results

The frame mentioned above was analyzed using ten historically significant earthquake records. These records are as follows: Imperial Valley, Chichi, Corralitos, Emeryville, Trinidad, Kobe, Kocaeli, Loma Prieta, Northridge, Sakaria. These records were matched with Vancouver soil class "C" response spectrum before the analysis. The spectrum matching was done using the SeismoMatch (2015) software which utilizes the wavelets algorithm developed by Abrahamson

(1992) and Hancock et al. (2006). The scaled spectral acceleration versus time period (Sa-T) plot of the matched records is shown in Figure 4-24.

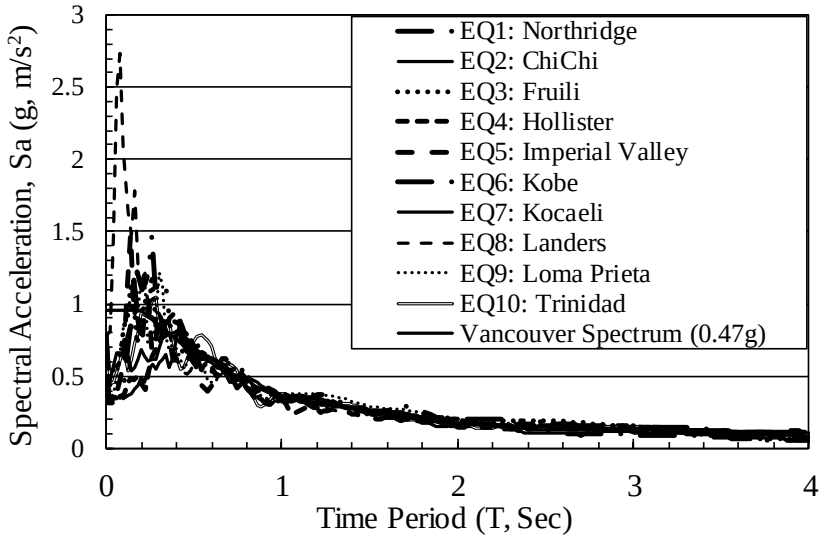

Figure 4-24: Matched response spectra of the ten earthquake records

After the spectrum matching, these ten earthquake records were used to run the nonlinear dynamic time history analysis on the braced frame. From these analyses results, the following parameters were chosen for investigation: Maximum roof drift %, Residual roof drift %, Maximum interstory drift %, and residual interstory drift %. Figure 4-25 shows the comparison between maximum roof drift % and residual roof drift % for the ten earthquake records.

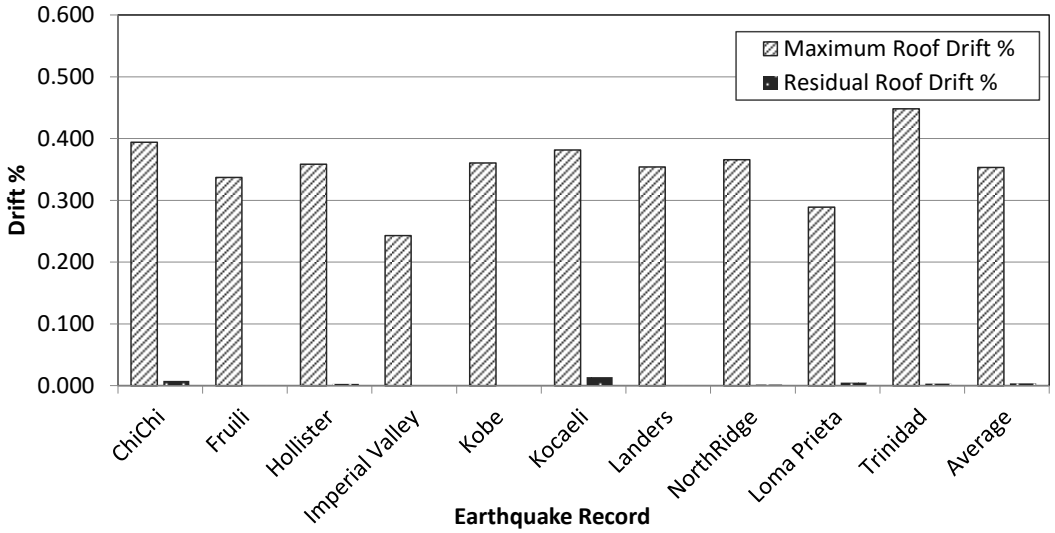

Figure 4-25: Maximum and residual roof drift %

It can be seen that the maximum roof drift % was just above 0.44% for the Trinidad earthquake record. Furthermore, the maximum "residual roof drift %" was found to be 0.014% for the Kocaeli earthquake record. For the 18m tall building frame, this equates to a value of 2.5mm. This low residual roof drift ratio can be attributed to the efficacy of this novel self-centering bracing system.

Figure 4-26(a) and (b) compares the maximum and residual interstory drift ratios for the ten earthquake records. The maximum interstory drift ratios for all ten earthquake records are very close to one another except the Trinidad earthquake. The maximum interstory drift ratios were observed mostly in the 3m and 12m level, which are the 1st and 4th floor of the building respectively.

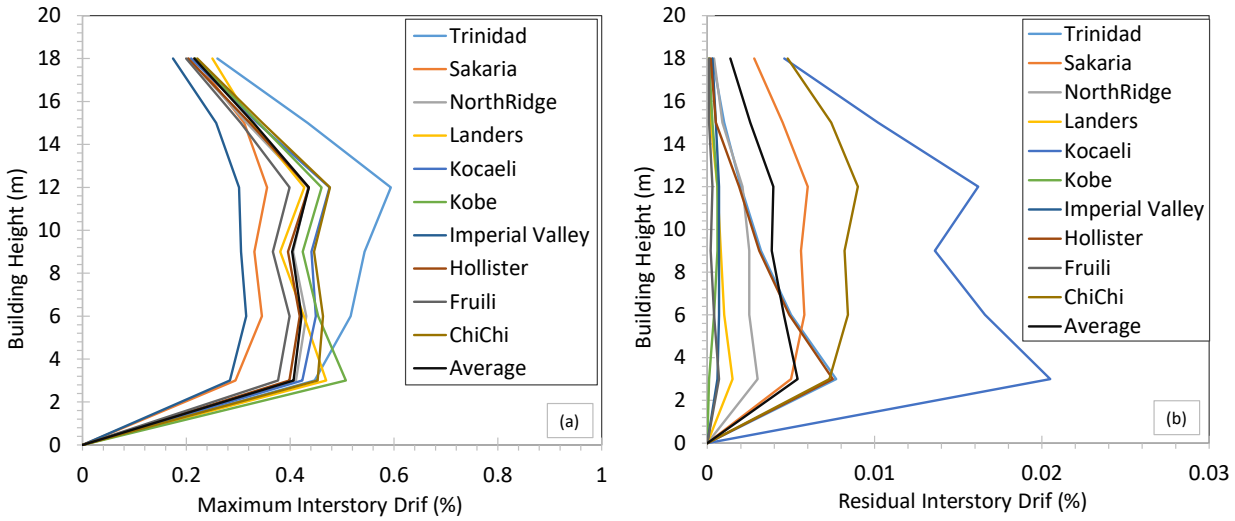

Figure 4-26: (a) Maximum interstory Drift % (b) Residual interstory Drift %

The maximum value is 0.59% which is around 1/4th of the code specified limit of 2.5% for the "Other Building" category. Furthermore, the average value was found to be around 0.4% only. On the other hand, the residual interstory drift values were found to vary more significantly between the earthquake records. The range is from almost zero to 0.02%, which is a much wider range (w.r.t max to min ratio) compared to the maximum interstory drift ratios. Like the previous plot, the maximum values are mostly observed at 3m and 12m level (First floor and fourth floor respectively). The average of the maximum was found to be around 0.005%. This value is much lower than traditional BRB frames which experience on an average 0.3% residual interstory drift ratio (Zhu and Zhang 2007).

Figure 4-27 shows the brace hysteresis for the Trinidad earthquake record. Six figures from (a) to (f) represents brace hysteresis from first to the sixth floor. It can be observed that the nonlinearity is highest on the first floor and it gradually becomes linear at the 5th and 6th floor. It can also be noted that for this low plastic deformation, the residual deformation is insignificant. Therefore, if the braces do not significantly deform in the nonlinear range, the residual deformation can be safely ignored.

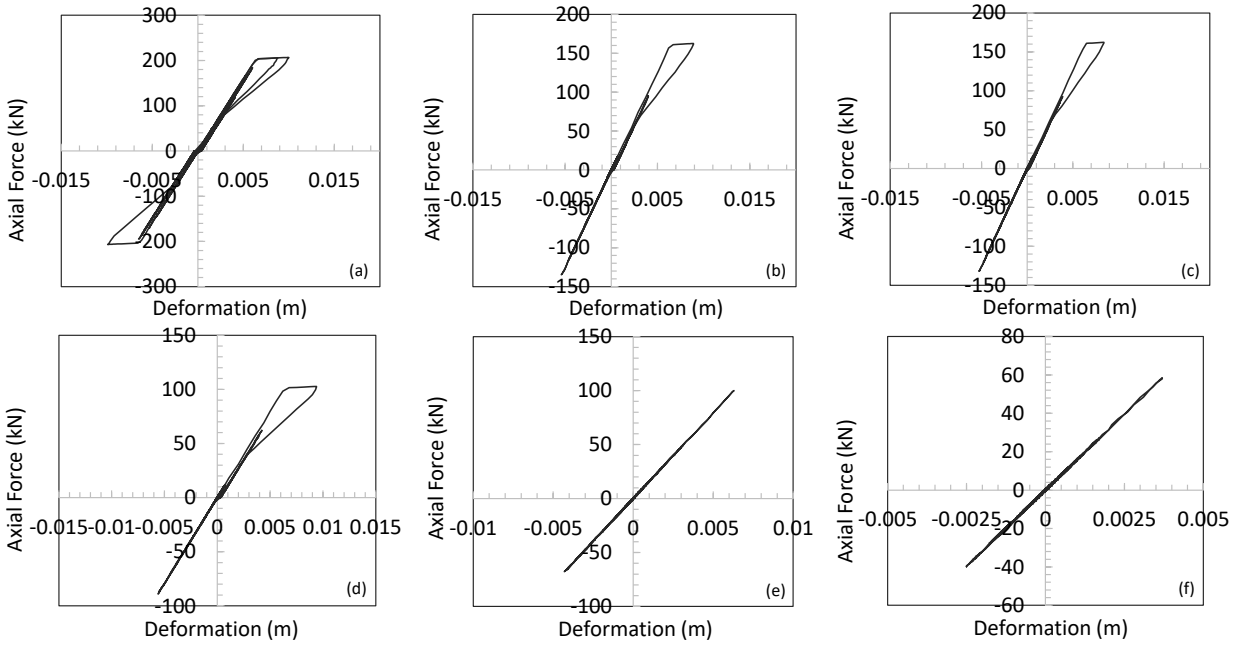

Figure 4-27: Brace hysteresis for Trinidad earthquake (a) First story (b)Second story (c)Third story (d)Fourth story (e) Fifth story and (f) Sixth story

4.14 Summary

A tension only uniaxial mechanical SE SMA material model has been developed with residual deformation simulation capability. Next, it was utilized in a custom-built MATLAB finite element solver developed for the PBSC bracing system. Quasi-static input loading history was used, and the resultant hysteresis was found to exhibit sliding behavior. The resultant hysteresis was analyzed, tested and a novel flag-shaped hysteresis with sliding response was developed. This hysteresis model was integrated into the S-FRAME Structural analysis and design software. A six-storied steel building utilizing the PBSC bracing system was designed using Vancouver soil class 'C' response spectrum. A braced frame of the building was modeled in two dimensions, and it was subjected to ten earthquake records scaled to Vancouver spectrum. Nonlinear dynamic time history analyses were carried out on the braced frame, and nodal responses were captured. Next, maximum and residual interstory drift ratios were calculated. The maximum interstory drift ratios were found well below the code specified limit. The residual interstory drift ratio was found to be insignificant

(below 0.05%). Furthermore, a similar trend was observed for the maximum and residual roof drift ratios. Based on the observed response, it can be concluded that the PBSC bracing system is excellent in controlling residual deformation in buildings. This implies that a structure fitted with this bracing system will be capable of self-centering after an earthquake.

CHAPTER 5: SEISMIC RESPONSE MODIFICATION FACTORS FOR THE PBSC BRACING SYSTEM

5.1 General

The PBSC bracing system is a novel seismic force resisting system developed by the author. Therefore, recommended values of seismic response modification factors are not available in the code for this system. Hence, it is necessary to determine these key parameters which will enable the designers to analyze and design these structures against seismic loading. There are two essential parameters which are needed for designing building frames against seismic loading as per the National Building Code of Canada (NBCC 2010). These factors are known as the Overstrength (R_o) and the ductility related force reduction factors (R_d). Together, they are also known as the response modification factor (R). In this chapter the seismic response modification factor of steel frames equipped with piston based self-centering SMA bracing system is evaluated using the method outlined in FEMA P695 (FEMA 2009) guideline. The evaluation is done in terms of collapse margin ratio (CMR), which is defined as the ratio between the median collapse earthquake intensity to the maximum considered earthquake intensity at the fundamental period of the building. For this study, four, six and eight storied 4-bay wide PBSC braced frame models are considered. These frames were designed using relevant code standard (NBCC 2010) and trial values of response modification factors (R_d and R_o). Frame elements (e.g. columns and beams) were designed using CSA S16-09 (CSA 2009) standard. The buildings were assumed to be in a high seismic zone in western Canada (Vancouver). Later, this trial value was examined and evaluated using the collapse margin ratio defined in FEMA P695 (FEMA 2009). In order develop the archetypes needed for the evaluation using collapse margin ratio, nonlinear building frame

models were built in a state-of-the-art finite element analysis and design software called S-FRAME. Nonlinear hysteresis behavior of these braces was modeled using the SMA flag hysteresis model with sliding response developed in chapter 4. A set of 44 near-field ground motion records from 22 individual seismic events provided in the FEMA P695 (FEMA 2009) document was used to perform incremental dynamic time history analysis (IDA) on the building frames mentioned above. Besides IDA, nonlinear static pushover analysis was also carried out for the determination of seismic overstrength factor. From this analysis, median collapse earthquake intensities were determined, and these values were used to calculate the collapse margin ratio. These collapse margin ratios were adjusted for spectral shape factor and period based ductilities of these frames. The adjusted collapse margin ratios were compared against acceptable limits provided in FEMA P695 guideline. If the values of these adjusted collapse margin ratio fell outside the acceptable range, new R_d and R_o values were selected, and the whole procedure was repeated until they were found acceptable. After multiple trials, the results from all the archetypes showed that the seismic performance factors calculated in this study satisfy the acceptance criteria. Designing PBSC braced buildings using these factors could provide an adequate margin against collapse under the maximum earthquake hazard defined in the code (NBCC 2010). The scope of this study is limited to only four, six and eight storied PBSC braced frames. Furthermore, this study mostly focuses on the seismicity of Western Canada. Therefore, response modification factors determined in this study should only be used for the short and medium tall building in Western Canada. For much taller or shorter buildings, these factors have to be reinvestigated. Furthermore, for a different geographic region with different seismicity, these factors need to be recalculated by taking these regional factors into consideration.

5.2 Force based design procedure

The current force-based design procedure outlined in the NBCC (2010) permits the designer to reduce the elastic seismic base shear force demand by R_d*R_o factor (Lee et al. 1999). This reduction in the design base shear force rests on the observation that a well-detailed structure is capable of resisting base shear force higher than the design value (R_o) and can also experience significant deformation without collapse (R_d) (Kim and Choi 2005). These factors significantly reduce the design base shear force. The designer then only needs to perform linear elastic (static or dynamic) analysis using this reduced base shear force. A structure thus designed is expected to deform inelastically to dissipate seismic energy during a design level seismic event. The structural components (e.g., beams and columns) that are designed for this lower force would experience much higher deformation. This method eliminates the need for the designer to perform nonlinear analysis on their building models. Due to this simplicity, R_d and R_o are the most important parameters in force based seismic design. Canadian building design code (NBCC 2010) provides empirical values of R_d and R_o for many different structural systems such as reinforced concrete moment resisting frames, steel moment resisting frames, shear walls and braced frames etc. The code provides the following equation for calculating the design base shear force.

$$V_d = \frac{S(T_a) M_v I_E W}{R_d R_o} \quad (5.1)$$

Here,

$S(T_a)$ = Spectral acceleration demand

M_v = Factor to account for higher mode effects

I_E = Structural importance factor

W = Seismic weight of the structure

Finally, V_d is the design base shear

The numerator in equation 1 represents the elastic base shear demand or V_E. It consists of spectral acceleration demand or $S(T_a)$. This value comes from the design response spectra of the seismic zone and the fundamental period of the structure to be designed. The next parameter is M_v which takes higher mode effect of the structure into account. Recommended values for this parameter are provided in Table 4.1.8.11 of NBCC (2010). The value of M_v ranges from 1.0 to 2.5. Another important parameter is called the importance factor (I_E). The more important the structure (e.g. Post-disaster, hospitals or schools), the higher the value of this parameter. The value of I_E ranges from 0.8 (low importance) to 1.5 (post-disaster). This parameter ensures that important structures are designed with higher base shear force compared to less important ones; which is expected to increase the safety of important structures against a seismic hazard. The last parameter in the numerator is "*W*" or the seismic weight of the structure. All weights which contribute to the seismic mass of the structure are considered; this includes dead load, parts of the storage and the snow load and full content of any tank supported by the structure. These parameters in the numerator result in the elastic base shear. The response modification factors, "R_d" and "R_o" are in the denominator; therefore, the higher the value of these factors, the lower the value of design base shear force, V_d. Therefore, higher values of these factors result in a much more economical design.

Figure 5-1 depicts the definition of R_d and R_o using an example pushover plot of a building. This example pushover curve shows the lateral strength of a structure in terms of base shear force and roof top displacement. An idealized version of this pushover curve is overlaid on top of the actual pushover curve. The idealization is done to find out the yield strength and yield displacement of the system, which are necessary for the R_d and R_o factor calculation. This idealized curve

represents the structures lateral strength in an elastic-perfectly plastic manner. FEMA 356 (FEMA 2000) recommendations are followed for this idealization process.

In Figure 5-1, V_y is the yield base shear of the structure. As it is hard to locate the exact yield point on a curved surface (actual backbone curve), the idealized base shear vs. roof displacement curve was used to estimate the yield base shear. The corresponding displacement value is the yield displacement (Δ_y). The ratio of these two parameters (V_y/Δ_y) represents the initial stiffness of the structure (K_i). V_d represents the design strength of the structure. This is the base shear force the structure was designed to withstand. Due to structural redundancy, safety factors and overdesign (e.g. using same beam or column sections on every floor), building structures yield at a much higher load than their design strength, which is known as the overstrength. The value of the overstrength factor is calculated by dividing the V_y with V_d. Equation 5.2 shows the formula for calculating the overstrength factor (R_o).

$$R_o = \frac{V_y}{V_d} \tag{5.2}$$

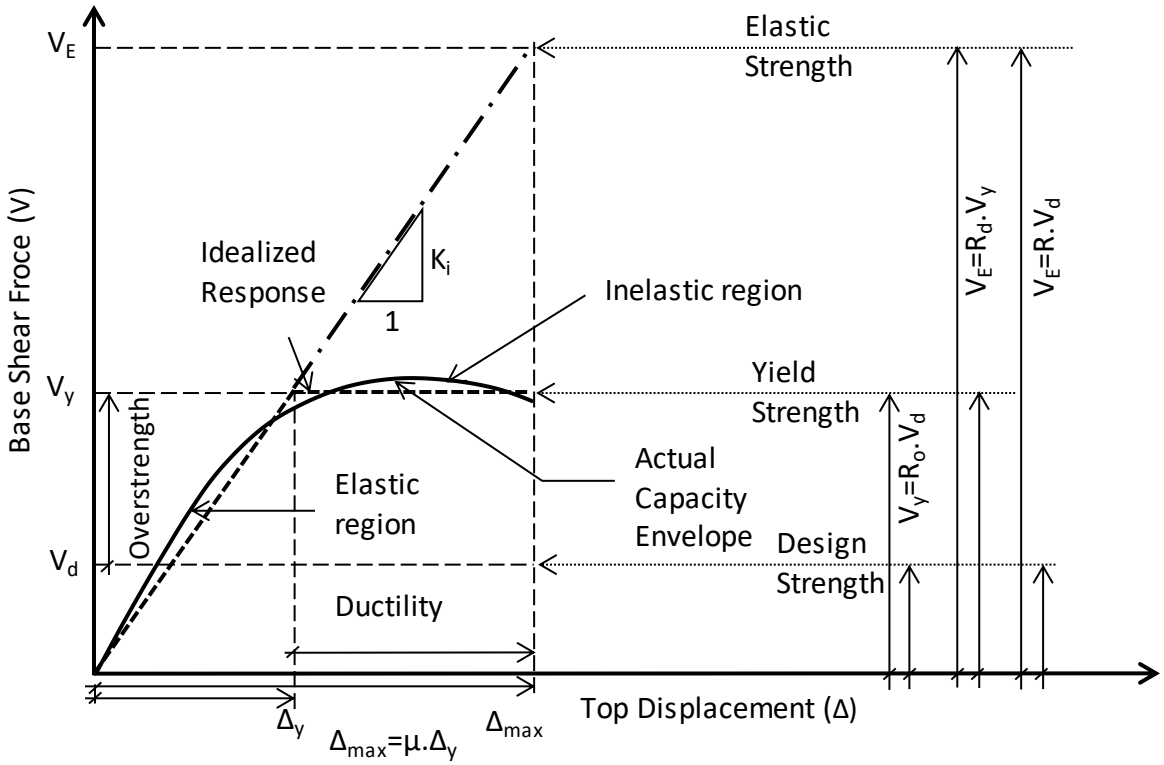

Figure 5-1: Relationships between force reduction (R_d), overstrength (R_o), response modification factor (R) and displacement ductility (μ)

Ductility related force reduction factor is another crucial parameter in seismic design. If a structure is designed to remain fully elastic under seismic loading, then the structure will exhibit a different response compared to the actual nonlinear response. The relationship between the base shear force and the roof displacement will remain linear. It was observed that for a certain structural period range an elastic structures displacement response under dynamic excitation is almost same as that of a nonlinear structure; also known as the equal displacement approximation (Newmark and Hall 1982). However, the author observed that this does not hold true for a short period (stiff) structures. Therefore, the linear elastic structure, if flexible enough will experience almost same displacement under the same earthquake event; this will, in turn, result in a much higher base shear force. We can call this base shear (V_E) or the elastic base shear demand. If we divide this fictitious elastic base shear force (V_E) with the yield base shear force (V_y), we get the

ductility related force reduction factor (R_d). On the other hand, the ratio between the elastic base shear force (V_E) and the design base shear force (V_d) is known as the response modification factor (R). Equation 5.3 and Equation 5.4 shows the formula for R_d and R. As per Kim and Choi (2004), a greater value of 'R' indicates higher energy dissipation capacity.

$$R_d = \frac{V_E}{V_Y} \tag{5.3}$$

$$R = R_d R_o = \frac{V_E}{V_d} \tag{5.4}$$

Another important parameter is the ductility (μ); defined as the ratio between the maximum displacement (Δ_{max}) and the yield displacement (Δ_y) of the structure under consideration. Similar to the previous parameters, these are also calculated from the idealized bilinear representation of the structure's backbone curve.

$$\mu = \frac{\Delta_{max}}{\Delta_Y} \tag{5.5}$$

5.3 Necessity of this study

Nowadays, the new seismic force resisting systems are getting introduced in every code update cycle. The capability of these new systems in resisting seismic load is not clear; therefore, it is vital to quantify the seismic performance of these new systems (FEMA 2009). As PBSC is a novel bracing system and there is no rational seismic design guideline for it, it is of utmost importance that the seismic performance factors be determined for structures equipped with this bracing system.

Use of SMA based self-centering bracing system in buildings has been studied in the past by many researchers (Auricchio et al. 2006; Moradi et al. 2014; Zhang and Zhu 2007). These studies found that utilizing shape memory alloy in the bracing system could decrease the residual damage of the buildings. However, few of them came up with a proper design method or designing

structures with these bracing systems. As discussed earlier, R_d and R_o are two essential parameters in force based seismic design of structures. The code provides empirical values for different types of structural force resisting systems. Most of these factors were proposed based on observations or empirical studies. The proposed factors are mostly conservative and result in overdesign. Recently, studies were carried out to investigate the adequacy or propose values of response modification factors for different types of structures like cold-formed steel special bolted moment frames (Sato and Uang 2013), steel special moment-frame buildings (Miyamoto et al. 2011; Zareian et al. 2010), concrete buildings reinforced with superelastic shape memory alloy rebars (Hossain et al. 2015), cold-formed steel strap braced walls (Comeau et al. 2010), self-centering concentrically braced frames (Tahmasebi et al. 2014) and seismic-resistant friction damped braced frame system with buckling restrained columns (Blebo and Roke 2015). All of these studies were carried out using FEMA P695 (FEMA 2009) guideline which provides a rational method for calculating response modification factor for new structural systems or evaluating the code proposed values for well-established structural systems.

NBCC (2010) requires that buildings designed using code specified seismic hazard level should have a very low probability of collapse thus preventing loss of lives. However, it is not well defined on how to achieve this collapse safety as experimental validation would require large-scale test setup which could test up to global collapse limit (Haselton et al. 2010). Researcher and practitioners nowadays tend to quantify the performance criteria with which they design the structures (Ghobarah 2001). Luckily, due to advancement performance-based seismic design tools and technologies it is now easier than ever to determine the collapse safety of various structural systems with moderate to high accuracy using nonlinear collapse simulation techniques on a probabilistic basis. In this chapter, collapse margin ratio (CMR) of 4,6 and 8 storied PBSC braced

frames will be calculated using the FEMA P695 methodology to determine the required seismic response modification factors.

5.4 Description of the FEMA P695 methodology

The FEMA P695 guideline offers a rational method for determining building response parameters and system performance. If the method is properly implemented in the design process for various seismic force resisting systems, during a seismic event, it will provide equivalent safety against collapse in contrast to inherent safety against collapse intended by the current seismic design codes (FEMA 2009). FEMA P695 utilizes collapse margin ratio (CMR) for determining building seismic performance factors; which is defined in the guideline (FEMA 2009) as the ratio between median spectral acceleration (5% damped) at the collapse level ground motion, S_{CT} (or corresponding displacement, SD_{CT}) to the spectral acceleration of the maximum considered earthquake (MCE) ground motion (5% damped), S_{MT} (or corresponding displacement, SD_{MT}), at the fundamental period of the seismic force resisting system.

$$CMR = \frac{S_{CT}}{S_{MT}} = \frac{SD_{CT}}{SD_{MT}} \tag{5.6}$$

Another definition of the collapse margin ratio (CMR) could be given as follows: CMR is the amount by which S_{MT} must be increased to achieve building collapse by half (50%) of the earthquake ground motion records in a record set suggested by FEMA P695. Collapse margin ratio depends on the following factors: uncertainty in analysis, design, construction and ground motion variability. These factors are collectively considered in a collapse fragility curve. This curve depicts the collapse probability of the seismic-force-resisting system with respect to the ground motion intensity (FEMA 2009).

A flow diagram of the FEMA P695 based seismic performance factor determination method is shown in Figure 5-2. The method starts with designing model buildings using a trial value response modification factor, R or the multiplication of R_d and R_o as per Canadian building design code (NBCC 2010). After the design of the building, nonlinear archetype models are created using hysteresis response of the primary force resisting elements, such as beams, columns, braces, and connections. The hysteresis response and the primary force-deformation backbone curves can be determined using experimental investigation, continuum nonlinear 3D finite element analysis or fiber modeling. Once the building archetype models are created, pushover analysis is carried out for the determination of ductility and overstrength factor. In the next step, 22 far-field (recorded at sites located more than 10km from the fault rupture) ground motions record pairs are normalized with respect to the peak ground velocity of the record set and scaled to the design response spectrum. However, scaling to the design response spectrum can be skipped as during analysis the record group is scaled with several scaling factors to generate the IDA curves.

In the next step, the selected ground motion records are collectively scaled and nonlinear dynamic time history analysis is carried out on the building archetypes. This process is repeated until median collapse is achieved; which is the intensity at which half of the records in the set causes collapse to the building model. Collapse is determined by dynamic instability or excessive lateral displacements. This process although similar but differs from the incremental dynamic analysis concept proposed by Vamvatsikos et al. (2002). In the next step, a collapse fragility curve is defined from the collapse data obtained from the IDA results using cumulative distribution function. This plot relates the probability of collapse to the ground motion intensity (Ibarra et al. 2002).

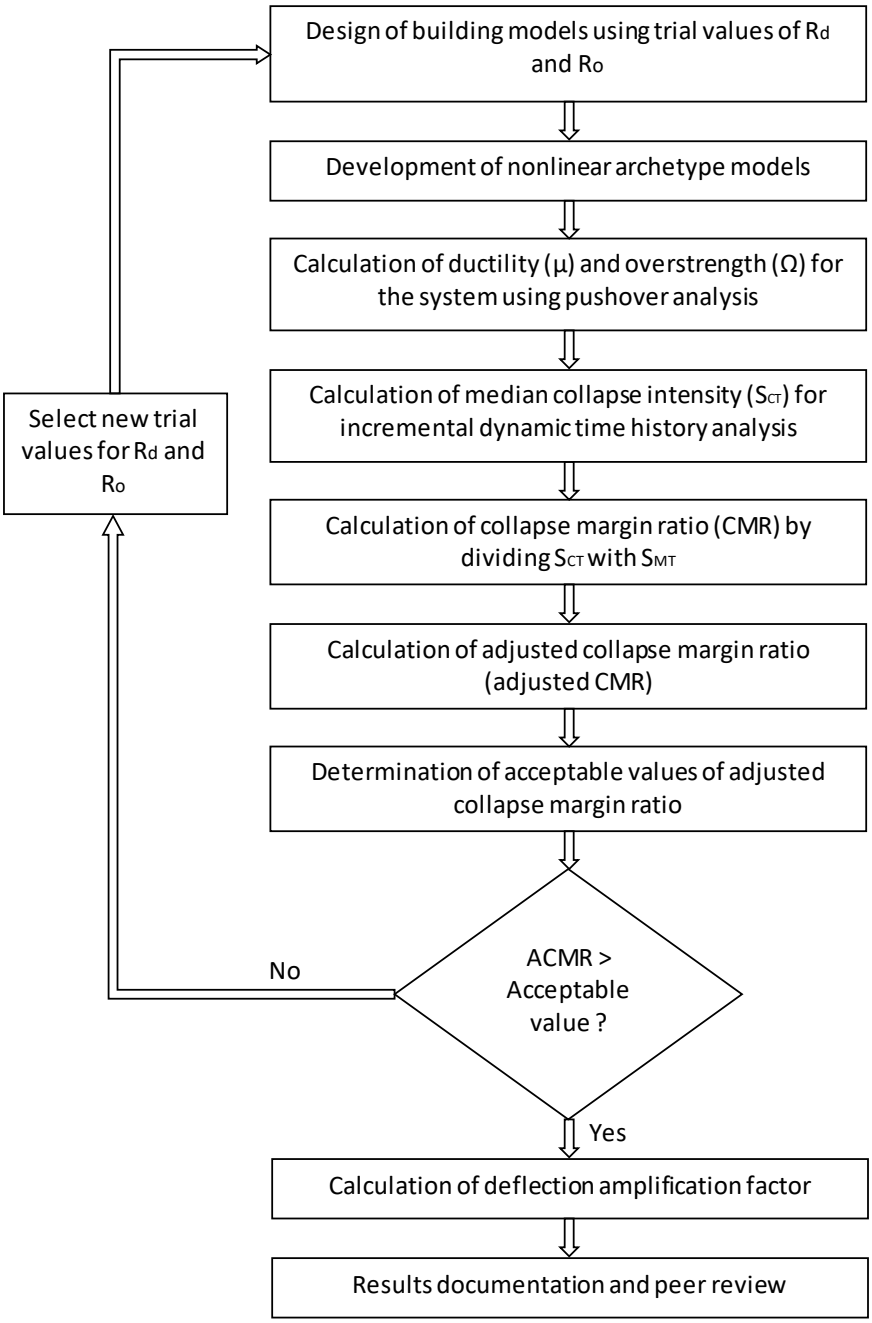

Figure 5-2: Determination of seismic performance factors (FEMA 2009)

This median collapse ground motion intensity is denoted as S_{CT}; whereas, the intensity of maximum considered earthquake spectral acceleration at the fundamental period of the building is denoted as S_{MT}. Maximum considered earthquake is defined as the intensity of an earthquake event

with 2% probability of exceedance in 50 years. As per Poisson's distribution, the return period of such an earthquake is once in 2475 years. In ASCE 7-05 (ASCE 2005), the design response spectrum is taken as 2/3rd of the MCE response spectrum. However, in Canadian building code (NBCC 2010), 2% in 50 years earthquake hazard level is used for design. However, for any structural force resisting system having an R_d value higher than or equal to 1.5, the code limits the maximum spectral acceleration for design to 2/3rd of S_a (0.2) or 2/3rd of the maximum value of the response spectrum. Therefore, these two design standards are very similar to each other in this regard. Hence, FEMA P695(FEMA 2009) method is applicable for evaluating building seismic performance factors in Canadian building design context.

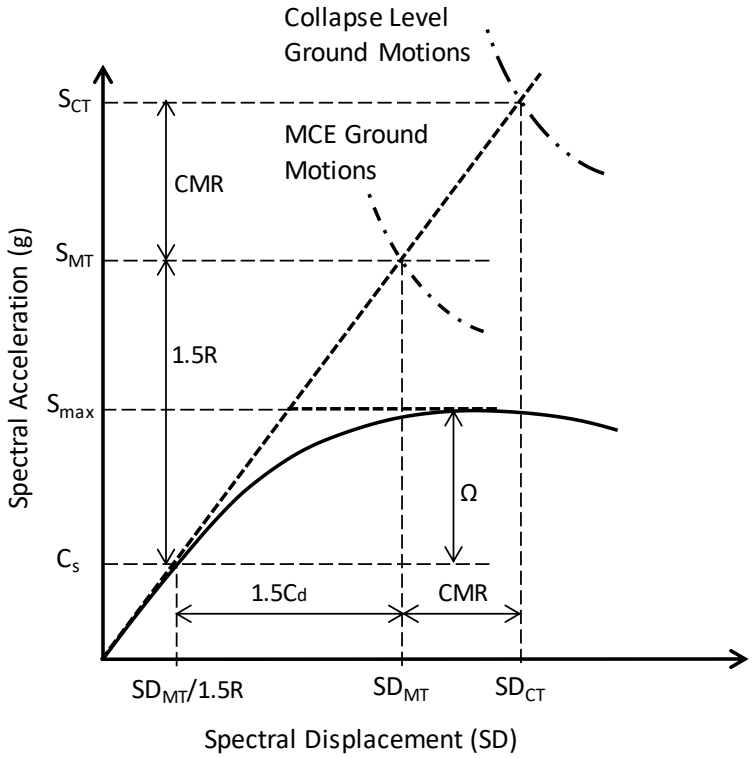

Figure 5-3: Illustrations of seismic performance factors (adapted from FEMA (2009))

After the determination of S_{CT}, these values are divided by S_{MT} to get the value of collapse margin ratio (CMR). In the next step, the calculated value of CMR is adjusted for the following

factors: effects of spectral shape, record to record variability, design requirement uncertainty (test data and modeling uncertainty), etc. This adjusted value is known as the adjusted collapse margin ratio (ACMR). After the adjustment, the ACMR value is checked against acceptable limits defined in the guideline. If the ACMR value is higher than the acceptable CMR value, then the trial value of "R" or "R_dR_o" is accepted. On the other hand, if the ACMR value is not found satisfactory, then the whole evaluation process is repeated with a new trial value of "R" or "R_dR_o".

5.5 Design and modeling of the PBSC braced frames

Steel braced frames with three different heights (four, six and eight storied) and same layout plans were selected for this study. These buildings were designed using seismic design procedures of National Building Code of Canada (NBCC 2010). The site for these buildings was chosen as the coastal region of the Vancouver city. The maximum spectral acceleration of the design response spectra is 0.95g at the constant acceleration zone. Figure 5-4 illustrates the response spectra chosen for the design.

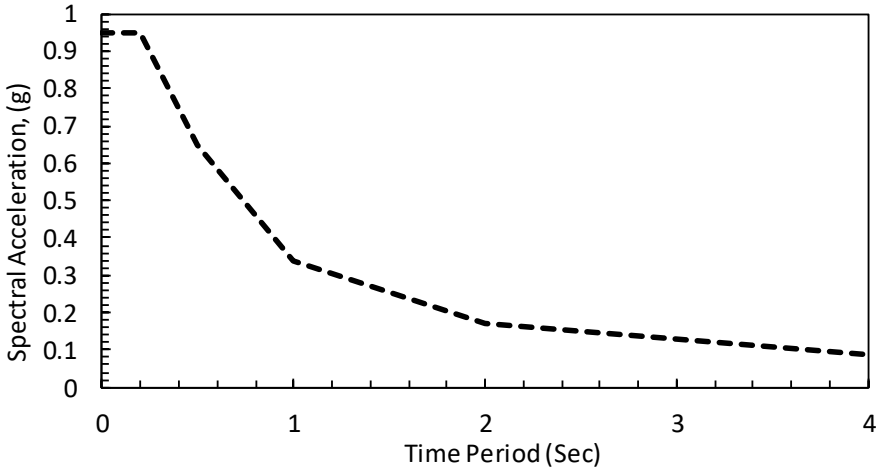

Figure 5-4: Vancouver soil class "C" response spectrum

The importance factor for these buildings was taken as 1.0 as these are considered "residential constructions." As regular plans and elevations were chosen, the higher mode effect was also taken

as 1.0. For soil class "C," the F_a and F_v values were taken as 1.0. In the first trial, the R_d and R_o values were selected as 8.0 and 1.3 respectively. However, after some preliminary analysis, these values were found to be outside the acceptable limit provided in the FEMA P695 guideline. Therefore, in the second trial, R_d and R_o values were taken as 6.0 and 1.1 respectively. A well-known structural analysis and design software called S-FRAME V11.2.6 (S-FRAME 2016) was used for the seismic design and section size determination for these buildings. The beams and braces were modeled with pin ended connections which prevented them from resisting or transferring end moments. The column supports were also modeled using hinges. This modeling procedure ensures that the braced frames resist lateral forces only through the axial action of the braces. This was done to eliminate lateral strength contribution from elements other than the braces to understand the seismic performance of the structure solely due to this novel bracing system. As PBSC braces have two different materials in the system (Steel and SMA), it is difficult to calculate the brace stiffness before the final design before knowing the length of each element. Furthermore, commercially available structural analysis and design software such as S-FRAME, SAP2000, ETABS, STAAD Pro do not have SMA material built into them. However, the elastic properties could be provided as input for building the model necessary for design calculations. However, modeling such a way sometimes hamper the automatic steel design process. To prevent this, the braces were modeled using standard hollow circular steel sections without the SMA ties. However, as the steel shaft and the SMA ties are arranged in a series the actual stiffness of the PBSC brace (shaft and SMA ties in a series) would be less than a whole section made of steel shaft only. To match the expected stiffness, the PBSC brace stiffness was separately calculated and it was provided as a section property modifier in the S-FRAME Software. For this design, it was found that an axial stiffness modifier of 0.69 or 31% reduction was appropriate. The detailed calculation

can be found in Appendix A. Using this stiffness modifier and modeling technique described above, 4, 6 and 8-storied three-dimensional steel building frame models were built in S-FRAME Software. Isometric views of these building frames are shown in Figure 5-5. The slabs are hidden from this view for clarity.

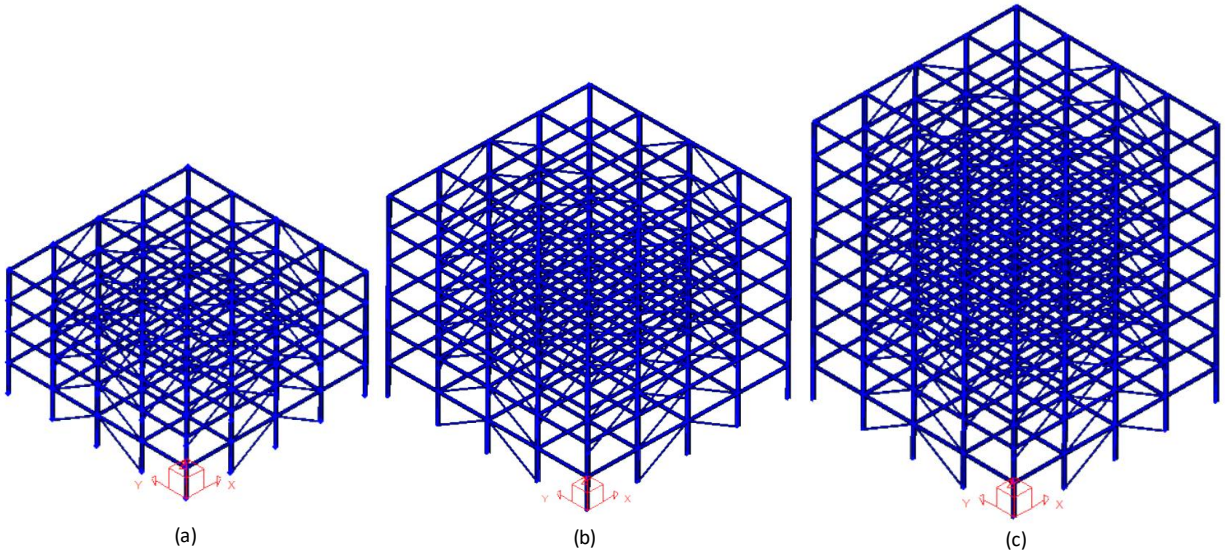

Figure 5-5: Three-dimensional model of the (a) four (b) six and (c) eight-storied PBSC building

After the seismic design was done and the section sizes were determined (Figure 5-6), the following steps were carried out. As nonlinear incremental dynamic analysis procedure is very computationally demanding, two-dimensional models were used instead of the three-dimensional ones. Individual perimeter braced frames from each of these three building models were taken for performance evaluation using nonlinear analysis. The nonlinear behavior of these braces was modeled using zero-length link elements positioned at the end of the braces. A detailed PBSC brace design procedure used for this analysis is given in Appendix A. As nonlinearity of the SMA bars is directly taken into consideration by the link elements, the stiffness of the shaft needs to be adjusted to match the actual PBSC bracing system which the shaft and link combination in the model is simulating. As the SMA bars are represented by zero-length elements, the shaft had to be

modeled longer than its actual designed size. This increased length decreases the axial stiffness of the brace by a factor of (L_i/L_a), where L_i is the increased length and L_a is the designed length. Therefore, in the nonlinear model, the axial stiffness was modified by a factor equal to the inverse of the previous factor, or (L_a/L_i). In the final step, the nonlinear hysteretic parameters of the PBSC braces were calculated using the method given in Appendix A.

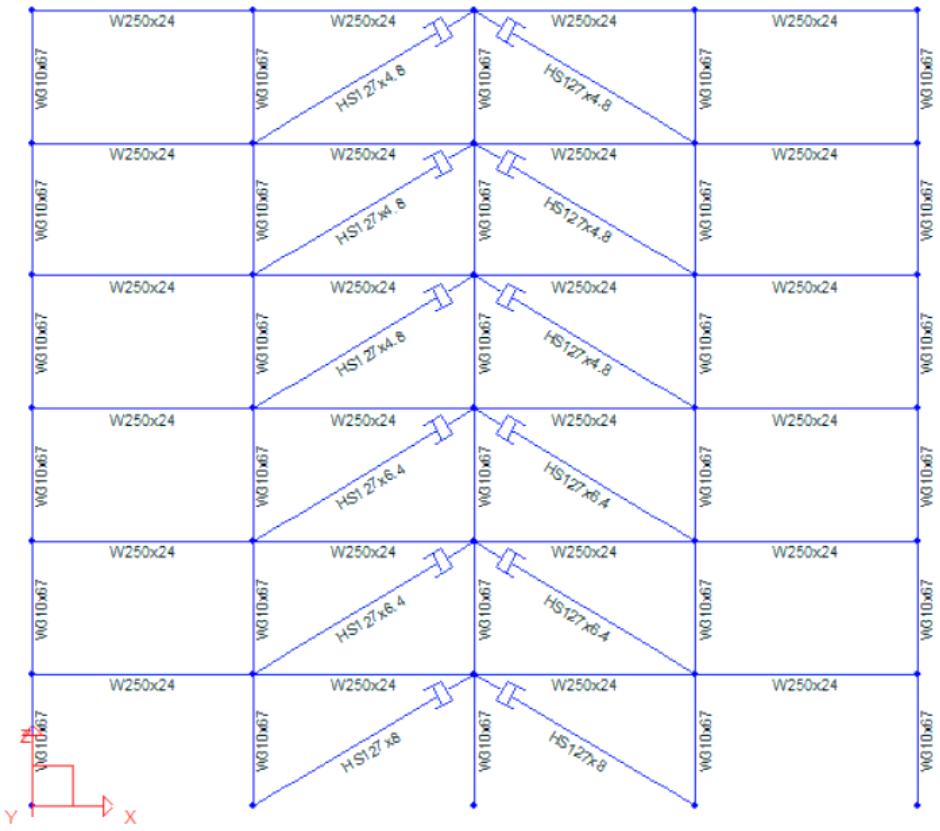

Figure 5-6: The designed six-storied PBSC frame showing the required section sizes

5.1 Incremental dynamic time history analysis

The incremental dynamic analysis of the index archetype is a two-step process. In the first step, ground motion records were selected, normalized and scaled. In the next step, several hundreds of nonlinear dynamic time history analyses are carried out by scaling these records. This two-step procedure is discussed in detail below.

5.1.1 Ground motion record selection and scaling

The FEMA P695 methodology provides two sets of ground motion records for the collapse assessment of the building archetypes using incremental dynamic time history analysis. One record set contains 22 far-field record pairs (Table 5-1) and another set containing 28 near-field (recorded at sites located less than 10km from the fault rupture) record pairs. However, only far-field record set is necessary for collapse evaluation; the near-field record set is provided as supplemental information. If required, this record set could be used to examine issues arising from near-fault directivity effects; which is done for practical reasons since there are numerous issues in the characterization of near-field hazards as well as ground motion effects. On the other hand, for this analysis, only two horizontal orthogonally separated records are used from each event. The vertical component of the excitation is ignored as this direction is not considered of vital importance for collapse assessment.

Table 5-1: Twenty-two far-field earthquake record details for collapse evaluation

Event ID	M_w	Event Name	Year	Recording Station	Fault Type	Epicentral Distance	PGA_{max} (g)	PGV_{max} (cm/s)
1	6.7	Northridge	1994	Beverly Hills	Thrust	13.3	0.52	63
2	6.7	Northridge	1994	Canyon Country	Thrust	26.5	0.48	45
3	7.1	Duzce, Turkey	1999	Bolu	Strike-Slip	41.3	0.82	62
4	7.1	Hector Mine	1999	Hector	Strike-Slip	26.5	0.34	42
5	6.5	Imperial Valley	1979	Delta	Strike-Slip	33.7	0.35	33
6	6.5	Imperial Valley	1979	El Centro Array #11	Strike-Slip	29.4	0.38	42
7	6.9	Kobe, Japan	1995	Nishi-Akashi	Strike-Slip	8.7	0.51	37
8	6.9	Kobe, Japan	1995	Shin-Osaka	Strike-Slip	46	0.24	38
9	7.5	Kocaeli, Turkey	1999	Duzce	Strike-Slip	98.2	0.36	59
10	7.5	Kocaeli, Turkey	1999	Arcelik	Strike-Slip	53.7	0.22	40
11	7.3	Landers	1992	Yermo Fire Station	Strike-Slip	86	0.24	52
12	7.3	Landers	1992	Coolwater	Strike-Slip	82.1	0.42	42
13	6.9	Loma Prieta	1989	Capitola	Strike-Slip	9.8	0.53	35
14	6.9	Loma Prieta	1989	Gilroy Array #3	Strike-Slip	31.4	0.56	45
15	7.4	Manjil, Iran	1990	Abbar	Strike-Slip	40.4	0.51	54
16	6.5	Superstition Hills	1987	El Centro Imp. Co.	Strike-Slip	35.8	0.36	46
17	6.5	Superstition Hills	1987	Poe Road (temp)	Strike-Slip	11.2	0.45	36
18	7.0	Cape Mendocino	1992	Rio Dell Overpass	Thrust	22.7	0.55	44
19	7.6	Chi-Chi, Taiwan	1999	CHY101	Thrust	32	0.44	115
20	7.6	Chi-Chi, Taiwan	1999	TCU045	Thrust	77.5	0.51	39
21	6.6	San Fernando	1971	LA-Hollywood Stor	Thrust	39.5	0.21	19
22	6.5	Fruili, Italy	1976	Tolmezzo	Thrust	20.2	0.35	31

The near-field record set contains all high-magnitude events (PGA > 0.2g, PGV > 0.15 m/sec and M_w > 6.5) from the Pacific Earthquake Engineering Research Center (PEER) Next-Generation Attenuation (NGA) database. Large-magnitude earthquakes usually have a long duration and dominate collapse risk, which is important for collapse evaluation of nonlinear material or element hysteresis with gradual strength degradation. The record set includes event records from soft rock and stiff soil sites. The records are from shallow crustal sources, mostly thrust or strike-slip faults (FEMA 2009).

The records were selected in a way to encounter some conflicting objectives. From a single earthquake event, no more than two strongest records were chosen to avoid event bias. The record

set includes an adequate number of earthquake records to allow the calculation of record to record variability (RTR) and median collapse intensity (S_{CT}). However, an explicit calculation for RTR is not required; as an alternative, previous development studies and research is used to estimate values of RTR, and this is built in the computation process of the total system collapse uncertainty (FEMA 2009).

The main objective of the far-field record set is to deliver a fully defined ground motion record set for collapse evaluation of all seismic design categories located in any seismic hazard zone and founded on any soil condition in a consistent manner. All records in the set are from real seismic events, no synthetic record was used, based on the assumption that regional variation of ground motions is not be considered (FEMA 2009). These records were scaled to represent a specific intensity; usually the collapse intensity of the index archetype under consideration. There are two major steps in the ground motion record scaling process. In the first step, the median peak ground velocity (PGV) of the record set was determined. In the next step, this median value was divided by the PGV of each event. This ratio is known as the normalization factor for the i^{th} record (NM_i). Later, these normalization factors were multiplied with the corresponding ground motion record data to calculate the normalized records. The normalization factors for all 22 far-field events are provided in Table 5-2. This normalization process removed the unwarranted inconsistency between records due to intrinsic differences in source type, source distance, site conditions and event magnitude. However, this process does not affect record to record variability.

Table 5-2: Normalization factor for far-field record set

Event ID	Comp. 1 Sa (g)	Comp. 2 Sa (g)	PGV_{peer} (cm/s)	Normalization factor	Normalized PGA_{max} (g)	Normalized PGV_{max}
1	1.02	0.94	57.2	0.65	0.34	41
2	0.38	0.63	44.8	0.83	0.4	38
3	0.72	1.16	59.2	0.63	0.52	39
4	0.35	0.37	34.1	1.09	0.37	46
5	0.26	0.48	28.4	1.31	0.46	43
6	0.24	0.23	36.7	1.01	0.39	43
7	0.31	0.29	36	1.03	0.53	39
8	0.33	0.23	33.9	1.1	0.26	42
9	0.43	0.61	54.1	0.69	0.25	41
10	0.11	0.11	27.4	1.36	0.3	54
11	0.5	0.33	37.7	0.99	0.24	51
12	0.2	0.36	32.4	1.15	0.48	49
13	0.46	0.28	34.2	1.09	0.58	38
14	0.27	0.38	42.3	0.88	0.49	39
15	0.35	0.54	47.3	0.79	0.4	43
16	0.31	0.25	42.8	0.87	0.31	40
17	0.33	0.34	31.7	1.17	0.53	42
18	0.54	0.39	45.4	0.82	0.45	36
19	0.49	0.95	90.7	0.41	0.18	47
20	0.3	0.43	38.8	0.96	0.49	38
21	0.25	0.15	17.8	2.1	0.44	40
22	0.25	0.3	25.9	1.44	0.5	44

In the final step, as per FEMA P695 guideline, the normalized ground motion records were supposed to be collectively scaled (anchored) to a specific ground motion (response spectra of the seismic zone under consideration) intensity so that the median spectral acceleration of the set matches the MCE spectral acceleration at the fundamental period of the index archetype. However, this last step (anchoring) is not mandatory as the evaluation procedure requires scaling the records up until 50% of the records causes collapse. Therefore any initial scaling factor other than the anchoring factor also works for the evaluation. Figure 5-7 shows the normalized mean spectra of the unscaled far-field ground motion record set compared to the Vancouver 2% in 50-year soil class “C” response spectra.

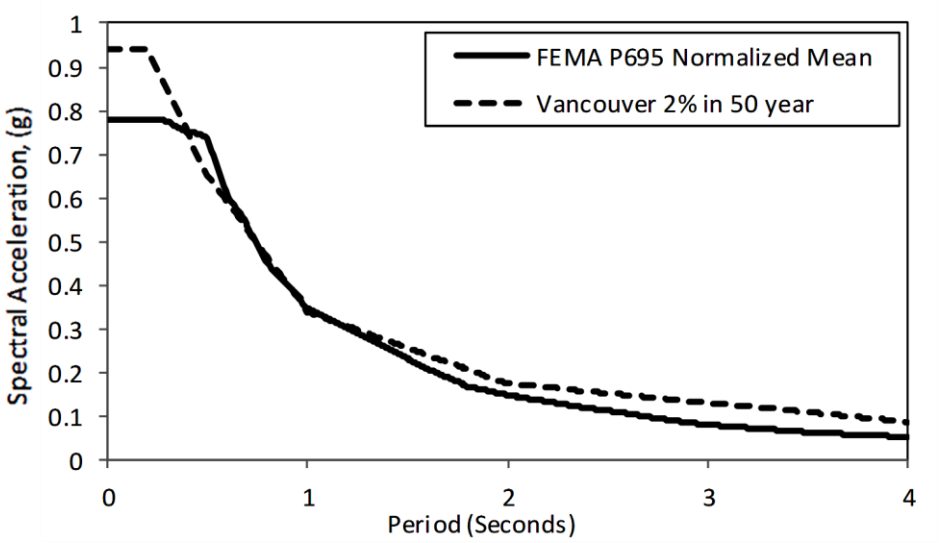

Figure 5-7: FEMA P695 normalized mean spectra compared to the Vancouver soil class "C" response spectra

5.1.2 IDA results

After the far-field records had been normalized and scaled, nonlinear dynamic time history analyses were carried out starting from a small-scale factor (around 0.5). This scaling factor was incremented by 0.5 for subsequent analysis until median collapse was observed. The collapse of the PBSC index archetype was set at 6.8% elongation of the NiTinol bars. This elongation corresponds to the austenite to martensite finishing stress for the specific NiTinol bars. After this strain, NiTinol bar fully transforms to martensite. At this phase, the stiffness of the NiTinol bar increases to the initial stiffness thus attracting significantly higher forces. Based on the design assumption that the connections of the PBSC brace to the frame corners will not be designed for stresses greater than this, it is expected that the connections will fail at this stress and will result in a side sway collapse for the frame. As NiTinol bars are only 1m long as per the design (Appendix A), which is approximately one-sixth length of the brace, it resulted in 2.66% interstory drift ratio for the frame.

Following settings were chosen in the S-FRAME Software for the nonlinear dynamic time history analysis. For numerical integration "Newmark" method has been selected with α and δ values 0.25 and 0.5 respectively. For damping coefficient calculation, "Rayleigh" damping method was chosen with 5% damping for both stiffness and mass proportional coefficients. For Rayleigh damping matrix formation, both mass and stiffness matrix was formed using initial geometry. The seismic mass was formed from the following formula as per FEMA (2009).

Seismic mass = 1.05*Dead Load + 0.25 Live Load (5.1)

The resulting IDA curves (Figure 5-8(a)-(c)) show the incremental dynamic analysis results of the four, six and eight storied PBSC index archetypes. The IDA curves have a distinct yield zones near 1% interstory drift ratio, after which the response becomes much flatter. However, around 2.6%-2.8% the curves again stiffen up due to martensite phase stiffening. After this point, the curves seem to stiffen up and attract a significant amount of spectral acceleration. From the calculation presented in Appendix A, it can be understood that at 2.66% interstory drift ratio the NiTinol bars in the PBSC braces exceed Austenite to martensite finishing stress and starts to stiffen up. The effect of the brace stiffening is clearly visible in Figure 5-8 near the above mentioned interstory drift ratio percentage.

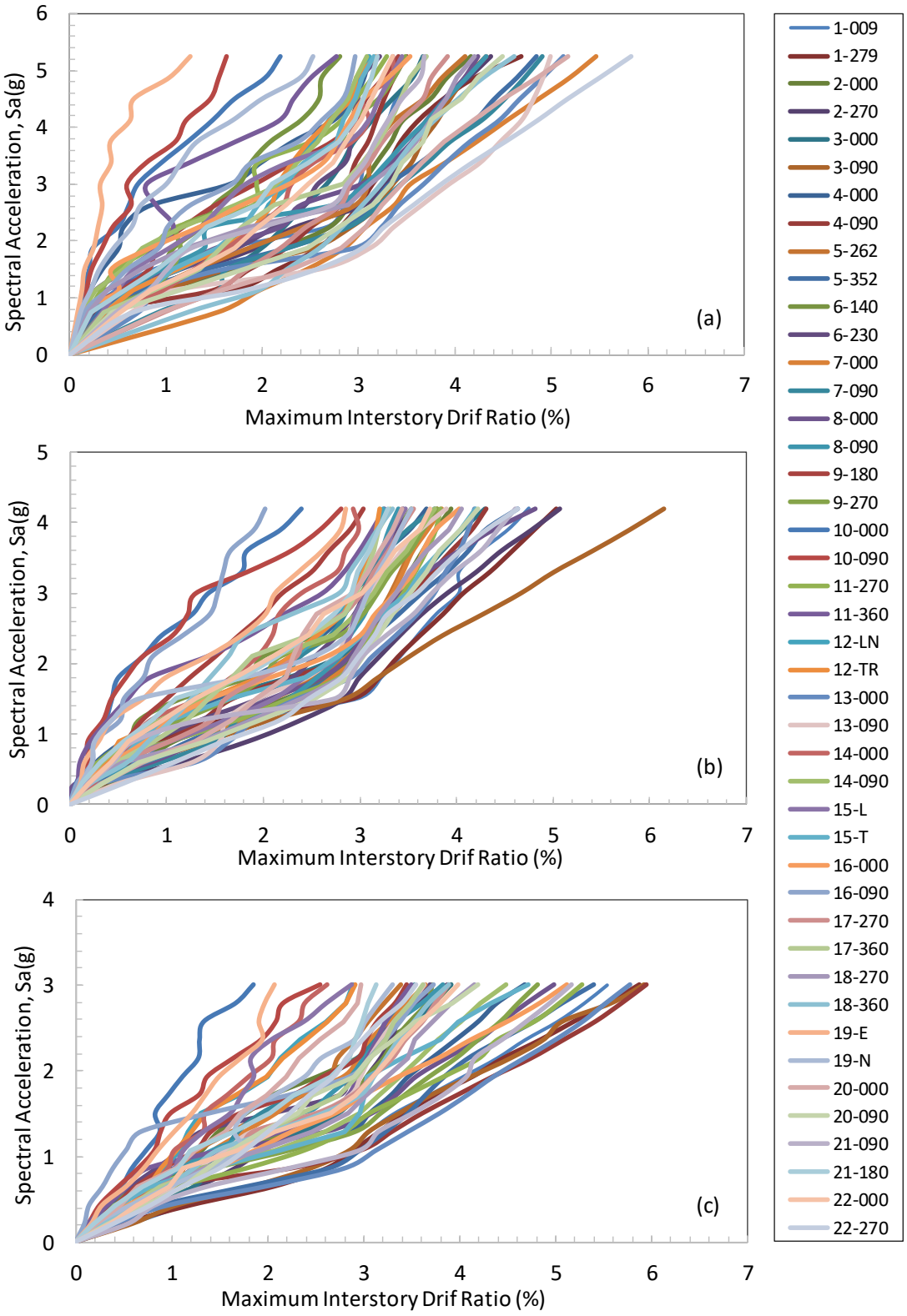

Figure 5-8: Spectral acceleration vs maximum interstory drift ratio IDA curves for (a) 4-storied (b) 6-storied and (c) 8-storied PBSC braced frame

5.2 Collapse margin ratio calculation

The collapse margin ratio for the individual index archetypes was calculated using the following method. From the individual spectral acceleration (S_a) vs. interstory drift ratio IDA curves, the failure spectral acceleration (S_a) values were determined at 2.66% interstory drift ratio. These failure S_a values were used to plot cumulative distribution function/curves (Figure 5-9). From these curves, the S_a values at 50% cumulative probability were calculated, which is known as the median collapse intensity (S_{CT}) at 5% damping. From the period of individual PBSC index archetypes and Vancouver soil class "C" response spectrum, the MCE spectral acceleration S_{MT} was found. The ratio of S_{CT}/S_{MT} was calculated and presented in Table 5-3. This ratio represents the collapse margin ratio of the PBSC index archetypes.

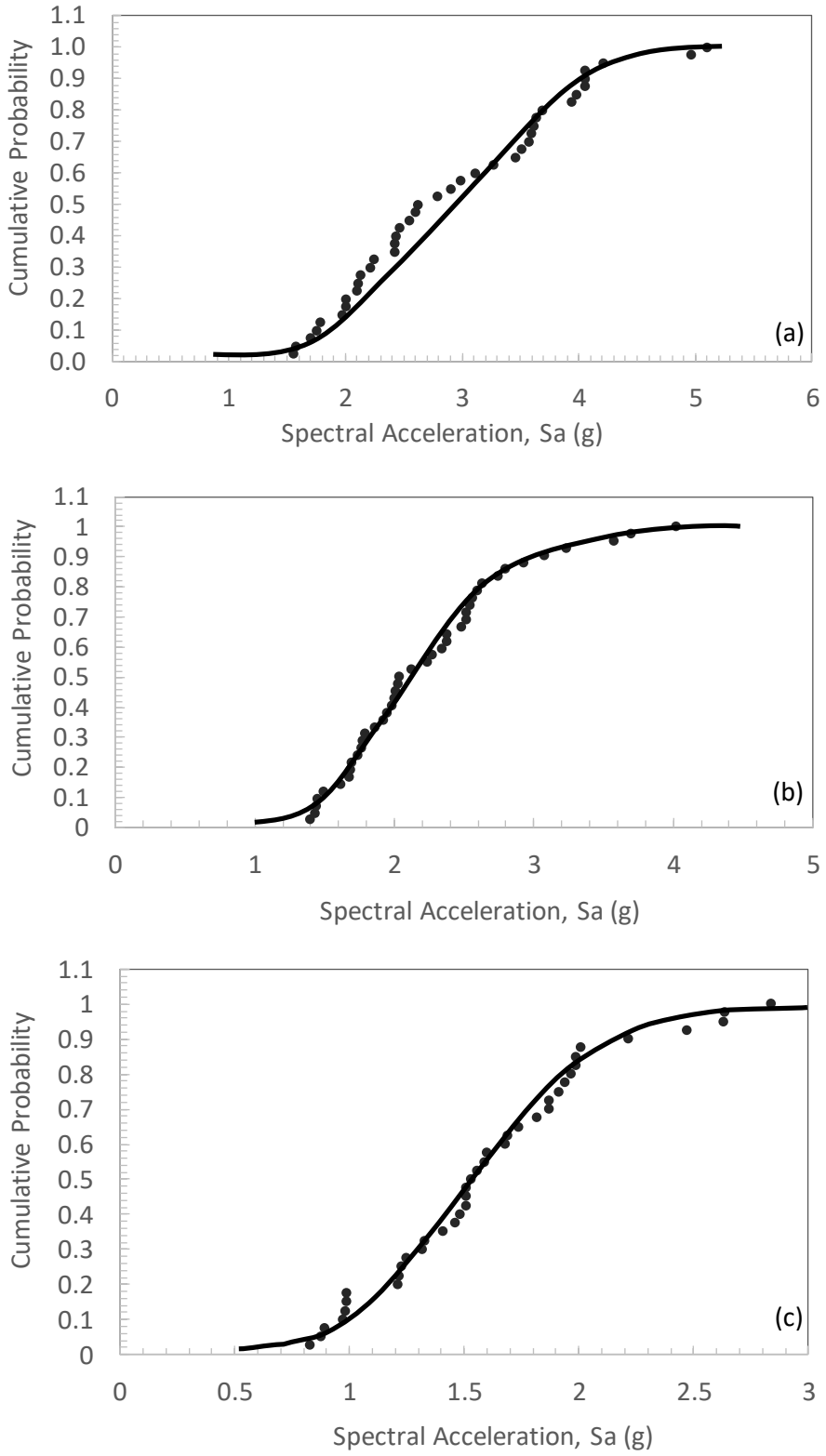

Figure 5-9: Cumulative distribution function of collapse level spectral acceleration values for (a) 4-storied (b) 6-storied and (c) 8-storied PBSC braced frame

From Table 5-3, the collapse margin ratios for the three archetypes ranges from 3.50-3.67; which are high ratios indicating the structures have a very low probability of collapse under MCE spectral acceleration. However, adjustment of these values is required for final judgment.

Table 5-3: Calculation of median collapse intensity and collapse margin ratio

	4 Storied	6 Storied	8 Storied
Median Collapse Intensity, S_{CT} (g)	2.75	2.1	1.55
MCE Spectral Acceleration, S_{MT} (g)	0.75	0.6	0.429
Collapse Margin Ratio, CMR	3.67	3.50	3.61

5.2.1 Adjusted collapse margin ratio

The collapse margin ratios calculated above were adjusted to compare with the acceptable values provided in FEMA P695 (2009). Validation of trial value for response modification factor has also been performed based on the acceptability of the adjusted collapse margin ratio (*ACMR*). Calculation of collapse margin ratio and collapse capacity can be considerably influenced by frequency content (spectral shape) of the ground motion records. For this reason, spectral shape factors (*SSF*) were calculated for each index archetype models. This factor is dependent on period based ductility (μ_T), which was calculated using nonlinear static and Eigenvalue analysis of the archetype models. The period based ductility is a critical parameter for this analysis as it is directly related to *ACMR* using equation 5.5.

$$ACMR = SSF \times CMR \tag{5.5}$$

SSF values for different seismic design categories, building time periods and period based ductilities (μ_T) are provided in Table 7-1a and Table 7-1b of FEMA (2009). The period based ductility (μ_T) of an index archetype can be calculated using equation 5.6.

$$\mu_T = \frac{\delta_u}{\delta_{y,eff}} \tag{5.6}$$

In this equation, δ_u is the ultimate roof displacement and $\delta_{y,eff}$ is the effective roof yield displacement. The parameter δ_u in equation 5.6 was calculated from the pushover curves discussed later in this chapter and the parameter $\delta_{y,eff}$ is calculated using equation 5.7.

$$\delta_{y,eff} = C_0 \frac{V_{max}}{W} \frac{g}{4\pi^2} (\max(T, T_1))^2 \tag{5.7}$$

In equation 5.7, V_{max} is the maximum base shear force (from pushover analysis), W is the weight of the building, g is the acceleration due to gravity, T is the fundamental period of the building from the building code formula, and T_1 is the period of the building from modal/Eigenvalue analysis. C_o is a factor relating roof displacement to the fundamental single-degree-of-freedom mode displacement. C_o was calculated using equation 5.8.

$$C_0 = \emptyset_{1,r} \frac{\sum_{x=1}^{N} m_x \ \emptyset_{1,x}}{\sum_{x=1}^{N} m_x \ \emptyset^2{}_{1,x}} \tag{5.8}$$

In this equation, m_x is the mass of level x. $\varphi_{1,x,}$ and $\varphi_{1,r}$ are the ordinates of the modal displacements of level x and the roof respectively. N represents the number of level in the building archetype under consideration. If the building mode shape ordinates are scaled in a way to make the maximum ordinate equal to unity, then C_o represents modal participation factor.

In the first step of calculating adjusted collapse margin ratio, modal analyses were carried out on the PBSC building archetypes. The mode shape pseudo-displacement values with respect to frame heights are plotted in Figure 5-10. As per FEMA (2009) guideline, horizontal loading patterns for pushover analysis were generated from the corresponding mode, which is shown in Figure 5-11.

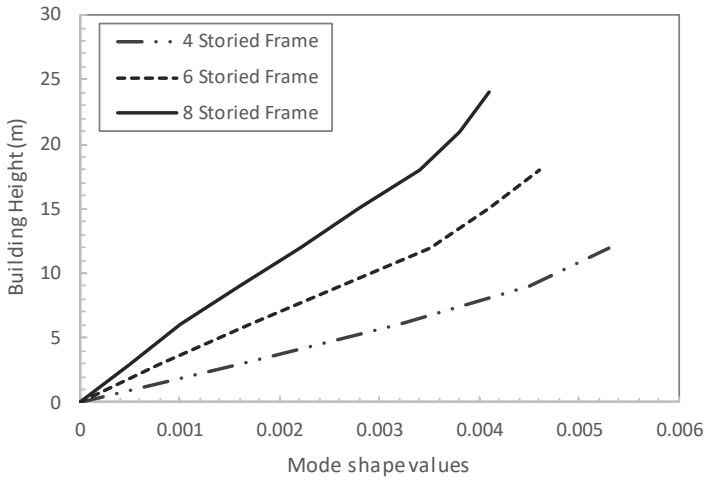

Figure 5-10: Fundamental mode shapes for the (a) 4-storied (b) 6-storied and (c) 8-storied PBSC building archetypes

This mode shape proportional horizontal load was applied to the left most perimeter column of each frame, and nonlinear quasi-static analysis with a linearly increasing (ramp) function was carried out. This ramp function was created using a duration of 10 seconds. This large load application duration was selected to eliminate any dynamic effect during the analysis. The function value starts from zero at time zero and reaches unity at ten seconds. The quasi-static analysis was run in one hundred equal time steps for smooth output curves. The maximum values of this modal shape proportional load patterns were carefully adjusted to produce expected pushover response. If the load was too low, the archetypes were not reaching yield or nonlinearity; on the contrary, loads with too high values were making the models unstable. Therefore, trial and error analysis were carried out to achieve the optimum load values for the pushover curve. For brevity, the trial and error steps are not shown here. Figure 5-11 shows the final magnitude of the forces applied to the archetypes as per their fundamental mode shapes.

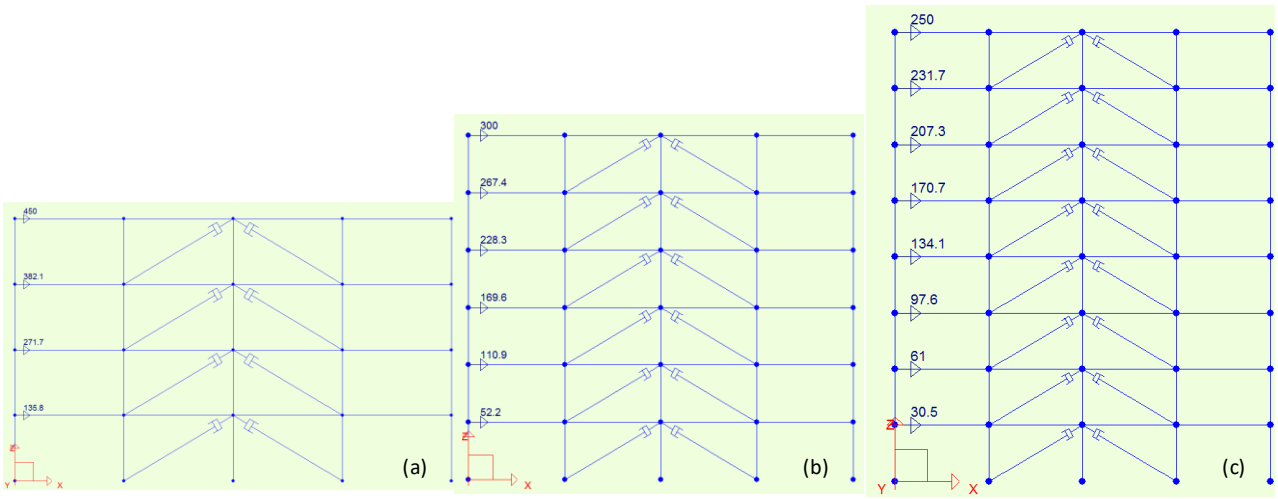

Figure 5-11: Mode shape proportional horizontal loading pattern for the (a) 4-storied (b) 6-storied and (c) 8-storied PBSC braced frame

During the pushover analysis, the displacement of the top node of the middle column was monitored along the base shear force. After the analysis, the roof displacements vs. base shears for the 4,6 and 8-storied frames were plotted and are shown in Figure 5-12(a)-(c). It was found out that all three pushover curves are similar in shape. The yield base shear forces are very close to one another. However, the maximum/ultimate displacements were vastly different between the frames. Due to the short height, the 4-storied frame, it has the smallest maximum deformation and vice versa.

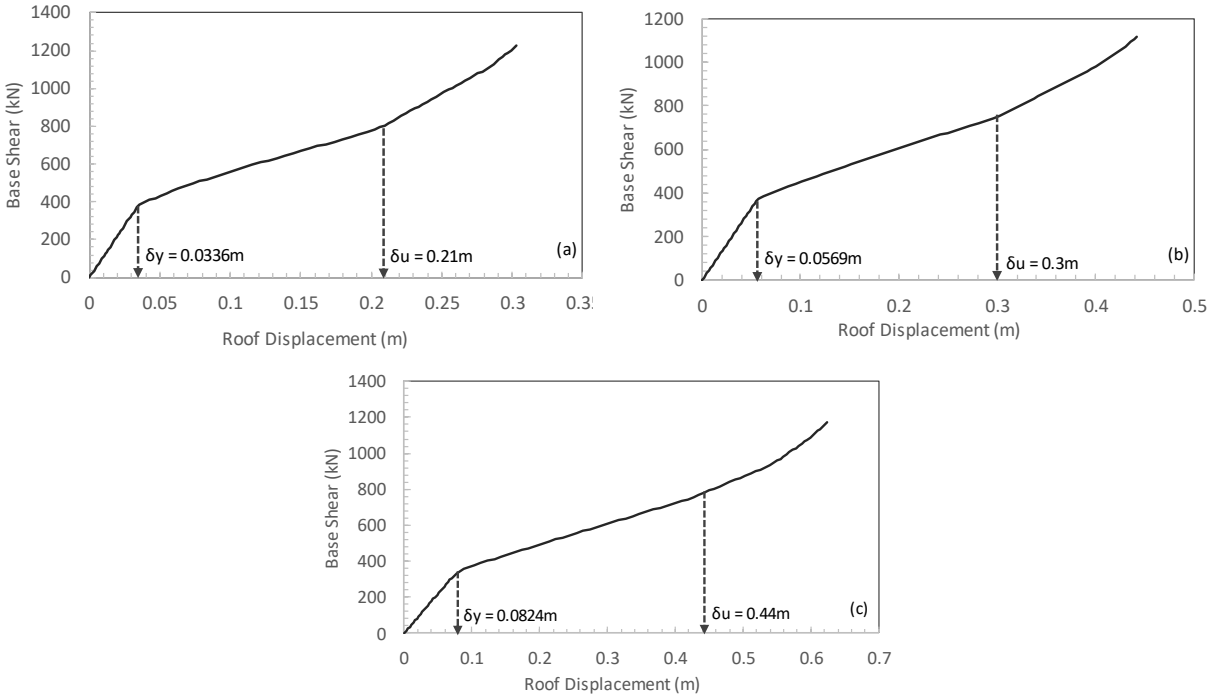

Figure 5-12: Pushover curves for the (a) 4-storied (b) 6-storied and (c) 8-storied frame

After the ultimate displacement (δ_u) values had been calculated using the pushover analyses discussed previously, a detailed calculation was carried out to calculate *Co* which is shown in Table 5-4 to Table 5-6. Each row except the last one in these tables represents a single level/story of the building. For each level, the weight, mass, and ordinates of the mode shape ($\varphi_{1,x}$) are shown. The last row shows the total for the columns required for the calculation of C_o. The final column shows the C_o value calculated for each building archetype using equation 5.8. The required $\varphi_{1,r}$ values can be found in Figure 5-10.

Table 5-4: C_0 coefficient calculation for 4-storied PBSC braced frame

Description	Weight (kN)	Mass (kg)	$\varphi_{1,x}$	$\varphi_{1,x}^2$	$m_x\varphi_{1x}$	$m_x*\varphi_{1x}^2$	C_0
Roof	126.65	12914.42	0.0053000	0.0000281	68.45	0.36	1.305
Story 3	176.83	18031.73	0.0045000	0.0000203	81.14	0.37	
Story 2	177.16	18064.97	0.0032000	0.0000102	57.81	0.18	
Story 1	177.48	18098.21	0.0016000	0.0000026	28.96	0.05	
Total	658.12	67109.33			236.35	0.96	

Table 5-5: C_0 coefficient calculation for 6-storied PBSC braced frame

Description	Weight (kN)	Mass (kg)	$\varphi_{1,x}$	$\varphi_{1,x}^2$	$m_x\varphi_{1x}$	$m_x*\varphi_{1x}^2$	C_0
Roof	126.34	12883.39	0.0046000	0.0000212	59.26	0.27	1.35
Story 5	176.20	17967.47	0.0041000	0.0000168	73.67	0.30	
Story 4	176.50	17998.49	0.0035000	0.0000123	62.99	0.22	
Story 3	176.83	18031.73	0.0026000	0.0000068	46.88	0.12	
Story 2	177.16	18064.97	0.0017000	0.0000029	30.71	0.05	
Story 1	177.48	18098.21	0.0008000	0.0000006	14.48	0.01	
Total	1010.52	103044.27			288.00	0.98	

Table 5-6: C_0 coefficient calculation for 8-storied PBSC braced frame

Description	Weight (kN)	Mass (kg)	$\varphi_{1,x}$	$\varphi_{1,x}^2$	$m_x\varphi_{1x}$	$m_x*\varphi_{1x}^2$	C_0
Roof	126.34	12883.39	0.0041	0.0000168	52.82	0.217	1.37
Story 7	176.50	17998.49	0.0038	0.0000144	68.39	0.260	
Story 6	175.90	17936.45	0.0034	0.0000116	60.98	0.207	
Story 5	176.20	17967.47	0.0028	0.0000078	50.31	0.141	
Story 4	176.50	17998.49	0.0022	0.0000048	39.60	0.087	
Story 3	176.83	18031.73	0.0016	0.0000026	28.85	0.046	
Story 2	177.16	18064.97	0.001	0.0000010	18.06	0.018	
Story 1	177.48	18098.21	0.0005	0.0000003	9.05	0.005	
Total	1362.92	138979.21			328.07	0.981	

In the next step, effective yield displacements were calculated from equation 5.7. Some of the required parameters e.g. ultimate displacements (δ_u) and maximum base shear capacities were taken from Figure 5-12. Time periods for these frames were calculated as per equation (5.9) of NBCC (2010).

$$T = 0.025h_n \qquad (5.9)$$

Using the frame heights, building weights, time periods, ultimate displacement and base shear capacity it was found out that the effective yield displacements for 4, 6 and 8-storied frames are 0.06m, 0.092m and 0.138m respectively. By calculating the ratio of $\delta_u/\delta_{y,\,eff,}$ the following period based ductility values were found (3.50, 3.27 and 3.20) for the 4, 6 and 8-storied frame respectively. As per expectation, the period based ductility decreased with the increase of frame

height. A similar trend for decreasing ductility with story height was observed in Haque and Alam (2015b) for rack clad building structures.

Table 5-7: Period based ductility calculation

Parameters	4-Storied	6-Storied	8-Storied
Frame height, h_n	12	18	24
Ultimate displacement, δ_u	0.21	0.3	0.44
Maximum base shear capacity, V_{max}	800	760	780
Building weight, W	658.12	1010.52	1362.92
Time period as per code equation, T	0.3	0.45	0.6
Time period from modal analysis, T_1	0.39	0.6032	0.84
max(T,T_1)	0.39	0.6032	0.84
C_0	1.31	1.35	1.37
$\delta_{y,eff}$	0.060	0.092	0.138
μ_T	3.50	3.27	3.20

In the final step, spectral shape factor and adjusted collapse margin ratio were calculated using time periods and period based ductility values calculated earlier. SSF values for different fundamental time periods and period based ductilities are given in Table 7-1b (*SDC* D_{max}) of FEMA (2009). The *SSF* values were interpolated from the above mention table and are shown in Table 5-8. Adjusted collapse margin ratios were calculated using equation 5.5, and it was found that the values ranged from 4.24 to 4.47. Average value of *ACMR* was found to be 4.37.

Table 5-8: Spectral shape factor (*SSF*) calculation

	4-Storied	6-Storied	8-Storied
Time Period, T	0.39	0.60	0.84
Period based ductility, μ_T	3.50	3.27	3.20
SSF	1.2	1.21	1.238
CMR	3.67	3.50	3.61
ACMR	4.40	4.24	4.47
Average *ACMR*	4.37		

5.2.1 Acceptable values of collapse margin ratio

The *ACMR* values calculated above were checked against the acceptable values provided in Table 7-3 of FEMA (2009). The table provides acceptable values of adjusted collapse margin ratios

($ACMR_{10\%}$ and $ACMR_{20\%}$) for different levels of total system collapse uncertainty (β_{TOT}) and values of acceptable collapse probabilities (10% and 20%). The table mentioned above was generated based on the assumption that the collapse level uncertainty distribution is lognormal with a median of S_{CT} and lognormal standard deviation equal to β_{TOT}. The FEMA table mentioned above also provides acceptable ACMR values for other levels (5%, 15%, and 25%) of collapse probabilities. However, they are provided only for reference and comparison. Higher values of collapse probability and lower values of total system collapse uncertainty requires lower values of adjusted collapse margin ratio and vice versa.

5.2.1.1 Total system collapse uncertainty

System collapse capacity is a highly variable parameter, and many sources of uncertainties influence it. Therefore, it is essential to take all significant sources of uncertainty into account in collapse response to incorporate their effects in the collapse evaluation process. There are various sources of collapse uncertainties e.g.: record to record uncertainty (*RTR*), design requirement uncertainty (*DR*), test data uncertainty (*TD*), modeling uncertainty (*MDL*).

Record-to-record uncertainty occurs due to the variability in the response of building archetype models under different earthquake records. This variability is evident in the IDA plots shown in Figure 5-8. This variability in interstory drift ratio response can be attributed to the difference in frequency content and dynamic characteristics of the ground motion records in the far-field record set. Furthermore, this variability is also dependent on the far-field ground motion record set's hazard characterization. From previous studies (Haselton 2006; Ibarra and Krawinkler 2005a; b; Zareian and Krawinkler 2006) it was found out that the value of β_{RTR} ranges from 0.35 to 0.45 and it is fairly consistent among various building types. It was found from previous research and studies

that archetypes with μ_T values higher than or equal to 3.0 have a fixed β_{RTR} value of 0.40. For μ_T values lower than 3.0, the β_{RTR} value can be calculated using equation 5.10. However, the β_{RTR} value must be equal to or higher than 0.20. As all μ_T values for the PBSC index archetypes were found larger than 3.0 (Table 5-7), the β_{RTR} value was found to be 0.40.

$$\beta_{RTR} = 0.1 + 0.1\,\mu_T \qquad (5.10)$$

The next uncertainty is known as the design requirement related uncertainty (β_{DR}). This uncertainty is dependent on the robustness and completeness of the design requirements. This uncertainty is quantified with respect to the quality of design requirements. Robustness and completeness of test data related uncertainty are taken care of by the test data uncertainty parameter (β_{TD}). This uncertainty is quantified with respect to the test data quality. The last uncertainty parameter is Modeling uncertainty (β_{MDL}). This uncertainty represents how well a full range of structural response characteristics and associated design parameters are represented by the index archetype models. This parameter also represents how well the archetypes simulate collapse behavior by direct simulation or non-simulated checks of the components. β_{MDL} is measured by the quality of archetype models.

The total collapse uncertainty is denoted by the lognormal standard deviation parameter (β_{TOT}). It is calculated by combining the uncertainties mentioned above and expressed using the following equation. The range of values for the parameters in Equation 5.11 are given below.

$$\beta_{TOT} = \sqrt{\beta_{RTR}^2 + \beta_{DR}^2 + \beta_{TD}^2 + \beta_{MDL}^2} \qquad (5.11)$$

Where,

β_{TOT} = total system collapse uncertainty (0.275 - 0.950)

β_{RTR} = record-to-record collapse uncertainty (0.20 - 0.40)

β_{DR} = design requirements-related collapse uncertainty (0.10 – 0.50)

β_{TD} = test data-related collapse uncertainty (0.10 – 0.50)

β_{MDL} = modeling-related collapse uncertainty (0.10 – 0.50)

For the PBSC archetypes the following values were selected for the above-mentioned uncertainty parameters: $\beta_{RTR} = 0.40$, $\beta_{DR} = 0.2$, β_{TD} = 0.35, and β_{MDL} = 0.35. These values were chosen based on the assumptions discussed below.

As per equation 5.10 and μ_T values in Table 5-8, the calculated value of β_{RTR} is 0.40. For the other three uncertainty parameters related to design requirements, test data, and nonlinear models, the following scale was used for selecting values for the corresponding β parameters. The scale is as follows for the qualities of each uncertainty parameter: (A) Superior, β = 0.10; (B) Good, β = 0.20; (C) Fair, β = 0.35; and (D) Poor, β = 0.50. As Canadian building design requirement is strict and of a very high standard and the parameter value of 0.2 was chosen for $\beta_{DR.}$ Although no tests were performed for the PBSC bracing system, good quality test data is available in the literature for shape memory alloy used in the system; therefore, a fair rating with value 0.35 was chosen for the β_{TD} parameter. The archetype model was carefully designed and modeled with nonlinear lumped plasticity based hysteresis model specifically developed for this bracing system. However, nonlinear connection models were not modeled due to lack of data; therefore, a quality rating of fair (β = 0.35) was chosen for the nonlinear model uncertainty parameter $\beta_{MDL.}$ Putting this values in equation 5.11 gives a value of 0.67 for $\beta_{TOT.}$

5.2.1.2 Acceptable values of collapse margin ratio

In this section, acceptable values of collapse margin ratios are calculated using the total collapse uncertainty and adjusted collapse margin ratio calculated in the previous sections of this chapter. Table 5-9 shows the acceptable CMR values for 10% and 20% probabilities of collapse.

These values are taken from Table 7-3 of FEMA (2009). The minimum ACMR value of the individual archetypes was checked against $ACMR_{20\%}$, and the average ACMR across the performance group was checked against $ACMR_{10\%}$. Both of the ACMR values were found to be higher than the acceptable CMR values, which indicate that collapse probability of the PBSC index archetypes are lower than the FEMA (2009) suggested limit; which means under MCE ground motion an individual archetype has lower than 20% probability of collapse and the whole group on average has less than 10% probability of collapse. Therefore, the R_d and R_o value selected for designing the PBSC index archetypes are adequate for ensuring safety against collapse under MCE ground motion intensity.

Table 5-9: Acceptable values of collapse margin ratio

Description	Value
Total System Collapse Uncertainty, β_{TOT}	0.67
ACMR $_{10\%}$	2.35
ACMR $_{20\%}$	1.75
ACMR average across performance group	4.37
Minimum of individual ACMR	4.24

5.3 Overstrength Factor

The overstrength factor (R_o) was checked using pushover analysis to compare against the initial value assumed at the beginning of this study. To find out the overstrength factor the yield base shear force was divided by the base shear force at first component yielding for all three frames. These base shear forces along with the calculation of overstrength factor are shown in Table 5-10. It was found that the average value of the overstrength factor for the PBSC braced frame is 1.07 which is very close to 1.10 assumed in design. Hence, no re-design/re-analysis is required for the determination of R_o factor.

Table 5-10: Overstrength Factor (R_o) calculation

	4 Storied	6 Storied	8 Storied
Yield Force	420	390	355
Vd (first yield)	371.9	372	343
Overstrength	1.13	1.05	1.03
Average	1.07		

5.4 Summary

Three PBSC braced frame models were created in S-FRAME Structural analysis and design software. These building frames were designed using (NBCC 2010) building code and (CSA 2009) design standard. These buildings were designed using arbitrary values of R_d = 6.0 and R_o = 1.1. After the design, nonlinear archetypes were built using hysteresis model developed for the PBSC bracing system. Finally, incremental dynamic time history analysis was carried out on the nonlinear archetypes using 44 far-field ground motion records which were normalized with respect to the record set's median PGV. From this analysis, the median collapse earthquake intensities were calculated, and they were used to calculate collapse margin ratios. These collapse margin ratios were adjusted for spectral shape factor and finally compared against acceptable limits. It was found out that all individual archetypes and the group passed the acceptable limit of collapse margin ratios. Therefore, it could be concluded that the initial seismic performance factor values (R_d = 6.0 and R_o = 1.1) are adequate for seismic design of this system.

CHAPTER 6: SEISMIC FRAGILITY COMPARISON BETWEEN PBSC AND BRB BRACING SYSTEM

6.1 General

This chapter concentrates on the seismic vulnerability assessment of PBSC braced frames using fragility functions. Fragility functions were developed to determine the probability of exceedance of certain damage states for this bracing system. The damage states were defined with respect to maximum interstory drift ratios. These fragility functions were generated using probabilistic seismic demand models (PSDM). The data for the fragility functions were calculated from nonlinear dynamic time history analysis with a suite of 44 far-field ground motion records. To understand the advantages and disadvantages of the PBSC bracing system, a similar analysis was carried out on the buckling restraint bracing (BRB) system. Both structural force resisting systems were designed using NBCC 2010 building code and CSA S16-14 standard. Bilinear kinematic hysteresis model was used to represent the axial force-deformation hysteresis of the buckling restrained braces; on the other hand, modified SMA flag hysteresis model with residual and sliding response was utilized to represent the nonlinear response of the PBSC bracing system. The fragility functions provided a great insight into the vulnerability of PBSC brace frames against different levels of earthquake intensity and helped in understanding the impact of using SMA in the bracing system in contrast to steel. This study found that the use of SMA in a bracing system (PBSC) could significantly reduce the vulnerability of steel frames in terms of transient interstory drift ratio compared to the counterpart for most of the damage states under consideration. The scope of this study is limited to only short to medium-tall buildings and the seismicity of Western

Canada. Further studies should be carried out if the application of the outcome of this study falls outside the scope mentioned above.

6.2 Research significance

Canada's western coast, particularly Vancouver Island, and Vancouver area are considered as the most earthquake hazard prone areas. Vancouver is Canada's gateway to the Pacific, and a large portion of the Canadian economy is dependent on the well-being of this region; therefore, the economic impact of a major earthquake event in this region could be severe. Any high-intensity earthquake event could cause major damage to the infrastructure which could in turn cripple the economy of this nation. Therefore, seismic vulnerability assessment of the building infrastructure of this region is of high importance. This study focuses on the seismic fragility assessment of the novel PBSC braced frames designed for this region and provides a recommendation on how to improve their performance.

6.3 Description of the building models

Similar to the building seismic performance factor study (Chapter 5), three 4x4 bay wide building frames with different story heights (four, six and eight storied) were selected for this study (Figure 5-5). Two sets of these models were created; one set for the PBSC bracing system and the other for the buckling restrained bracing system. The BRB and PBSC building models were analyzed and designed as per NBCC (2010) seismic design provisions. The steel sections were designed using CSA (2009). However, the PBSC braced frames were designed using $R_d = 6.0$ and $R_o = 1.1$, which was found from the building seismic performance factor study done earlier. The PBSC braces were designed using the design method shown in Appendix A.

6.4 Finite element modeling and analysis

All of the building frames models mentioned above were built in the S-FRAME (2016) structural analysis and design software. This software utilizes finite element method for creating analysis models. After the design of the buildings, nonlinear analysis models were created using lumped plasticity models. Link elements were introduced at the brace ends for representing their load deformation hysteresis under cyclic loading. Consistent mass matrix formulation was used rather than the lumped mass matrix to achieve better accuracy. Furthermore, for Rayleigh damping matrix formulation, both stiffness and mass matrices were derived from the initial geometry of the structure.

Nonlinear dynamic time history analysis was carried out on the three PBSC braced frame models to find out maximum interstory drift response under different earthquake records. The Newmark (1959) time history integration method was used for this analysis. Similar to the incremental dynamic analysis done for the building seismic performance factor calculation, the following values for alpha and delta parameters were chosen: alpha = 0.25 and delta = 0.50. Geometric nonlinearities were also taken into consideration which included large P-delta effect. To reduce analysis complexity and limit the number of finite element models, structural geometric variabilities (plan and elevation) and material strength uncertainties are not taken into consideration in this study.

6.5 Earthquake records

Due to the scarcity of a vast number of strong earthquake records for British Columbia, strong ground motion records were chosen from all over the world instead. The records were selected from the far-field record set provided in the (FEMA 2009) guideline. Using the ground motion

record information available in the guideline, the records were downloaded from PEER NGA strong motion database. The record set contains ground motion records from twenty-two individual earthquake events. Every one of these events has two horizontal and one vertical component. For this analysis, only the horizontal components of the ground motions were used. In total 44 ground motion records were used for analyzing the PBSC and BRB building frames. The records are from rocky soil type with a moment magnitude (M_w) greater than or equal to 6.5. Only far-field record set was selected due to the inherent complexity associated with the characterization of the near-field records. Figure 6-1 represents the response spectra of the 44 far-field ground motion records. In the same figure, the mean and the mean plus one and two standard deviation response spectra are also plotted. These ground motion records were applied in the in-plane direction of the PBSC and BRB braced frames. After each time history analysis, if nonlinearity was not observed, then the earthquake records were scaled up until significant nonlinear behavior or collapse were observed. This ensures that building responses were recorded at higher PGA values not covered in the ground motion record set.

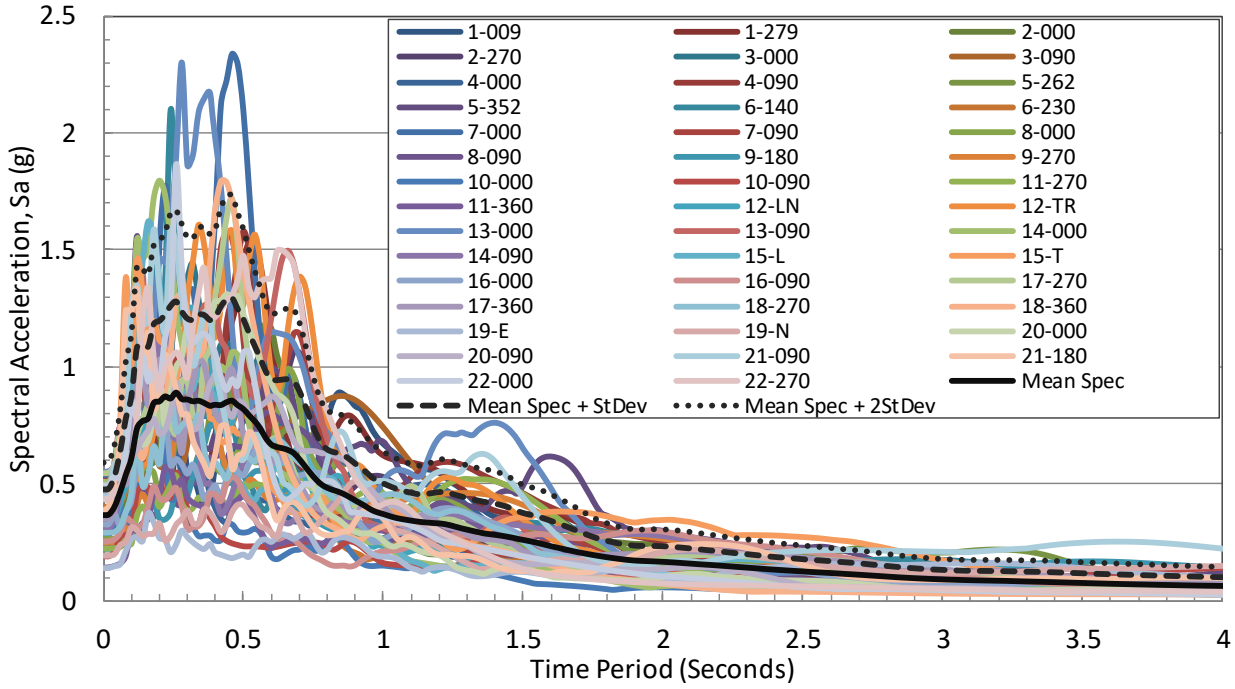

Figure 6-1: Response spectra of the selected 44 far-field ground motion records.

6.6 Results and discussions

The logarithmic relationship between spectral acceleration (S_a) and interstory drift ratio percentage for the three PBSC and three BRB braced frames are shown in Figure 6-2(a)-(c). A regression analysis was carried out using this data to find out two important parameters "*a*" and "*b*", required for the development of fragility functions. These parameters are calculated from the tangent and intercept values of the ln(ISDR%) vs. ln(S_aT) plot. The equation for "*a*" and "*b*" are given in equations 6.1 and 6.2. If the equation of the plot is written in the "$y = mx+c$" format, then

$$a = e^c \tag{6.1}$$

$$b = m \tag{6.2}$$

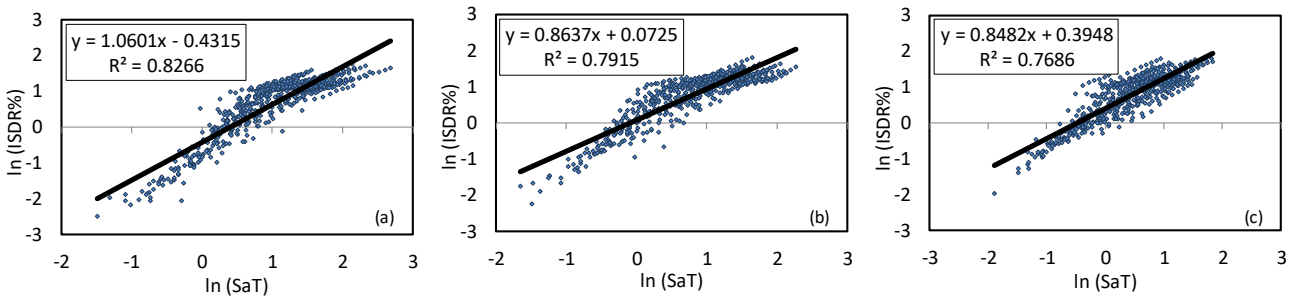

Figure 6-2: ln(ISDR%) vs. ln(S_aT) distribution for the (a) four (b)six and (c)eight-storied PBSC braced frame

The fragility curves for the four, six and eight storied PBSC braced frames are shown in Figure 6-3(a)-(c) respectively. Each figure compares four different damage states; they are as follows: Operational (O), immediate occupancy (IO), life safety (LS), and collapse prevention (CP). These damage states were defined using FEMA (2000) guideline and the work of Fahnestock et al. (2006). The interstory drift ratio values for these damage states are shown in Table 6-1. For the PBSC bracing system, unlike the other three damage states, the collapse prevention (CP) damage state was not directly adopted from the above-mentioned guidelines and reports; instead this limit was calculated from the brace design procedure shown in Appendix A. The CP limit state of the PBSC bracing system is a variable quantity which can be manipulated by changing the brace design. For example, designing the brace with longer NiTinol bar would increase the collapse prevention ISDR% and vice versa. For the current design with 1m long NiTinol bars, the ISDR% at CP limit state was found to be 2.66%. If 2m long SMA bars were used in the design, then this limit would increase by two-folds to 5.33%. However, before reaching that high interstory drift ratio other structural components (beams, columns, and connections) would fail, making the use of longer NiTinol bar inefficient. Therefore, the length of the NiTinol bars should be selected based on the required/demand ISDR% and other component limit states while minimizing the cost of the brace.

Table 6-1: Damage states based on interstory drift ratio percentage

Damage State	PBSC	BRB
Operational (O)	0.5	0.5
Immediate Occupancy (IO)	1	1
Life Safety (LS)	2	2
Collapse Prevention (CP)	2.66	4

Figure 6-3(a) shows fragility curves with four different damage states for the four-storied PBSC braced frame. From this figure, it can be comprehended that the four-storied frame is very robust and has almost no probability of collapse up to a spectral acceleration of 2.0g. After this spectral acceleration value, the likelihood of collapse gradually increases to 0.72 for a S_a value of 14.0g; which is a very high spectral acceleration and unlikely to occur during the lifetime of the building. On the other hand, the life safety damage state curve is much steeper compared to the collapse prevention damage state curve. There is no probability of life safety damage until 1.0g spectral acceleration; however, there is around 10% probability at S_a = 2.0g. This curve gradually reaches a value close to unity at S_a = 14.0g. The third curve under discussion is the Immediate occupancy damage state curve. It can be seen that, at S_a = 1.0g, there is approximately 5% probability of damage for the four-storied frame. This curve is much steeper compared to the previous two curves discussed earlier. At S_a = 2.0g, the probability of damage is around 50%, which is very high compared to the previous curves. The final curve is for operational damage state, which is the steepest among the four. From this figure, it can be seen that there is approximately 97% probability of damage even at a low S_a value of 0.5g.

Fragility curves for six-storied PBSC frame are shown in Figure 6-3(b). From this figure, it can be seen that the six-storied frame has a slightly higher probability of collapse for all four damage states compared to the four-storied frame. At Sa =1.0g there is a very slight (around 1%)

probability of collapse for the six-storied frame which increases close to 10% at S_a = 2.2g. The life safety damage state reaches the same 10% probability of damage at S_a = 0.7g. For Immediate occupancy damage state, it requires only 0.4g spectral acceleration to arrive at the same probability of damage. Finally, the operational damage state curve has a 99% probability of exceedance at S_a equal to 0.225g.

Figure 6-3(c) depicts the four-damage state fragility curve for the eight-storied PBSC braced frame. The fragility curves in this figure are similar to the six-storied frame. However, the curves are slightly steeper compared to the previous ones. If we compare the S_a values for 10% probabilities of exceedance for each damage states, we can see that the collapse prevention damage state curve achieves this at 1.1g. The life safety and immediate occupancy damage state achieve this same probability at 0.35g and 0.22g respectively; while the operational damage state achieves this at less than 0.05g spectral acceleration.

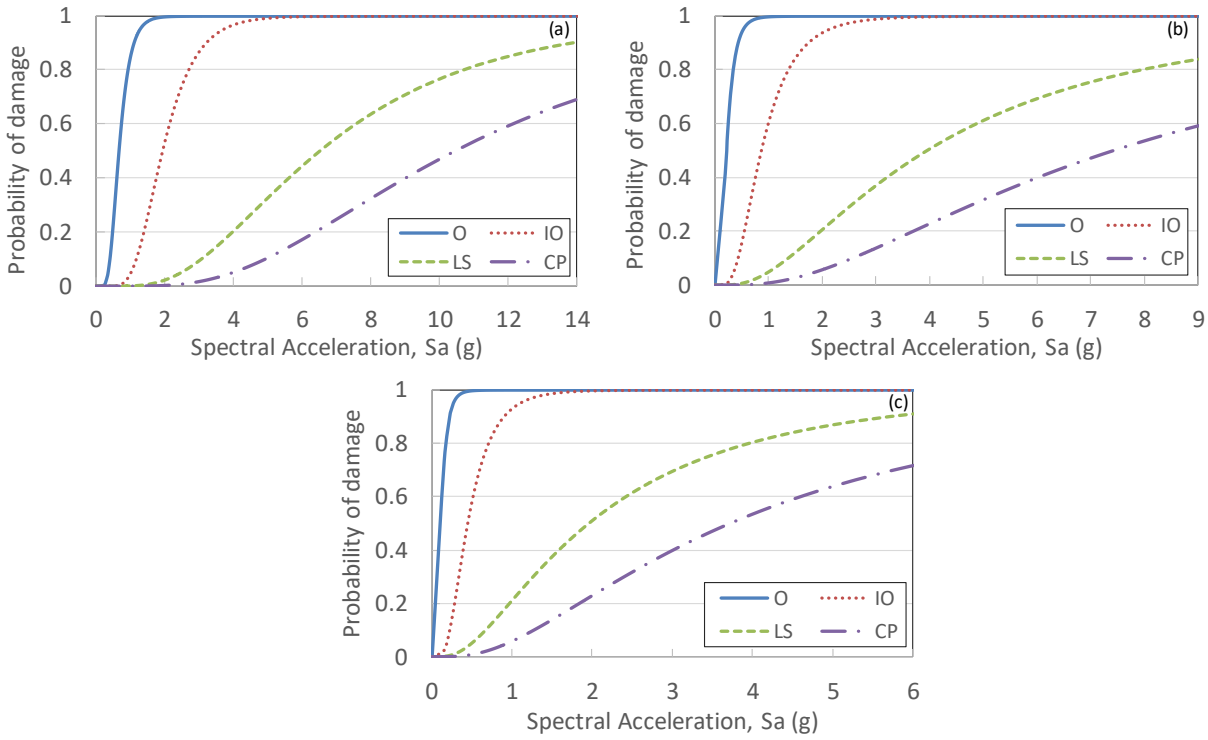

Figure 6-3: Fragility curve for (a) four (b) six and (c) eight-storied PBSC braced frame

The above mentioned three frames were compared against each other with respect to the four damage states discussed above. It was found out that for these damage states, the four-storied PBSC frame has the lowest probability of damage. On the other hand, the eight-storied frame has the highest probability of damage while the six-storied frame has damage probabilities in between these two frames. Therefore, for the PBSC frame, an increase in building height equates to an increase in damage probability for the same earthquake intensity level.

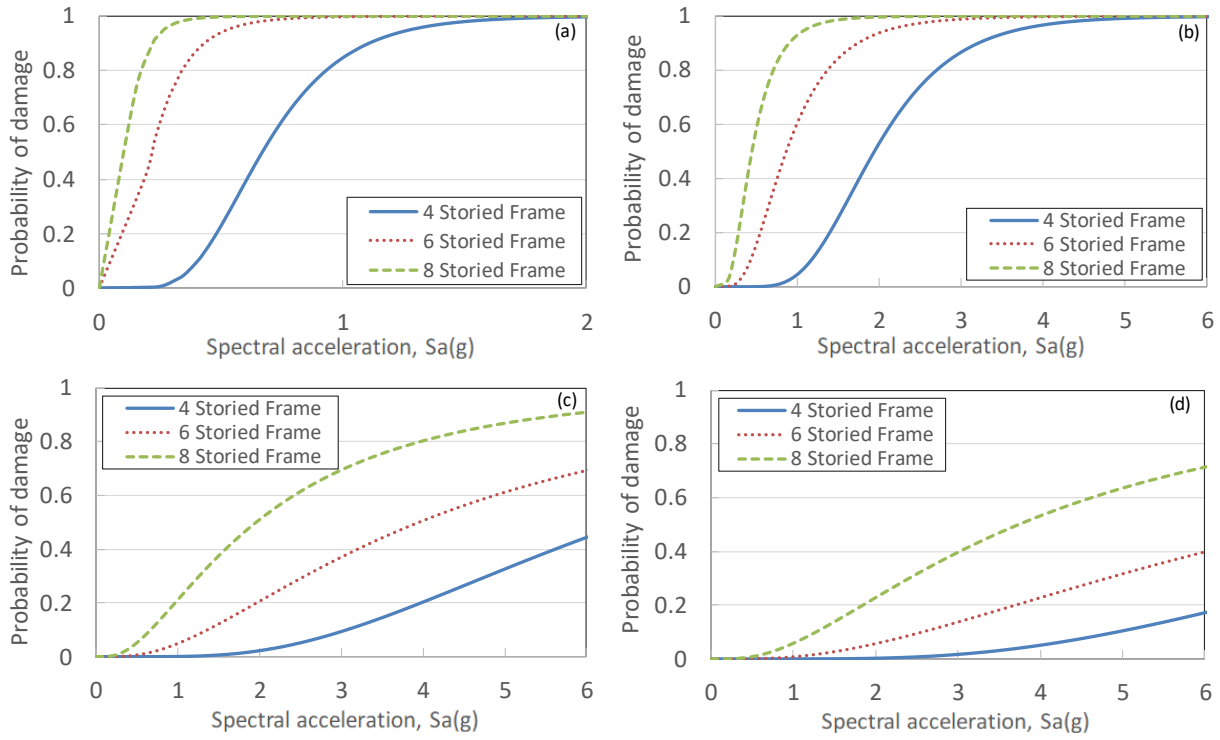

Figure 6-4: Different damage states compared between three PBSC frames (a) operational (b) immediate occupancy (c) life safety and (d) collapse prevention

6.7 Buckling restraint bracing system

The fragility analysis mentioned above was carried out on buckling restrained braced frames for comparison with the PBSC bracing system. The four, six and eight-storied building frames used for PBSC bracing system were designed using standard star seismic braces. ETABS (2015) building analysis and design software was utilized for the analysis and design of the BRB frames. Similar to the PBSC braced frame design, the buildings were assumed to be in a soil class "C" site in Vancouver. The frames were designed using an R_d value of 4.0 and R_o value of 1.2. From the design, it was found out that Star Seismic BRB section 1.0 was adequate in resisting the design earthquake loading. This section has a core area of 645mm^2. The initial stiffness is 30230kN/m and the post-yield stiffness is 513.9kN/m, yield force is 197.94kN and tension strength 233.53kN/m.

After the design, same 44 far-field earthquake records (Figure 6-1) from PEER NGA database were used to carry out nonlinear dynamic time history analysis on the three BRB frame models which were used earlier for the PBSC building frames. Similar to the previous analysis, some of the earthquake records were scaled to include higher spectral acceleration values not covered in the original unscaled record set.

From the incremental dynamic time history analysis results and equation 6.1, equation 6.2 and Figure 6-5(a), the values of "*a*" and "*b*" are 0.7888 and 0.9367 respectively. These parameters were used to calculate mean and standard deviation for the four damage states (Operational, Immediate occupancy, life safety and collapse prevention) discussed earlier.

Figure 6-5(a)-(c) shows the natural logarithmic relationship between the earthquake spectral intensity and interstory drift ratio percentage for the four, six and eight storied BRB frames.

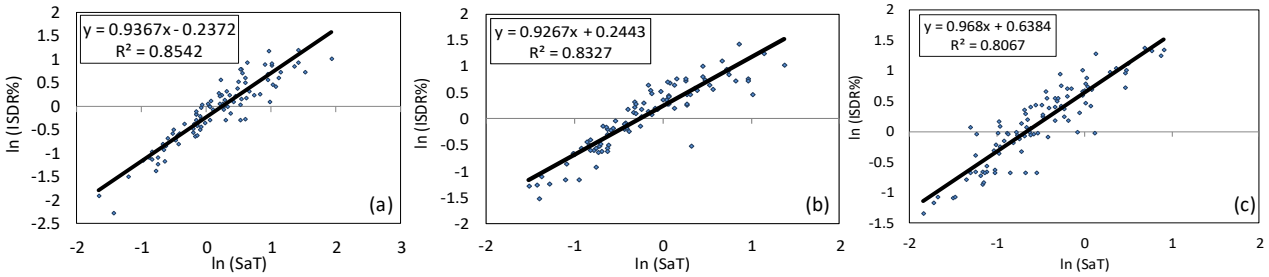

Figure 6-5: ln(ISDR%) vs. ln(SaT) distribution for the (a) four-storied (b) six-storied and (c) eight storied BRB frame

Figure 6-6(a)-(c) shows the fragility curves for the four, six and eight-storied brb frame. The above mentioned four damage states are shown in this figure. The four storied BRB frame was analyzed up to a spectral acceleration value of 7g. It was found out that even at that high intensity, there was almost no probability of collapse. However, at the same intensity, there is approximately 60% probability of exceeding the life safety damage state. The other two damage states, for example, the operational and immediate occupancy level achieved 100% probability of

exceedance at 1.0g and 4.0g respectively. Similar fragility curves were found for the six-storied BRB frame. However, the six-storied frame was subjected to a maximum spectral intensity of 4.0g. At this intensity, it was observed that the frame has less than 10% probability of exceeding the collapse damage state; however, the life safety damage state reached approximately 80% probability at the same intensity level. The remaining two damage states: operational and immediate occupancy level achieved 100% probability at around 0.6g and 2.0g respectively. Finally, if we analyze the fragility curve of the eight-storied BRB frame then we can see that at 2.5g spectral acceleration the frame reached almost 20% probability of exceeding the collapse prevention damage state. At the same spectral acceleration level, the life safety damage state achieved over 90% probability of exceedance; whereas the immediate occupancy and operational level achieved 100% probability at 1.0g and 0.4g respectively.

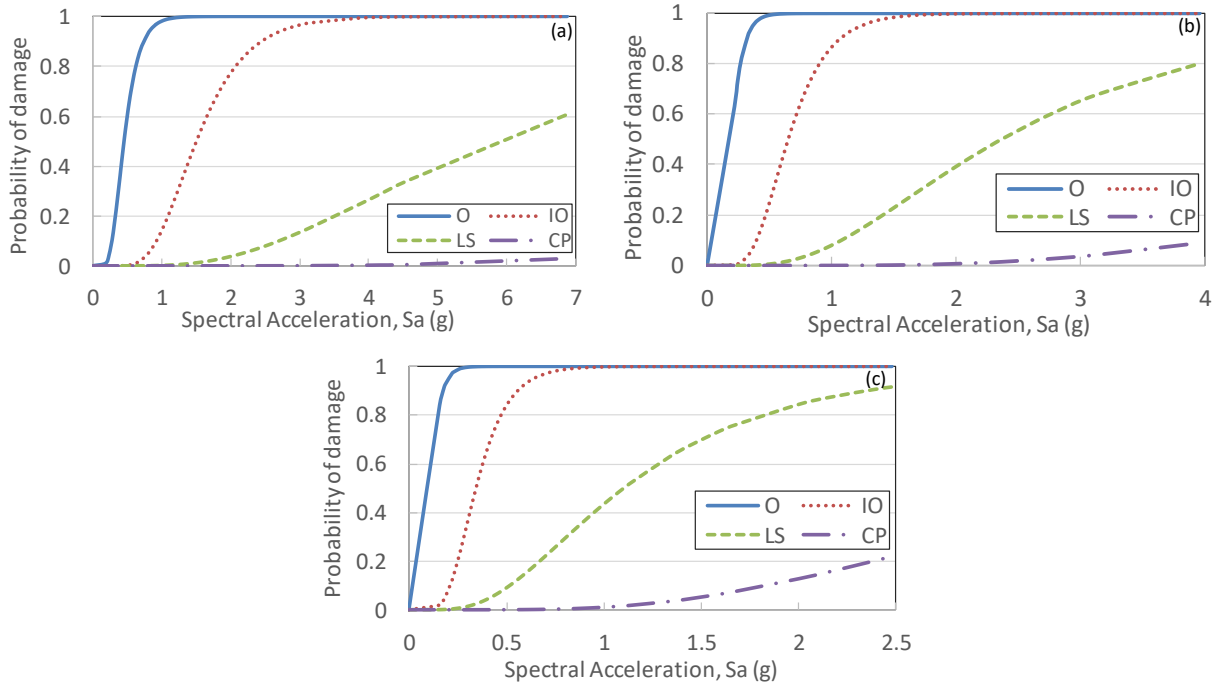

Figure 6-6: Fragility curve for (a) four (b) six and (c) eight-storied BRB braced frame

The above mentioned three frames were compared against each other with respect to the individual damage states. It can be observed that for all four damage states (O, IO, LS, and CP), the probability of damage is lowest for the four-storied frame and highest for the eight-storied frame while six-storied frame remaining in the middle. It was found out that with increasing building height the probability of damage for each damage state increases.

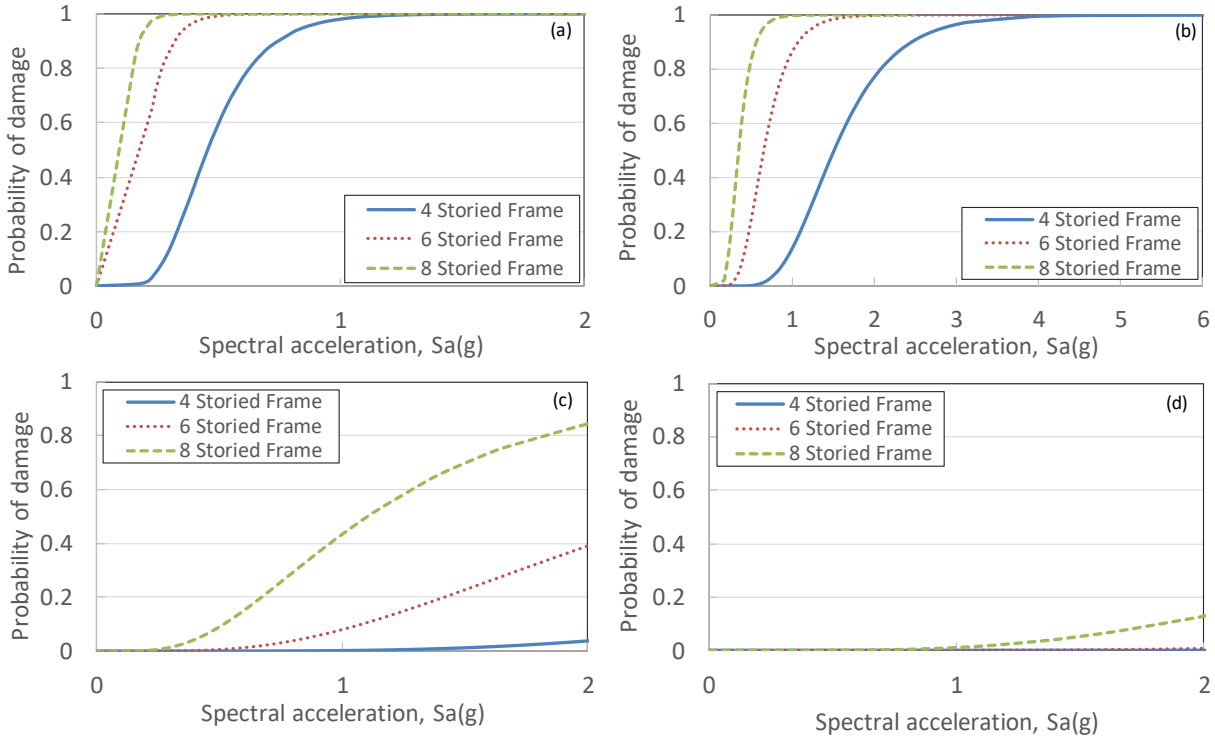

Figure 6-7: Different damage state compared between three BRB frames (a) operational (b) immediate occupancy (c) life safety and (d) collapse prevention

6.8 Fragility comparison between PBSC and BRB frames

The fragility functions were compared between the PBSC and the BRB frames in Figure 6-8. Figure 6-8(a) shows the fragility comparison between four-storied PBSC and BRB frames. It was observed that for operational, immediate occupancy and life safety damage states the PBSC braced frame has a higher fragility curve than the BRB frame; which indicates less probability of exceedance for these three damage states at the same earthquake intensity level. However, for the

collapse prevention damage state, the BRB frame outperformed the PBSC frame. This is due to higher interstory drift capacity of BRB frame (ISDR 0.04) compared to the PBSC frame (ISDR 0.0266) at this damage state.

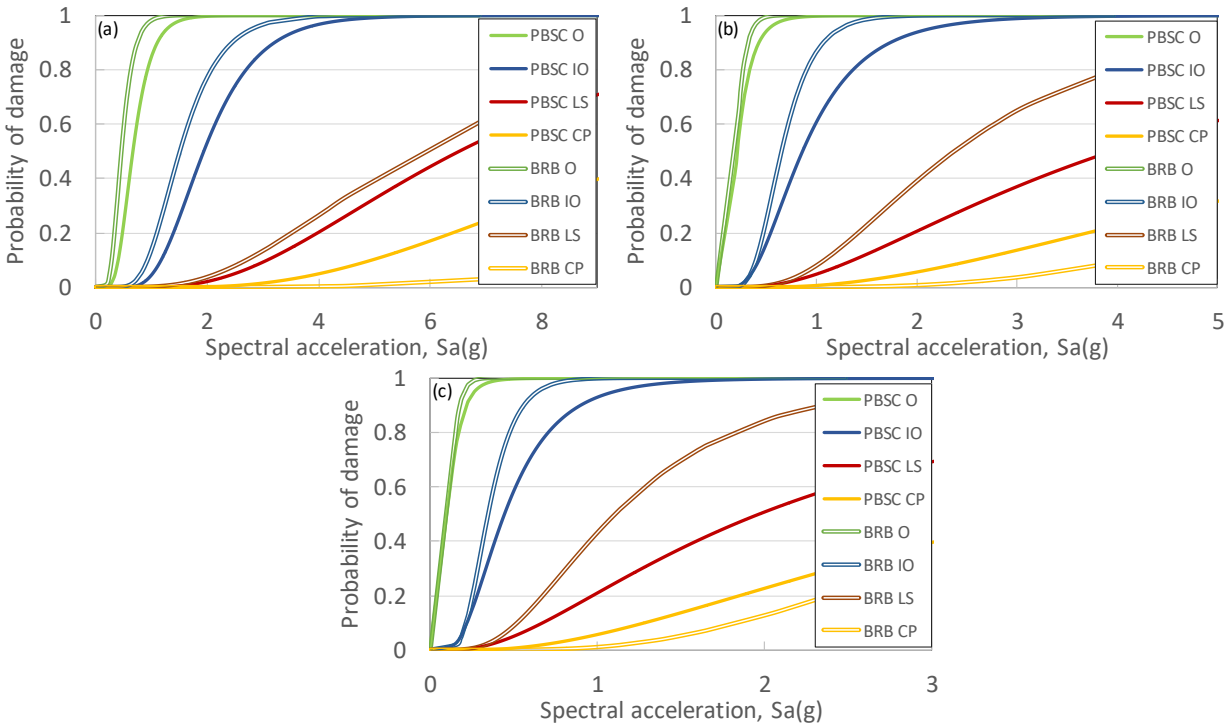

Figure 6-8: Fragility curves compared between PBSC and BRB frames for (a) four (b) six and (c) eight-storied frames

However, for the above analysis, the PBSC braces were designed with only 1m long SMA bars for most economic design; which limited its collapse prevention interstory drift ratio capacity to 2.66% (Appendix A). However, this collapse prevention interstory drift limit can be increased to 4% by either of the following three modifications: (a) Increasing the SMA tie bar lengths to (4/2.66) or 1.5 times the previous length or 1500mm. (b) a different composition of the SMA alloy with a higher recoverable strain (e.g. 9% or greater (Dolce and Cardone 2001)) or (c) a combination of (a) and (b) for an economical alternative. Using method (c) stated above; the brace design was modified. The recoverable strain of SMA bars was set at 9%, and their lengths were increased to

1100mm from 1000mm to have the least impact on the overall stiffness of the braced frame. This modification resulted in a maximum elongation capacity of 1100*.09 or 99mm for the NiTinol bars; including the elastic deformation of the brace shaft the total elongation is approximately 101mm or 1.73% for a 5830mm long brace. Converting this brace elongation to interstory drift ratio using the equation provided in Appendix A, we get a maximum ISDR capacity of 4%. Using this design modification, the fragility analysis was repeated to check the performance against BRB bracing system for the collapse prevention damage state. The result of this comparison is shown in Figure 6-9. In this figure, all three PBSC frames have less probability of collapse for the same spectral acceleration compared to the BRB frames. Therefore, the design of the PBSC bracing system can be easily modified to increase or decrease its damage limit states, which gives great flexibility to the engineers to optimize their design.

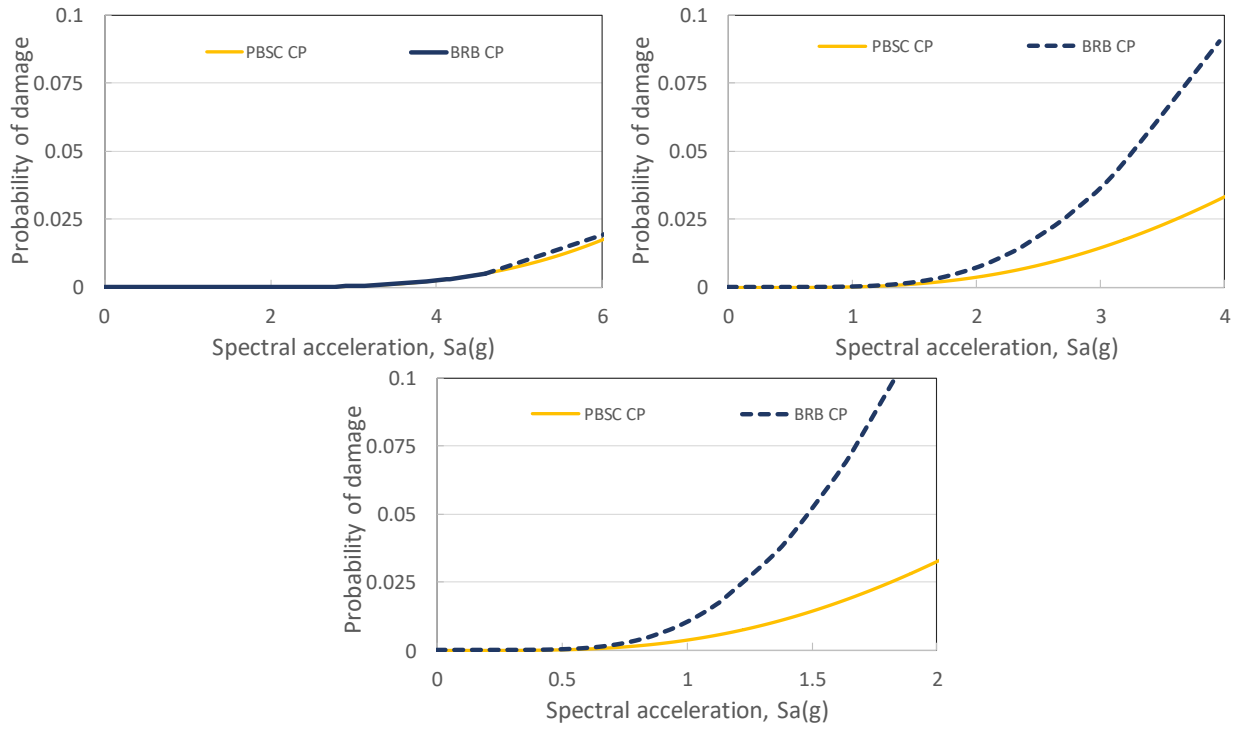

Figure 6-9: Collapse level fragility curves compared between PBSC and BRB frames for (a) four (b) six and (c) eight-storied frames for the modified PBSC brace design.

6.9 Summary

Four, six and eight-storied braced frames were analyzed and designed with both PBSC and BRB bracing systems to compare their seismic performance with respect to fragility function. The PBSC frames were designed with the R_d and R_o values calculated in the previous chapter; whereas, the BRB braces were designed using the code provided values. After the design, nonlinear dynamic time history analysis was carried out on this frames to determine their fragility functions against four damage states. The results revealed the following:

1. For the PBSC bracing system, taller frames are more vulnerable to seismic loading compared to the shorter ones for the same spectral acceleration demand. The similar trend was observed for the BRB frames. However, taller frames usually attract less spectral acceleration from an earthquake compared to a shorter frame. This is due to the higher fundamental period of the taller frames compared to the shorter ones.
2. Both PBSC and BRB frame groups have almost no probability of collapse against spectral acceleration values near 1.0g, which is the maximum probable spectral acceleration in Canada.

For operational, immediate occupancy and life safety performance levels the PBSC frames outperformed the BRB frames in terms of damage probability. However, for the collapse prevention damage state, the BRB showed better performance compared to the PBSC bracing system. However, the collapse fragility of PBSC bracing system could be increased by simply increasing the length of SMA ties or by changing the plateau strain of SMA; which could be achieved by changing the composition of the SMA alloy.

CHAPTER 7: CONCLUSIONS

7.1 Summary

Most of the current seismic force resisting systems utilize energy dissipation mechanism for resisting seismic loading. The piston based self-centering bracing system is taking a different approach in resisting this load. Instead of heavily depending on nonlinear hysteretic energy dissipation this system is relying on its superior self-centering capability. As the system is novel and there are no seismic design guidelines for this system, this thesis is a pioneering effort in shedding some light into this area. To understand this system and other competing systems in this space, a comprehensive literature review is also provided for the readers.

The author has provided schematic diagrams of the system and explained the mechanism of the system in detail. In the next step, the author has built detailed nonlinear finite element models of this bracing system in an advanced finite element analysis software (ABAQUS 2014). The model was developed using solid elements for high accuracy. SMA material hysteresis model developed by Auricchio and Sacco (1997) was used for modeling the SMA bars. Nonlinear quasi-static analysis with cyclic loading on the system revealed excellent self-centering capability indicated by flag-shaped hysteresis. However, the hysteresis material model discussed above does not simulate the residual deformation of SMA, therefore in the next step, the author developed a new hysteresis model for NiTinol based SMAs with residual deformation. This material model was integrated into a MATLAB based finite element program developed for analyzing the PBSC bracing system. After carrying out the nonlinear quasi-static analysis with the PBSC bracing system, the author discovered a novel hysteresis for the brace. This hysteresis exhibits both residual deformation and sliding response. To understand the seismic behavior of buildings

utilizing the PBSC bracing system, this hysteresis model was coded and implemented in a commercial structural analysis and design software know as S-FRAME.

National building code of Canada utilizes force based seismic design procedure for designing buildings against seismic loading; which requires the determination of overstrength and ductility related force reduction factors. The author adopted FEMA P695 methodology for determining these factors for this novel structural system. Three building models were designed, and nonlinear models were built in S-FRAME Software environment. During the design process, the initial values of R_d and R_o were chosen to be 6.0 and 1.1 respectively. Then the author carried out incremental dynamic time history analysis on these building frame models using 44 normalized strong motion records retrieved from the PEER NGA strong motion database. From the analysis, it was found out that the adjusted collapse margin ratios were higher than the acceptable limits; therefore, the tentative values of R_d and R_o selected during the design are satisfactory.

This study also presented the performance comparison between the PBSC and the BRB frames designed under same seismic and gravity loading conditions. Three frames from each group were designed as per NBCC (2010), and their performances were evaluated and compared with respect to fragility functions. Four limit states (Operational, immediate occupancy, life safety and collapse prevention) were defined as per FEMA (2000) guideline. From the fragility analysis, it was found out that, for both PBSC and BRB frames the seismic vulnerability increases with the increase in building height for a specific spectral acceleration. Furthermore, it was found that both systems have very low probability of achieving the collapse damage states even at the high seismic spectral intensity of 3.0g. Finally, it was found that the BRB frame is more vulnerable under operational, immediate occupancy and life safety damage states but less vulnerable for collapse prevention

damage state compared to the PBSC braced frame under the same spectral acceleration level. However, it was also found out that the seismic fragility of collapse prevention damage state for the PBSC bracing system can be improved if longer SMA bars are utilized. This would make PBSC bracing system provide similar or better margin of safety against collapse at the same earthquake intensity.

7.2 Limitations of this study

The limitations of this study are as follows:

1. This study mostly focused on one configuration of the brace where SMA bars are continuous through the piston plate. Another configuration where the bars are discontinued at the piston plate was not studied in detail. However, results published earlier showed similar hysteresis behavior.
2. Sensitivity studies were not carried out for finding out the optimal part sizes for the PBSC brace; this was done based on the assumption that these parts/components (e.g. shaft, sleeve, and nuts) will be designed as per the established codes/standards. These components should be capacity protected to ensure that yielding and nonlinear deformation only takes place in the SMA tie bars.
3. Two-dimensional frame analyses were carried out instead of three-dimensional ones. This was done to reduce analysis time.
4. Only braces were considered nonlinear in the analysis. However, the beam-to-column and column-to-foundation connections could exhibit some moment-rotation stiffness and hysteresis even they are not designed for that purpose. This behavior was ignored in this study.

5. No experimental investigation was carried out on the PBSC bracing system. However, the residual deformation based SMA material hysteresis model was validated against experimental results. Furthermore, a small scale PBSC brace prototype has recently been built in the UBC Okanagan's ALAMS lab, and its test results will be published in subsequent studies.

7.3 Conclusion

The following conclusions can be drawn from this study

1. The finite element analysis on the PBSC bracing system showed flag-shaped hysteresis response. This hysteresis indicates good self-centering capability with moderate hysteresis damping.
2. The PBSC bracing system is more flexible or can be designed to be more flexible compared to traditional or buckling restrained bracing system due to the one-third elastic modulus of NiTinol compared to steel. Furthermore, the length of the NiTinol SMA bars could also be adjusted and the stiffness of bracing system and the structure could be adjusted. A lower stiffness results in a lower period and eventually lower base shear force from the response spectrum analysis; which could eventually lead to smaller sections required from the design and thus cost savings.
3. Although the PBSC bracing system has exhibited a sliding response, no perceptible negative impact was found on the seismic performance of the buildings. Excellent self-centering was observed after the earthquake loading was over. The residual interstory drift ratios were found insignificant which indicates almost no or meager repair cost after an earthquake event.

4. The overstrength and ductility related force related force reduction factors were found to be 6.0 and 1.1. The ductility related force reduction factor was found higher than most other systems given in NBCC (2010). Therefore, more detailed analysis with a greater number of stories and bays with many different brace configurations should be carried out to determine a more conservative value.
5. The fragility analysis of the PBSC bracing system showed good performance against all limit states (except collapse prevention) for earthquake intensities covered in the design response spectra of Canada. The collapse level fragility of the PBSC braced frame was found to be underperforming against BRB frame however that can be improved by tweaking the brace design (e.g. increasing the SMA bar lengths)

7.4 Recommendations for future research

The following recommendations are given for future research regarding the PBSC bracing system

1. Prototype models should be built in the lab for testing the cyclic performance of the PBSC bracing system.
2. The self-centering capability of portal frames equipped with the PBSC braces should be investigated experimentally using quasi-static cyclic load tests.
3. Shake table testing should be carried out to find out the seismic performance of single storied steel buildings equipped with the PBSC bracing systems.
4. Sensitivity analysis should be conducted on the coupler design to check their slip deformation relationship with the SMA bars and how it could be prevented by changing shape, size, and number of screws. The seismic performance factor determination study

should be extended to cover many different brace configurations (X, EBF, V etc.), the number of bays, the number of stories, etc.

5. The use of PBSC brace in a moment frame should be investigated. This would require nonlinear model creation with nonlinear beams, columns and foundation elements. Soil structure interaction models could be utilized for more accurate results.
6. The self-centering capability of reinforced concrete moment resisting frames utilizing PBSC bracing system should be investigated. Similar studies should be carried out on timber frames to find out the braces applicability in these structural systems.
7. Seismic performance evaluation of multi-column bridge bents strengthened/retrofitted with the PBSC bracing system should also be investigated.
8. Effect of extreme temperatures on the cyclic performance of PBSC bracing system should be investigated.
9. Effect of strain rate on the hysteresis behavior of the PBSC bracing system should be determined using experimental investigation. In the next step, a hysteresis model capable of simulating the strain rate effect should be developed from these experimental results.
10. The performance of the PBSC braced frames against wind load should be investigated.
11. A life-cycle cost analysis study should be carried out on the PBSC bracing system. The result should be compared against the counterparts such as BRB, SCED, MANSIDE and traditional bracing systems. As the PBSC bracing system could bring back a structure to its original position, the life-cycle cost analysis could show its true advantage over the competition despite the high initial cost.

12. A detailed market evaluation study should be carried out to determine the potential market size, location, public interest and growth potential for this bracing system.

REFERENCES

ABAQUS. (2014). “Theory manual.” Dassault Systèmes Simulia Corp.

Alam, M. S., a Youssef, M., Nehdi, M. (2007). “Utilizing shape memory alloys to enhance the performance and safety of civil infrastructure: a review.” *Canadian Journal of Civil Engineering*, 34(9), 1075–1086.

Alam, M. S., Bhuiyan, M. A. R., and Billah, A. H. M. M. (2012). “Seismic fragility assessment of SMA-bar restrained multi-span continuous highway bridge isolated by different laminated rubber bearings in medium to strong seismic risk zones.” *Bulletin of Earthquake Engineering*, 10(6), 1885–1909.

ASCE. (2005). “Minimum Design Loads for Buildings and Other Structures, ASCE 7-05.” *American Society of Civil Engineers*, Reston, Virginia.

Asgarian, B., and Moradi, S. (2011). “Seismic response of steel braced frames with shape memory alloy braces.” *Journal of Constructional Steel Research*, Elsevier Ltd, 67(1), 65–74.

Asgarian, B., and Shokrgozar, H. R. (2009). “BRBF response modification factor.” *Journal of Constructional Steel Research*, Elsevier Ltd, 65(2), 290–298.

Auricchio, F., Fugazza, D., and Desroches, R. (2006). “Earthquake performance of steel frames with with nitinol braces.” *Journal of Earthquake Engineering*, 10(1), 45–66.

Auricchio, F., and Sacco, E. (1997). “A one-dimensional model for superelastic shape-memory alloys with different elastic properties between austenite and martensite.” *International Journal of Non-Linear Mechanics*, 32(6), 1101–1114.

Billah, A. H. M. M., and Alam, M. S. (2015). “Seismic fragility assessment of concrete bridge pier reinforced with superelastic shape memory alloy.” *Earthquake Spectra*, 31(3), 1515–1541.

Blebo, F. C., and Roke, D. A. (2015). “Seismic-resistant friction-damped braced frame system with buckling restrained columns.” *Structural Congress*, Structures Congress, Portland,

Oregon, 2241–2250.

Bystricky, P., and Fanucci, J. P. (2010). “Buckling restrained brace for structural reinforcement and seismic energy dissipation and method of producing same.” Patent US7707788 B2.

Carr, A. J. (2008). “Ruaumoko - A Program for Inelastic Time-History Analysis.” Dept. C. Eng. Univ., Canterbury, New Zealand.

Christopoulos, C., Tremblay, R., Kim, H.-J., and Lacerte, M. (2008). “Self-Centering Energy Dissipative Bracing System for the Seismic Resistance of Structures: Development and Validation.” *Journal of Structural Engineering*, American Society of Civil Engineers, 134(1), 96–107.

Chung-Che, C., Chung, P., and Tsai, W.-J. (2014). “Dual-core self-centering buckling-restrained brace.” Patent US8763320 B1.

Comeau, G., Velchev, K., and Rogers, C. A. A. (2010). “Development of seismic force modification factors for cold-formed steel strap braced walls.” *Canadian Journal of Civil Engineering*, 37(2), 236–249.

CSA. (2009). "CSA-S16-09: design of steel structures." *Canadian Standards Association*, Mississauga (Ontario, Canada),.

DesRoches, R., McCormick, J., and Delemont, M. (2004). “Cyclic Properties of Superelastic Shape Memory Alloy Wires and Bars.” *Journal of Structural Engineering*, American Society of Civil Engineers, 130(1), 38–46.

Dezfuli, F. H., Alam, M. S. (2013). “Shape memory alloy wire-based smart natural rubber bearing.” *Smart Materials and Structures*, IOP Publishing, 22(4), 45013.

Dhondt, G. (2014). “Twenty-node brick element with reduced integration (C3D20R and F3D20R).” retrieved from http://webmitedu/calculix_v27/CalculiX/ccx_27/doc/.

Dolce, M., and Cardone, D. (2001). “Mechanical behaviour of shape memory alloys for seismic applications 2. Austenite NiTi wires subjected to tension.” *International Journal of*

Mechanical Sciences, 43, 2657–2677.

Dolce, M., and Cardone, D. (2006). "Theoretical and Experimental Studies for the Application of Shape Memory Alloys in Civil Engineering." *Journal of Engineering Materials and Technology*, 128(3), 302.

Dolce, M., Cardone, D., and Marnetto, R. (2000). "Implementation and testing of passive control devices based on shape memory alloys." *Earthquake Engineering & Structural Dynamics*, 29(v), 945–968.

Dolce, M., Cardone, D., and Marnetto, R. (2001). "SMA recentering devices for seismic isolation of civil structures." *Proc. SPIE*, 238–249.

Duerig, T. W., Melton, K. N., and Stöckel, D. (2013). *Engineering aspects of shape memory alloys*. Butterworth-Heinemann.

Eguchi, R. T., Goltz, J. D., Taylor, C. E., Chang, S. E., Flores, P. J., Johnson, L. A., Seligson, H. A., and Blais, N. C. (1998). "Direct economic losses in the Northridge earthquake: a three-year post-event perspective." *Earthquake Spectra*, 14(2), 245–264.

Elnashai, A. S., Gencturk, B., Kwon, O. S. O.-S., Al-Qadi, I. L., Hashash, Y., Roesler, J. R., Kim, S. J. S. J., Jeong, S.-H., Dukes, J., and Valdivia, A. (2010). "The Maule (Chile) earthquake of February 27, 2010: Consequence assessment and case studies." *MAE Center Report No. 10-04*.

Elwood, K. J. (2013). "Performance of concrete buildings in the 22 February 2011 Christchurch earthquake and implications for Canadian codes 1." *Canadian Journal of Civil Engineering*, NRC Research Press, 40(3), 759–776.

Fahnestock, L. A., Sause, R., Ricles, J. M. (2006). "Analytical and Large-Scale Experimental Studies of Earthquake-Resistant Buckling-Restrained Braced Frame Systems." Lehigh University, ATLSS Report No. 06-01, 3525(610).

Fahnestock, L. A., Ricles, J. M., Sause, R. (2007). "Experimental Evaluation of a Large-Scale

Buckling-Restrained Braced Frame.” *Journal of Structural Engineering*, 133(9), 1205–1214.

FEMA. (2000). “Prestandard and Commentary for the Seismic Rehabilitation of Buildings (FEMA 356).” Federal Emergency Management Agency, Washington, DC.

FEMA. (2009). "*FEMA P695: Quantification of Building Seismic Performance Factors*." Federal Emergency Management Agency, Washington, DC.

Gall, K., Sehitoglu, H., Chumlyakov, Y. I., Kireeva, I. V., and Maier, H. J. (1999). “The Influence of Aging on Critical Transformation Stress Levels and Martensite Start Temperatures in NiTi: Part II—Discussion of Experimental Results.” *Journal of Engineering Materials and Technology*, 121(1), 28.

Ghobarah, A. (2001). “Performance-based design in earthquake engineering: state of development.” *Engineering structures*, 23(8), 878–884.

Gray, M. G., Christopoulos, C., and Packer, J. A. (2010). “Cast steel yielding fuse for concentrically braced frames.” *9th US National and 10th Canadian Conference on Earthquake Engineering 2010, Including Papers from the 4th International Tsunami Symposium*, 4235–4244.

Gray, M. G., Christopoulos, C., and Packer, J. A. (2012a). “Full-scale testing of the cast steel yielding brace system.” *Stessa 2012: Proceedings of the 7th International Conference on Behaviour of Steel Structures in Seismic Areas*, 769–774.

Gray, M. G., Christopoulos, C., and Packer, J. A. (2014a). “Cast Steel Yielding Brace System for Concentrically Braced Frames: Concept Development and Experimental Validations.” *Journal of Structural Engineering*, 140(4), 4013095.

Gray, M. G., Christopoulos, C., Packer, J. A., and Lignos, D. G. (2012b). “Development, Validation, and Modeling of the New Cast Steel Yielding Brace System.” *20th Analysis and Computation Specialty Conference*, 71–82.

Gray, M. G., De Oliveira, J. C. C., Binder, C. C. J. I., Christopoulos, C., and Binder, J. I. (2014b).

"Effects of Post-Yield Stiffening and Strengthening on the Collapse Performance of Non-Buckling Braced Frames." *Tenth U.S. National Conference on Earthquake Engineering*.

Hane, K. F., and Shield, T. W. (1999). "Microstructure in the cubic to monoclinic transition in titanium-nickel shape memory alloys." *Acta Materialia*, 47(9), 2603–2617.

Haque, A. B. M. R., and Alam, M. S. (2014). "Piston-Based Self-Centering Brace Apparatus." Patent US 20160326742 A1.

Haque, A. B. M. R., and Alam, M. S. (2015a). "Cyclic Performance of a Piston Based Self-Centering Bracing System." *Structures Congress 2015*, 2360–2371.

Haque, A. B. M. R., and Alam, M. S. (2015b). "Preliminary investigation on the overstrength and force reduction factors for industrial rack clad buildings." *The 11th Canadian Conference on Earthquake Engineering*, Canadian Association for Earthquake Engineering, Victoria, BC.

Haselton, C. B. (2006). "Assessing seismic collapse safety of modern reinforced concrete moment frame buildings." Stanford University.

Haselton, C. B., Liel, A. B., Deierlein, G. G., Dean, B. S., and Chou, J. H. (2010). "Seismic collapse safety of reinforced concrete buildings. I: Assessment of ductile moment frames." *Journal of Structural Engineering*, 137(4), 481–491.

Hinchman, A. (2013). "Buckling-restrained brace." Patents US8869468 B2.

Hossain, A., Alam, M. S., and Rteil, A. (2015). "Seismic Force Reduction Factors for Concrete Buildings Reinforced With Superelastic Shape Memory Alloy Rebars." *The 11th Canadian Conference on Earthquake Engineering*.

Hu, J. W., Choi, D. H., and Kim, D. K. (2013). "Inelastic behavior of smart recentering buckling-restrained braced frames with superelastic shape memory alloy bracing systems." *Proceedings of the Institution of Mechanical Engineers, Part C: Journal of Mechanical Engineering Science*, SAGE Publications, 227(4), 806–818.

Ibarra, L. F., and Krawinkler, H. (2005a). *Global collapse of frame structures under seismic*

excitations. Pacific Earthquake Engineering Research Center.

Ibarra, L., and Krawinkler, H. (2005b). “Effect of uncertainty in system deterioration parameters on the variance of collapse capacity.” *9th International Conference on Structural Safety and Reliability, Rome, Italy*.

Ibarra, L., Medina, R., and Krawinkler, H. (2002). “Collapse assessment of deteriorating SDOF systems.” *Proceedings of the 12th European Conference on Earthquake Engineering*, 9–13.

Iwata, M., and Murai, M. (2006). “Buckling-restrained brace using steel mortar planks; performance evaluation as a hysteretic damper.” *Earthquake engineering & structural dynamics*, Wiley Online Library, 35(14), 1807–1826.

Khachaturyan, A. G. (1983). “Theory of structural phase transformations in solids.” *John Willey, New York, NY*, 17, 1733–1743.

Kim, J., and Choi, H. (2005). “Response modification factors of chevron-braced frames.” *Engineering Structures*, 27(2), 285–300.

Kulak, G., Fisher, J., and Struik, J. (1987). “Guide to design criteria for bolted and riveted joints.” *Wiley-Interscience*.

Lafortune, P., McCormick, J., DesRoches, R., and Terriault, P. (2007). “Testing of Superelastic Recentering Pre-Strained Braces for Seismic Resistant Design.” *Journal of Earthquake Engineering*, Taylor & Francis, 11(3), 383–399.

Lee, L. H., Han, S. W., and OH, Y. H. (1999). “Determination of ductility factor considering different hysteretic models.” *Earthquake engineering & structural dynamics*, 28(9), 957–977.

Ma, N., Song, G., and Tarefder, R. A. (2004). “Vibration control of a frame structure using shape memory alloy braces.” *The Third International Conference on Earthquake Engineering (Nanjing, China)*.

MATLAB. (2012). “MATLAB Documentation." MathWorks.

McCormick, J., DesRoches, R., Fugazza, D., and Auricchio, F. (2007). “Seismic assessment of concentrically braced steel frames with shape memory alloy braces.” *Journal of Structural Engineering-Asce*, 133(6), 862–870.

Miller, D. J., Fahnestock, L. A., Eatherton, M. R. (2012). “Development and experimental validation of a nickel-titanium shape memory alloy self-centering buckling-restrained brace.” *Engineering Structures*, Elsevier Ltd, 40, 288–298.

Miyamoto, H. K., Gilani, A. S. J., Wada, A., and Ariyaratana, C. (2011). “Identifying the collapse hazard of steel special moment-frame buildings with viscous dampers using the FEMA P695 methodology.” *Earthquake Spectra*, 27(4), 1147–1168.

Moradi, S., Alam, M. S., and Asgarian, B. (2014). “Incremental dynamic analysis of steel frames equipped with NiTi shape memory alloy braces.” *the Structural Design of Tall and Special Buildings*, 23(18), 1406–1425.

NBCC. (2010). “National building code of canada.” Institute for Research in Construction, National Research Council of Canada, Ottawa, Ontario, Canada,.

Nemat-Nasser, S., and Guo, W. G. (2006). “Superelastic and cyclic response of NiTi SMA at various strain rates and temperatures.” *Mechanics of Materials*, 38(5–6), 463–474.

Newmark, N. M. (1959). “A method of computation for structural dynamics.” *Journal of the engineering mechanics division*, ASCE, 85(3), 67–94.

Newmark, N. M., and Hall, W. J. (1982). “Earthquake spectra and design.” *Earth System Dynamics*, 1.

NRC. (2016). “Seismic zones in Western Canada:Background on Earthquakes in Western Canada.” *Natural Resources Canada*, Retrieved from http://www.earthquakescanada.nrcan.gc.ca/zones/westcan-en.php (Jan. 20, 2016).

Otsuka, K., and Shimizu, K. (1986). “Pseudoelasticity and shape memory effects in alloys.” *International Metals Reviews*, 31(1), 93–114.

Otsuka, K., and Wayman, C. M. (1998). “Mechanism of shape memory effect and superelasticity.” *Shape memory materials*, Cambridge University Press Cambridge, UK, 27–49.

Otsuka, K., and Wayman, C. M. (1999). *Shape memory materials*. Cambridge University press.

Perkins, J. (1981). “Ti--Ni and Ti--Ni--X shape memory alloys.” *Metals Forum*, 153–163.

S-FRAME. (2016). “S-Frame Structural Analysis and Design. S-Frame Reference Manual.” S-FRAME Software, Inc., Richmond, BC.

Sato, A., and Uang, C. M. (2013). “A FEMA P695 study for the proposed seismic performance factors for cold-formed steel special bolted moment frames.” *Earthquake Spectra*, 29(1), 259–282.

Scawthorn, C., and Yanev, P. I. (1995). “17 January 1995, Hyogo-ken Nambu, Japanese earthquake.” *Engineering Structures*, Elsevier, 17(3), 146–157.

SeismoSoft. (2016). “SeismoStruct - A computer program for static and dynamic nonlinear analysis of framed structures, V 7.0.” Seismosoft srl.

Speicher, M. S. (2009). “Cyclic testing and assessment of shape memory alloy recentering systems.” Georgia Institute of Technology, (May).

Tadaki, T., Otsuka, K., and Shimizu, K. (1988). “Shape memory alloys.” *Annual Review of Materials Science*, Annual Reviews 4139 El Camino Way, PO Box 10139, Palo Alto, CA 94303-0139, USA, 18(1), 25–45.

Tahmasebi, E., Sause, R., Ricles, J.M., Chancellor, N.B. and Akbas, T., (2014). "Probabilistic collapse performance assessment of self-centering concentrically braced frames." In Proceedings of the 10th US National Conference on Earthquake Engineering, Anchorage, AK, USA (pp. 21-25).

Takeuchi, T., Hajjar, J. F., Matsui, R., Nishimoto, K., and Aiken, I. D. (2010). “Local buckling restraint condition for core plates in buckling restrained braces.” *Journal of Constructional Steel Research*, Elsevier Ltd, 66(2), 139–149.

Takeuchi, T., Nakamura, H., Kimura, I., Hasegawa, H., Saeki, E., and Watanabe, A. (2004). "Buckling restrained braces and damping steel structures." Patent US6826874 B2.

Tremblay, R., and Christopoulos, C. (2012). "Self-centering energy dissipative brace apparatus with tensioning elements." Patent US20120266548 A1.

Vamvatsikos, D., and Cornell, C. A. (2002). "Incremental dynamic analysis." *Earthquake Engineering and Structural Dynamics*, 31(3), 491–514.

Wayman, C. M. (1964). *Introduction to the crystallography of martensitic transformations*. Macmillan.

Wayman, C. M., and Duerig, T. W. (1990). "An introduction to martensite and shape memory." *Butterworth-Heinemann, Engineering Aspects of Shape Memory Alloys(UK), 1990*, 3–20.

Yang, C.-S. W., DesRoches, R., Leon, R. T., Walter Yang, C. S. (2010). "Design and analysis of braced frames with shape memory alloy and energy-absorbing hybrid devices." *Engineering Structures*, Elsevier Ltd, 32(2), 498–507.

Youssef, M. A., Alam, M. S., and Nehdi, M. (2008). "Experimental Investigation on the Seismic Behavior of Beam-Column Joints Reinforced with Superelastic Shape Memory Alloys." *Journal of Earthquake Engineering*, Taylor & Francis Group, 12(7), 1205–1222.

Zareian, F., and Krawinkler, H. (2006). "Simplified performance-based earthquake engineering." Stanford University Stanford, CA, USA.

Zareian, F., Lignos, D. G., and Krawinkler, H. (2010). "Evaluation of seismic collapse performance of steel special moment resisting frames using FEMA P695 (ATC-63) methodology." *Structures Congress 2010*, p 1275-1286.

Zhang, Y., and Zhu, S. (2007). "A shape memory alloy-based reusable hysteretic damper for seismic hazard mitigation." *Smart Materials & Structures*, 16(5), 1603–1613.

Zhu, S., and Zhang, Y. (2007). "Seismic behaviour of self-centring braced frame buildings with reusable hysteretic damping brace." *Earthquake engg & structural dynamics*, 1329–1346.

APPENDICES

Appendix A: Design method for PBSC braced frame

A.1 Brace elongation to interstory drift ratio

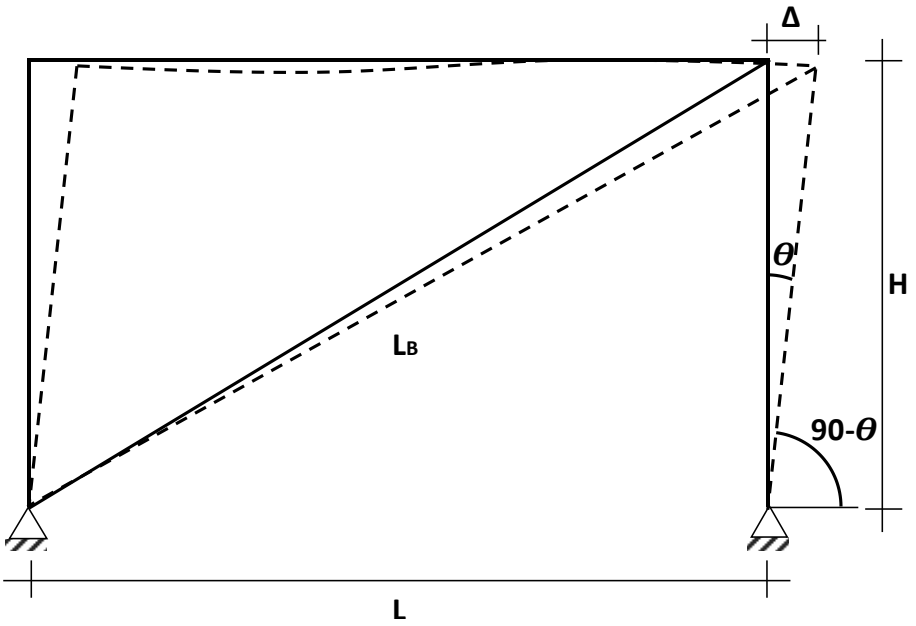

Figure A-1: Elongated brace length calculation

Assuming θ is a very small angle, the vertical projection of the column does not change after lateral displacement Δ (Figure A-1).

Therefore, interstory drift ratio (ISDR) as per equation A-1,

$$ISDR = \frac{\Delta}{H} = Sin(\theta) \qquad (A\text{-}1)$$

We know that, for a very small angle (in radians), $Sin(\theta) = \theta$

Therefore,

$$\theta = \frac{\Delta}{H} \qquad (A\text{-}2)$$

The original length of the brace, L_B is given by

$$L_B = \sqrt{L^2 + H^2} \qquad \textit{(A-3)}$$

Horizontal projection of the brace after lateral deformation/brace elongation = $L+H*Cos(90-\theta)$

Vertical projection of the brace after lateral deformation/Brace elongation = $H*Sin(90-\theta)$

Elongated length of the brace = $[\{ L+H*Cos(90-\theta)\}^2+\{ H*Sin(90-\theta)\}^2]^{0.5}$

$= [\{ L+H*Sin\theta\}^2+\{ H*Cos\theta\}^2]^{0.5}$

$= [L^2+2*L*H*Sin\theta+H^2*Sin^2\theta+H^2*Cos^2\theta]^{0.5}$

$= [L^2+2*L*H*Sin\theta+H^2*(Sin^2\theta+Cos^2\theta)]^{0.5}$

$= [L^2+H^2+2LHSin\theta]^{0.5}$

Brace elongation ratio, $\lambda_r = [\frac{L^2+H^2+2LHSin\theta}{L^2+H^2}]^{0\cdot5}$

$\lambda_r = [1 + \frac{2LHSin\theta}{L^2+H^2}]^{0\cdot5}$

$\lambda_r = [1 + \frac{2LH*\frac{\Delta}{H}}{L^2+H^2}]^{0\cdot5}$

$\lambda_r = [1 + \frac{2LH*\frac{\Delta}{H}}{{L_B}^2}]^{0\cdot5}$ *(A-4)*

Let's assume $L = 5000mm$ and $H = 3000mm$, for an *ISDR* or Δ/H value of 0.025 or 2.5% ISDR%

Brace elongation ratio = $[1 + \frac{2LH*\frac{\Delta}{H}}{L^2+H^2}]^{0.5}$

$= [1 + \frac{2*5000*3000*.025}{5000^2+3000^2}]^{0.5}$

$= [1.022059]^{0.5}$

$= 1.010969 \approx$ *1.011*

Amount of elongation *1.010969-1 = .010969 or 1.0969%*

Therefore, for a 5000mm wide by 3000mm high frame configuration the brace elongation percentage divided by interstory drift ratio percentage is *1.0969/2.5 = 0.4387*.

If we use NiTinol bars with the following material properties (Table A-1), we can see that for a plateau strain value of 0.06, the strain at Austenite to martensite finishing stress (ε_{amf}) is *0.06816*; which can be calculated using equation A-5.

$$\varepsilon_{amf} = \varepsilon_L + \sigma_{amf}/E_{sma} \qquad \textit{(A-5)}$$

If 1000mm long NiTinol bars are used, the maximum elongation will be 68.16mm at σ_{amf}. If we divide this elongation by the brace length (L_B) of 5830.95mm we get an elongation of 1.16%. Therefore, the expected interstory drift ratio at this brace elongation value is *1.16/0.4387 = 2.66%*.

As the stiffness of NiTinol bars beyond σ_{amf} stress level increases drastically, it can be assumed that the PBSC brace to steel frame connections will not be designed for this high degree of stress. Therefore, connections between the brace and the frame might start to fail after σ_{amf} stress in the SMA bars. Therefore, for 1000mm long NiTinol bars, the maximum interstory drift ratio at the collapse prevention damage state could be conservatively set to 2.66%. However, if 4% interstory

drift ratio at this limit state is desired then the following modifications could be made to the design: (a) brace length should be increased to (4*1000/2.66) or 1503mm. (b) a different composition of the SMA alloy with a higher recoverable strain (e.g. 9%) could be used.

A.2 Hysteresis parameters for PBSC braced frame

The following equations (A6 to A12) were used to calculate the PBSC link hysteresis parameters in the S-FRAME Structural analysis and design software. The SMA material properties used for the calculation of these parameters are given in Table A-1.

Table A-1: Sample material properties for NiTinol SMA bars

Properties	Values	Unit
Austenite to martensite starting stress, σ_{ams}	400	N/mm^2
Austenite to martensite finishing stress, σ_{amf}	510	N/mm^2
Martensite to austenite starting stress, σ_{mas}	370	N/mm^2
Martensite to austenite finishing stress, σ_{maf}	130	N/mm^2
Modulus of elasticity, E_{sma}	62500	N/mm^2
Yield Strain, ε_{ams}	0.0064	
Plateau Strain, ε_L	0.06	
Strain at austenite to martensite finishing stress, ε_{amf}	0.06816	

The required nonlinear parameters are yield force of the brace (P_y), initial stiffness (K_i), post-yield stiffness (K_p), austenite to martensite finishing force (P_{amf}), martensite to austenite starting force (P_{mas}), unloading force turn factor (α) and residual deformation factor (β).

$$P_y = \sigma_{ams} * A_{sma} \quad \textit{(A-6)}$$

$$k_i = E_{sma} * A_{sma}/L_{sma} \quad \textit{(A-7)}$$

$$k_p = \left(\frac{\sigma_{amf}-\sigma_{ams}}{\varepsilon_{amf}-\varepsilon_{ams}}\right) * A_{sma}/L_{sma} \quad \textit{(A-8)}$$

$$P_{amf} = \sigma_{amf} * A_{sma} \quad \textit{(A-9)}$$

$$P_{amf} = \sigma_{mas} * A_{sma} \quad (A\text{-}10)$$

$$\alpha = \frac{\sigma_{maf}}{\sigma_{ams}} \quad (A\text{-}11)$$

$$0 \leq \beta \leq 1 \quad (A\text{-}12)$$

Here,

A_{sma} = Total cross-sectional area of SMA bars resisting either tension or compression

L_{sma} = Length of SMA bars for tension or compression

A sample of calculated values for these parameters are given in Table A-2. These values have been computed using the material property data provided in Table A-1. For this calculation, it was assumed that the brace has 2-10.1mm dia SMA bars each having a length of 1000mm.

Table A-2: PBSC brace link hysteresis parameters

Properties	Values	Unit
Yield force, P_y	64	kN
Initial Stiffness, K_i	10014	kN/m
Post-Yield Stiffness, K_p	285.40	kN/m
Austenite to martensite finishing force, P_{amf}	81.72	kN
Martensite to austenite starting force, P_{mas}	59.29	kN
Unloading force turn factor, α	0.33	
Residual deformation factor, β	0.1	

A.3 Axial stiffness modifier for design

During building design, it is not feasible to explicitly model the PBSC bracing system with the cylinder/sleeve, internal NiTinol tie bars and end plates in traditional structural design software like S-FRAME, SAP2000 or ETABS etc. To resolve this issue, a simplified method has been proposed to incorporate the actual stiffness of the PBSC brace in the software. The method requires the use of axial stiffness modification factors. These factors can be manually calculated before the analysis of the PBSC braced frames.

For the PBSC braced frame design model, the braces could be modeled using elastic truss elements. If the braces are modeled as single elements, then their stiffness do not match the PBSC brace which has stiffness contribution from the brace shaft and the NiTinol tie bars. The stiffness of the cylinder can be ignored as it is much stiffer compared to the other two elements. If we model the brace in finite element software with a prismatic steel member, then the stiffness of the brace can be expressed using equation A-13

$$K_b = \frac{A_b * E_{steel}}{L_b} \quad \textit{(A-13)}$$

Where,

A_b = Cross sectional area of steel brace

E_{steel} = Modulus of elasticity of steel (200 GPa)

L_b = Length of the brace

However, the brace stiffness comes from two parts connected in series: NiTinol bar part and the shaft.

The stiffness of the NiTinol part and the shaft can be expressed using equation A-14 and A-15

$$K_{sma} = \frac{A_{sma} * E_{sma}}{L_{sma}} \quad \textit{(A-14)}$$

$$K_{shaft} = \frac{A_{shaft} * E_{steel}}{L_{shaft}} \quad \textit{(A-15)}$$

The equivalent stiffness of the brace (K_{eq}) can be calculated as follows

$$\frac{1}{K_{eq}} = \frac{1}{K_{sma}} + \frac{1}{K_{shaft}} \quad \textit{(A-16)}$$

$$\frac{1}{K_{eq}} = \frac{1}{\frac{A_{sma} * E_{sma}}{L_{sma}}} + \frac{1}{\frac{A_{shaft} * E_{steel}}{L_{shaft}}} \quad \textit{(A-17)}$$

Assumptions,

$A_{sma} = (F_{y,steel}/F_{y,sma})A_{shaft} = fA_{shaft}$

Modular ratio = $E_{steel}/E_{sma} = r$

NiTinol tie length to brace length, $(L_{sma}/L_b) = n$

Steel shaft length to brace length, $(L_{shaft}/L_b) = m$

Substituting the above-mentioned relationships in equation A-17 we get

$$\frac{1}{K_{eq}} = \frac{1}{\frac{fA_{shaft}E_{steel}}{rnL_b}} + \frac{1}{\frac{A_{shaft}E_{steel}}{mL_b}}$$

$$\frac{1}{K_{eq}} = \frac{1}{\frac{fK_b}{rn}} + \frac{1}{\frac{K_b}{m}}$$

$$\frac{1}{K_{eq}} = \frac{rn}{fK_b} + \frac{m}{K_b}$$

$$\frac{1}{K_{eq}} = \left(\frac{rn}{f} + m\right)\frac{1}{K_b}$$

$$\frac{1}{K_{eq}} = (\frac{rn + fm}{f})\frac{1}{K_b}$$

$$K_{eq} = (\frac{f}{rn+fm})K_b \qquad \textit{(A-18)}$$

Assuming $F_{y,steel} = 350\ MPa$, $F_{y,sma} = 400\ MPa$, $E_{steel} = 200\ GPa$, $E_{sma} = 62.5\ GPa$, $L_b = 5.83m$ (assuming 5m wide by 3m tall bay), $L_{sma} = 1m$ *and* L_{shaft} = 4.83m, we get the following values for *f, r, n* and *m.*

$f = 0.875$

$r = 3.2$

n = 0.1715

m = 0.8284

Substituting these values in equation A-18 we get

$$K_{eq} = 0.687 * K_b$$

This multiplier (0.687) was used as an axial stiffness modified for the braces in the finite element model.

A.4 Axial stiffness modifier for nonlinear analysis

During the nonlinear dynamic time history analysis, link elements are used at the end of the braces to simulate the nonlinear load deformation hysteresis and stiffness of the NiTinol bars. However, the link elements in most of the structural analysis and design software are modeled as zero-length elements. Which means the SMA ties are getting represented without any length in the model. This makes the shaft longer than their actual length and reduces the brace axial stiffness. To correct the stiffness, a different axial stiffness multiplier should be used for nonlinear analysis. This ratio can be simply calculated using the ratio between the modeled length of the brace and the actual length of the brace shaft if links represented the actual length of the NiTinol bars. This equivalent brace stiffness is given by equation A-19.

$$K_{eq} = (\frac{L_b}{L_{shaft}}) * K_b \qquad \textit{(A-19)}$$

Using, L_b = 5.83m (assuming 5m wide by 3m tall bay), and L_{shaft} = 4.83m (assuming 1m long SMA bars), we get the following expression from equation A-19.

$$K_{eq} = 1.207 * K_b$$

This higher than one axial stiffness modification factor increases the brace stiffness and corrects for the extra length modeled.

A.5 A step-by-step guideline for PBSC brace frame design

The following step-by-step guideline should be used to design a PBSC braced frame

1. Analysis of the frame: Analysis should be carried out on the desired/selected frame with braces as modeled as elastic truss elements. The braces should be pin-connected to the frame; therefore, they should only carry axial forces. The axial stiffness of the braces should be modified to take the stiffness of the SMA bars into account as per section A.3.
2. Seismic analysis: Response spectrum, linear dynamic time history or equivalent lateral force based analysis should be carried out to determine the seismic demand forces on the braces. On the other hand, a sophisticated nonlinear analysis could also be performed for the brace frame design. However, this would require nonlinear modeling of the braces using hysteresis models. The parameters for the link hysteresis would be difficult to guess without prior linear analysis; therefore, this would require numerous trial and error. Therefore, it is recommended to use the linear static or linear dynamic analysis for the design.
3. Brace design: The PBSC braces should be designed using the forces calculated in step 2. For the design of the braces, the SMA bars should be designed using factored demand and unfactored resistance. However, the steel components should be designed using factored demand and factored resistance. Furthermore, an additional load amplification factor of 1.1-1.2 (based on engineering judgment) should be utilized for the design of the shaft and the sleeve. This additional load amplification factor should ensure capacity protection for

these elements. The design of these components should follow the axial compression member design procedure of the relevant code/standard of the jurisdiction. However, the design of the SMA ties should be based on simple tensile stress check. The required area of the ties should be calculated using equation A-20.

$$A_{tie} = \frac{T_f}{\sigma_{ams}} \quad \textit{(A-20)}$$

Where,

A_{tie} = Required area of SMA tie bars

T_f = Factored force demand on the brace (max of tension/compression)

σ_{ams} = Austenite to martensite starting stress

4. SMA Tie Bar length: The length of the SMA tie bars should be determined based on the required interstory drift ratio capacity. Equation A-4 can be used to determine the elongated length of the brace for a design interstory drift ratio. The amount of elongation should be designed to occur mostly in the SMA tie bars. The shaft and sleeve should deform only in the elastic range. Therefore, the SMA tie bar lengths should be chosen in a way that this elongation falls within the recoverable strain limit of the SMA bar. Equation A-21 should be used for calculating the required length of the SMA tie bar.

$$L_{sma} = (\lambda_r - 1) * L_B/\varepsilon_{amf} \quad \textit{(A-21)}$$

Here,

L_{sma} = Required length of SMA bars for tension or compression

λ_r = Brace elongation ratio (elongated length/original length)

L_B = Brace length

ε_{amf} = Austenite to martensite finishing strain

Appendix B: MATLAB finite element program

```
clc;
clear all;
close all;

%Information about external force array input xls file
filename = 'loads.xlsx';
sheet = 'LH';
xlRange = 'B:B';
Load_History = xlsread(filename, sheet, xlRange);

%Variable used for turning on SMA hysteresis for the ties
sma_ties_used=1;

%Number of data points in the excel file
Load_History_Size=size(Load_History);
Data_Points=Load_History_Size(1);
Tie_Length=1;
Shaft_Length=0.01;

%Calculation for the Interior and Exterior Ties. In the stiffness matrix
%double the number of ties is used. One set for taking tension and the
%other set for taking compression
No_Of_Ties=2;
Tie_dia =.018; %Diameter of each ties
Area_Of_Ties=pi*Tie_dia^2*0.25*No_Of_Ties;

%Calculation for the Shaft
Dshft_centerline = 0.11905; %Centerline dimension
t_shft=.00795; %Wall thickness
Dos=Dshft_centerline+t_shft/2; %Outer diameter
Dis=Dshft_centerline-t_shft/2;  %Inner diameter
Area_of_Shaft=pi*(Dos^2-Dis^2)*.25; %This area should come from a standard section

%disp('Cross sectional area of bar segments')
A=[Area_Of_Ties, Area_of_Shaft]; %First data is for cylinder and second data is for
the brace shaft
A_backup=A;
%disp('Lengths of bar segments');
L=[Tie_Length,Shaft_Length];%First item is for cylinder length and the second item is
for brace shaft length
L_bckp=L; %Populating L_bckup matrix

%Creating a deformed length matrix for corresponding loading data points
Total_Deformed_length=zeros(1,Data_Points);
Tie_Deformed_length=zeros(1,Data_Points);
Shaft_Deformed_length=zeros(1,Data_Points);
Tie_Load_History=zeros(1,Data_Points);

%Number of Bar segments, n
n=2;
Undeformed_length=L(1)+L(2);

%Modulus of elasticity of the material in Ties
if sma_ties_used==0
    Em_ties=2e11;
    Fy_ties=350e6;
    Fu_ties=450e6;
else
    Em_ties=62.5e9;
```

```
    Fy_ties=400e6;
    Fu_ties=510e6;
end

%Modulus of elasticity of the material in Shaft
Em_shaft=2e11;
%Poissons's Ratio, use zero if engineering stresses are used in the material model.
Use
%0.3 (Steel) 0.33 (SMA) if true stress strain curves are used in the material model.
%v=0.33;
v_Ties=0;
v_Shaft=0;
v = [v_Ties, v_Shaft];
% Member initial material elasticity kept for backup
Em=[Em_ties,Em_shaft];
%disp('Variable Modulus of elasticity of bar segments needed for stiffness matrix');
Ev=[Em(1),Em(2)];
%Yield stress of steel
Fy=[Fy_ties,350e6];
Fu=[Fu_ties,450e6];
%Positive and negative yield stress matrix
Fypos=[1*Fy(1),1.0*Fy(2)];
Fyneg=[-1*Fy(1),-1.0*Fy(2)];
%Positive ultimate stress matrix
Fupos=[1*Fu,1.0*Fu];
%disp('Yield strain (m/m):');
ey_pos=[Fypos(1)/Em(1),Fypos(2)/Em(2)];
%disp('Yield displacement (m):');
dy_pos=[ey_pos(1)*L(1),ey_pos(2)*L(2)];
dy_neg=[-ey_pos(1)*L(1),-ey_pos(2)*L(2)];
%Strain at ultimate stress
eu=[0.1,0.1];
%Plastic Strain
ep=eu-ey_pos;
%Post yield elasticity ratio
r=[((Fupos(1)-Fypos(1))/ep(1))/Em(1),((Fupos(2)-Fypos(2))/ep(2))/Em(2)];
%Positive yield forces for the elements
Pypos=[Fypos(1)*A(1),Fypos(2)*A(2)];

%Buckling load of the shaft
k_shaft=1.0;
I_shaft=(pi*(Dos^4-Dis^4))/64;
r_shaft=(I_shaft/A(2))^.5;
Pbuck_shaft=-pi^2*Em(2)*A(2)/(k_shaft*L(2)/r_shaft)^2;

%Buckling monitoring variables
shaft_buckled=0;

%Ultimate strain monitoring variables
tie_ult_strain_excd=0;
shaft_ult_strain_excd=0;

%disp('Stiffness of bar segments');
Kcoeff=[A(1)*Ev(1)/L(1),A(2)*Ev(2)/L(2)];
k=zeros(2,2,n);
%Global Displacement Matrix
GlobalU=zeros(n+1,1);

Load_History=Load_History*A(1)*Fupos(1)*1.0;

%Local Stiffness matrix formation
for i=1:n,
```

```
    k(1,1,i)=1;
    k(1,2,i)=-1;
    k(2,1,i)=-1;
    k(2,2,i)=1;
end

Tie_tensile_length_bckp=L(1);
Tie_compressive_length_bckp=L(1);

%Global Variable for sharing with the sma hysteresis function
global Strain_Max;
global Residual_Strain;
global Ei;
global Sams;
global Samf;
global Smas;
global Smaf;
global Ep;
global SMA_Yield_Strain;
global residual_ratio;
global Smax
global Strain_Crspnd_Pos;
global Strain_amf;
global Brace_Under_Tension;
global Strain_Max_Tension;
global Strain_Max_Compression;
global Residual_Strain_Tension;
global Residual_Strain_Compression;

Ei = 62.5e9;
Sams = Fy_ties;
Samf = Fu_ties;
Smas = 370e6;
Smaf = 130e6;
Smax=Sams;
Strain_Plateau=0.06;
SMA_Yield_Strain = Sams / Ei;
Strain_Max = SMA_Yield_Strain;
Strain_Max_Tension = SMA_Yield_Strain;
Strain_Max_Compression = SMA_Yield_Strain;
Residual_Strain=0;
Residual_Strain_Tension = 0;
Residual_Strain_Compression = 0;
Strain_L = Samf / Ei;
Ep = (Samf - Sams) / (Strain_Plateau + Strain_L - SMA_Yield_Strain);
residual_ratio = 0.1;
Strain_Crspnd_Pos = SMA_Yield_Strain;
Strain_amf = Strain_Plateau + Strain_L;
Brace_Under_Tension = (Load_History(2)-Load_History(1))/abs((Load_History(2)-
Load_History(1)))


for j=1:Data_Points, %Program's main counter for going through every data point

    %Implementation of hysteresis rules
    if j>1 %Only evaluate starting from second data point
        for i=1:n, %This loop goes through the bar elements one by one
            if Load_History(j)>=Load_History(j-1) %If load is increasing
                if Load_History(j)>0 %If the arrangement is in tension
                    if (i==1)
                        if sma_ties_used==1
                            if (Load_History(j-1)<=0)
```

```
                                L(i)=Tie_tensile_length_bckp;
                            end
                            if j<Data_Points

Ev(i)=sma_hysteresis((Load_History(j)/A(i)),(L(i)/Tie_Length-
1),(Load_History(j+1)/A(i)),(L_bckp(i)/Tie_Length-1));
                            else

Ev(i)=sma_hysteresis((Load_History(j)/A(i)),(L(i)/Tie_Length-
1),(Load_History(j)/A(i)),(L_bckp(i)/Tie_Length-1));
                            end
%                             if (Load_History(j-1)<=0)
%                                 L(i)=Tie_tensile_length_bckp;
%                             end
                            Kcoeff(i)=A(i)*Ev(i)/L(i);
                        else%If only steel ties are used
                            if (Load_History(j-1)<=0)
                                L(i)=Tie_tensile_length_bckp;
                            end

[Ev(i),Fypos(i),Fyneg(i)]=steel_hysteresis(Load_History(j)/A(i),Load_History(j-
1)/A(i),Fypos(i),Fyneg(i),Fy(i),r(i));
%                             if (Load_History(j-1)<=0)
%                                 L(i)=Tie_tensile_length_bckp;
%                             end
                            Kcoeff(i)=A(i)*Ev(i)/L(i);
                        end

                    elseif (i==2)

[Ev(i),Fypos(i),Fyneg(i)]=steel_hysteresis(Load_History(j)/A(i),Load_History(j-
1)/A(i),Fypos(i),Fyneg(i),Fy(i),r(i));
                            Kcoeff(i)=A(i)*Ev(i)/L(i);
                        end

                else %If the arrangement is in compression
                    if (i==1) %Calculation for the ties
                        if sma_ties_used==1
                            if j<Data_Points

Ev(i)=sma_hysteresis((Load_History(j)/A(i)),(L(i)/Tie_Length-
1),(Load_History(j+1)/A(i)),(L_bckp(i)/Tie_Length-1));
                            else

Ev(i)=sma_hysteresis((Load_History(j)/A(i)),(L(i)/Tie_Length-
1),(Load_History(j)/A(i)),(L_bckp(i)/Tie_Length-1));
                            end
                            Kcoeff(i)=A(i)*Ev(i)/L(i);
                        else %If only steel ties are used

[Ev(i),Fypos(i),Fyneg(i)]=steel_hysteresis(Load_History(j)/A(i),Load_History(j-
1)/A(i),Fypos(i),Fyneg(i),Fy(i),r(i));
                            Kcoeff(i)=A(i)*Ev(i)/L(i);
                        end
                    elseif i==2

[Ev(i),Fypos(i),Fyneg(i)]=steel_hysteresis(Load_History(j)/A(i),Load_History(j-
1)/A(i),Fypos(i),Fyneg(i),Fy(i),r(i));
                            Kcoeff(i)=A(i)*Ev(i)/L(i);
                        end
                end
```

```
            elseif Load_History(j)<Load_History(j-1)  %if Load is decreasing
                if Load_History(j)>=0 %If the arrangement is in tension

                    if (i==1)
                        if sma_ties_used==1
                            if j<Data_Points

Ev(i)=sma_hysteresis((Load_History(j)/A(i)),(L(i)/Tie_Length-
1),(Load_History(j+1)/A(i)),(L_bckp(i)/Tie_Length-1));
                            else

Ev(i)=sma_hysteresis((Load_History(j)/A(i)),(L(i)/Tie_Length-
1),(Load_History(j)/A(i)),(L_bckp(i)/Tie_Length-1));
                            end
                            Kcoeff(i)=A(i)*Ev(i)/L(i);
                        else  %If only steel ties are used. negative sign is applied
before the load argument as the compression for the whole brace is tension for the
ties.

[Ev(i),Fypos(i),Fyneg(i)]=steel_hysteresis(Load_History(j)/A(i),Load_History(j-
1)/A(i),Fypos(i),Fyneg(i),Fy(i),r(i));
                            Kcoeff(i)=A(i)*Ev(i)/L(i);
                        end
                    elseif (i==2)

[Ev(i),Fypos(i),Fyneg(i)]=steel_hysteresis(Load_History(j)/A(i),Load_History(j-
1)/A(i),Fypos(i),Fyneg(i),Fy(i),r(i));
                             Kcoeff(i)=A(i)*Ev(i)/L(i);
                    end
                else %If the arrangement is in compression and getting loaded in
compression
                    if (i==1) %For the ties
                        if sma_ties_used==1
                            if (Load_History(j-1)>=0)
                                L(i)=Tie_compressive_length_bckp;
                            end
                            if j<Data_Points

Ev(i)=sma_hysteresis((Load_History(j)/A(i)),(L(i)/Tie_Length-
1),(Load_History(j+1)/A(i)),(L_bckp(i)/Tie_Length-1));
                            else

Ev(i)=sma_hysteresis((Load_History(j)/A(i)),(L(i)/Tie_Length-
1),(Load_History(j)/A(i)),(L_bckp(i)/Tie_Length-1));
                            end
%                             if (Load_History(j-1)>=0)
%                                 L(i)=Tie_compressive_length_bckp;
%                             end
                            Kcoeff(i)=A(i)*Ev(i)/L(i);
                        else %If only steel ties are used. negative sign is applied
before the load argument as the compression for the whole brace is tension for the
ties.
                            if (Load_History(j-1)>=0)
                                L(i)=Tie_compressive_length_bckp;
                            end

[Ev(i),Fypos(i),Fyneg(i)]=steel_hysteresis(Load_History(j)/A(i),Load_History(j-
1)/A(i),Fypos(i),Fyneg(i),Fy(i),r(i));
%                             if (Load_History(j-1)>=0)
%                                 L(i)=Tie_compressive_length_bckp;
%                             end
                            Kcoeff(i)=A(i)*Ev(i)/L(i);
```

```
                        end

                    elseif (i==2)

[Ev(i),Fypos(i),Fyneg(i)]=steel_hysteresis(Load_History(j)/A(i),Load_History(j-
1)/A(i),Fypos(i),Fyneg(i),Fy(i),r(i));
                        Kcoeff(i)=A(i)*Ev(i)/L(i);
                    end
                end
            end
        end
    end

%Keeping a backup of the previous steps length matrix
L_bckp=L;

%     disp('Calculated Modulus of elasticity of bar segments')
%     Ev;
%     disp(['Iteration Step :', num2str(j)] )
    %Global Stiffness matrix formation
    GlobalK=zeros(n+1,n+1);
    %k2 is a temporary stiffness matrix holder
    k2=zeros(n+1,n+1);
%     disp('Bar lengths :')
%     L;
    for i=1:n,
        k2(i:i+1,i:i+1)=k(:,:,i);
        GlobalK=GlobalK+Kcoeff(i)*k2(:,:);
        k2=zeros(n+1,n+1);
    end
    GlobalK;

    ReducedK=zeros(n,n);
    %Elimination of first row-column of the global stiffness matrix
    ReducedK=GlobalK(2:n+1,2:n+1);
    ReducedK;
    F=zeros(1,n+1);

%     disp('Applied force at bar end')
    if j==1
        F(1,n+1)=Load_History(j);
    else
        %Load increment is applied only
        F(1,n+1)=Load_History(j)-Load_History(j-1);
    end

    %Transpose of F matrix
%     disp('Force Matrix')
    F=F';
    ReducedF=zeros(n,1);
    ReducedF=F(2:n+1,1:1);

    %Global Displacement matrix
%     disp('Global Displacement matrix (m)')
    ReducedGlobalU=zeros(n,1);
    ReducedGlobalU=ReducedK\ReducedF;

    GlobalU(2:n+1,1:1)=ReducedGlobalU(1:n,1:1);
    GlobalU;

    GlobalF=zeros(n+1,1);
    for i=1:n+1,
```

```
        GlobalF(i,1)=GlobalK(i:i,1:n+1)*GlobalU;
    end

    for i=1:n,
        L(i)=L(i)+GlobalU(i+1)-GlobalU(i);
    end
%     disp('Bar lengths :')
    L;

    Tie_Deformed_length(j)=L(1);
    Shaft_Deformed_length(j)=L(2);
    if j>1
        if (Load_History(j)>0)
            Tie_tensile_length_bckp=L(1);
        elseif (Load_History(j)<0)
            Tie_compressive_length_bckp=L(1);
        end
    end
    %Tie Area change due to poisson's ratio. Absolute value of the percent
    %elongation is taken as ties are always in tension (Positive strain).
    A(1)=pi*(Tie_dia*(1-abs(Tie_Deformed_length(j)/Tie_Length-
1)*v(1)))^2*0.25*No_Of_Ties;

    %Shaft Area change due to poisson's ratio
    if Dis == 0
        A(2)=pi*(Dos*(1-(Shaft_Deformed_length(j)/Shaft_Length-1)*v(2)))^2*.25;
    else
        Dos=Dshft_centerline+t_shft*(1-(Shaft_Deformed_length(j)/Shaft_Length-
1)*v(2)); %Outer diameter
        Dis=Dshft_centerline-t_shft*(1-(Shaft_Deformed_length(j)/Shaft_Length-
1)*v(2));  %Inner diameter
        A(2)=pi*(Dos^2-Dis^2)*.25; %This area should come from a standard section
    end

    %Total deformed brace length calculation
    for i=1:n,
        if (Load_History(j)>=0)%If the brace is under tension
            if (i==1)
                Total_Deformed_length(j)=Total_Deformed_length(j)+L(i);
            elseif (i==2)
                Total_Deformed_length(j)=Total_Deformed_length(j)+L(i);
            end
        else %If the brace is under compression
            if (i==1)
                Total_Deformed_length(j)=Total_Deformed_length(j)+L(i);
            elseif (i==2)
                Total_Deformed_length(j)=Total_Deformed_length(j)+L(i);
            end
        end
    end

    %Monitoring buckling occurance
    if (Load_History(j)<=Pbuck_shaft)
        shaft_buckled=1;
    end

    %Monitoring ultimate strain exceedance
    if (abs(L(1)/Tie_Length)>=1.1)
        tie_ult_strain_excd=1;
    elseif (abs(L(2)/Shaft_Length)>=1.1)
        shaft_ult_strain_excd=1;
    end
```

```
end

%%%%%%%%%%%%%%%%%%%
%Plots and Outputs%
%%%%%%%%%%%%%%%%%%%

%Removing the tie compressive loads as they were not used for the
%calculation and reversing the sign for the global load to make it tensile
%for the ties
for k=1:Data_Points,
    if Load_History(k)<0
        Tie_Load_History(k)=-Load_History(k);
    else
        Tie_Load_History(k)=0;
    end
end
%Coordinate calculation for the buckling load plot
Deformation_Range=zeros(1,2);
Deformation_Range(1)=(max(Total_Deformed_length)-Undeformed_length);
Deformation_Range(2)=(min(Total_Deformed_length)-Undeformed_length);
% Deformation_Range;
Shaft_Buckling_Plot=[Pbuck_shaft,Pbuck_shaft];

%Coordinate calculation for ultimate strain points
Load_Range=zeros(1,2);
Load_Range(1)=max(Load_History);
Load_Range(2)=min(Load_History);
Tie_Strain_Range=[eu(1),eu(1)];
Shaft_Strain_Range=[eu(2),eu(2)];

subplot(1,4,1)
plot(Load_History/1000)
ylabel('Axial Force (kN)');
xlabel('Iteration Step');
grid on;

subplot(1,4,2)
plot((Total_Deformed_length-Undeformed_length)*1000)
ylabel('Axial Deformation (mm)');
xlabel('Iteration Step');
grid on;

subplot(1,4,3)
plot( (Total_Deformed_length-Undeformed_length)*1000, Load_History/1000)
ylabel('Axial Force in the brace (kN)');
xlabel('Axial Deformation (mm)');
grid on;

subplot(1,4,4)
if (shaft_buckled==1)
    plot( (Shaft_Deformed_length-Shaft_Length)*1000,
Load_History/1000,Deformation_Range*1000,Shaft_Buckling_Plot/1000)
else
    plot( (Shaft_Deformed_length-Shaft_Length)*1000, Load_History/1000)
end

ylabel('Axial Force in Shaft (kN)');
xlabel('Axial Deformation (mm)');
grid on;


disp('Printing some initially calculated matrix for review')
```

```
A_backup;
Undeformed_length;
ep;
r;
Pypos;

if (shaft_buckled==1)
    disp('Shaft buckled')
end
```

Appendix C: MATLAB material models

Tension only SE SMA uniaxial material model

```
function Esma = sma_hysteresis(Stress1,Strain1,Stress2,Strain0) %Function requires
current stress strain point, Next stress point and one step earlier strain

%Global Variables
global Strain_Max;
global Residual_Strain;
global Ei;
global Sams;
global Samf;
global Smas;
global Smaf;
global Ep;
global SMA_Yield_Strain;
global Smax;
global residual_ratio;
global Strain_Crspnd_Pos;
global Strain_amf;
global Brace_Under_Tension;
global Strain_Max_Tension;
global Strain_Max_Compression;
global Residual_Strain_Tension;
global Residual_Strain_Compression;
E1=0;
Q1Q4_Strain = Smaf/Ei;
Q1Q4_Stress = Smaf;

if (Stress2>0)
    Brace_Under_Tension = 1;
    Strain_Max = Strain_Max_Tension;
    Residual_Strain = Residual_Strain_Tension;
elseif (Stress2<0)
    Brace_Under_Tension = 0;
    Strain_Max = Strain_Max_Compression;
    Residual_Strain = Residual_Strain_Compression;
end

Stress2=abs(Stress2);
Stress1=abs(Stress1);
Strain1=abs(Strain1);
Strain0=abs(Strain0);

if (Stress2>=Stress1)     %Stress increasing
```

```
    if (Strain1 > Strain_Max)

        Strain_Max = Strain1;
        Residual_Strain = (Strain_Max - SMA_Yield_Strain) * residual_ratio;
        if (Brace_Under_Tension == 1)
            Strain_Max_Tension = Strain_Max;
            Residual_Strain_Tension = Residual_Strain;
        elseif (Brace_Under_Tension == 0)
            Strain_Max_Compression = Strain_Max;
            Residual_Strain_Compression = Residual_Strain;
        end
    end

    Smax= (Sams * Ei + Ei * Ep * (Strain1 - SMA_Yield_Strain) - Stress1 * Ep) / (Ei -
Ep);
    Strain_Crspnd_Pos = (Strain1 * Ei + Sams - Ep * SMA_Yield_Strain - Stress1) / (Ei
- Ep);
    if (Stress1 >= 0 && Stress1 < Smax)
        if (Stress2 <= Smax)
            Esma = Ei;
        elseif (Stress2 > Smax && Stress2 <= Samf)
            Esma =(Stress2-Stress1)/(Strain_Crspnd_Pos+(Stress2-Smax)/Ep-Strain1);
        elseif (Stress2 > Samf)
            Esma = (Stress2-Stress1)/(Strain_amf+(Stress2-Samf)/Ei-Strain1);
        end
    elseif (Stress1 >= Smax && Stress1 < Samf)
        if (Stress2 <= Samf)
            Esma = Ep;
        else
            Esma = (Stress2-Stress1)/(Strain_amf+(Stress2-Samf)/Ei-Strain1);
            %Esma = Ei;
        end
    elseif (Stress1 >= Samf)
        Esma = Ei;
    end
elseif (Stress2 < Stress1) %Stress decreasing
    if (Brace_Under_Tension == 1)
        Q1Q4_Strain = (Ei / (Ei - E1)) * Residual_Strain_Tension + Smaf/Ei;
        Q1Q4_Stress = ((Q1Q4_Strain - Residual_Strain_Tension) * Ei);
    elseif (Brace_Under_Tension == 0)
        Q1Q4_Strain = (Ei / (Ei - E1)) *Residual_Strain_Compression + Smaf/Ei;
        Q1Q4_Stress = ((Q1Q4_Strain -Residual_Strain_Compression) * Ei);
    end

    if (Stress1 > Smas)
        if (Stress2>=Smas)
            Esma = Ei;
        elseif (Stress2<Smas && Stress2>=Q1Q4_Stress)
            Smas_Strain=(Smas - Stress1) / Ei + Strain1;
            E1 = (Smas - Smaf) / (Smas_Strain - Smaf / Ei);
            Esma = E1;
        elseif (Stress2<Q1Q4_Stress)
            Esma = (Stress1-Stress2)/(Strain1-Q1Q4_Strain+(Q1Q4_Stress-Stress2)/Ei);
        end
    elseif (Stress1 > Q1Q4_Stress && Stress1 <= Smas)
        if (Stress2 >= Q1Q4_Stress)
            E1 = (Stress1 - Smaf) / (Strain1 - Smaf / Ei);
            Esma = E1;
        else
            Esma = (Stress1-Stress2)/(Strain1-Q1Q4_Strain+(Q1Q4_Stress-Stress2)/Ei);
        end
    elseif (Stress1 <= Q1Q4_Stress)
```

```
        Esma = Ei;
    end
end
```

Material model for steel

```
function [Esteel,Fy_pos_out,Fy_neg_out] =
steel_hysteresis(Stress1,Stress0,Fy_pos,Fy_neg,Fy,r)
Ei = 200e9;
Ep=Ei*r;

if (Stress1>=Stress0)     %Loading in tension
    if (Stress1<Fy_pos)
        Esteel=Ei;
    elseif (Stress1>=Fy_pos)
        Esteel=Ep;
        Fy_pos=Stress1;
        Fy_neg=Fy_pos-2*Fy;
    end
elseif (Stress1 < Stress0) %Loading in compression
    if (Stress1>Fy_neg)
        Esteel=Ei;
    elseif (Stress1<=Fy_neg)
        Esteel=Ep;
        Fy_neg=Stress1;
        Fy_pos=Fy_neg+2*Fy;
    end
end
Fy_pos_out=Fy_pos;
Fy_neg_out=Fy_neg;
```

Appendix D: PBSC brace hysteresis model

```
Private Sub CommandButton1_Click()

    Dim i, N As Integer                                         'Loop Variables
    Dim k1, k2, k3, k4, k5, k6, Fy, PMax, PMin, NMin, NMax As Double 'Positive Initial
stiffness = k1, Positive Post elatic stiffness = k2,   Yield force in positive
direction= Fy, Positive force limit = PMax, Negative force limit = NMin
    Dim Deformation_Y_Pos, Deformation_Y_Neg As Double
    Dim Variable_Deformation_Y_Pos, Variable_Deformation_Y_Neg As Double
    Dim Deformation_Max_Pos, Deformation_Min_Pos As Double
    Dim Deformation_Min_Neg, Deformation_Max_Neg As Double
    Dim Force() As Double
    Dim Deformation() As Double
    Dim work As Double
    Dim Location() As Double
    Dim Tangent_Stiffness() As Double
    Dim Deformation_Before_Corner As Double
    Dim Q2Q3_Junction_Def, Q1Q4_Junction_Def As Double
    Dim Q2Q3_Junction_Force, Q1Q4_Junction_Force As Double
    Dim r1, ry As Double
    Dim Historical_Deformation_Max, Historical_Deformation_Min As Double
    Dim SMA_Rule As Integer
    Dim Slippage_Rule As Integer
    Dim SMA_Cutoff_Force As Double
    Dim SMA_Pos_Cutoff_Force, SMA_Neg_Cutoff_Force As Double
```

```
    Dim SMA_Pos_Cutoff_Def, SMA_Neg_Cutoff_Def As Double
    Dim SMA_Max_Force, SMA_Max_Pos_Force, SMA_Min_Neg_Force As Double
    Dim SMA_Max_Def, SMA_Min_Def As Double
    Dim Res_Def_Pos, Res_Def_Neg As Double
    Dim PMax_Array(), Deformation_Max_Pos_Array(), NMin_Array(),
Deformation_Min_Neg_Array(), PMin_Array(), Deformation_Min_Pos_Array(), k5_Array(),
k6_Array(), Q1Q4_Junction_Def_Array(), Q1Q4_Junction_Force_Array() As Double
    Dim Q2Q3_Junction_Def_Array(), Q2Q3_Junction_Force_Array(),
SMA_Pos_Cutoff_Force_Array(), SMA_Neg_Cutoff_Force_Array(), NMax_Array(),
Historical_Deformation_Max_Array(), Historical_Deformation_Min_Array(),
Res_Def_Pos_Array(), Res_Def_Neg_Array() As Double
    Dim Variable_Deformation_Y_Pos_Array(), Variable_Deformation_Y_Neg_Array() As
Double


    For k = 1 To 18
    load_num = k

    Fy = Worksheets("Final").Cells(1, 2).Value
    k1 = Worksheets("Final").Cells(2, 2).Value
    r1 = Worksheets("Final").Cells(3, 2).Value
    r2 = Worksheets("Final").Cells(4, 2).Value
    alpha = Worksheets("Final").Cells(5, 2).Value
    beta = Worksheets("Final").Cells(6, 2).Value
    ry = Worksheets("Final").Cells(7, 2).Value
    N = Worksheets("Load Cases").Cells(1, 2 * load_num - 1).Value
    SMA_Rule = Worksheets("Final").Cells(11, 2).Value
    SMA_Cutoff_Force = Worksheets("Final").Cells(12, 2).Value
    SMA_Max_Force = Worksheets("Final").Cells(13, 2).Value
    Slippage_Rule = Worksheets("Final").Cells(14, 2).Value


    If (k1 <= 0 Or k2 < 0 Or Fy < 0 Or k2 >= k1 Or beta > 1 Or load_num <= 0 Or
load_num > 18 Or SMA_Rule < 0 Or SMA_Rule > 1 Or Slippage_Rule < 0 Or Slippage_Rule >
1 Or SMA_Cutoff_Force > Fy Or SMA_Cutoff_Force < alpha * Fy Or SMA_Max_Force <= Fy Or
ry > 1 Or ry < 0) Then
        MsgBox "Invalid Entry", vbOKOnly
        Exit Sub
    End If

    ReDim Force(N) As Double
    ReDim Deformation(N) As Double
    ReDim Tangent_Stiffness(N) As Double
    ReDim Location(N) As Double

    For i = 0 To N - 1 'Preloading deformation data for faster testing and debugging
        Deformation(i) = Worksheets("Load Cases").Cells(i + 3, 2 * load_num - 1).Value
    Next i

    ReDim PMax_Array(N), Deformation_Max_Pos_Array(N), NMin_Array(N),
Deformation_Min_Neg_Array(N), PMin_Array(N), Deformation_Min_Pos_Array(N),
k5_Array(N), k6_Array(N), Q1Q4_Junction_Def_Array(N), Q1Q4_Junction_Force_Array(N) As
Double
    ReDim Q2Q3_Junction_Def_Array(N), Q2Q3_Junction_Force_Array(N),
SMA_Pos_Cutoff_Force_Array(N), SMA_Neg_Cutoff_Force_Array(N), NMax_Array(N),
Historical_Deformation_Max_Array(N), Historical_Deformation_Min_Array(N),
Res_Def_Pos_Array(N), Res_Def_Neg_Array(N), Variable_Deformation_Y_Pos_Array(N),
Variable_Deformation_Y_Neg_Array(N) As Double

    k2 = r1 * k1
    Tangent_Stiffness(0) = k1
    Location(0) = 0
```

```
    PMax = Fy
    NMin = -Fy
    Deformation_Y_Pos = Fy / k1
    Deformation_Y_Neg = -Fy / k1
    k3 = k1 * beta
    k4 = r2 * k1
    work = 0
    Deformation_Max_Pos = Fy / k1
    Deformation_Min_Neg = -Fy / k1
    Deformation_Before_Corner = 0

    Historical_Deformation_Max = Deformation_Y_Pos
    Historical_Deformation_Min = Deformation_Y_Neg

    Q1Q4_Junction_Def = alpha * Deformation_Y_Pos
    Q2Q3_Junction_Def = alpha * Deformation_Y_Neg

    'Needed for SMA hysteresis rule
    SMA_Pos_Cutoff_Force = SMA_Cutoff_Force
    SMA_Neg_Cutoff_Force = -SMA_Cutoff_Force

    SMA_Pos_Cutoff_Def = SMA_Pos_Cutoff_Force / k1 'Test code
    SMA_Neg_Cutoff_Def = SMA_Neg_Cutoff_Force / k1 'Test code

    SMA_Max_Pos_Force = SMA_Max_Force
    SMA_Min_Neg_Force = -SMA_Max_Force

    SMA_Max_Def = (SMA_Max_Pos_Force - Fy) / k2 + Deformation_Y_Pos
    SMA_Min_Def = (SMA_Min_Neg_Force + Fy) / k2 + Deformation_Y_Neg

    Res_Def_Pos = 0
    Res_Def_Neg = 0

    Variable_Deformation_Y_Pos = Fy / k1
    Variable_Deformation_Y_Neg = -Fy / k1



    'Start of the program's main loop
    For i = 0 To N - 2 Step 1
        If (Deformation(i + 1) = Deformation(i)) Then
            Force(i + 1) = Force(i)
            Tangent_Stiffness(i + 1) = Tangent_Stiffness(i)
            Location(i + 1) = 0
        ElseIf (Deformation(i + 1) > Deformation(i)) Then
            If (i > 0) Then
                If (Deformation(i) < Deformation_Before_Corner) Then
                    If (Deformation(i) < Historical_Deformation_Min) Then
                        Historical_Deformation_Min = Deformation(i)
'Set the current rotation as the minimum of all times
                        Res_Def_Neg = (Historical_Deformation_Min - Deformation_Y_Neg)
* ry
                    End If
                    If (Force(i) <= SMA_Neg_Cutoff_Force) Then
                        SMA_Neg_Cutoff_Def = (SMA_Neg_Cutoff_Force - Force(i)) / k1 +
Deformation(i)
                        If (alpha * Deformation_Y_Neg = SMA_Neg_Cutoff_Def) Then
                            k6 = 0
                        Else
                            k6 = (-alpha * Fy - SMA_Neg_Cutoff_Force) / (alpha *
Deformation_Y_Neg - SMA_Neg_Cutoff_Def) 'Slope of the line connecting (SMA negative
```

```
cutoff force, corresponding deformation) point and (-alpha*Fy, -alpha*deformation_y)
point
                        End If
                    ElseIf (Force(i) < Q2Q3_Junction_Force) Then
                        If (alpha * Deformation_Y_Neg = Deformation(i)) Then
                            k6 = 0
                        Else
                            k6 = (-alpha * Fy - Force(i)) / (alpha * Deformation_Y_Neg
- Deformation(i)) 'Slope of the line connecting (SMA negative cutoff force,
corresponding deformation) point and (-alpha*Fy, -alpha*deformation_y) point
                        End If
                    End If


                    If (k6 = k1) Then
                        Q2Q3_Junction_Def = Deformation_Y_Neg * alpha
                        Q2Q3_Junction_Force = Q2Q3_Junction_Def * k1
                    Else
                        Q2Q3_Junction_Def = (k1 / (k1 - k6)) * Res_Def_Neg +
Deformation_Y_Neg * alpha
                        Q2Q3_Junction_Force = (Q2Q3_Junction_Def - Res_Def_Neg) * k1
                    End If
                End If
            End If

            If (Force(i) >= 0) Then
                PMax = (Fy * k1 + k1 * k2 * (Res_Def_Pos - Deformation_Y_Pos)) / (k1 -
k2)
                Deformation_Max_Pos = (Res_Def_Pos * k1 + Fy - k2 * Deformation_Y_Pos)
/ (k1 - k2)
                If (Deformation(i) < SMA_Max_Def) Then
                    If (Force(i) = 0) Then
                        If (Deformation(i + 1) <= Res_Def_Pos) Then
                            Force(i + 1) = 0
                            Tangent_Stiffness(i + 1) = 0
                            Location(i + 1) = 1.211
                        ElseIf (Deformation(i + 1) > Res_Def_Pos And Deformation(i +
1) <= SMA_Max_Def) Then
                            If ((k1 * (Deformation(i + 1) - Res_Def_Pos)) <= PMax)
Then
                                Force(i + 1) = k1 * (Deformation(i + 1) - Res_Def_Pos)
                                Tangent_Stiffness(i + 1) = k1
                                Location(i + 1) = 1.212
                            Else
                                Force(i + 1) = k2 * (Deformation(i + 1) -
Deformation_Max_Pos) + PMax
                                Tangent_Stiffness(i + 1) = k2
                                Location(i + 1) = 1.213
                            End If
                        ElseIf (Deformation(i + 1) > SMA_Max_Def) Then
                            Force(i + 1) = k1 * (Deformation(i + 1) - SMA_Max_Def) +
SMA_Max_Pos_Force
                            Tangent_Stiffness(i + 1) = k1
                            Location(i + 1) = 1.214
                        End If
                    ElseIf (Force(i) < PMax) Then 'if current force is less than the
limit
                        If (k1 * (Deformation(i + 1) - Deformation(i)) + Force(i) <=
PMax) Then 'if next force is also less than the limit
                            Force(i + 1) = k1 * (Deformation(i + 1) - Deformation(i))
+ Force(i)
                            Tangent_Stiffness(i + 1) = k1
```

```
                            Location(i + 1) = 1.215
                        Else    'if next force is more than the limit
                            If (k2 * (Deformation(i + 1) - Deformation_Max_Pos) + PMax
<= SMA_Max_Pos_Force) Then
                                Force(i + 1) = k2 * (Deformation(i + 1) -
Deformation_Max_Pos) + PMax
                                Tangent_Stiffness(i + 1) = k2
                                Location(i + 1) = 1.216
                            Else
                                Force(i + 1) = k1 * (Deformation(i + 1) - SMA_Max_Def)
+ SMA_Max_Pos_Force
                                Tangent_Stiffness(i + 1) = k1
                                Location(i + 1) = 1.217
                            End If
                        End If
                    ElseIf (Force(i) >= PMax) Then
                        If (Deformation(i + 1) <= SMA_Max_Def) Then
                            Force(i + 1) = k2 * (Deformation(i + 1) - Deformation(i))
+ Force(i)
                            Tangent_Stiffness(i + 1) = k2
                            Location(i + 1) = 1.218
                        Else
                            Force(i + 1) = k1 * (Deformation(i + 1) - SMA_Max_Def) +
SMA_Max_Pos_Force
                            Tangent_Stiffness(i + 1) = k1
                            Location(i + 1) = 1.219
                        End If
                    End If
                ElseIf (Deformation(i) >= SMA_Max_Def) Then
                    Force(i + 1) = k1 * (Deformation(i + 1) - Deformation(i)) +
Force(i)
                    Tangent_Stiffness(i + 1) = k1
                    Location(i + 1) = 1.22
                End If
            ElseIf (Force(i) < 0) Then 'if current force is negative and deformation
is increasing
                If (k1 * Deformation(i) - Force(i) - k1 * Res_Def_Neg < 0) Then 'Any
point on the left side of the line with stiffness k1 and going through (Res_def_neg,
0) point
                    If (Force(i) <= SMA_Neg_Cutoff_Force) Then 'If current force level
is less than the Martensite to Austenite starting stress
                        If (k1 * (Deformation(i + 1) - Deformation(i)) + Force(i) <=
SMA_Neg_Cutoff_Force) Then 'If next force level is also less than the Martensite to
Austenite starting stress
                            Force(i + 1) = k1 * (Deformation(i + 1) - Deformation(i))
+ Force(i)
                            Tangent_Stiffness(i + 1) = k1
                            Location(i + 1) = 2.1
                        ElseIf (k1 * (Deformation(i + 1) - Deformation(i)) + Force(i)
> SMA_Neg_Cutoff_Force) Then 'If next force level is more than the Martensite to
Austenite starting stress
                            If (Deformation(i + 1) <= Q2Q3_Junction_Def) Then
                                Force(i + 1) = k6 * (Deformation(i + 1) -
SMA_Neg_Cutoff_Def) + SMA_Neg_Cutoff_Force
                                Tangent_Stiffness(i + 1) = k6
                                Location(i + 1) = 2.11
                            ElseIf (Deformation(i + 1) > Q2Q3_Junction_Def) Then
                                PMax = (Fy * k1 + k1 * k2 * (Res_Def_Pos -
Deformation_Y_Pos)) / (k1 - k2)
                                Deformation_Max_Pos = (Res_Def_Pos * k1 + Fy - k2 *
Deformation_Y_Pos) / (k1 - k2)
```

```
                                If (k1 * (Deformation(i + 1) - Q2Q3_Junction_Def) +
Q2Q3_Junction_Force <= 0) Then
                                    Force(i + 1) = k1 * (Deformation(i + 1) -
Q2Q3_Junction_Def) + Q2Q3_Junction_Force
                                    Tangent_Stiffness(i + 1) = k1
                                    Location(i + 1) = 2.14
                                ElseIf (k1 * (Deformation(i + 1) - Q2Q3_Junction_Def)
+ Q2Q3_Junction_Force > 0) Then
                                    If (Deformation(i + 1) <= Res_Def_Pos) Then
                                        Force(i + 1) = 0
                                        Tangent_Stiffness(i + 1) = 0
                                        Location(i + 1) = 2.15
                                    ElseIf (Deformation(i + 1) > Res_Def_Pos) Then
                                        If ((k1 * (Deformation(i + 1) - Res_Def_Pos))
<= PMax) Then
                                            Force(i + 1) = k1 * (Deformation(i + 1) -
Res_Def_Pos)
                                            Tangent_Stiffness(i + 1) = k1
                                            Location(i + 1) = 2.16
                                        Else
                                            If ((k2 * (Deformation(i + 1) -
Deformation_Max_Pos) + PMax) <= SMA_Max_Pos_Force) Then
                                                Force(i + 1) = k2 * (Deformation(i +
1) - Deformation_Max_Pos) + PMax
                                                Tangent_Stiffness(i + 1) = k2
                                                'Variable_Deformation_Y_Pos =
Deformation_Max_Pos
                                                Location(i + 1) = 2.17
                                            Else
                                                Force(i + 1) = k1 * (Deformation(i +
1) - SMA_Max_Def) + SMA_Max_Pos_Force
                                                Tangent_Stiffness(i + 1) = k1
                                                Location(i + 1) = 2.18
                                            End If
                                        End If
                                    End If
                                End If
                            End If
                        ElseIf (Force(i) > SMA_Neg_Cutoff_Force And Force(i) <
Q2Q3_Junction_Force) Then
                            If ((k6 * (Deformation(i + 1) - Deformation(i)) + Force(i)) <=
Q2Q3_Junction_Force) Then
                                Force(i + 1) = k6 * (Deformation(i + 1) - Deformation(i))
+ Force(i)
                                Tangent_Stiffness(i + 1) = k6
                                Location(i + 1) = 2.2
                            Else
                                PMax = (Fy * k1 + k1 * k2 * (Res_Def_Pos -
Deformation_Y_Pos)) / (k1 - k2)
                                Deformation_Max_Pos = (Res_Def_Pos * k1 + Fy - k2 *
Deformation_Y_Pos) / (k1 - k2)
                                If (k1 * (Deformation(i + 1) - Q2Q3_Junction_Def) +
Q2Q3_Junction_Force <= 0) Then
                                    Force(i + 1) = k1 * (Deformation(i + 1) -
Q2Q3_Junction_Def) + Q2Q3_Junction_Force
                                    Tangent_Stiffness(i + 1) = k1
                                    Location(i + 1) = 2.23
                                Else
                                    If (Deformation(i + 1) <= Res_Def_Pos) Then
                                        Force(i + 1) = 0
                                        Tangent_Stiffness(i + 1) = 0
```

```
                                    Location(i + 1) = 2.24
                                ElseIf (Deformation(i + 1) > Res_Def_Pos) Then
                                    If ((k1 * (Deformation(i + 1) - Res_Def_Pos)) <=
PMax) Then
                                        Force(i + 1) = k1 * (Deformation(i + 1) -
Res_Def_Pos)
                                        Tangent_Stiffness(i + 1) = k1
                                        Location(i + 1) = 2.25
                                    Else
                                        If ((k2 * (Deformation(i + 1) -
Deformation_Max_Pos) + PMax) <= SMA_Max_Pos_Force) Then
                                            Force(i + 1) = k2 * (Deformation(i + 1) -
Deformation_Max_Pos) + PMax
                                            Tangent_Stiffness(i + 1) = k2
                                            'Variable_Deformation_Y_Pos =
Deformation_Max_Pos
                                            Location(i + 1) = 2.26
                                        Else
                                            Force(i + 1) = k1 * (Deformation(i + 1) -
SMA_Max_Def) + SMA_Max_Pos_Force
                                            Tangent_Stiffness(i + 1) = k1
                                            Location(i + 1) = 2.27
                                        End If
                                    End If
                                End If
                            End If

                        End If
                    ElseIf (Force(i) >= Q2Q3_Junction_Force) Then
                        PMax = (Fy * k1 + k1 * k2 * (Res_Def_Pos - Deformation_Y_Pos))
/ (k1 - k2)
                        Deformation_Max_Pos = (Res_Def_Pos * k1 + Fy - k2 *
Deformation_Y_Pos) / (k1 - k2)
                        If (k1 * (Deformation(i + 1) - Deformation(i)) + Force(i) <=
0) Then
                            Force(i + 1) = k1 * (Deformation(i + 1) - Deformation(i))
+ Force(i)
                            Tangent_Stiffness(i + 1) = k1
                            Location(i + 1) = 2.32
                        Else
                            If (Deformation(i + 1) <= Res_Def_Pos) Then
                                Force(i + 1) = 0
                                Tangent_Stiffness(i + 1) = 0
                                Location(i + 1) = 2.33
                            ElseIf (Deformation(i + 1) > Res_Def_Pos) Then
                                If ((k1 * (Deformation(i + 1) - Res_Def_Pos)) <= PMax)
Then
                                    Force(i + 1) = k1 * (Deformation(i + 1) -
Res_Def_Pos)
                                    Tangent_Stiffness(i + 1) = k1
                                    Location(i + 1) = 2.34
                                Else
                                    If ((k2 * (Deformation(i + 1) -
Deformation_Max_Pos) + PMax) <= SMA_Max_Pos_Force) Then
                                        Force(i + 1) = k2 * (Deformation(i + 1) -
Deformation_Max_Pos) + PMax
                                        Tangent_Stiffness(i + 1) = k2
                                        Location(i + 1) = 2.35
                                    Else
                                        Force(i + 1) = k1 * (Deformation(i + 1) -
SMA_Max_Def) + SMA_Max_Pos_Force
                                        Tangent_Stiffness(i + 1) = k1
```

```
                                    Location(i + 1) = 2.36
                                End If
                            End If
                        End If
                    End If
                ElseIf (k1 * Deformation(i) - Force(i) - k1 * Res_Def_Neg >= 0) Then
                    PMax = (Fy * k1 + k1 * k2 * (Res_Def_Pos - Deformation_Y_Pos)) /
(k1 - k2)
                    Deformation_Max_Pos = (Res_Def_Pos * k1 + Fy - k2 *
Deformation_Y_Pos) / (k1 - k2)
                    If (k1 * (Deformation(i + 1) - Deformation(i)) + Force(i) <= 0)
Then
                        Force(i + 1) = k1 * (Deformation(i + 1) - Deformation(i)) +
Force(i)
                        Tangent_Stiffness(i + 1) = k1
                        Location(i + 1) = 2.42
                    Else
                        If (Deformation(i + 1) <= Res_Def_Pos) Then
                            Force(i + 1) = 0
                            Tangent_Stiffness(i + 1) = 0
                            Location(i + 1) = 2.43
                        ElseIf (Deformation(i + 1) > Res_Def_Pos) Then
                            If ((k1 * (Deformation(i + 1) - Res_Def_Pos)) <= PMax)
Then
                                Force(i + 1) = k1 * (Deformation(i + 1) - Res_Def_Pos)
                                Tangent_Stiffness(i + 1) = k1
                                Location(i + 1) = 2.44
                            Else
                                If ((k2 * (Deformation(i + 1) - Deformation_Max_Pos) +
PMax) <= SMA_Max_Pos_Force) Then
                                    Force(i + 1) = k2 * (Deformation(i + 1) -
Deformation_Max_Pos) + PMax
                                    Tangent_Stiffness(i + 1) = k2
                                    'Variable_Deformation_Y_Pos = Deformation_Max_Pos
                                    Location(i + 1) = 2.45
                                Else
                                    Force(i + 1) = k1 * (Deformation(i + 1) -
SMA_Max_Def) + SMA_Max_Pos_Force
                                    Tangent_Stiffness(i + 1) = k1
                                    Location(i + 1) = 2.46
                                End If
                            End If
                        End If
                    End If
                End If
            End If
            Deformation_Before_Corner = Deformation(i)
        ElseIf (Deformation(i + 1) < Deformation(i)) Then
'deformation decreasing
            If (i > 0) Then
                If (Deformation(i) > Deformation_Before_Corner) Then
' Corner point determination
                    If (Deformation(i) > Historical_Deformation_Max) Then
                        Historical_Deformation_Max = Deformation(i) 'At every corner
point the historical deformation max is changing!!! I have to check the logic behind
this
                        If (Slippage_Rule = 0) Then
                            Res_Def_Pos = (Historical_Deformation_Max -
Variable_Deformation_Y_Pos) * ry + Res_Def_Neg
                        Else
```

```
                        Res_Def_Pos = (Historical_Deformation_Max -
Deformation_Y_Pos) * ry
                    End If
                End If
                If (Force(i) >= SMA_Pos_Cutoff_Force) Then
                    SMA_Pos_Cutoff_Def = (SMA_Pos_Cutoff_Force - Force(i)) / k1 +
Deformation(i)
                    If (alpha * Deformation_Y_Pos = SMA_Pos_Cutoff_Def) Then
                        k5 = 0
                    Else
                        k5 = (alpha * Fy - SMA_Pos_Cutoff_Force) / (alpha *
Deformation_Y_Pos - SMA_Pos_Cutoff_Def)
                    End If
                ElseIf (Force(i) > Q1Q4_Junction_Force) Then
                    If (alpha * Deformation_Y_Pos = Deformation(i)) Then
                        k5 = 0
                    Else
                        k5 = (alpha * Fy - Force(i)) / (alpha * Deformation_Y_Pos
- Deformation(i))
                    End If
                End If
                If (k5 = k1) Then
                    Q1Q4_Junction_Def = alpha * Deformation_Y_Pos
                    Q1Q4_Junction_Force = Q1Q4_Junction_Def * k1
                Else
                    Q1Q4_Junction_Def = (k1 / (k1 - k5)) * Res_Def_Pos +
Deformation_Y_Pos * alpha
                    Q1Q4_Junction_Force = ((Q1Q4_Junction_Def - Res_Def_Pos) * k1)
                End If
            End If
        End If

        If (Force(i) <= 0) Then
            NMin = (-Fy * k1 + k1 * k2 * (Res_Def_Neg - Deformation_Y_Neg)) / (k1
- k2)
            Deformation_Min_Neg = (Res_Def_Neg * k1 - Fy - k2 * Deformation_Y_Neg)
/ (k1 - k2)
            If (Deformation(i) > SMA_Min_Def) Then
                If (Force(i) = 0) Then
                    If (Deformation(i + 1) >= Res_Def_Neg) Then
                        Force(i + 1) = 0
                        Tangent_Stiffness(i + 1) = 0
                        Location(i + 1) = -1.2
                    ElseIf (Deformation(i + 1) < Res_Def_Neg And Deformation(i +
1) >= SMA_Min_Def) Then
                        If ((k1 * (Deformation(i + 1) - Res_Def_Neg)) >= NMin)
Then
                            Force(i + 1) = k1 * (Deformation(i + 1) - Res_Def_Neg)
                            Tangent_Stiffness(i + 1) = k1
                            Location(i + 1) = -1.21
                        Else
                            Force(i + 1) = k2 * (Deformation(i + 1) -
Deformation_Min_Neg) + NMin
                            Tangent_Stiffness(i + 1) = k2
                            Location(i + 1) = -1.22
                        End If
                    ElseIf (Deformation(i + 1) < SMA_Min_Def) Then
                        Force(i + 1) = k1 * (Deformation(i + 1) - SMA_Min_Def) +
SMA_Min_Neg_Force
                        Tangent_Stiffness(i + 1) = k1
                        Location(i + 1) = -1.23
                    End If
```

```
                    ElseIf (Force(i) > NMin) Then
                        If (k1 * (Deformation(i + 1) - Deformation(i)) + Force(i) >=
NMin) Then
                            Force(i + 1) = k1 * (Deformation(i + 1) - Deformation(i))
+ Force(i)
                            Tangent_Stiffness(i + 1) = k1
                            Location(i + 1) = -1.24
                        Else
                            If (k2 * (Deformation(i + 1) - Deformation_Min_Neg) + NMin
>= SMA_Min_Neg_Force) Then
                                Force(i + 1) = k2 * (Deformation(i + 1) -
Deformation_Min_Neg) + NMin
                                Tangent_Stiffness(i + 1) = k2
                                Location(i + 1) = -1.25
                            Else
                                Force(i + 1) = k1 * (Deformation(i + 1) - SMA_Min_Def)
+ SMA_Min_Neg_Force
                                Tangent_Stiffness(i + 1) = k1
                                Location(i + 1) = -1.26
                            End If
                        End If
                    ElseIf (Force(i) <= NMin) Then
                        If (Deformation(i + 1) >= SMA_Min_Def) Then
                            Force(i + 1) = k2 * (Deformation(i + 1) - Deformation(i))
+ Force(i)
                            Tangent_Stiffness(i + 1) = k2
                            Location(i + 1) = -1.27
                        Else
                            Force(i + 1) = k1 * (Deformation(i + 1) - SMA_Min_Def) +
SMA_Min_Neg_Force
                            Tangent_Stiffness(i + 1) = k1
                            Location(i + 1) = -1.28
                        End If
                    End If
                ElseIf (Deformation(i) <= SMA_Min_Def) Then
                    Force(i + 1) = k1 * (Deformation(i + 1) - Deformation(i)) +
Force(i)
                    Tangent_Stiffness(i + 1) = k1
                    Location(i + 1) = -1.29
                End If
            ElseIf (Force(i) > 0) Then 'if current force is positive and deformation
is decreasing
                If (k1 * Deformation(i) - Force(i) - k1 * Res_Def_Pos > 0) Then 'Any
point on the right side of the line with stiffness k1 and going through (Res_def_pos,
0) point
                    If (Force(i) >= SMA_Pos_Cutoff_Force) Then 'If current force level
is more than the Martensite to Austenite starting stress
                        If (k1 * (Deformation(i + 1) - Deformation(i)) + Force(i) >=
SMA_Pos_Cutoff_Force) Then
                            Force(i + 1) = k1 * (Deformation(i + 1) - Deformation(i))
+ Force(i)
                            Tangent_Stiffness(i + 1) = k1
                            Location(i + 1) = -2.1
                        Else 'if next force/force is less than the
SMA_pos_cutoff_force
                            If (Deformation(i + 1) >= Q1Q4_Junction_Def) Then
                                Force(i + 1) = k5 * (Deformation(i + 1) -
SMA_Pos_Cutoff_Def) + SMA_Pos_Cutoff_Force
                                Tangent_Stiffness(i + 1) = k5
                                Location(i + 1) = -2.21
                            Else
```

```
                                NMin = (-Fy * k1 + k1 * k2 * (Res_Def_Neg -
Deformation_Y_Neg)) / (k1 - k2)
                                Deformation_Min_Neg = (Res_Def_Neg * k1 - Fy - k2 *
Deformation_Y_Neg) / (k1 - k2)
                                If (k1 * (Deformation(i + 1) - Q1Q4_Junction_Def) +
Q1Q4_Junction_Force >= 0) Then
                                    Force(i + 1) = k1 * (Deformation(i + 1) -
Q1Q4_Junction_Def) + Q1Q4_Junction_Force
                                    Tangent_Stiffness(i + 1) = k1
                                    Location(i + 1) = -2.24
                                ElseIf (k1 * (Deformation(i + 1) - Q1Q4_Junction_Def)
+ Q1Q4_Junction_Force < 0) Then
                                    If (Deformation(i + 1) >= Res_Def_Neg) Then
                                        Force(i + 1) = 0
                                        Tangent_Stiffness(i + 1) = 0
                                        Location(i + 1) = -2.25
                                    ElseIf (Deformation(i + 1) < Res_Def_Neg) Then
                                        If ((k1 * (Deformation(i + 1) - Res_Def_Neg))
>= NMin) Then
                                            Force(i + 1) = k1 * (Deformation(i + 1) -
Res_Def_Neg)
                                            Tangent_Stiffness(i + 1) = k1
                                            Location(i + 1) = -2.26
                                        Else
                                            If ((k2 * (Deformation(i + 1) -
Deformation_Min_Neg) + NMin) >= SMA_Min_Neg_Force) Then
                                                Force(i + 1) = k2 * (Deformation(i +
1) - Deformation_Min_Neg) + NMin
                                                Tangent_Stiffness(i + 1) = k2
                                                Location(i + 1) = -2.27
                                            Else
                                                Force(i + 1) = k1 * (Deformation(i +
1) - SMA_Min_Def) + SMA_Min_Neg_Force
                                                Tangent_Stiffness(i + 1) = k1
                                                Location(i + 1) = -2.28
                                            End If
                                        End If
                                    End If
                                End If
                            End If
                        ElseIf (Force(i) < SMA_Pos_Cutoff_Force And Force(i) >
Q1Q4_Junction_Force) Then
                            If ((k5 * (Deformation(i + 1) - Deformation(i)) + Force(i)) >=
Q1Q4_Junction_Force) Then
                                Force(i + 1) = k5 * (Deformation(i + 1) - Deformation(i))
+ Force(i)
                                Tangent_Stiffness(i + 1) = k5
                                Location(i + 1) = -2.3
                            Else
                                NMin = (-Fy * k1 + k1 * k2 * (Res_Def_Neg -
Deformation_Y_Neg)) / (k1 - k2)
                                Deformation_Min_Neg = (Res_Def_Neg * k1 - Fy - k2 *
Deformation_Y_Neg) / (k1 - k2)
                                If ((k1 * (Deformation(i + 1) - Q1Q4_Junction_Def) +
Q1Q4_Junction_Force) >= 0) Then
                                    Force(i + 1) = k1 * (Deformation(i + 1) -
Q1Q4_Junction_Def) + Q1Q4_Junction_Force
                                    Tangent_Stiffness(i + 1) = k1
                                    Location(i + 1) = -2.33
                                Else
                                    If (Deformation(i + 1) >= Res_Def_Neg) Then
```

```
                                    Force(i + 1) = 0
                                    Tangent_Stiffness(i + 1) = 0
                                    Location(i + 1) = -2.34
                                ElseIf (Deformation(i + 1) < Res_Def_Neg) Then
                                    If ((k1 * (Deformation(i + 1) - Res_Def_Neg)) >=
NMin) Then
                                        Force(i + 1) = k1 * (Deformation(i + 1) -
Res_Def_Neg)
                                        Tangent_Stiffness(i + 1) = k1
                                        Location(i + 1) = -2.35
                                    Else
                                        If ((k2 * (Deformation(i + 1) -
Deformation_Min_Neg) + NMin) >= SMA_Min_Neg_Force) Then
                                            Force(i + 1) = k2 * (Deformation(i + 1) -
Deformation_Min_Neg) + NMin
                                            Tangent_Stiffness(i + 1) = k2
                                            Location(i + 1) = -2.36
                                        Else
                                            Force(i + 1) = k1 * (Deformation(i + 1) -
SMA_Min_Def) + SMA_Min_Neg_Force
                                            Tangent_Stiffness(i + 1) = k1
                                            Location(i + 1) = -2.37
                                        End If
                                    End If
                                End If
                            End If
                        ElseIf (Force(i) <= Q1Q4_Junction_Force) Then
                            NMin = (-Fy * k1 + k1 * k2 * (Res_Def_Neg -
Deformation_Y_Neg)) / (k1 - k2)
                            Deformation_Min_Neg = (Res_Def_Neg * k1 - Fy - k2 *
Deformation_Y_Neg) / (k1 - k2)
                            If (k1 * (Deformation(i + 1) - Deformation(i)) + Force(i) >=
0) Then
                                Force(i + 1) = k1 * (Deformation(i + 1) - Deformation(i))
+ Force(i)
                                Tangent_Stiffness(i + 1) = k1
                                Location(i + 1) = -2.43
                            Else
                                If (Deformation(i + 1) >= Res_Def_Neg) Then
                                    Force(i + 1) = 0
                                    Tangent_Stiffness(i + 1) = 0
                                    Location(i + 1) = -2.44
                                ElseIf (Deformation(i + 1) < Res_Def_Neg) Then
                                    If ((k1 * (Deformation(i + 1) - Res_Def_Neg)) >= NMin)
Then
                                        Force(i + 1) = k1 * (Deformation(i + 1) -
Res_Def_Neg)
                                        Tangent_Stiffness(i + 1) = k1
                                        Location(i + 1) = -2.45
                                    Else
                                        If ((k2 * (Deformation(i + 1) -
Deformation_Min_Neg) + NMin) >= SMA_Min_Neg_Force) Then
                                            Force(i + 1) = k2 * (Deformation(i + 1) -
Deformation_Min_Neg) + NMin
                                            Tangent_Stiffness(i + 1) = k2
                                            Location(i + 1) = -2.46
                                        Else
                                            Force(i + 1) = k1 * (Deformation(i + 1) -
SMA_Min_Def) + SMA_Min_Neg_Force
                                            Tangent_Stiffness(i + 1) = k1
                                            Location(i + 1) = -2.47
```

```
                                    End If
                                End If
                            End If
                        End If
                    End If
                Else 'Any point on the left side of the line with stiffness k1 and
going through (Res_def_pos, 0) point
                    NMin = (-Fy * k1 + k1 * k2 * (Res_Def_Neg - Deformation_Y_Neg)) /
(k1 - k2)
                    Deformation_Min_Neg = (Res_Def_Neg * k1 - Fy - k2 *
Deformation_Y_Neg) / (k1 - k2)
                    If (k1 * (Deformation(i + 1) - Deformation(i)) + Force(i) >= 0)
Then
                        Force(i + 1) = k1 * (Deformation(i + 1) - Deformation(i)) +
Force(i)
                        Tangent_Stiffness(i + 1) = k1
                        Location(i + 1) = -2.53
                    Else
                        If (Deformation(i + 1) >= Res_Def_Neg) Then
                            Force(i + 1) = 0
                            Tangent_Stiffness(i + 1) = 0
                            Location(i + 1) = -2.54
                        ElseIf (Deformation(i + 1) < Res_Def_Neg) Then
                            If ((k1 * (Deformation(i + 1) - Res_Def_Neg)) >= NMin)
Then
                                Force(i + 1) = k1 * (Deformation(i + 1) - Res_Def_Neg)
                                Tangent_Stiffness(i + 1) = k1
                                Location(i + 1) = -2.55
                            Else
                                If ((k2 * (Deformation(i + 1) - Deformation_Min_Neg) +
NMin) >= SMA_Min_Neg_Force) Then
                                    Force(i + 1) = k2 * (Deformation(i + 1) -
Deformation_Min_Neg) + NMin
                                    Tangent_Stiffness(i + 1) = k2
                                    Location(i + 1) = -2.56
                                Else
                                    Force(i + 1) = k1 * (Deformation(i + 1) -
SMA_Min_Def) + SMA_Min_Neg_Force
                                    Tangent_Stiffness(i + 1) = k1
                                    Location(i + 1) = -2.57
                                End If
                            End If
                        End If
                    End If
                End If
            End If
            Deformation_Before_Corner = Deformation(i)
        End If

        PMax_Array(i) = PMax
        Deformation_Max_Pos_Array(i) = Deformation_Max_Pos
        NMin_Array(i) = NMin
        Deformation_Min_Neg_Array(i) = Deformation_Min_Neg
        PMin_Array(i) = PMin
        Deformation_Min_Pos_Array(i) = Deformation_Min_Pos
        k5_Array(i) = k5
        k6_Array(i) = k6
        Q1Q4_Junction_Def_Array(i) = Q1Q4_Junction_Def
        Q1Q4_Junction_Force_Array(i) = Q1Q4_Junction_Force
        Q2Q3_Junction_Def_Array(i) = Q2Q3_Junction_Def
        Q2Q3_Junction_Force_Array(i) = Q2Q3_Junction_Force
        SMA_Pos_Cutoff_Force_Array(i) = SMA_Pos_Cutoff_Force
```

```
        SMA_Neg_Cutoff_Force_Array(i) = SMA_Neg_Cutoff_Force
        NMax_Array(i) = NMax
        Historical_Deformation_Max_Array(i) = Historical_Deformation_Max
        Historical_Deformation_Min_Array(i) = Historical_Deformation_Min
        Res_Def_Pos_Array(i) = Res_Def_Pos
        Res_Def_Neg_Array(i) = Res_Def_Neg
        Variable_Deformation_Y_Pos_Array(i) = Variable_Deformation_Y_Pos
        Variable_Deformation_Y_Neg_Array(i) = Variable_Deformation_Y_Neg
    Next i

    Dim Test_Case As Integer
    Dim Sheet_Name As String
    Test_Case = Worksheets("Final").Cells(16, 2).Value
    If (load_num > 9) Then
        Sheet_Name = "SDOF_crv (" & CStr(Test_Case) & CStr(load_num) & ")"
    Else
        Sheet_Name = "SDOF_crv (" & CStr(Test_Case) & "0" & CStr(load_num) & ")"
    End If
    Sheets.Add.Name = Sheet_Name

    Worksheets(Sheet_Name).Cells(1, 1).Value = SMA_Rule + 6
    Worksheets(Sheet_Name).Cells(1, 2).Value = Fy
    Worksheets(Sheet_Name).Cells(1, 3).Value = k1
    Worksheets(Sheet_Name).Cells(1, 4).Value = r1
    Worksheets(Sheet_Name).Cells(1, 5).Value = r2
    Worksheets(Sheet_Name).Cells(1, 6).Value = alpha
    Worksheets(Sheet_Name).Cells(1, 7).Value = beta
    Worksheets(Sheet_Name).Cells(1, 8).Value = ry
    Worksheets(Sheet_Name).Cells(1, 9).Value = SMA_Cutoff_Force
    Worksheets(Sheet_Name).Cells(1, 10).Value = SMA_Max_Force
    Worksheets(Sheet_Name).Cells(1, 11).Value = Slippage_Rule

    For i = 0 To N - 1
        Worksheets(Sheet_Name).Cells(i + 2, 1).Value = Deformation(i)
        Worksheets(Sheet_Name).Cells(i + 2, 2).Value = Force(i)
    Next i
    DrawChart

    Erase Force, Deformation, Tangent_Stiffness, Location
    Erase PMax_Array, Deformation_Max_Pos_Array, NMin_Array,
Deformation_Min_Neg_Array, PMin_Array, Deformation_Min_Pos_Array, k5_Array, k6_Array,
Q1Q4_Junction_Def_Array, Q1Q4_Junction_Force_Array, Variable_Deformation_Y_Pos_Array,
Variable_Deformation_Y_Neg_Array
    Erase Q2Q3_Junction_Def_Array, Q2Q3_Junction_Force_Array,
SMA_Pos_Cutoff_Force_Array, SMA_Neg_Cutoff_Force_Array, NMax_Array,
Historical_Deformation_Max_Array, Historical_Deformation_Min_Array, Res_Def_Pos_Array,
Res_Def_Neg_Array

    Next k

End Sub

Public Function Larger(ByVal Num1 As Double, ByVal Num2 As Double) As Double
    If (Num1 >= Num2) Then
        Larger = Num1
    Else
        Larger = Num2
    End If
End Function

Public Function Smaller(ByVal Num1 As Double, ByVal Num2 As Double) As Double
    If (Num1 <= Num2) Then
```

```
        Smaller = Num1
    Else
        Smaller = Num2
    End If
End Function

Sub DrawChart()
    Dim LastRow As Long
    Dim Rng1 As Range
    Dim ShName As String
    With ActiveSheet
        LastRow = .Range("A" & .Rows.Count).End(xlUp).Row
        Set Rng1 = .Range("A2:A" & LastRow & ", B2:B" & LastRow)
        ShName = .Name
    End With

    Charts.Add
    With ActiveChart
        .ChartType = xlXYScatterLines
        .SetSourceData Source:=Rng1
        .Location Where:=xlLocationAsObject, Name:=ShName
    End With

    With ActiveChart.SeriesCollection(1)
        .MarkerStyle = xlMarkerStyleNone
    End With

    ActiveChart.SeriesCollection(1).Select
    With Selection.Format.Line
        .Visible = msoTrue
        '.DashStyle = msoLineSysDash
        .ForeColor.RGB = RGB(60, 60, 60) 'now it works
    End With

End Sub
```